



**National Library
of Canada**

**Bibliothèque nationale
du Canada**

Canadian Theses Service

Service des thèses canadiennes

**Ottawa, Canada
K1A 0N4**

NOTICE

The quality of this microform is heavily dependent upon the quality of the original thesis submitted for microfilming. Every effort has been made to ensure the highest quality of reproduction possible.

If pages are missing, contact the university which granted the degree.

Some pages may have indistinct print especially if the original pages were typed with a poor typewriter ribbon or if the university sent us an inferior photocopy.

Reproduction in full or in part of this microform is governed by the Canadian Copyright Act, R.S.C. 1970, c. C-30, and subsequent amendments.

AVIS

La qualité de cette microforme dépend grandement de la qualité de la thèse soumise au microfilmage. Nous avons tout fait pour assurer une qualité supérieure de reproduction.

S'il manque des pages, veuillez communiquer avec l'université qui a conféré le grade.

La qualité d'impression de certaines pages peut laisser à désirer, surtout si les pages originales ont été dactylographiées à l'aide d'un ruban usé ou si l'université nous a fait parvenir une photocopie de qualité inférieure.

La reproduction, même partielle, de cette microforme est soumise à la Loi canadienne sur le droit d'auteur, SRC 1970, c. C-30, et ses amendements subséquents.



National Library
of Canada

Bibliothèque nationale
du Canada

Canadian Theses Service Service des thèses canadiennes

Ottawa, Canada
K1A 0N4

The author has granted an irrevocable non-exclusive licence allowing the National Library of Canada to reproduce, loan, distribute or sell copies of his/her thesis by any means and in any form or format, making this thesis available to interested persons.

The author retains ownership of the copyright in his/her thesis. Neither the thesis nor substantial extracts from it may be printed or otherwise reproduced without his/her permission.

L'auteur a accordé une licence irrévocable et non exclusive permettant à la Bibliothèque nationale du Canada de reproduire, prêter, distribuer ou vendre des copies de sa thèse de quelque manière et sous quelque forme que ce soit pour mettre des exemplaires de cette thèse à la disposition des personnes intéressées.

L'auteur conserve la propriété du droit d'auteur qui protège sa thèse. Ni la thèse ni des extraits substantiels de celle-ci ne doivent être imprimés ou autrement reproduits sans son autorisation.

ISBN 0-315-55403-5

THE UNIVERSITY OF ALBERTA

**SYNTHESIS AND CHARACTERIZATION OF THE HEXAPROTIC
LIGAND TRIS(2-AMINOETHYL)AMINE HEXAACETIC ACID (TAHA)**

**BY
ARUNA SHARMA**

**A THESIS
SUBMITTED TO THE FACULTY OF GRADUATE STUDIES AND
RESEARCH IN PARTIAL FULFILLMENT OF THE REQUIREMENT FOR
THE DEGREE OF MASTER OF SCIENCE**

DEPARTMENT OF CHEMISTRY

**EDMONTON, ALBERTA
FALL, 1989**

THE UNIVERSITY OF ALBERTA

RELEASE FORM

NAME OF AUTHOR: Aruna Sharma


TITLE OF THESIS: Synthesis and Characterization of the hexaprotic ligand
tris (2-aminoethyl)amine hexaacetic acid (TAHA)

DEGREE: Master of Science

YEAR THIS DEGREE GRANTED: 1989

Permission is hereby granted to THE UNIVERSITY OF ALBERTA
LIBRARY to reproduce single copies of this thesis and to lend or sell such
copies for private, scholarly or scientific research only.

The author reserves other publication rights, neither the thesis nor
extensive extracts from it may be printed or otherwise reproduced without the
author's written permission.



(A. Sharma)
57 Mitchell Ave.

Red Deer, Alberta

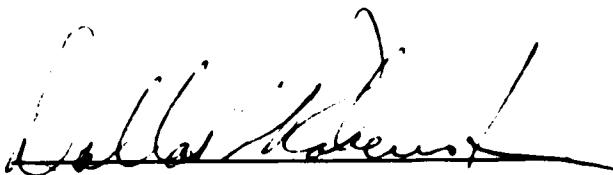
T4N 5S3

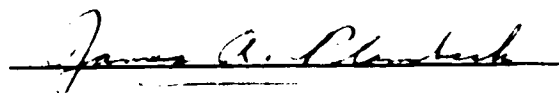
Date: Oct 6 1989

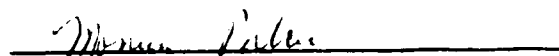
THE UNIVERSITY OF ALBERTA

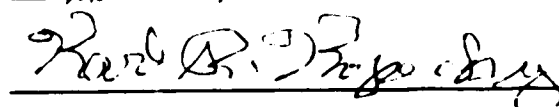
FACULTY OF GRADUATE STUDIES AND RESEARCH

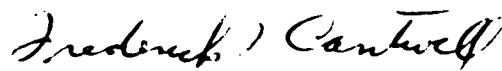
The undersigned certify that they have read, and recommend to the Faculty of Graduate Studies and Research for acceptance, a thesis entitled **Synthesis and Characterization of the Hexaprotic Ligand Tris (2-aminoethyl)amine hexaacetic acid (TAHA)** submitted in partial fulfillment of the requirements for the degree of **Master of Science**.


(Supervisor)








(Chairman)

Date: Oct. 6, 1989

**Boldly
dedicated to all the
PhD. Candidates
who obtained a Masters of Science:
for all their untold secrets
and
for all their success
Past, Present and Future.**

**Simply
dedicated to T.A.K.
because I said I would
once
when we were both younger and freer
and
....just because....**

ABSTRACT

Paramagnetic lanthanide ions chelated to polyaminocarboxylate ligands are of considerable importance as magnetic resonance imaging (MRI) contrast enhancing agents. More specifically, lanthanide ions such as gadolinium (Gd^{+3}) are of particular interest due to their efficiency in reducing the proton relaxation times of water. These ions are complexed to a ligand, such as diethylenetriaminepentaacetic acid (DTPA), to reduce the toxic effects of the metal. This thesis describes the synthesis of a new ligand, tris(2-aminoethyl)amine hexaacetic acid (TAHA) with the structural formula $N(CH_2CH_2N(CH_2COOH)_2)_3$ as a potential candidate as a new contrast agent for MRI. This ligand has ten possible coordination sites available for binding to a metal ion. Therefore, it could complex to metals with a very high stability constant, which in turn would prevent free metal ion from being released in vivo.

TAHA was characterized by potentiometric methods (both pH and pHg titrations), as well as 1H NMR methods. Six acid dissociation constants in aqueous solutions were calculated, and various metal ligand formation constants were obtained and tabulated. The metal ions studied in depth were mercury(II), lanthanum, and calcium. The lanthanide series, and various selected metals were also studied in terms of their interaction with TAHA.

This work illustrates the complex nature of metal-TAHA interactions; the potential of $Gd(TAHA)^{-3}$ as a contrast agent for MRI is uncertain at this time; future work involving both in vitro and in vivo studies to further characterize its chemistry are necessary.

ACKNOWLEDGEMENTS

**"The most satisfying privilege of higher education is
after all that is done is done
and after all that is complete is finished;
one has the honor of writing....."**

Dr. D.L. Rabenstein, supervisor, is acknowledged.

Financial support from the National Science and Engineering Research Council of Canada received during the course of this work, is gratefully acknowledged.

For numerous stimulating, helpful, and beneficial discussions I gratefully acknowledge the following people from the University of California, Riverside: Ms. J. Pleasants, Dr. T. Schierling, and Dr. W. Guo. These people took the time, interest, energy, and offered input that was most valuable during the course of this work, and especially during the end. I would also like to acknowledge the following professors at the University of Alberta, for discussions on both research and non-research concerns: Dr. F. Cantwell, Dr. B. Kratochvil, and Dr. J. Plambeck.

I would like to acknowledge the excellent personnel at the electronics shop, the machine shop and the photocopying room at both the University of California, Riverside and at the University of Alberta. I would also like to thank the secretarial staff for assistance in various matters including mailing of my paycheck. I would also like to acknowledge the other academic and nonacademic staff at the Department of Chemistry, University of Alberta, for information and assistance during the three years I was registered as an extramural student at the University of California, Riverside. I would also like to thank the staff at the Faculty of Graduate Studies, University of Alberta, for information and advice upon my return to Edmonton.

Thanks go to Dr. K. Kasperski for information regarding the Macintosh and assistance, as well advice, regarding the figures; her patience, endurance, time, and occasional nudge, are appreciated.

I am very indebted to my long time friend, Ms. K. Gill and her husband, Mr. R. Gill, for the complete access to their home and computer. Their patience, trust, and confidence are appreciated.

A thesis cannot, I feel, be completed on laboratory research, scientific knowledge, hard work, and endurance alone--I would therefore like to take this opportunity to thank the following people, without whom this work would not have been presented at this time.

Firstly, I would like to acknowledge and send my deepest appreciation to my parents who have given me support, faith, acceptance, and determination to succeed as measured by that which in the end is all that matters: myself and the Universe in which I belong. On a more practical and physical plane, I would like to thank my parents for all the financial support during the three years I was living in Riverside on a Canadian paycheck (when the dollar was 1.42000...).

I would also like to acknowledge my brother Bob and my sister Rita, for everything, especially for making me smile and laugh.

I would like to thank my friends, both in California and Canada, for their support, conversation, and simply being Friends when it was not convenient nor beneficial. These few people know who they are and need not be mentioned, except in the knowledge that they have been more than just acknowledged.

TABLE OF CONTENTS

CHAPTER	PAGE
I. INTRODUCTION	1
II. EXPERIMENTAL	
A. Chemicals.....	10
B. Solution Preparation	
1. Preparation and Standardization of EDTA.....	11
2. Preparation and Standardization of Metal Solutions	13
3. Preparation and Standardization of Carbonate Free Potassium Hydroxide.....	14
C. Instrumentation	
1. pH Measurements	16
2. pHg Method	18
3. ¹ H NMR Measurements.....	30
D. Computing Methods	
1. NMR Curve Fitting	34
2. Nonlinear Least Squares Calculations.....	36
3. Other Calculations.....	37
III. SYNTHESIS AND CHARACTERIZATION OF TRIS(2- AMINOETHYL)AMINE HEXAPROTIC ACID (TAHA)	
A. Synthesis, Purification, and General Properties of Ligand	38
B. Calculation of Acid Dissociation Constants	
1. Introduction.....	45
2. Method 1	48
3. Method 2	55
4. Method 3	59
5. Discussion	67
C. ¹ H NMR Studies of the Acid/Base Chemistry of TAHA.....	75
D. Summary..	84

TABLE OF CONTENTS (continued)

CHAPTER	PAGE
IV. METAL TAHA BINDING STUDIES	
A. Introduction.....	88
B. Mercury	
1. Potentiometric Studies	90
2. ¹ H NMR studies.....	115
3. Summary.....	134
C. Lanthanum	
1. Potentiometric Studies	138
2. ¹ H NMR studies.....	151
3. Summary.....	177
D. Calcium.....	178
1. Potentiometric Studies	180
2. ¹ H NMR studies.....	186
3. Summary.....	198
E. Other Metals Studied	
1. Rare Earth Metals.....	200
2. Other Metals	213
3. Summary.....	223
V. DISCUSSION.....	226
REFERENCES	228
APPENDIX 1. Sample subroutine for KINET used for the calculation of the acid dissociation constants for a triprotic acid, using pH versus volume of titrant	237
APPENDIX 2. Infrared spectrum of TAHA dissolved in water	239
APPENDIX 3. Mass spectra (EI) of TAHA obtained at 180 °C and 240 °C	240

TABLE OF CONTENTS (continued)

	PAGE
APPENDIX 4. Acid Dissociation constants (ionic strength of 0.1 M KNO ₃ and a temperature of 25.00 °C)	
A. EDTA, EGTA, DTPA, tren.....	241
B. Hexaprotic Acids (TAHA, TTHA, TAPHA and triaminoethylamine hexaprotic acid).....	242
C. Other Ligands.....	243

LIST OF TABLES

TABLE	DESCRIPTION	PAGE
1.	Calculated stability constants for metal complexes of EDTA and DTPA at constant ionic strength and temperature ($\mu = 0.1 \text{ M KNO}_3$, 25.00°C).....	29
2.	Summary of general properties of the ligand TAHA (tris(2-aminoethyl)amine).....	44
3.	Calculated x and y values for the determination of K_2 and K_3 , using Method 1.....	52
4.	Calculated x and y values for the determination of K_4 and K_5 using Method 1.....	56
5.	Comparison of the six acid dissociation constants of TAHA obtained from the three different methods.	58
6.	Tabulation of experimentally determined \bar{n} values, along with the A values and pH's, for the determination of the first three acid dissociation constants using the method of Bjerrum.....	64
7.	Acid dissociation constants for TAHA in H_2O and D_2O ($\mu = 0.1 \text{ M KNO}_3$, 25.00°C).....	69
8.	Tabulation of $[\text{Hg}^{+2}]$ and the overall formation constants $\beta_{\text{Hg}_2\text{L}}$ and $\beta'_{\text{Hg}_2\text{L}}$, for the bimetal complex $\text{Hg}_2(\text{TAHA})^{-2}$	96
9.	Tabulation of the concentrations of various mercury containing species, Hg^{+2} , $\text{Hg}(\text{OH})^+$, and $\text{Hg}(\text{TAHA})^{-4}$, and conditional formation constants, as a function of pH.....	102

LIST OF TABLES (continued)

TABLE	DESCRIPTION	PAGE
10.	Tabulation of the stability constants for protonated mercury-TAHA complexes ($\mu = 0.1 \text{ M KNO}_3$, $25.00 \text{ }^\circ\text{C}$).....	110
11.	Comparison of the logarithm of K_{HgHL} values for various mono-protonated mercury-ligand complexes ($\mu = 0.1 \text{ M KNO}_3$, $25.00 \text{ }^\circ\text{C}$).	112
12.	Tabulation of the chemical shift, linewidth, and assignment of each resonance in the ^1H NMR spectrum for the mercury-TAHA system (Figure 28).	117
13.	Numerical output of deconvolution results shown in Figures 35A and 35B for a solution in which the ratio of Hg^{+2} :TAHA is 1.0:1.0.	133
14.	Tabulation of various species (ML and $\text{M}(\text{OH})_n$ complexes) as a function of pH for the pHg data, for a solution in which the ratio of Hg^{+2} : La^{+3} :TAHA is 1.0:2.0:2.0.....	144
15.	Summary of all the ^1H NMR resonances observed for the lanthanum-TAHA system, as well as assignment of the complex giving rise to each resonance.	154
16.	Tabulation of the stability constants for the lanthanum-TAHA system ($\mu = 0.1 \text{ M, KNO}_3$, $25 \text{ }^\circ\text{C}$).	164
17.	Tabulation of pH^* , chemical shifts, linewidths, and relative integrals for the two ^1H NMR resonances labelled as peak 1 and peak 11 in Figure 49A.....	173

LIST OF TABLES (continued)

TABLE	DESCRIPTION	PAGE
18.	Summary of the effect of change in temperature on peak half widths, as shown in Figure 51.	175
19.	Tabulation of the stability constants calculated for the calcium-TAHA system ($\mu = 0.1 \text{ M KNO}_3$, $25.00 \text{ }^\circ\text{C}$).	183
20.	Tabulation of the logarithm of K_{CaL} for various ligands ($\mu = 0.1 \text{ M KNO}_3$, $25.00 \text{ }^\circ\text{C}$).	199
21.	Tabulation of initial concentrations used for potential-pH diagrams presented in Figure 65.	203
22.	Tabulation of pK_{eq}^M in the potential-pH independent region for various rare earth metals with TAHA.	210
23.	Tabulation of concentrations used for potential-pH diagrams presented in Figure 69.	216
24.	Tabulation of pK_{eq}^M and the potential-pH independent region for various metals with TAHA.	216
25.	Tabulation of concentrations of various species for the nickel-TAHA system.	220

LIST OF FIGURES

FIGURE	DESCRIPTION	PAGE
1.	A schematic of the double walled cell utilized for the determination of metal ligand stability constants using the pHg Method.	19
2.	Potential-pH diagrams for the determination of metal EDTA complexes in a solution with an ionic strength of 0.1 M (KNO ₃) at 25.00 °C.	26
3.	Potential-pH diagrams for the determination of metal DTPA complexes in a solution with an ionic strength of 0.1 M (KNO ₃) at 25.00 °C.	27
4.	The temperature calibration curve for the Varian XL 500 spectrometer obtained using Equation [24].	32
5.	A. Pulse sequence for the single pulse experiment B. Pulse sequence for the Jump and Return experiment.....	33
6.	Equation, including structures, depicting the synthesis of the ligand TAHA from tris (2-aminoethyl)amine and chloroacetic acid using the method of Moor. Methylene protons, T1, T2, and T3, as well as the N1 (or central) and N2 nitrogen atoms on TAHA, are labelled.....	39
7.	¹ H NMR spectrum of a solution of EDTA and TAHA at pH* 3.0. ...	42
8.	Potentiometric (pH) titration of TAHA as a function of the A value where A is defined as moles of base added per mole of TAHA present. A. Titration performed in H ₂ O; B. Titration performed in D ₂ O.....	46

LIST OF FIGURES (continued)

FIGURE	DESCRIPTION	PAGE
9.	A x-y plot of (x,y) values that are tabulated in Table 3.	51
10.	Illustration of the graphical solution for the determination of K_2 and K_3 using the values presented in Table 3.	53
11.	Illustration of the graphical solution for the determination of K_4 and K_5	57
12.	Straight line plot for the determination of the stepwise association constants, K_1^* and K_2^* , using the method of Bjerrum.	62
13.	Formation curve, \bar{n} versus pH, for the dissociation of the carboxylate groups of TAHA; in this case the A value range is between 0 to 3 for a triprotic acid.	63
14.	Formation curve, \bar{n} versus pH, in which TAHA is considered as an hexaprotic acid.	66
15.	Distribution curve in H_2O at constant ionic strength and temperature ($\mu=0.1$ M KNO_3 and 25.00 °C).	70
16.	Distribution curve in D_2O at constant ionic strength and temperature ($\mu=0.1$ M KNO_3 and 25.00 °C).	71
17.	A schematic of the microscopic dissociation constants of TAHA carboxylate groups	74
18.	Representative 1H NMR spectra of TAHA as a function of pH*	77

LIST OF FIGURES (continued)

FIGURE	DESCRIPTION	PAGE
19.	Chemical shift (ppm) versus pH* for the T1, T2, and T3 methylene proton resonances of TAHA.....	78
20.	A schematic of the microscopic dissociation constants of TAHA amino groups.....	83
21.	Comparison of TAHA with other ligands using α^* versus pH plots; the term α^* is defined as $\alpha^* = [\alpha_6]^{-1}$	86
22.	Titration curves of pH versus A value for the mercury-TAHA system; the L represents the ligand TAHA ($\mu=0.1$ M KNO ₃ and 25.00 °C).	91
23.	Plot of logarithm of $\beta'_{\text{Hg}_2\text{L}}$ and $\beta_{\text{Hg}_2\text{L}}$ as a function of pH.	97
24.	Potential-pH diagram for a solution in which the Hg ⁺² :TAHA ratio is 1.00:1.60.....	101
25.	Plot of K_{HgL}^C as a function of pH for duplicate runs of Hg ⁺² :TAHA in a ratio of 1.0:2.0.	105
26.	Plot of the linear regression analysis for the calculation of K_{HgHL} and $K_{\text{HgH}_2\text{L}}$ using Equation [101].	109
27.	Plot of the logarithm of K_{HgHL} versus sum of pK's (Σ pK's) for several mercury-ligand complexes.	114
28.	Typical ¹ H NMR spectrum for a 1.0:1.0 solution of Hg ⁺² :TAHA (1.06 mM Hg ⁺² , 5.32 mM TAHA) obtained in the pH* range 4.26 to 7.09.	116
29.	¹ H NMR spectra for a 1.0:1.0 solution of Hg ⁺² :TAHA (1.06 mM Hg ⁺² , 5.32 mM TAHA) as a function of pH*.....	119

LIST OF FIGURES (continued)

FIGURE	DESCRIPTION	PAGE
30.	Comparison of the ^1H NMR resonances due to the T1 and T3 methylene protons of TAHA complexed to mercury as a function of pH^*	121
31.	Comparison of the ^1H NMR resonances due to T2 and T3 methylene protons of TAHA complexed to mercury as a function of pH^*	122
32.	Comparison of the two ^1H NMR resonances, assigned as peak 1 and peak 4 in Figure 28, due to the T2 methylene protons of TAHA complexed to mercury.....	124
33.	Chemical shift (ppm) as a function of pH^* for the mercury-TAHA system.	126
34.	^1H NMR spectra of a sample in which the Hg^{+2} :TAHA ratio is 2.7:1.0, A. In the presence of precipitate, B. After the precipitate was completely dissolved by the addition of carbonate free KOD.....	129
35.	Deconvolution output of a 1.0:1.0 ratio of Hg^{+2} :TAHA at pH^* 5.17. A. Input parameters indicated that the total number of resonances present is seven. B. Input parameters indicated that the total number of resonances is eight.	131
36.	Summary of all possible equilibria involved in the interaction of mercury with TAHA.....	135
37.	Titration curves of pH versus A value for the lanthanum-TAHA system in various concentrations; L represents the ligand TAHA ($\mu=0.1$ M KNO_3 and 25.00°C).	139

LIST OF FIGURES (continued)

FIGURE	DESCRIPTION	PAGE
38.	Potential-pH diagram (curve C) for a solution in which the ratio of $\text{Hg}^{+2}:\text{La}^{+3}:\text{TAHA}$ is 1.0:2.0:2.0.....	142
39.	Plot of $\text{pK}_{\text{eq}}^{\text{La}}$ versus pH.....	148
40.	Plot of the logarithm of $K_{\text{LaL}}^{\text{C}}$ as a function of pH.	150
41.	^1H NMR spectrum at $\text{pH}^* 3.09$ for the lanthanum-TAHA system.....	152
42.	Chemical shift (ppm) as a function of pH^* for the lanthanum-TAHA system.	153
43.	Representative ^1H NMR spectra as a function of pH^* in the range 3.55 to 4.24 for the lanthanum-TAHA system	156
44.	Fraction of the total intensity of peaks 7 and 8, assigned in Figure 41, as a function of pH.	157
45.	Representative ^1H NMR spectra as a function of pH^* in the range 3.76 to 9.52 for the lanthanum-TAHA system.	158
46.	Deconvolution output of a 1.0:1.0 ratio of $\text{La}^{+3}:\text{TAHA}$ at $\text{pH}^* 3.55$	161
47.	Plot of conditional formation constants for $\text{LaH}_2\text{L}^{-1}$, (K_1^{C}), and LaHL^{-3} , (K_2^{C}), as a function of pH^*	163
48.	Plot of the logarithm of K_{LaHL} versus the sum of $\text{pK}'\text{s}$, ($\Sigma \text{pK}'\text{s}$), for several lanthanum-ligand complexes.....	167

LIST OF FIGURES (continued)

FIGURE	DESCRIPTION	PAGE
49.	^1H NMR spectra in which the final $\text{La}^{+3}:\text{TAHA}$ ratio was 2.3:1.0, plotted as a function of pH^* . A. Chemical shift (ppm) range is 3.70 to 4.10, depicting the region in which bound T3 methylene protons are observed.....	168
49.	(continued) B. chemical shift (ppm) range is 2.40 to 3.80, depicting the bound T1 and T2 methylene protons.	169
50.	Plot of chemical shift (ppm) versus pH^* of all ^1H NMR resonances in which the $\text{La}^{+3}:\text{TAHA}$ ratio was 2.3:1.0.	172
51.	Representative ^1H NMR spectra as a function of temperature, in which the $\text{La}^{+3}:\text{TAHA}$ ratio was 2.3:1.0.....	174
52.	Summary of all possible equilibria involved in the interaction of lanthanum with TAHA.	179
53.	Titration curves of pH versus A value for the calcium-TAHA system at various concentrations; L represents the ligand TAHA ($\mu=0.1$ M KNO_3 and 25.00°C).....	181
54.	Potential-pH diagram for a solution in which the ratio of $\text{Hg}^{+2}:\text{Ca}^{+2}:\text{TAHA}$ is 1.0:2.0:2.0.....	184
55.	Plot of $\text{pK}_{\text{eq}}^{\text{Ca}}$ and $\log K_{\text{CaL}}^{\text{C}}$ as a function of pH	185
56.	Representative ^1H NMR spectra of the calcium-TAHA system, as a function of pH^*	187

LIST OF FIGURES (continued)

FIGURE	DESCRIPTION	PAGE
57.	Representative ^1H NMR spectra of the calcium-TAHA system, as a function of temperature, in which the Ca^{+2} :TAHA ratio was 1.08:1.00, at $\text{pH}^* 6.11$	188
58.	Representative ^1H NMR spectra of the calcium-TAHA system, as a function of temperature, in which the Ca^{+2} :TAHA ratio was 1.08:1.00, at $\text{pH}^* 10.10$	190
59.	Chemical shift (ppm) versus pH^* for the titration of Ca^{+2} :TAHA in a ratio of 1.08:1.00.....	191
60.	Deconvolution output of a 1.08:1.00 ratio of Ca^{+2} :TAHA at $\text{pH}^* 6.17$	193
61.	Plot of the logarithm of $K_{\text{CaL}}^{\text{C}}$ (K^{C}), versus pH^* for the calcium-TAHA system.	194
62.	A plot of the linear regression analysis from which the formation constants $K_{\text{CaHL}}^{\text{D}}$ and $K_{\text{CaH}_2\text{L}}^{\text{D}}$ was performed as described in text.	197
63.	Potential-pH diagram for a solution in which the ratio of Hg^{+2} : M^{+3} :TAHA is 1.0:2.0:2.0, where M^{+3} represents the trivalent rare earth metal ion.	201

LIST OF FIGURES (continued)

FIGURE	DESCRIPTION	PAGE
64.	Plot of pK_{eq}^M and $\log K_{ML}^C$ as a function of pH. A. praseodymium (Pr^{+3}). B. neodymium (Nd^{+3}). C. samarium (Sm^{+3}). D. europium (Eu^{+3}). E. gadolinium (Gd^{+3}). F. terbium (Tb^{+3}). G. dysprosium (Dy^{+3}). H. holmium (Ho^{+3}). I. erbium (Er^{+3}). J. ytterbium (Yb^{+3})205	205
65.	Potential-pH diagram (left y axis) and mmoles base added (right y axis) versus pH for the holmium-TAHA system.....208	208
66.	Plot of $pK_{eq(av)}^M$ versus atomic number (Z) for the interaction of rare earth metals with TAHAs.....211	211
67.	Plot of $pK_{eq(av)}^M$ versus ionic radius (\AA) for the interaction of rare earth metals with TAHAs.....212	212
68.	Titration curves of pH versus A value for the cadmium-TAHA system at various concentrations; L represents the ligand TAHAs ($\mu=0.1$ M KNO_3 and $25.00^\circ C$).214	214
69.	Potential-pH diagram for a solution in which the ratio of $Hg^{+2}:M^{+n}:TAHA$ is 1.0:2.0:2.0.....215	215
70.	Plot of pK_{eq}^M and logarithm of K_{ML}^C as a function of pH. A. Cadmium (Cd^{+2}), B. Zinc (Zn^{+2}).....218	218
71.	Plot of $[HgL]$ versus pK_{eq}^{Ni}221	221

LIST OF FIGURES (continued)

FIGURE	DESCRIPTION	PAGE
72.	Titration curves of pH versus A value for the nickel-TAHA system at various concentrations; L represents the ligand TAHA ($\mu=0.1$ M KNO_3 and 25.00°C).....	222
73.	Plot of $\text{pK}_{\text{eq}}^{\text{M}}$ and logarithm of $\text{K}_{\text{PbL}}^{\text{C}}$ as a function of pH. A. Lead (Pb^{+2}), B. Strontium (Sr^{+2}).....	224

I. INTRODUCTION

Nuclear magnetic resonance imaging, often termed magnetic resonance imaging (MRI), has become a rapidly growing field in the last several years. MRI has shown exceptional promise as a useful diagnostic tool for the study of human diseases; one of the major goals in MRI is to maximize one's ability to visualize and differentiate adjacent tissue regions in the body on the basis of differences in anatomy, physiology, or pathological processes. Such images are dependent on the proton density and the proton relaxation times, both spin-lattice (T_1) and spin-spin (T_2) relaxation times, of the water protons present in tissue.

Contrast agents are, by definition, exogenous reagents used in MRI which alter the T_1 and T_2 relaxation times of the water protons, allowing for an increased enhancement (contrast) of the images obtained by MRI. Such agents are administered intravenously or orally.

The increased interest and rapid growth in the theory, design, and clinical research of contrast agents is due in part to its application in medical diagnosis. For example, Lauffer (1) has reported that, in general, the required dose of paramagnetic contrast agents, at roughly 0.5 to 5.0 grams per person, is much higher than the concentration of metal ions or complexes utilized in radioscinotography. However, iodine-containing contrast agents used in computer tomography and other radiological procedures routinely used today require a much higher dosage, approximately 50.0 to 200.0 grams per person. It is believed that with the development of nontoxic chelates the "contrast-enhanced NMR exam is likely to be safer than the similar computer tomography procedures"(1).

In the last several years there have been several reviews on contrast

agents (1-15). In this introduction, a brief overview of the use and limitations of contrast agents will be presented.

The most useful contrast agents are those that are paramagnetic; of these paramagnetic agents, the trivalent metal ion of gadolinium, (Gd^{+3}), is of particular interest due to its effectiveness in reducing the T_1 and T_2 relaxation times of water protons. This is due to the seven unpaired electrons of the Gd^{+3} ion and the fact that the magnetic dipole moment of the electron is about one thousand times larger than that of protons. However, Gd^{+3} is extremely toxic with a LD_{50} (lethal dose causing 50% death in animal studies) of 0.5 mmole per kilogram in rats (16). For this reason Gd^{+3} must be chelated to a ligand; an especially useful chelator for Gd^{+3} is DTPA (diethylenetriamine pentaacetic acid). Weinmann *et al.* (16) have reported that the LD_{50} for $Gd(DTPA)^{-2}$ in rats is ten millimole per kilogram, which is a fifty fold increase in tolerance over Gd^{+3} . As will be discussed later, $Gd(DTPA)^{-2}$ has been approved for clinical studies with doses varying from 0.005 to 0.4 millimole per kilogram (2). Because of its efficiency in reducing the toxic effects of Gd^{+3} , as well as its effectiveness in decreasing relaxation times, the use of $Gd(DTPA)^{-2}$ as a contrast agent has been well established and documented (16-29). The structure of $Gd(DTPA)^{-2}$, which is an octadentate chelate, has been studied by Goldstein *et al.* (25). Of the nine coordination sites on the gadolinium ion, three are occupied by nitrogen atoms and five by carboxylate groups of DTPA. The remaining coordination site is occupied by a water molecule which undergoes rapid exchange with other water molecules in the outer sphere of the $Gd(DTPA)^{-2}$ complex; this provides a mechanism through which T_1 and T_2 relaxation times are mediated by the paramagnetic gadolinium ion. For the $Gd(DTPA)^{-2}$ complex, a high stability constant of 1×10^{22} has been reported (30). Swenberg and Meovius (2) calculate that this high stability factor

corresponds to having only 3.0×10^{-14} M Gd^{+3} present in the free state at any one time, under physiological conditions, when $Gd(DTPA)^{-2}$ is injected at a dose of 1.0×10^{-7} M.

The study of both the toxicity and the stability of a potential contrast agent is very important. While the testing and mechanistic understanding of metal complex toxicity often requires the expertise of toxicologists and pharmacologists, chemists can offer a tremendous contribution in the development of safe chelates largely by the synthesis of new ligands and their derivatives, as well as the elucidation of the dissociation and association mechanisms involved in both aqueous and serum solutions.

The toxic effects of a chelate can arise from a variety of factors. Firstly, toxicity may be due to the free metal ion initially uncomplexed by the ligand, or released by dissociation of the metal ligand complex. For example, Gd^{+3} can complex to calcium binding sites, often with an higher affinity due to its greater charge:radius ratio. Secondly, toxic effects may arise from the free ligand initially present in excess to ensure complete complexation of the paramagnetic metal ion (which is usually much more toxic than the ligand), or the presence of free ligand may also be due to dissociation of the metal ligand complex *in vivo*. This area is less well understood and characterized than free metal toxicity. This type of toxicity can stem from the sequestration of essential metal ions such as calcium and magnesium as well as 'organic toxic effects'. The third type of toxicity is from the metal ligand complex itself, which may arise from a wide variety of specific and nonspecific effects. For example, for the contrast agent $Gd(DTPA)^{-2}$, the toxicity of the high doses required in LD_{50} determinations may be due to a nonspecific hypertonic effect; that is to say, that a difference in the osmotic pressure between the intracellular and extracellular tissue is established after injection of large quantities of the complex with its counter ion.

As a result of the osmotic gradient, water is drawn out of the cells, causing cellular and circulatory unbalances, and/or damage. Other areas in which the metal ligand complex may cause toxicity include enzyme inhibition, nonspecific protein conformational effects, alteration of the membrane potential, and interaction with biological macromolecules or cellular membranes.

It is important to note that the in vivo stability of the metal ligand complex is specifically a kinetic and not a thermodynamic requirement. The contrast agent utilized should be efficiently excreted from the body within a few hours after administration and therefore the stability of the complex is only required for the residence time. It is therefore necessary to establish the dissociation kinetics as well as the thermodynamic stability constant in serum.

The dissociation kinetics are related to the thermodynamics of complexation via the following equation where k_a and k_d are defined as the association and dissociation rate constants and K_{ML} is defined as the thermodynamic stability constant.

$$K_{ML} = \frac{k_a}{k_d} \quad [1]$$

The study of the thermodynamics of complexation is important in identifying the source of the metal ligand stability. However, the presence of thermodynamic sinks other than that of the metal ligand complex exist in biological systems: these states will not be reached if the dissociation rate of the complex is sufficiently slow. The most important of such "sinks" for trivalent metal ions in serum is their precipitation with anions such as hydroxide (e.g. $Gd(OH)_3$), phosphate (e.g. $GdPO_4$), and carbonate (e.g. $Gd_2(CO_3)_3$). In the case of Gd^{+3} precipitation with phosphate and carbonate is more important than

precipitation with hydroxide ions.

Other chelates such as $\text{Mn}(\text{EDTA})^{-2}$, $\text{Cr}(\text{EDTA})^{-2}$, and $\text{Gd}(\text{EDTA})^{-1}$ have been studied as contrast agents. However, they have not been as effective as $\text{Gd}(\text{DTPA})^{-2}$ in the area of producing enhanced contrast and low toxicity. For example, the toxicity of $\text{Gd}(\text{EDTA})^{-2}$ is comparable to that of GdCl_3 , presumably due to the relatively low stability of the $\text{Gd}(\text{EDTA})^{-1}$ complex with a stability constant of 1×10^{17} (30), some five orders of magnitude less than that of $\text{Gd}(\text{DTPA})^{-2}$. It is assumed that complexes such as $\text{Gd}(\text{EDTA})^{-1}$ undergo significant dissociation in vivo which releases free Gd^{+3} causing severe toxic effects associated with the free gadolinium ion, as described earlier.

In general, metal chelates of DTPA are distributed throughout the extracellular space and do not cross the intact blood brain/barrier; such complexes are rapidly eliminated by the kidneys (22). Because of this, there has been considerable interest in the area of tissue targeting contrast agents such as $\text{Gd}(\text{DTPA})^{-2}$. Linking $\text{Gd}(\text{DTPA})^{-2}$ to bovine serum albumin (BSA) or to IgG monoclonal antibodies to increase tissue specificity towards specific organs or tumors has been studied (31-34). Lauffer *et. al.* (34) have found that the T_1 relaxivities increased from 3.8 for $\text{Gd}(\text{EDTA})^{-1}$ to 66.0 for BSA- $\text{Gd}(\text{EDTA})^{-1}$ and 70.0 for IgG- $\text{Gd}(\text{EDTA})^{-1}$. In this case, relaxivity is used to summarize the overall effectiveness of a paramagnetic agent in enhancing the T_1 and T_2 relaxation times. It is defined as the increase in the proton relaxation rates, $1/T_1$ and $1/T_2$, above that with saline alone and has units of $\text{sec}^{-1} \text{mM}^{-1}$.

Recently there has also been considerable interest in the use of water soluble metalloporphyrins (35-37) due to the tendency of porphyrins to become localized in tumors. Marzola and Cannistraro (37) have reported that the tetrasodium-meso-tetra(4-sulfonatophenyl) porphyrin (TTPS) complexed to Gd^{+3} produces a strong effect on proton relaxation times that is comparable to

Gd⁺³ alone. The authors have stated that such behavior of the complex may allow its administration at lower doses when compared to Gd(DTPA)⁻², as well as having the advantage of selective uptake by tumors.

Another widely growing area in the study of tissue targeting of contrast agents is the use of liposomes. Liposomes offer the advantage of being able to incorporate monoclonal antibodies, BSA, and other proteins into the phospholipid bilayer; also, liposomes may be prepared with a variety of phospholipids, allowing for greater flexibility in its use as a carrier of contrast agents to specific tissues. The use of liposomes carrying Gd(DTPA)⁻² has been studied by Kabalka *et al.* (38). Gamble and Schmidt (39) have also studied liposome encapsulated Gd(DTPA)⁻² injected into mice, and have reported an increased relaxation rate of water protons, as well as the liposomes being tissue specific for tumors. The authors have also incorporated cholesterol into the bilayer to promote vesicle stability and water exchange across the bilayer. The use of liposomes for paramagnetic enhancement in MRI has been recently reviewed by Gore *et al.* (40).

As mentioned earlier, the complex Gd(DTPA)⁻² has received considerable attention as a contrast agent; its effects have been well documented in both medical and chemical journals. As a result, Gd(DTPA)⁻² is often used as a prototype for comparison of other potential contrast agents. Also, since 1984, Gd(DTPA)⁻² has been approved for clinical studies on humans. Since then, a number of such studies have been reported for contrast enhancement of the kidneys and extracellular regions (41-45), as well as its use in the study of brain tumors (46-49). All such reports indicate an increased contrast enhancement *in vivo* with no toxic effects on the volunteers involved in the studies. As an example, Weinmann *et al.* (43) have monitored the level of Gd(DTPA)⁻²/dimeglumine in the plasma and renal excretion of twenty healthy

men after the injection of 0.005 to 0.250 millimole per kilogram of the complex. The authors reported that $\text{Gd}(\text{DTPA})^{-2}$ is rapidly removed from the body and is detected in the renal excretion one hour after administration, with a corresponding decrease of the complex in the plasma. They concluded that no toxicity or side effects were observed and that $\text{Gd}(\text{DTPA})^{-2}$ had a total renal clearance similar to DTPA and other exogenous, inert, substances.

To my knowledge the only other paramagnetic contrast agent approved for clinical use is iron oxide in the form of super paramagnetic ferrite crystals which have a fifty fold greater magnetic susceptibility per mole of metal than gadolinium chelates; this study was reported by Stark *et al.* (50) in July 1988.

To date, the ligand DOTA (1,4,7,10-tetraazacyclododecane-N,N',N'',N'''-tetraacetic acid) complexed to Gd^{+3} shows considerable promise in the area of contrast enhancement for MRI (51-54). The $\text{Ln}(\text{DOTA})^{-2}$ complexes, where Ln represents the rare earth metals, have very high stability constants (54); for example, the stability constant of $\text{Gd}(\text{DOTA})^{-2}$ is 1×10^{28} (54) compared to 1×10^{22} for $\text{Gd}(\text{DTPA})^{-2}$ (30). Knop *et al.* (55) have compared the use of $\text{Gd}(\text{DOTA})^{-2}$ and $\text{Gd}(\text{DTPA})^{-2}$ as contrast agents in rats and rhesus monkeys. The authors concluded that the broad distribution and relaxation rates of both complexes are similar. Based on these preliminary results the authors suggested that $\text{Gd}(\text{DOTA})^{-2}$ and similar macrocyclic Gd^{+3} chelates, can be considered as alternatives to $\text{Gd}(\text{DTPA})^{-2}$.

Although $\text{Gd}(\text{DTPA})^{-2}$ has been approved for clinical studies there is the problem of the presence of free gadolinium ions as was discussed earlier. There is a major concern over the extent to which $\text{Gd}(\text{DTPA})^{-2}$ may be toxic due to the release of ionic gadolinium within the central nervous system. The higher stability constant of $\text{Gd}(\text{DOTA})^{-2}$ would suggest that the long term toxicity of this complex would be lower than $\text{Gd}(\text{DTPA})^{-2}$; this would clearly indicate an

advantage for the use of $\text{Gd}(\text{DOTA})^{-2}$ over that of $\text{Gd}(\text{DTPA})^{-2}$.

As mentioned earlier, the development of new ligands which may prove to be superior to DTPA as a chelator of Gd^{+3} for MRI is an important area of study. In this thesis the synthesis of a new polyamino polycarboxylic acid, tris(2-aminoethyl)amine hexaacetic acid (TAHA), with the structural formula $\text{N}(\text{CH}_2\text{CH}_2\text{N}(\text{CH}_2\text{COOH})_2)_3$, was studied. This ligand has a total of ten coordination sites available for binding to Gd^{+3} and therefore the gadolinium complex of TAHA was expected to have an higher stability constant than the complex $\text{Gd}(\text{DTPA})^{-2}$.

Before a ligand can be considered as a potential contrast agent its solution chemistry must be well characterized. This thesis describes the behavior of this ligand in terms of the acid base chemistry and characterizes its interaction with a variety of metals. Chapter III describes the synthesis and general properties of TAHA as well as the calculation of the acid dissociation constants in H_2O and D_2O . Chapter IV is divided into two portions. The first part presents the results of potentiometric and ^1H NMR studies of the complexation of the metals mercury (Hg^{+2}), lanthanum (La^{+3}), and calcium (Ca^{+2}) with TAHA. The stability constants and equilibrium constants for the complexation reactions are presented and discussed. As will be made clear in this chapter, the interaction of the hexaprotic ligand TAHA (L) with the above metals is very complex. The ligand TAHA tends to form protonated metal ligand complexes (MH_nL) as well as polynuclear metal ligand complexes consisting of both bimetal complexes such as M_2L , and mixed metal complexes such as $\text{MM}'\text{L}$, where M and M' are two different metal ions. The possibility of the existence of hydroxyl complexes such as $\text{ML}(\text{OH})_n$ or $\text{MM}'\text{L}(\text{OH})_n$ is also considered. The stability constants of the metal complexes of Hg^{+2} , La^{+3} , and Ca^{+2} with TAHA will also be compared with the corresponding stability

constants of other polyamino polycarboxylic acids. In the second part of Chapter IV the results of potentiometric studies of the complexation of TAHA with the lanthanide series, and with the metals nickel (Ni^{+2}), cadmium (Cd^{+2}), zinc (Zn^{+2}), lead (Pb^{+2}), and strontium (Sr^{+2}), are discussed.

The last chapter is a summary and general discussion of the ligand TAHA.

II. EXPERIMENTAL

A. Chemicals

Tris(2-aminoethyl)amine (98%, $(\text{H}_2\text{NCH}_2\text{CH}_2)_3\text{N}$) and chloroacetic acid (ClCH_2COOH) were obtained from Aldrich Chemical Company. Lanthanum nitrate(III) hexahydrate (99.999%, $\text{La}(\text{NO}_3)_3 \cdot 6\text{H}_2\text{O}$), samarium(III) nitrate hexahydrate (99.9%, $\text{Sm}(\text{NO}_3)_3 \cdot 6\text{H}_2\text{O}$), praseodymium(III) nitrate hexahydrate (99.999% $\text{Pr}(\text{NO}_3)_3 \cdot 6\text{H}_2\text{O}$), neodymium(III) nitrate hexahydrate (99.95%, $\text{Nd}(\text{NO}_3)_3 \cdot 6\text{H}_2\text{O}$), europium(III) nitrate hexahydrate (99.999%, $\text{Eu}(\text{NO}_3)_3 \cdot 6\text{H}_2\text{O}$), gadolinium(III) nitrate pentahydrate (99.999%, $\text{Gd}(\text{NO}_3)_3 \cdot 5\text{H}_2\text{O}$), terbium(III) nitrate hexahydrate, (99.999%, $\text{Tb}(\text{NO}_3)_3 \cdot 6\text{H}_2\text{O}$), dysprosium(III) nitrate pentahydrate (99.99%, $\text{Dy}(\text{NO}_3)_3 \cdot 5\text{H}_2\text{O}$, holmium(III) nitrate pentahydrate (99.99%, $\text{Ho}(\text{NO}_3)_3 \cdot 5\text{H}_2\text{O}$), erbium(III) nitrate pentahydrate (99.9%, $\text{Er}(\text{NO}_3)_3 \cdot 5\text{H}_2\text{O}$), and ytterbium(III) nitrate pentahydrate (99.9%, $\text{Yb}(\text{NO}_3)_3 \cdot 5\text{H}_2\text{O}$) were obtained as gold labelled products from Aldrich Chemicals with the corresponding product analysis performed by inductively coupled plasma (ICP). These metal salts contained trace (ppm) level impurities which usually consisted of other lanthanides at concentrations varying from 0.0 ppm for lanthanum to 166.0 ppm for europium. They also contained trace levels of alkaline earth metals such as calcium and magnesium. Because of the low level of impurities present, these metal salts were used without further purification. Hexamine (hexamethylenetetramine), and diethylenetriaminepentaacetic acid (DTPA) were obtained from Sigma Chemicals. Disodium ethylenediaminetetraacetic acid (EDTA), Eriochrome Black T, xylene orange, zincon (2-carboxyl-2-hydroxy-5'-sulfoformazyl), lead nitrate ($\text{Pb}(\text{NO}_3)_2$), mercuric nitrate ($\text{Hg}(\text{NO}_3)_2 \cdot \text{H}_2\text{O}$), zinc metal (30 mesh), potassium nitrate (KNO_3), cadmium nitrate ($\text{Cd}(\text{NO}_3)_2 \cdot 6\text{H}_2\text{O}$), strontium nitrate ($\text{Sr}(\text{NO}_3)_2$), nickelous nitrate ($\text{Ni}(\text{NO}_3)_2 \cdot 6\text{H}_2\text{O}$), and t-butyl

alcohol, were obtained from Mallinkrodt.

Deuterium oxide (99.8% atom D), deuterium chloride (37 w/w%, 99% atom D) and potassium deuterioxide (40 w/w%, 98% D) were obtained from Aldrich Chemicals.

All other chemicals were obtained from Fisher Scientific and were used as received unless otherwise stated.

All water used for solution preparation was purified by passage of distilled water through a Milli Q Water Purification System (Millipore Corporation). The water purification procedure used by this system consisted of circulating the distilled water through an activated carbon column to remove organic molecules, deionization by passage through two ion exchange resins and a final filtration through a 0.22 μm pore size membrane filter. The final resistance was greater than 1.0×10^6 ohm cm. Prior to solution preparation, all freshly distilled deionized water was boiled for fifteen minutes and then cooled in a borosilicate glass bottle equipped with an outlet tube filled with 8-20 mesh Ascarite II (Arthur H. Thomas Company) to minimize exposure to carbon dioxide.

B. Solution Preparation

1. Preparation and Standardization of EDTA

A standard solution of EDTA was prepared using reagent grade $\text{EDTA} \cdot 2\text{H}_2\text{O}$ which had been previously dried overnight at 80 °C. A stock solution of approximately 0.015 M, stored in a borosilicate glass bottle, was prepared by dissolving the disodium salt of EDTA in water.

Standardization of the EDTA solution was performed by direct titration of a 0.1799 mM standard zinc solution buffered at pH 6.0 by the addition of 25 mL of a stock 20% hexamine buffer. The endpoint was determined using the metal

indicator xlenol orange (3,3'-bis-[N,N-di(carboxymethyl)aminomethyl]-o-cresol-sulphonephthalein), which at the endpoint undergoes a sharp color change from lemon-yellow to red. This method for the standardization of EDTA proved to be both rapid and reproducible, giving relative standard deviations between 2-5 ppt.

The standard zinc solutions were prepared as follows. Zinc metal was washed twice with dilute sulfuric acid to remove the presence of any surface oxide and rinsed with distilled deionized water until no trace of acid could be detected in the wash solution. The zinc metal was then washed twice with 99% ethanol, dried at room temperature and stored in a sealed, acid-washed bottle. An accurately weighed sample of the zinc metal was dissolved in a small volume of hydrochloric acid and neutralized to approximately pH 5.5 by KOH, before diluting to volume. The final stock solution of zinc was typically 0.03 M. Aliquots of the standard zinc solution were delivered from a calibrated 5 mL Fisher Brand pipet and titrated with EDTA for the standardization of the stock EDTA solution, which was then used for the standardization of other metal nitrate solutions.

For many of the experiments it was necessary to accurately know concentrations of the test solution. In such studies, where it was necessary to deliver accurate volumes of standard stock solutions, manually calibrated Fisher brand pipets (1, 2, 5, and 10 mL) were utilized. Calibration was performed in the usual manner by delivering water from the pipet into a vial, sealing and weighing the water delivered on a digital analytical balance (Fisher brand 100 AX). Calculation of the volumes delivered by each pipet was performed using the weight of water delivered and the density of water at ambient temperature.

2. Preparation and Standardization of Metal Solutions

Stock solutions, 0.02 M, of $\text{Cd}(\text{NO}_3)_2$, $\text{Ca}(\text{NO}_3)_2$, $\text{Sr}(\text{NO}_3)_2$, and $\text{Hg}(\text{NO}_3)_2$ were made up with KNO_3 to a final ionic strength of 0.1 M with reagent grade KNO_3 (Fisher Chemical Company). All of these solutions, except the calcium solution, were standardized by direct titration with EDTA using the appropriate buffer and metal indicator as described by Vogel (56). In some cases the solutions were also standardized by the addition of excess standardized EDTA and back titrating with the standard zinc solution.

When calcium is titrated with EDTA using Eriochrome Black T as the indicator, no sharp endpoint is obtained. In the presence of magnesium, there is a sharp color change from red to blue for the following reasons: the stability constant of $\text{Ca}(\text{EDTA})^{-2}$ is larger than the stability constant of $\text{Mg}(\text{EDTA})^{-2}$ by a factor of $1 \times 10^{2.27}$ (30), while the magnesium indicator complex (MgIn^-) is more stable than the calcium indicator complex (CaIn^-). Consequently, during EDTA titration of a solution containing magnesium and calcium ions, in the presence of Eriochrome Black T, EDTA first reacts with free calcium ions, then with free magnesium ions, and finally with the magnesium indicator complex. In the pH range between 7 and 11, the magnesium-indicator complex is red and the free indicator is blue. Thus, a sharp color transition from red to blue occurs:



For the direct EDTA titration of calcium, a $\text{Mg}(\text{EDTA})^{-2}$ complex was prepared by mixing equal volumes of 0.015 M EDTA and 0.015 M MgSO_4 . A few drops of the $\text{Mg}(\text{EDTA})^{-2}$ solution was added to the ammonia-ammonium chloride buffer at pH 10.0, which was then added to the stock calcium solution prior to the titration. The endpoint was determined when no reddish hue from the

Eriochrome Black T indicator was observed in the titration of calcium with standardized EDTA solution.

Although most of the rare earth salts were assumed to be pure as indicated by the analytical data obtained from Aldrich, several lanthanides ($\text{La}(\text{NO}_3)_3$, $\text{Pr}(\text{NO}_3)_3$, and $\text{Gd}(\text{NO}_3)_3$) were titrated to determine the per cent purity according to the method of Reilley (57) or the method of Lyle and Rahman (58). The method of Reilley involved the addition of excess EDTA to a solution of the metal, followed by back titration with a standardized zinc solution. A small amount of $\text{Hg}(\text{EDTA})^{-2}$ was added to the solution and the endpoint detected potentiometrically using a mercury indicating electrode as will be described in more detail later. The method of Lyle and Rahman involved direct titration of the lanthanide salts with EDTA using hexamine as the buffer (pH 5 to pH 6) and xylene orange as the metal indicator. Both these methods showed that the percent purity of the lanthanide salts was greater than 99.9%, which was in agreement with the ICP product analysis performed by Aldrich Laboratories; therefore all lanthanide salts were used without further purification.

All metal solutions were stored in acid clean borosilicate glass bottles, while the solid metal nitrates were stored in a desiccator after the percent purity had been determined.

3. Preparation and Standardization of KOH

Carbonate-free KOH was prepared by dissolving reagent grade KOH (Fisher Chemical Company) in freshly boiled water. The KOH was diluted to volume and passed through a column of Dowex 1-X8 20-50 mesh ion exchange resin (Baker Chemical Company) originally in the chloride form. Since the quaternary alkyl amine sites of this strongly basic anion exchange resin preferentially absorb carbonate ions over hydroxide ions, carbonate can be separated from the hydroxide ions. The Dowex resin was packed by gravity

in a column with the dimensions 64.0 x 1.0 cm. The packed column was washed once with dilute HCl and several times with the KOH solution. The KOH effluent was discarded until no chloride ions could be detected by precipitation upon the addition of a few drops of 0.1 M $\text{Ag}(\text{NO}_3)$. The final KOH solution was stored in either a sealed acid clean borosilicate glass bottle or polyethylene bottle, after bubbling for several minutes with carbon dioxide free nitrogen gas.

It was found that KOH that had been passed through the Dowex 1-X8 resin had a strong odor after being stored for two to three days, possibly from degradation of resin bi-products. The cause of the odor was determined to be due to the resin by observation that the odor was present after several days in a solution of resin immersed in very dilute (0.001 M and 0.0001 M) KOH. Standardization of KOH solution which had not been passed through the column, KOH solution which had just been passed through a regenerated column, and KOH which had been passed through the Dowex 1-X8 column and allowed to sit at room temperature until a distinct odor could be detected, indicated no statistically significant difference in the concentration of KOH. The relative standard deviations of the titrations were all within 1.0 ppt. However, because the cause of the odor could not be determined and it was uncertain whether possible degradation products would affect subsequent titrations, it was decided to use freshly prepared KOH passed through the Dowex 1-X8 column for all experiments requiring carbonate-free KOH. All KOH solutions were stored in acid clean borosilicate glass bottles with an outlet tubing containing CO_2 absorbant (Ascarite II).

The KOH was standardized by titration of reagent grade potassium hydrogen phthalate using phenolphthalein ($\text{pK}_{\text{In}} = 9.60$) as the acid-base indicator. Although KHP is not hygroscopic, it was dried at 110 °C to remove

trace adsorbed surface water, and then stored in a desiccator.

C. Instrumentation

1. pH Measurements

All pH measurements were made using a Fisher Accumet 520 digital pH meter. The performance of the pH meter was checked periodically using a mini test-pH electrode simulator (Fisher Scientific Company) which allowed for testing of the pH scale, temperature compensator, and the input impedance of the meter. The pH meter was equipped with a micro-combination glass electrode consisting of a glass body and a ceramic porous plug, which served as the liquid junction. A three-point calibration was performed using Fisher certified buffer solutions of pH 4.00 ± 0.01 (0.05 M potassium biphosphate buffer), pH 7.00 ± 0.01 (0.05 M potassium phosphate monobasic buffer), and pH 10.00 ± 0.02 (0.05 M potassium carbonate/potassium borate buffer). The pH 4.00 and pH 7.00 buffers were standardized and checked periodically with freshly prepared NBS standard solutions (59,60).

Measurements from which acid dissociation constants were calculated were performed in the following manner. The ligand to be titrated was dissolved and allowed to come to thermal equilibrium (approximately 2 hours at 25.00 ± 0.01 °C) in a double-walled flow cell connected to a water bath (Brinkman Model RMS 20). Carbonate-free KOH titrant was delivered using a Mettler DV11 autoburet. To prevent carbonate contamination, all connecting tubing was polyethylene (permeability to CO₂ approximately 1×10^{-9} mL-cm/sec² cm Hg) (61). The titrant was delivered through a 2 or 5 μ L Pederson curved micropipet; the tip remained in the solution throughout the duration of the titration. It was found that pH drift due to diffusion from the tip was negligible. All solutions were continuously bubbled with nitrogen gas during the course of the pH titration.

For potentiometric measurements in D₂O solutions, from which acid dissociation constants were calculated, a constant ionic strength of 0.1 M (KNO₃) was maintained, and the experimental method was identical to that described above except that the titrant was KOD that was standardized as described for the standardization of KOH and was prepared by dilution of 40% KOD with 99.8% D₂O.

Since an ionic strength of 0.1 M with KNO₃ was maintained for all solutions for which potentiometric data were collected, hydrogen ion activities were calculated using Equation [3]:

$$a_i = C_i \gamma_i \quad [3]$$

where C_i is the concentration, a_i is the activity, and γ_i is the activity coefficient of ion i . A value of $\gamma_H = 0.83$ was used for the activity coefficient of hydrogen at an ionic strength of 0.1 M KNO₃ (61).

pH meter readings for D₂O solutions were converted to pD values using the relationship defined in Equation [4]:

$$pD = pH_{\text{meter reading}} + 0.4 \quad [4]$$

This relationship assumes that two conditions are met. Firstly, that the glass electrode responds in a Nernstian fashion to changes in the deuterium ion activity in heavy water, in the same manner as the hydrogen ion activity in aqueous solutions. Secondly, that the deuterium ion activity must not alter the liquid-junction potential between the heavy water solutions and the aqueous electrode filling solution. Both these conditions have been shown to be met

(62). Hence, there is a constant difference between the operational pH, determined with a glass electrode in heavy water solutions, with reference to aqueous standards, and the assumed or expected pD. In this thesis, the uncorrected pH meter reading obtained in heavy water solutions will be denoted by pH*.

Several methods for calculating acid dissociation constants from potentiometric data were utilized; these methods will be fully described in the following chapter.

2. pHg Method

Formation constants of metal chelate complexes were determined by the pHg method (63-66). This method involves measurement of the potential with a J-tube mercury indicating electrode. A schematic diagram of the cell and the electrode is presented in Figure 1. pH measurements were made using a combination electrode as described earlier. Potential measurements were obtained with an Orion Research 611 pH-mV meter of which the potential output was periodically checked with a mini-test pH simulator that provides an accurately known potential between 0-1400 mV. These potentials were then compared with the potential output displayed by the pH meter. The J-tube mercury indicating electrode was constructed by the method of Holloway and Reilley (64). This electrode was designed to give a large mercury pool surface area in contact with the test solution, as well as to eliminate erratic potentials caused by seepage of the test solution to the platinum (Pt) wire, located in the bottom of the mercury cup. The Pt wire was completely encased in glass except at the points of contact with the mercury pool, and the mercury in the glass tube as shown in Figure 1. The dimensions of the mercury cup were 18 x 20 mm. An Ag-AgCl reference electrode equipped with a ground glass porous sleeve was used to prevent solution contamination, and to allow for a greater flow rate as

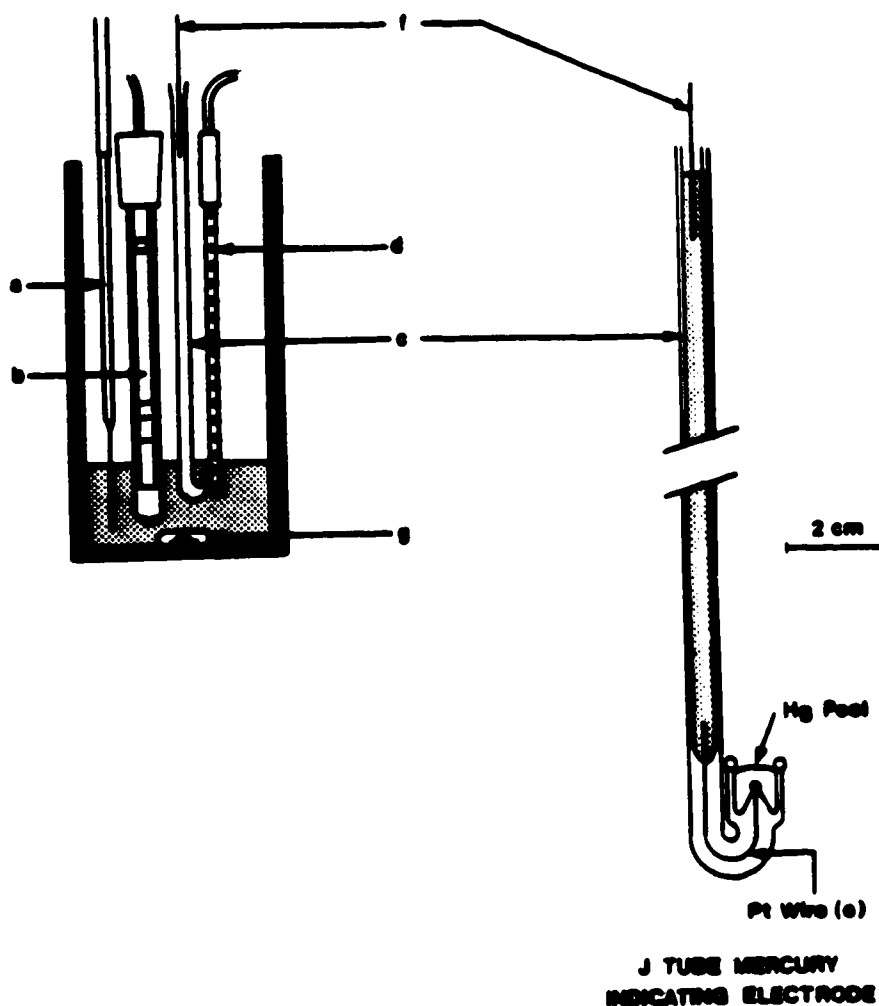


Figure 1. A schematic of the double walled cell utilized for the determination of metal ligand stability constants using the pHg Method. The cell has a maximum capacity of 45 cm³ and was thermostated at 25.00°C via connection to a water bath. The whole cell was tightly sealed except for a small hole to allow for N₂(g) to exit. The specific components are:

- | | |
|--|------------------------------|
| (a) inert N ₂ insert capillary | (b) reference electrode |
| (c) J tube mercury indicating electrode | (d) pH combination electrode |
| (e) platinum wire encased in glass capillary | (f) platinum wire contact |
| (g) magnetic stir bar | |

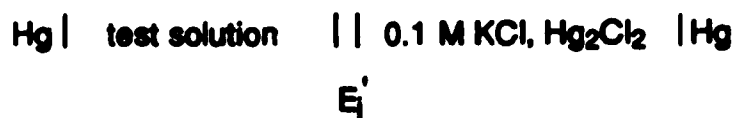
The mercury indicating electrode is expanded to scale to the right of the cell.

well as a larger contact area between the electrolyte solutions. When immersed in a solution of 0.1 M KNO_3 , a meter reading of 55 mV was obtained relative to a saturated calomel electrode (SCE). When this cell was used for the measurement of stability constants, potential equilibrium to within ± 1.0 mV was achieved within one minute.

The whole cell was thermostated at 25.00 ± 0.01 °C, sealed, and the solution continuously stirred while measurements were made. All solutions to be titrated were delivered using calibrated 1, 2, or 5 mL Fisher brand pipets. A final ionic strength of 0.1 M was maintained with KNO_3 .

Nitrogen gas was continuously bubbled through the solution to exclude oxygen that would otherwise limit the negative potential limit at the mercury electrode. Solutions were checked for the presence of chloride ions because the formation of insoluble mercurous halides reduces the positive potential limit of the mercury electrode. Surface coating on the mercury pool due to formation of metal oxides was generally not a problem. When surface oxide formation was observed, the experiment was repeated using lower concentrations of the metal ions.

When the pHg method is used to determine the stability constants of metal ligand complexes, the stability constant of the mercury-ligand complex (K_{HgL}) must first be determined. When the J tube mercury electrode is in contact with a solution of HgL and excess L, where L denotes the ligand, the cell may be represented in the following manner:



The potential of this cell is given by the following equation:

$$E = E_{\text{Hg}}^{\circ} + E_j' + \frac{RT}{2F} \ln [\text{Hg}^{+2}] \quad [5]$$

where E_{Hg}° is the standard potential of the reduction of Hg^{+2} to Hg° , and the potential of the reference electrode, E_j' is the liquid-junction potential between 0.1 M KNO_3 and 0.1 M KCl , which remains constant for a given set of experiments, R is the gas constant, T is the absolute temperature and F is defined as the faraday. Since E_j' is virtually constant between pH values 3 to 11, Equation [5] may be rewritten as

$$E = E_{\text{Hg}}^{\circ'} + \frac{RT}{2F} \ln [\text{Hg}^{+2}] \quad [6]$$

where $E_{\text{Hg}}^{\circ'}$ includes all the junction potentials involved and is a constant at any fixed ionic strength and temperature; $E_{\text{Hg}}^{\circ'}$ may be considered to be a formal reduction potential under the conditions used in this work ($\mu = 0.1$ M KNO_3 , 25.00 °C). When numerical values of RT at 25.00 °C and F are inserted into Equation [6] the following equation is obtained:

$$E = E_{\text{Hg}}^{\circ'} + 0.0296 \lg [\text{Hg}^{+2}] \quad [7]$$

The numerical value of $E_{\text{Hg}}^{\circ'}$ under these conditions may be evaluated by obtaining potential-pH diagrams of a well characterized mercury-ligand complex as will be detailed later in this chapter. As seen from Equation [7], the potential E is a linear function of the logarithm of the free mercury ion concentration in solution.

The formation constant for the mercury-ligand complex, HgL , is defined by Equations [8] and [9]:



$$K_{\text{HgL}} = \frac{[\text{HgL}]}{[\text{Hg}^{+2}] [\text{L}]} \quad [9]$$

In these and the following equations, the charge of the ligand, L , will be omitted for simplicity. It should be noted that if the ligand has a charge of $-m$, (L^{-m}), the mercury-ligand complex should be denoted as HgL^{-m+2} rather than HgL . The fraction of free ligand in the totally deprotonated form, α_{L} , at a particular pH, is given by Equation [10].

$$\alpha_{\text{L}} = \frac{[\text{L}]}{[\text{L}]'} = \frac{K_1 K_2 \dots K_n}{(\text{H}^+)^n + K_1 (\text{H}^+)^{n-1} + K_1 K_2 (\text{H}^+)^{n-2} \dots + K_1 K_2 \dots K_n} \quad [10]$$

where K_n are ligand acid dissociation constants, $[\text{L}]$ is the concentration of the ligand in its totally deprotonated form (i.e. $[\text{L}^{-m}]$), and $[\text{L}]'$ is the total concentration of the free ligand in solution. By combining Equations [9] and [10], the following equation is obtained:

$$[\text{Hg}^{+2}] = \frac{[\text{HgL}]}{[\text{L}]' \alpha_{\text{L}} K_{\text{HgL}}} \quad [11]$$

By substitution of Equation [11] into Equation [7], Equation [12] is obtained

$$E = E_{\text{Hg}}^{\circ'} + 0.0296 \log \frac{[\text{HgL}]}{[\text{L}]' \alpha_{\text{L}} K_{\text{HgL}}} \quad [12]$$

With the above equation, K_{HgL} may be determined experimentally by

measurement of the potential at the mercury electrode in a solution containing the free ligand and its mercury complex.

Once K_{HgL} is known, the stability constants of other metal-ligand complexes of L may be determined using this method. Hence the equilibria in a solution containing $HgL : ML : M$ at a ratio of 1.0:1.0:1.0 may be treated as a simple exchange reaction:



where M is either a bivalent or trivalent metal ion. The equilibrium constant, K_{eq} , for this reaction is defined as

$$K_{eq} = \frac{[Hg^{+2}][ML]}{[HgL][M]} \quad [14]$$

The stability constant, K_{ML} , is defined by the following equations



$$K_{ML} = \frac{[ML]}{[M][L]} \quad [16]$$

By combination of Equations [6] and [13], and then substitution into Equation [14], Equation [17] is obtained

$$K_{eq} = \frac{K_{ML}}{K_{HgL}} \quad [17]$$

Therefore the $[Hg^{+2}]$ can be defined by the combination and rearrangement of

Equations [9], [16], and [17] to give

$$[\text{Hg}^{+2}] = \frac{[\text{HgL}][\text{M}]\text{K}_{\text{ML}}}{[\text{ML}]\text{K}_{\text{HgL}}} \quad [18]$$

By substitution of Equation [18] into the Nernst Equation for the mercury electrode at 25 °C, Equation [7] becomes

$$E = E_{\text{Hg}}^{\circ} + 0.0296 \log \frac{[\text{HgL}][\text{M}]\text{K}_{\text{ML}}}{[\text{ML}]\text{K}_{\text{HgL}}} \quad [19]$$

From this equation, it is seen that the potential of the mercury electrode depends on the logarithm of K_{ML} of the particular metal complex involved, provided the concentration of the HgL , ML and M are kept constant. Once K_{HgL} is calculated using Equation [12] the value of K_{ML} may be calculated using Equation [19].

If the thermodynamic constant for HgL , (K_{HgL}), is much different from the conditional formation constant of HgL at the pH for which K_{ML} is calculated, $\text{K}_{\text{HgL}}^{\text{c}}$ may be used in Equation [19] where $\text{K}_{\text{HgL}}^{\text{c}}$ is the conditional formation constant measured under identical experimental conditions. The conditional formation constants are experimentally determined values and are useful because no assumptions are made in their calculation. Conditional formation constants are often used when protonation and complexation side reactions interfere with the formation of the HgL complex.

The values of $E_{\text{Hg}}^{\circ'}$ must remain constant throughout the pH titration. Since the term $E_{\text{Hg}}^{\circ'}$ contains several junction potentials, as shown by Equation [6], it was necessary to ensure that the $E_{\text{Hg}}^{\circ'}$ utilized for all calculations remained constant over a large pH range. The value of $E_{\text{Hg}}^{\circ'}$ under the experimental

conditions utilized in this work was determined in a "calibration" of the cell depicted in Figure 1 by obtaining potential-pH diagrams for well characterized complexes such as $\text{Hg}(\text{EDTA})^{-2}$ and $\text{Hg}(\text{DTPA})^{-3}$. Potential (mV) and pH measurements were made as a solution of $\text{Hg}(\text{EDTA})^{-2}$:EDTA in a ratio of 1:1 was titrated with carbonate free KOH from pH 2 to pH 11. Using the value of $K_{\text{Hg}(\text{EDTA})} = 10^{22.1}$ obtained by Holloway and Reilley (64), E_{Hg}° was treated as an unknown in Equation [12].

It was found that the E_{Hg}° thus calculated equaled 0.652 V, and remained constant over the pH range 2.0 to 9.6. The calculated E_{Hg}° deviated from this value at both lower and higher pH values, presumably due to the formation of protonated and hydroxyl HgL species, for which no correction was applied. A numerical value of 0.652 ± 0.001 V for E_{Hg}° was used for all pHg measurements.

A further check of this value was performed by the determination of stability constants for EDTA and DTPA complexes of mercury, gadolinium, cadmium, and strontium. The potential pH diagrams for metal complexes of EDTA and DTPA are presented in Figures 2 and 3 respectively. Curve A shows the experimentally determined potential as a function of pH for a solution that contains approximately equal amounts of the ligand and the corresponding mercury-ligand complex, from which K_{HgL} was calculated using Equation [12]. Calculation of K_{ML} was performed using the observed potential in the pH independent region of the potential pH curve for each ML complex using Equation [19]. Results for the calculation of K_{HgL} and K_{ML} for metal complexes of EDTA and DTPA are tabulated in Table 1, along with the corresponding literature values. The results in this table show that the logarithm of K_{ML} values determined by the pHg method are in good agreement with the literature values and it is therefore verified that E_{Hg}° (0.652 V) of the cell remained constant throughout the pH range of interest. The upper potential limit imposed on the

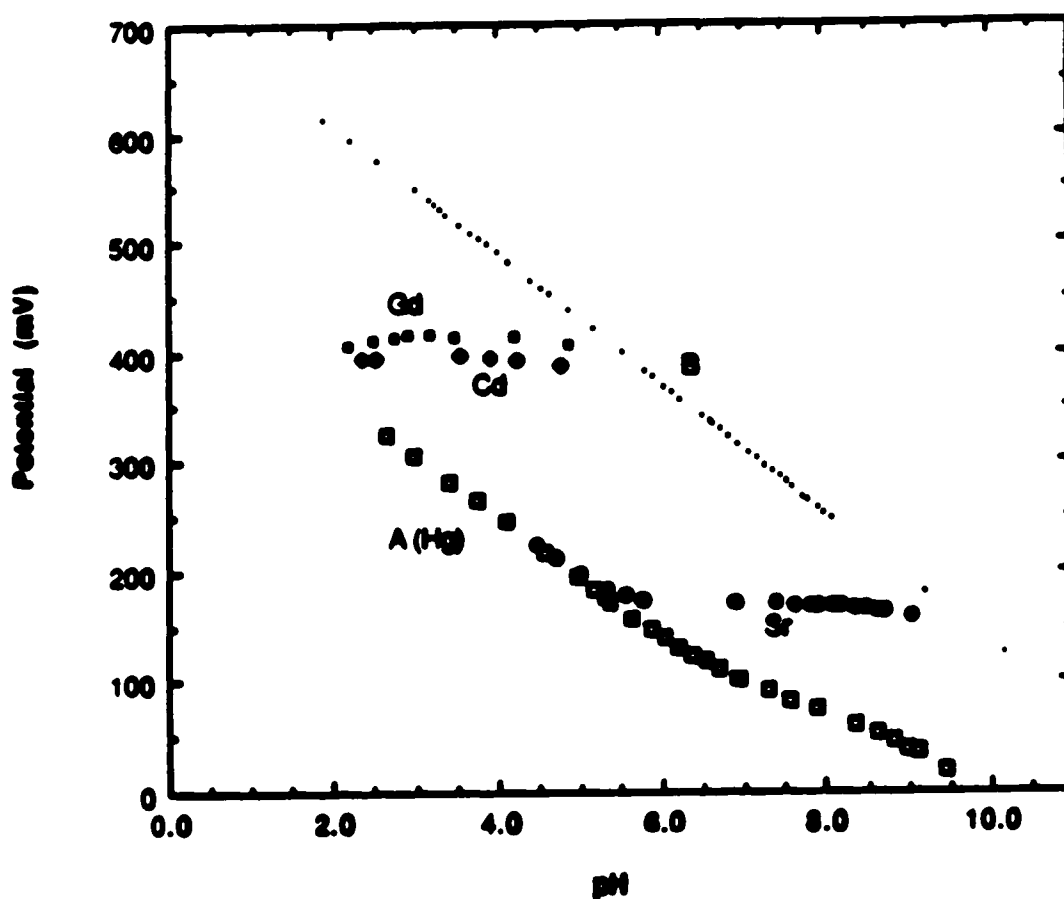


Figure 2. Potential-pH diagrams for the determination of metal EDTA complexes in a solution with an ionic strength of 0.1 M (KNO_3) at 25.00 °C. Curve A represents the potential-pH diagram of equal concentrations of EDTA and $\text{Hg}(\text{EDTA})^{2-}$; curve B represents the theoretical upper potential limit at the mercury electrode as described in text. The other curves represent the potential-pH diagrams of solutions in which the ratio of the $\text{Hg}(\text{EDTA})^{2-} : \text{M}(\text{EDTA})^{m-4} : \text{M}^{+m}$ is approximately equal. The exact concentrations of each species, and the calculated stability constants are given in Table 1.

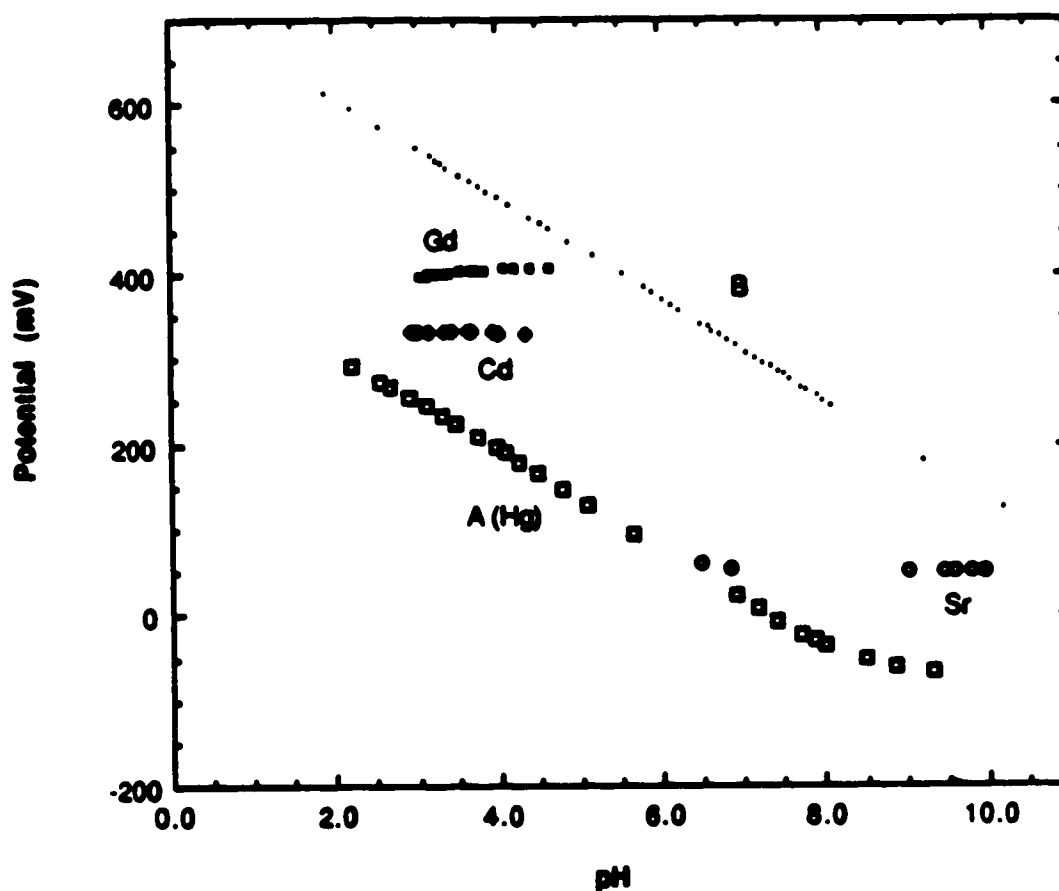


Figure 3. Potential-pH diagrams for the determination of metal DTPA complexes in a solution with an ionic strength of 0.1 M (KNO_3) at 25.00 °C. Curve B represents the potential-pH diagram of theoretical upper potential limit at the mercury electrode as described in text. The other curves represent the potential-pH diagrams of solutions of $\text{Hg}(\text{DTPA})\cdot 3:\text{M}(\text{DTPA})^m\cdot 5:\text{M}^{+m}$ in approximately equal concentrations. The exact concentration of each species, and the calculated stability constant, is given in Table 1.

mercury electrode system is due to the formation of mercuric oxide and can be calculated using the following equations obtained from Latimer (67).



$$K_{\text{HgO}} = [\text{Hg}^{+2}][\text{OH}^-]^2 = 10^{-25.5} \quad [21]$$

Solving for $[\text{Hg}^{+2}]$ in Equation [21] and substituting into Equation [7], results in Equation [22]:

$$E = E_{\text{Hg}}^{\circ'} + 0.0296 \log \left(\frac{K_{\text{HgO}}}{[\text{OH}^-]^2} \right) \quad [22]$$

Curve B in Figures 2 and 3 is the theoretical upper potential limit, as calculated using Equation [22].

An important requirement if the pHg method is to give correct values for K_{ML} , is that $K_{\text{ML}} < K_{\text{HgL}}$. Generally, this is not a problem since HgL complexes are usually of higher stability than most ML complexes. Schmid and Reilley (65) have reported that when the ratio $K_{\text{ML}}/K_{\text{HgL}} \geq 10^{-4}$, the mercury electrode itself is oxidized by the mercuric ions (Hg^{+2}) to form mercurous ions (Hg_2^{+2}). It would therefore be necessary to include the following formal equilibrium constant at 25 °C and $\mu = 0.1\text{M}$:

$$\frac{[\text{Hg}_2^{+2}]}{[\text{Hg}^{+2}]} = 85 \pm 2 \quad [23]$$

For all potentiometric experiments involving the J tube mercury indicating electrode, in the present work, such corrections were not necessary.

Table 1. Calculated stability constants for metal complexes of EDTA and DTPA at constant ionic strength and temperature ($\mu = 0.1 \text{ M KNO}_3$, 25.00°C).

metal	concentration (mM)		ligand	log K_{ML}	
	HgL	L		observed	reported
Hg ⁺²	1.18	1.18	DTPA	21.10 ± 0.2	21.50 ^a
Hg ⁺²	1.14	1.28	EDTA	27.10 ± 0.2	27.00 ^b

metal	concentration (mM)			ligand	log K_{ML}	
	HgL	ML	L		observed	reported
Cd ⁺²	1.18	1.18	1.31	DTPA	19.11 ± 0.02	19.0 ^a
	1.14	1.28	1.21	EDTA	16.26 ± 0.03	16.35 ^a , 16.4 ^b
Sr ⁺²	1.18	1.19	1.33	DTPA	9.62 ± 0.006	9.68 ^a
	1.14	1.28	1.25	EDTA	8.68 ± 0.02	8.68 ^a , 8.70 ^b
Gd ⁺²	1.18	1.18	1.00	DTPA	21.45 ± 0.1	22.26 ^a
	1.14	1.28	1.21	EDTA	16.97 ± 0.03	17.35 ^a

^a Reference 30

^b Reference 64

3. ^1H NMR Measurements

All ^1H NMR experiments were performed on Varian XL 400 or VXR 500 spectrometers operating in the pulse fourier transform mode. Data processing and analysis were performed using a Sun 3/160 Work Station equipped with Varian software. All ^1H NMR chemical shifts were measured relative to the methyl resonance of t-butanol which was added to the solution at concentrations of approximately 0.1 to 1 mM, depending on the concentration of the species present in the sample, and are reported relative to the methyl resonance of sodium-2,2-dimethyl-2-silapentane-5-sulfonate (DSS). The methyl resonance of t-butanol is 1.2365 ppm downfield from that of DSS.

For all ^1H NMR spectra, the deuterium resonance from D_2O provided an internal lock to correct for small fluctuations in the magnetic field. All NMR spectra, except those measured in the metal binding studies, were collected with a spectral width of 4000 or 5000 Hz and 16K data points. For metal binding studies, the spectral width was decreased in order to observe the region of interest with a high digital resolution (spectral width of 3196 Hz which gave a digital resolution of 0.344 Hz per point). Unless otherwise stated, spectra were zero filled to 32K and the free induction decay was multiplied by an exponentially decaying function to enhance the sensitivity; typically a line broadening of 0.2 to 0.3 Hz was used. Usually 50 transients were coadded, except when quantitative information was to be obtained from resonance intensities, in which case 150-200 transients were coadded.

Most NMR measurements were made at a probe temperature of 25 °C. In cases where the temperature was changed, the probe temperature was determined from the chemical shift separation of the hydroxyl (OH) and methylene (CH_2) resonances of ethylene glycol. The temperature calibration calculation was performed using the Van Geet equation(68,69), modified for a

500 MHz instrument:

$$T (K) = 466.5 - 0.203 \Delta\nu \quad [24]$$

where $\Delta\nu$ is the chemical shift difference between the OH and CH₂ resonances of ethylene glycol. A temperature calibration curve calculated using the above equation is presented in Figure 4. After adjustment to a given temperature, the sample was allowed to come to thermal equilibrium (approximately 20 minutes) before collection of the free induction decay. The sample temperature was maintained by flowing air around the sample tube while the probe temperature was sensed by a thermocouple. For temperatures above ambient, the air, normally at room temperature, was first heated to the desired temperature by heating elements before circulating around the sample. For temperatures below ambient, the air was first cooled by circulation in an ice water bath; the cooled air was then heated to the desired temperature by the heating elements before it was circulated around the sample tube.

The 90° pulse width was periodically determined by locating the pulse width at which a null point occurs, which is considered as the 180° pulse width. The 90° pulse width was then taken to be half the 180° pulse width. In typical ¹H NMR experiments, pulse widths between 60° and 90° were used.

Most ¹H NMR spectra were measured using the single pulse experiment (Figure 5A). In some experiments it was necessary to decrease the intensity of the resonance at 4.77 ppm due to the water protons. This was accomplished by the "Jump and Return Experiment" (70,71) depicted in Figure 5B. In this pulse sequence, the carrier is placed on the water resonance. A 90°_x pulse flips all the magnetization to the +y axis. During the delay period, τ , the magnetization of interest precesses in the xy plane while the solvent magnetization remains

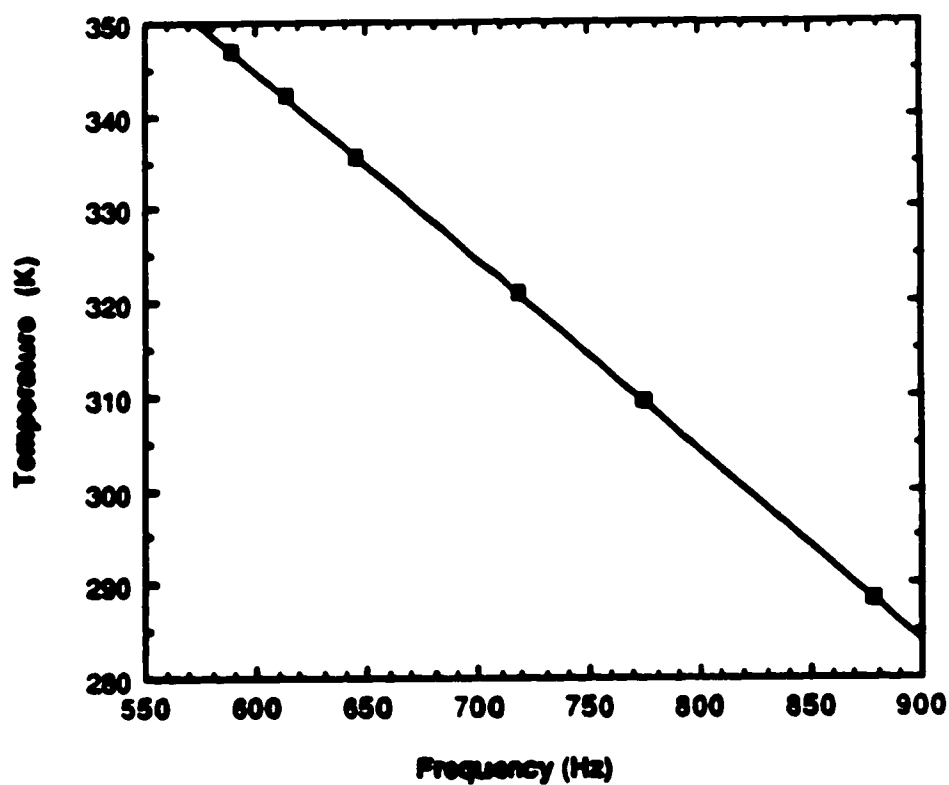


Figure 4. The temperature calibration curve for the Varian XL 500 spectrometer obtained using Equation [24]. The open symbols are the experimental data points, while the straight line represents the best fit line obtained by linear regression analysis.

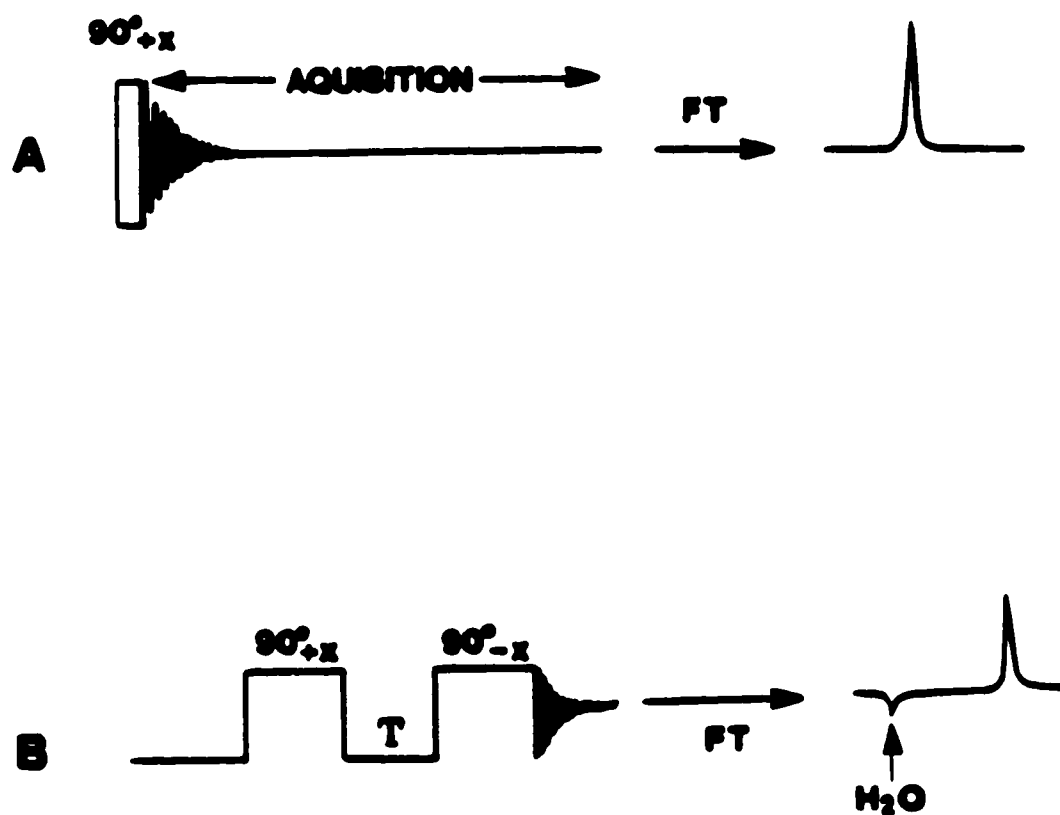


Figure 5. A. Pulse sequence for the single pulse experiment. B. Pulse sequence for the Jump and Return experiment.

stationary relative to the carrier. The delay time, τ , is equal to $1/4\Delta$, where Δ is the chemical shift difference between the water resonance and the resonance of interest (in Hz). Therefore, at the end of the delay period, the magnetization of interest will be on the x axis. The second 90° pulse is phase-shifted by 180° and brings the water resonance back to the +z axis, while the resonance of interest remains on the x axis, where it is detected. This method reduced the intensity of the water signal sufficiently, when compared to the single pulse experiment, so that observation of the resonances of interest was possible.

D. Computing Methods

1. NMR Curve Fitting

Under ideal conditions, the NMR signal gives rise to a Lorentzian lineshape where the width at the half-height is given by the following equation:

$$W_{1/2} = \frac{1}{\pi T_2} \quad [25]$$

where T_2 is the spin-spin relaxation time.

In a sample which consists of similar components with similar chemical shifts, a spectrum consisting of several overlapped Lorentzian peaks is observed, i.e. a "smearing out" of the peaks occurs. In NMR spectroscopy, deconvolution is the process where the observed overlapped spectrum is reduced to the individual Lorentzian components.

The Varian software includes a deconvolution curve-fitting program, similar to the original DECOMP (72-74) program utilized for resolving intensity and frequency assignments from unresolved multiplet patterns. In all metal binding studies performed using ^1H NMR, the Varian curve-fitting software was

utilized to obtain a calculated spectrum from the original overlapped spectrum. This program attempts to produce a final result which is as close as possible to the uncorrupted signal.

Computer memory allowed for a maximum of 2048 data points to be curve fitted at one time. Therefore, poorer digital resolution (0.780 Hz per point) was necessary when large regions were deconvolved. Better digital resolution (0.195 Hz per point) was possible when smaller regions were deconvolved, as was the case for the lanthanum and calcium ligand binding studies. For successful deconvolution into n components, the program required that there be $2n$ inflection points. When two peaks are extremely overlapped, and four inflection points can not be detected, the deconvolution program assumes that only one peak exists and will iterate on that basis, resulting in erroneous results.

For all curve-fitting, an exponential line broadening of 0.3 to 0.5 Hz was applied. Manual phasing and baseline corrections were performed on the region to be fitted, to prevent large errors due to the automatic linear baseline correction applied by the Varian deconvolution program.

Input parameters required by the deconvolution program were the frequencies of the lines, line intensities (maxima), linewidth at half-height ($W_{1/2}$) and the shape of the signal. In all deconvolutions, it was assumed that the shape of all signals was totally Lorentzian (i.e. no Gaussian component was present). From these input parameters, the program calculated initial area estimates that were necessary for the iterative procedure. Curve fitting was generally accomplished in 20 to 45 iterations which translated into 10 to 15 minutes of computer time. In cases where large tailing from broad peaks was present, increasing the region to be curve fitted (with the corresponding decrease in digital resolution) had no effect on the final results. It was found that, for broad peaks, good initial estimates for the input parameters were not

necessary to obtain reproducible final results.

The final output from the deconvolution consisted of the individual frequency, intensity, integral (performed by Simpson's Rule) and linewidth of each resonance present in the original spectrum.

Goodness-of-fit was determined by calculation of a chi square (χ^2) value. This calculation involves the assumption that the standard deviation of each data point is equal. The iteration involves minimizing χ^2 so that the probability of the calculated χ^2 for a given deconvoluted spectrum is less than the given degrees of freedom. The probability, or its complement, can be found in a general statistical textbook, or calculated, as outlined in Press *et al.* (72). For the present studies, probability values were not calculated; the calculations attempted only to minimize χ^2 .

2. Non-Linear Least Squares Calculations

Non-linear least squares calculations were done using a version of the nonlinear least squares program, KINET (75), modified for use on an IBM-PC running Fortran 77 (Version 3.13). With this program, the user must determine a model to which experimental data is to be fitted. This model is input as an Equation (EQN) in the subroutine within the main program. The program requires as input parameters the number of constants (maximum of 16), the number of data points (maximum of 99), the number of unknowns (maximum of 20) and the number of variables (maximum of 3 independent variables and one dependent variable), which are placed in a data file called KINDAT3 that arranges the data in a form suitable for KINET. KINET fits the data by varying the estimates of the unknown parameters to minimize the sum of the squares of the deviations of the experimental data from calculated values. Two methods may be used for the optimization of the unknown parameters. The first uses the matrix method described by Wentworth (76,77), modified to include an iteration

step as described by Pitha and Jones (78). This method converges rapidly and gives estimates for each unknown parameter together with a linear estimate of the standard deviation for the parameter which indicates the quality of fit. When more than one parameter is adjusted, a multicorrelation matrix is a part of the output. This matrix provides an indication of how closely the various parameters depend on each other, i.e. how closely two variables are "coupled". The second method uses the procedure of Powell (79) which uses a quadratically convergent algorithm to converge to estimates of each parameter. This is a directional set method to arrive at a global minimum as described by Press et al. (72).

Both these methods require good estimates of the unknown parameters. In order to ensure that the program has converged to a global (i.e. true) minimum rather than a local minimum, the initial estimates must be varied. If the program has converged to a global minimum, changes in the initial estimate will not alter the final results, (although the number of iterations will be larger, and if more than one parameter is being determined, divergence may occur).

KINET was used in an attempt to calculate acid dissociation constants from pH versus chemical shift data for the titration of the ligand with carbonate-free KOH.

3. Other Calculations

All other calculations were performed using Symphony (Version 1.1, released 1985). This program allows calculation and graphing using a spreadsheet format. All linear regression calculations were performed with Lotus 123 which allowed for the calculation of the theoretical best fit line using the spreadsheet. Less complicated equations were calculated using a Texas Instruments EL programmable calculator.

III. SYNTHESIS AND CHARACTERIZATION OF TRIS (2-AMINOETHYL) AMINE HEXAACETIC ACID (TAHA)

A. Synthesis, Purification and General Properties of Ligand

The polyaminopolycarboxylate ligand tris(2-aminoethyl)amine hexaacetic acid (TAHA) was synthesized by the method used by Moore (80) and Schwarzenbach and Ackermann (81) to synthesize EDTA. The following equation demonstrates the overall reaction (see Figure 6):



TAHA was synthesized by mixing 0.0668 moles of tris(2-aminoethyl)amine, commonly referred to as tren (10 ml, $\rho = 0.977 \text{ g cm}^{-3}$) in solution with 0.635 moles (approximately 60 grams) of chloroacetic acid dissolved in 50 ml water with low heating. Both solutions were cooled on ice before mixing. The pH was adjusted to 10 with KOH using the mixed indicator thymolphthalein/phenolphthalein which has a sharp color change from colorless to blue at pH 9.9. The mixture was slowly heated to a final temperature of 80-90 °C. The pH and temperature of the reaction mixture were maintained until no appreciable change in color was observed.

The reaction was monitored by ^1H NMR by removing aliquots from the reaction mixture, cooling and adjusting the pH between 3.0 to 4.5. Adjustment of pH was necessary since the tren and TAHA resonances had significant overlap in the ^1H NMR spectrum at pH 10, but in acidic solutions the resonances arising from the reactants were separated significantly from resonances due to the final product, TAHA. Using ^1H NMR it was determined

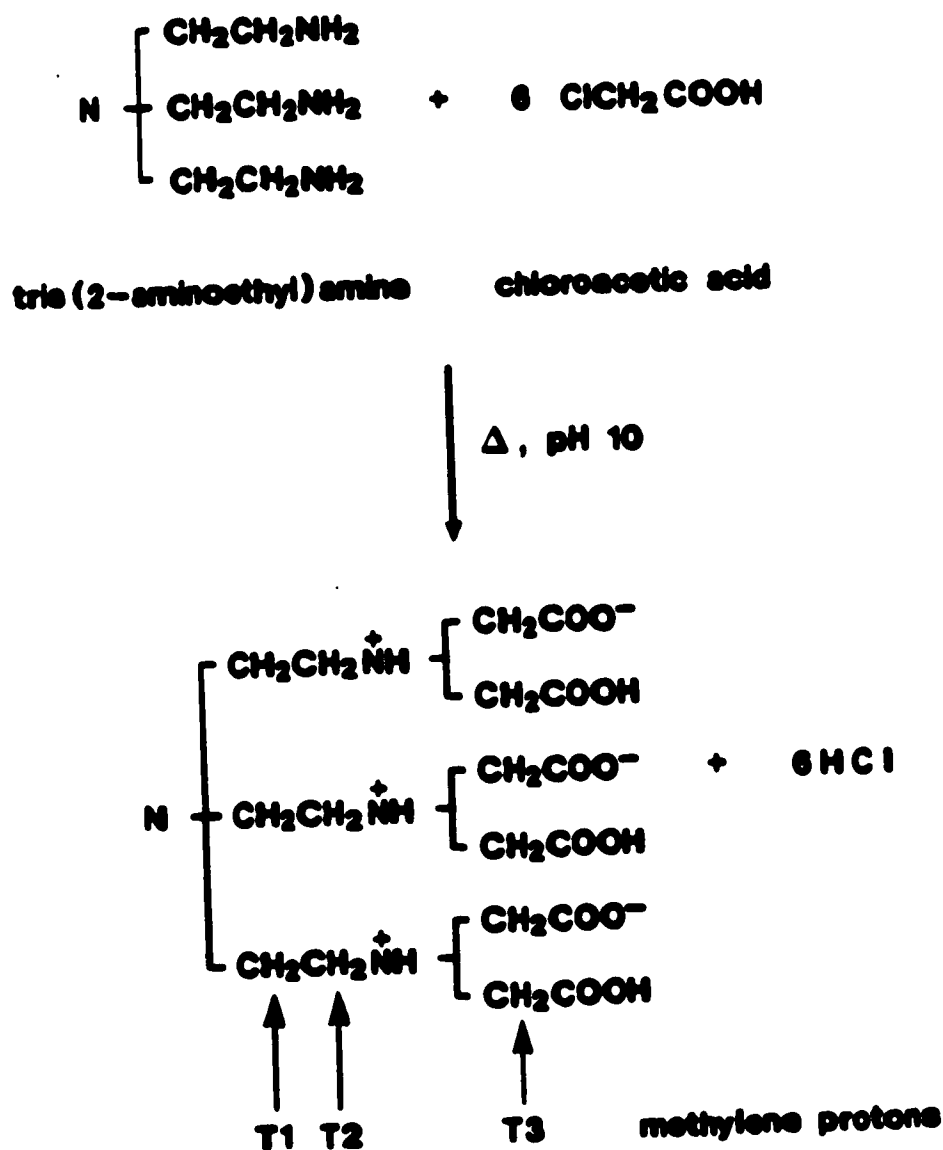


Figure 6. Equation, including structures, depicting the synthesis of the ligand TAHA from tris (2-aminoethyl)amine and chloroacetic acid using the method of Moore (80). The methylene protons, T1, T2, and T3 are labelled.

that the reaction proceeded very rapidly at elevated temperatures with many side reactions and intermediate by-products. It was therefore necessary to add more dissolved chloroacetic acid (approximately 25%) while maintaining the temperature and pH until the reaction was completed. The final ^1H NMR spectrum at this point indicated that less than 2% of the amine remained unreacted. The final solution, which was between 150-200 mL, was allowed to cool overnight at 4 °C; the precipitate, which consisted of KCl and reaction biproducts, was discarded. The mixture was then reduced in volume by approximately 30% by rotary evaporation at 35 °C until solid crystals started to appear. The mixture was then cooled and the precipitate, which consisted of mostly KCl, was discarded. This procedure was repeated three to four times. To insure that the product was not being discarded, ^1H NMR spectra was obtained for both the filtrate and precipitate at each stage of the above procedure. When the volume had been decreased to 50-75 mL, the pH was adjusted to between 2.0 to 2.3 and the solution was left for several days at 4 °C. After this time the product, TAHA, precipitated out of the reaction mixture as a fine white powder; at this time yield was approximately 70%.

Recrystallization and purification of the neutral ligand was performed in the following manner. The white powder was filtered and dissolved in a small volume of water while heating to a final temperature no greater than 35 °C. The solution was then slowly cooled to 4 °C, and allowed to sit overnight. It was sometimes necessary to add a few drops of ethanol to ensure nucleation. After gravity filtration, the filtrate was discarded and the solid was dried at room temperature. Because the final product was very insoluble in water, it was further purified to obtain a homogeneous sample by washing it twice with cold water, filtering, and discarding the filtrate. The final product, TAHA, was filtered by vacuum using a Buchner funnel, washed two times with ether, and dried at

70 °C for 24 hours. The ligand was then stored in a vacuum desiccator.

A solution of the neutral acid, TAHA, gave a negative test for chloride upon the addition of a few drops of 0.1 M AgNO₃, and a negative test for potassium with the addition of a few drops of HClO₄. Microanalysis of the ligand yielded the following results: C, 43.50%; H, 6.10%; N, 11.21%; the theoretical composition for the nonhydrated ligand (C₁₈H₃₀O₁₂N₄) is: C, 43.70%, H, 6.12%; N, 11.34%. The purity was also determined by ¹H NMR as follows. Disodium EDTA was purified as described by Vogel (56). Both EDTA and TAHA were dried overnight and a standard solution of EDTA and TAHA at pH* 3.0 was prepared. The purity of the TAHA was calculated to be 99 % from the relative areas of the EDTA and TAHA resonances. Figure 7 shows the spectrum obtained for the solution of EDTA and TAHA, along with the integrals. The two singlets labeled 'E' are due to the methylene protons of the acetate and ethylenic groups of EDTA.

In Figure 6, the assignment of the T1, T2 and T3 methylene protons, as well as the N1 and N2 nitrogen atoms, is presented. This identification will be referred to throughout this thesis; their assignment will be discussed in Section C of this chapter. The ratio of the T1:T2:T3 resonances was determined from the integrals in Figure 7 to be 0.99:1.00:2.01; the theoretical ratio being 1.0:1.0:2.0.

The infrared spectrum for an aqueous solution of TAHA, presented in Appendix 2, showed the typical N-C vibration at 1130 cm⁻¹ as well as the symmetrical and asymmetrical stretches of the COO group. There was also a band at 1140 cm⁻¹ which is characteristic of a C-N vibration when there is a "free" end or central nitrogen. This type of behavior is typical in alpha-aminopoly-carboxylic acids (82).

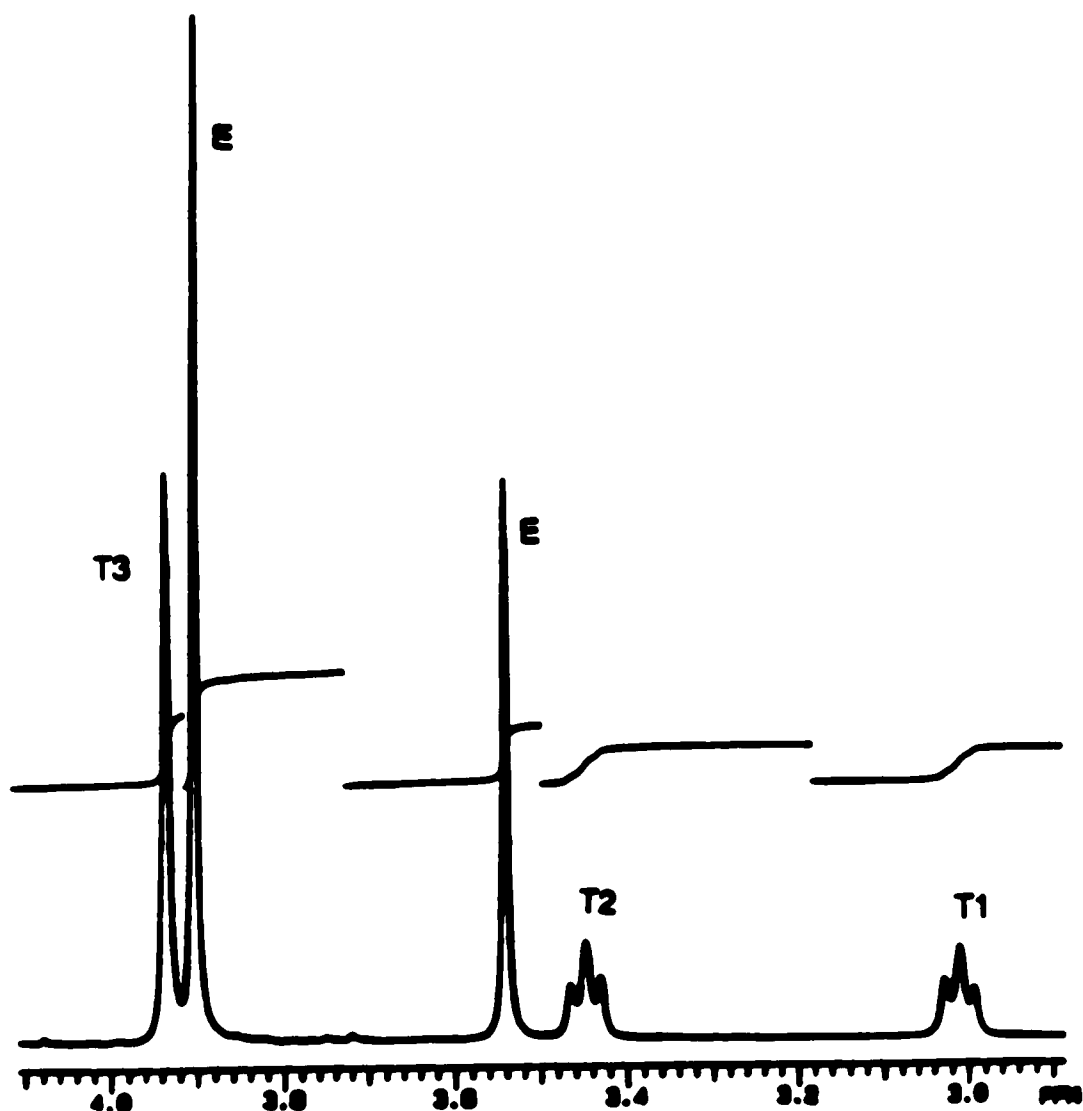


Figure 7. ¹H NMR spectrum of solution of EDTA and TAHA at pH* 3.0. The two singlets labelled 'E' are due to the methylene protons of the acetate and ethylene groups of EDTA, while the methylene resonances of TAHA are labelled as T1, T2, and T3, as assigned in Figure 6. The relative integrals of each resonance are presented above each resonance.

Mass spectra (EI. 180 and 240 °C) obtained for TAHA, presented in Appendix 3, indicated that the ligand fragments very easily; information thus obtained from mass spectra data proved to be less useful for characterization of the ligand.

The melting point was determined with an Ullmelt capillary melting point apparatus (Arthur H. Thomas Company). TAHA started to melt at 148°C and decomposed to a yellow powder, probably an amine derivative, at 189 °C. The melting point of Na₂H₂EDTA was also determined, to check the accuracy of the melting point apparatus. It was found that EDTA had a melting point of 250 °C which is identical to the melting point provided by Aldrich Chemical Laboratories.

Neutral TAHA was found to be insoluble in most organic solvents (methanol, ethanol, acetone, chloroform, hexane, dioxane, acetic anhydride, and isopropanol). Its solubility in water was measured using the method of Blaeder and Knight (83). A saturated solution was continuously stirred for two weeks at 25 °C. The saturated solution was then allowed to settle, and 5 mL aliquots of the clear supernatant were titrated with standardized KOH. The solubility of the neutral acid in H₂O was determined to be 3.073 ± 0.002 mM, while its solubility in 0.11 M KNO₃ was determined to be 3.349 ± 0.009 mM.

Aqueous solutions containing TAHA and several pH indicators were titrated while monitoring the pH with a pH meter, to identify an indicator which gave a sharp endpoint color change for use in the determination of the concentration of TAHA in a simple and rapid manner for subsequent experiments. Of the indicators tested it was found that the water soluble methyl red indicator ($pK_{IN} = 5.0$), which changes from red to peach to yellow between pH 4.2 to 6.3, was best suited for this purpose.

All the above results are summarized in Table 2.

Table 2. Summary of general properties of the ligand TAHA

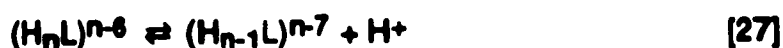
=====	
Property	Description
<hr/>	
Free Acid	H ₆ L
Appearance	fine, white powder
Molecular formula	C ₁₈ H ₃₀ N ₄ O ₁₂
Molar mass (non-hydrated)	494.22 g mol ⁻¹
Melting point	148 °C
Decomposition temperature	189 °C
Solubility,	
organic solvents	negligible
aqueous solution	3.073 ± 0.002 mM
aqueous solution (μ = 0.11 M KNO ₃)	3.347 ± 0.009 mM
Infrared spectrum (see Appendix 2)	all COO ⁻ stretches observed
(aqueous solution)	1130 cm ⁻¹ N-C vibration
	1140 cm ⁻¹ free end nitrogen
Mass spectrum (see Appendix 3)	fragments very easily
(EI. 240 °C)	
<hr/>	

B. Calculation of Acid Dissociation Constants

1. Introduction

This section deals with the determination of the acid dissociation constants for TAHA. Because the objective of this thesis research was to study the complexation of several divalent and trivalent metals ions by TAHA, it was necessary to know its acid dissociation constants so that the formation constant of its metal complexes could be determined.

The acid dissociation constants for TAHA are defined as follows:



$$K_n = \frac{[H^+][H_{n-1}L]^{n-7}}{[(H_nL)^{n-6}]} \quad [28]$$

where K_n is the acid dissociation constant and L is the ligand TAHA. Since TAHA is a hexaprotic acid $n_{\max} = 6$ for the neutral ligand.

Potentiometric titrations of the ligand with carbonate-free KOH in H_2O and D_2O are presented in Figures 8A and 8B. The sharp inflection at A equals 3, where A is defined as moles of base added per mole of the ligand, TAHA, corresponds to the titration of three of the six possible acidic protons; specifically three carboxylic acid groups are titrated. Between A values of 3 and 6 the three amino groups are titrated. There is also a smaller but distinct inflection point when A equals 5. This inflection is slightly steeper and more distinct in D_2O than in H_2O when the ionic strength is maintained constant at 0.1 M with KNO_3 .

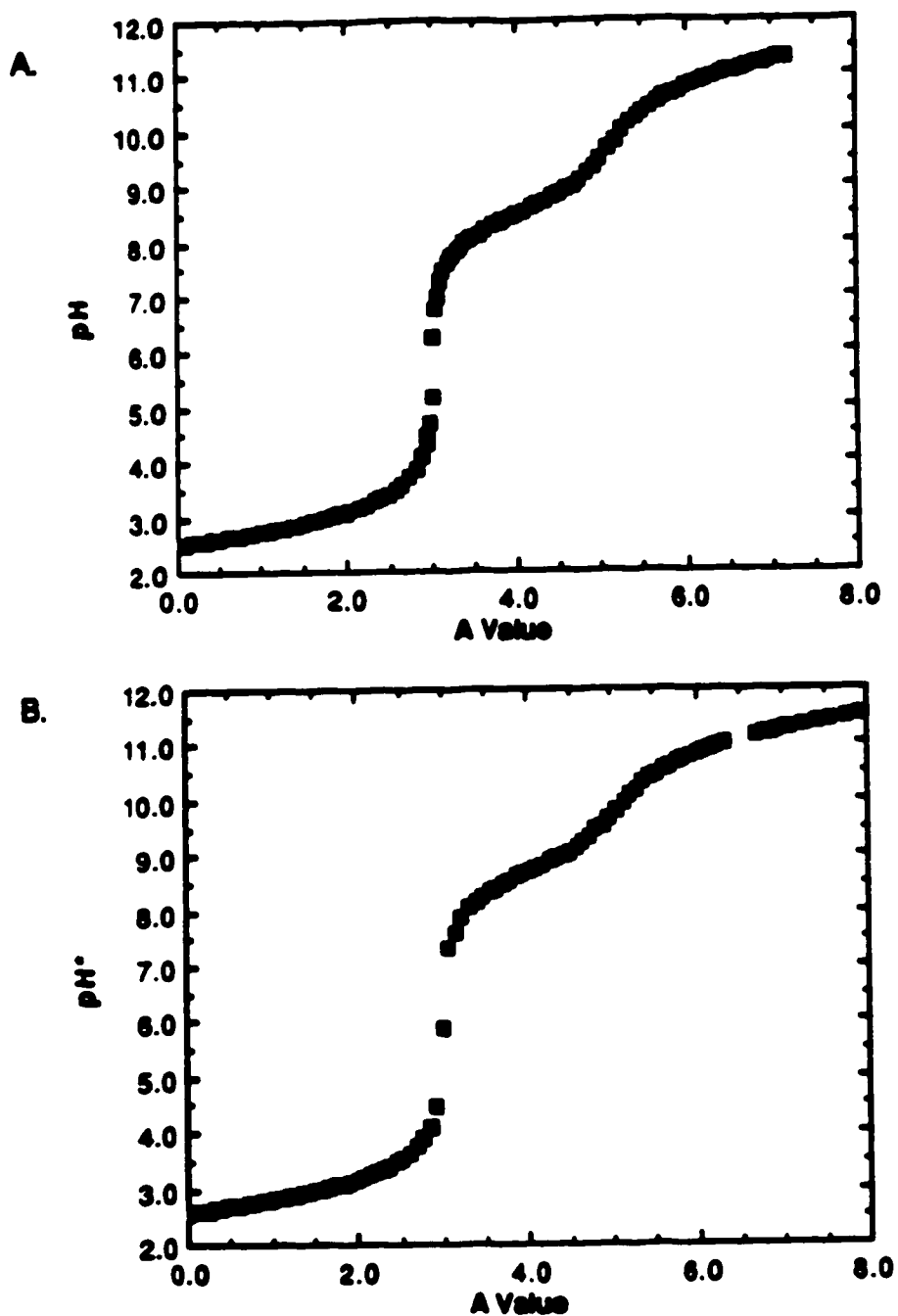


Figure 8. Potentiometric (pH) titration of TAHA as a function of the A value, where A is defined as moles of base added per mole of TAHA present. Both titrations were performed at constant ionic strength and temperature ($\mu=0.01$ KNO₃ and 25.00 °C). A. Titration performed in H₂O. B. Titration performed in D₂O.

Calculation of the six acid dissociation constants for the hexaprotic acid, H_6L , was greatly simplified by treating the potentiometric data in Figures 8A and 8B in terms of two separate triprotic acids. Treatment of the data in this manner, using electroneutrality and mass balance equations with the computer program KINET (a sample subroutine for the program is presented in Appendix 1), was attempted. Two methods were utilized in writing the appropriate subroutine equation for KINET. The first, which is often utilized for well behaved polyprotic acid, treats the volume of titrant, KOH, as a specified independent variable; a value of $[H^+]$ is then calculated using initial or refined estimates of the K_n values, and iteration is continued until convergence is attained. The second method involves letting $[H^+]$ serve as the independent variable and then calculating the volume of titrant which must be added to an analyte solution of a given concentration of H_3A to reach the experimental $[H^+]$ value. This method is often utilized for the calculation of ill-behaved polyprotic acids (84). Both methods failed to converge when implemented with the non-linear least squares curve fitting program KINET. This may be due to two of the three dissociation constants being strongly coupled to each other. Because this method was unsuccessful in the calculation of the dissociation constants for TAHA, three different graphical methods were used for the determination of the six acid dissociation constants as described below.

The following terms and definitions will be used for the derivations presented below:

- A = moles of base added per mole of ligand present
- C = initial concentration of the ligand
- H = concentration of hydrogen ion
- H_nL = concentration of protonated species of the ligand, where n varies from 0 to 3 for a triprotic acid

K_n = acid dissociation constant of the ligand where K_n is defined by Equation [28]

OH = concentration of hydroxyl ions calculated using the equation: $K_w = [OH^-][H^+]$
(where K_w is the dissociation constant of water).

In all of the the following derivations, charges have been omitted for simplicity.

2. Method 1

The first determination involves using the method of Wanninen (85), which has previously been used for determination of the acid dissociation constants of the pentaprotic acid DTPA by Ryskiewicz (86). With this method, K_2 and K_3 were determined by a graphical solution while K_1 was determined by an algebraic solution using the following equations:

$$C = H_3L + H_2L + HL + L \quad [29]$$

where C is the total concentration of the ligand TAHA. Using mass balance relationships, the following equations may be derived (where K^+ is the potassium ion concentration):

$$K^+ - OH + H = H_2L + 2HL + 3L \quad [30]$$

By definition K^+ equals AC , hence Equation [30] may be written as

$$AC - OH + H = H_2L + 2HL + 3L \quad [31]$$

Due to the low concentration of OH present at A values less than 3, Equation [31] may be rewritten as

$$AC + H = H_2L + 2HL + 3L \quad [32]$$

Substituting for H_2L from Equation [29] into Equation [32], one obtains:

$$AC + H - C = -H_3L + HL + 2L \quad [33]$$

Rewriting the right-hand side of Equation [33] in terms of the acid dissociation constants and $[H_2L]$, the following equation is obtained:

$$AC + H - C = -\frac{H}{K_1} H_2L + \frac{K_2}{H} H_2L + \frac{2K_2K_3}{H^2} H_2L \quad [34]$$

The $[H_2L]$ term is eliminated using equations similar to Equation [30] which consider the moles of base added at each given A value of a titration. In terms of AC, and H, Equation [34] may be rearranged to give:

$$AC + H - C = -\frac{H}{K_1} (AC + H) + \frac{K_2}{H} (2C - AC - H) + \frac{K_2K_3}{H^2} (3C - AC - H) \quad [35]$$

Equation [35] describes the relationship between the three acid dissociation constants K_1 , K_2 , and K_3 , in terms of AC, and the proton concentration. At A values greater than 1.0, the contribution of the H_3L term in Equations [33] and [34] may be neglected since after this value the first proton is completely titrated and so the concentration of the H_3L species is sufficiently low. The calculation

of K_2 and K_3 is performed by a graphical method that involves a quasilinearization procedure (8, 27) and the definition of the following terms:

$$x = \left(\frac{AC + H - C}{3C - AC - H} \right) [H]^2$$

and

$$y = \left(\frac{AC + H - C}{3C - AC - H} \right) [H]$$

For simplicity, Equation [35] may be rewritten (for experimental data points for which the A value is greater than 1) as :

$$K_2 = K_2 K_3 \frac{x}{y} + y \quad [36]$$

A plot of x versus y as identified above will give a parabolic plot such as that presented in Figure 9. The calculated x and y values at each given A value (for one experiment) are tabulated in Table 3 for reference. Each set of experimental data (x_1, y_1) is plotted individually as a straight line; for a number of experimental data points, there is a common point of intersection (x_0, y_0), defined as "P", which represents the solution of simultaneous equations. Figure 10 illustrates this type of plot for the (x, y) values tabulated in Table 3. In this plot, the x - y values were plotted for which the A values were greater than 1.5, where the contribution of the H_3L term is insignificant. In Figure 10, the abscissa at point P is equal to $K_2 K_3$ while the ordinate is equal to K_2 . For this set of experimental data K_3 is equal to 3.10×10^{-3} and K_2 is equal to 1.31×10^{-3} . After the graphical determination of K_2 and K_3 , K_1 is calculated algebraically using the K_2 and K_3 values and Equation [35]. At A values less than unity,

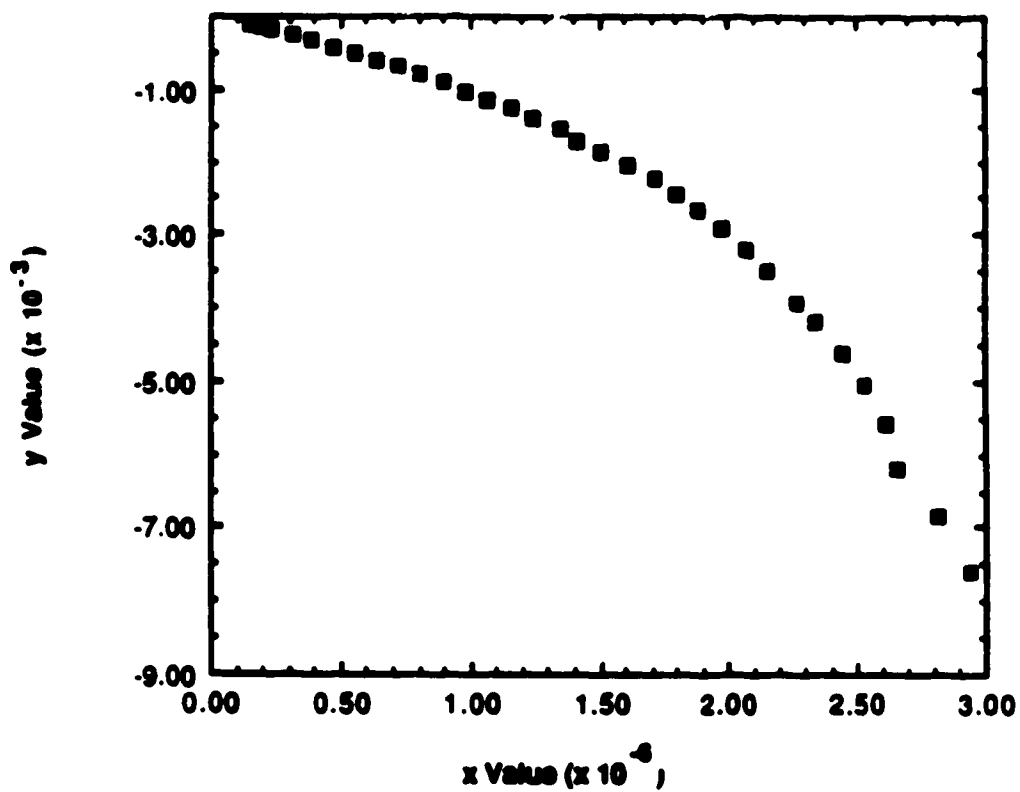


Figure 9. A x-y plot of (x,y) values that are tabulated in Table 3. The resultant curve is parabolic.

Table 3. Calculated x and y values for the determination of K_2 and K_3 using Method 1

A value	x value ($\times 10^{-6}$)	- y value ($\times 10^{-3}$)
1.613	3.05	8.52
1.737	2.66	6.18
1.819	2.53	5.04
1.902	2.34	4.18
2.026	2.07	3.20
2.109	1.88	2.68
2.233	1.61	2.06
2.316	1.41	1.71
2.440	1.16	1.27
2.522	9.87	1.03
2.605	8.09	8.02
2.688	6.40	6.03
2.812	3.91	3.41
2.915	1.93	1.51

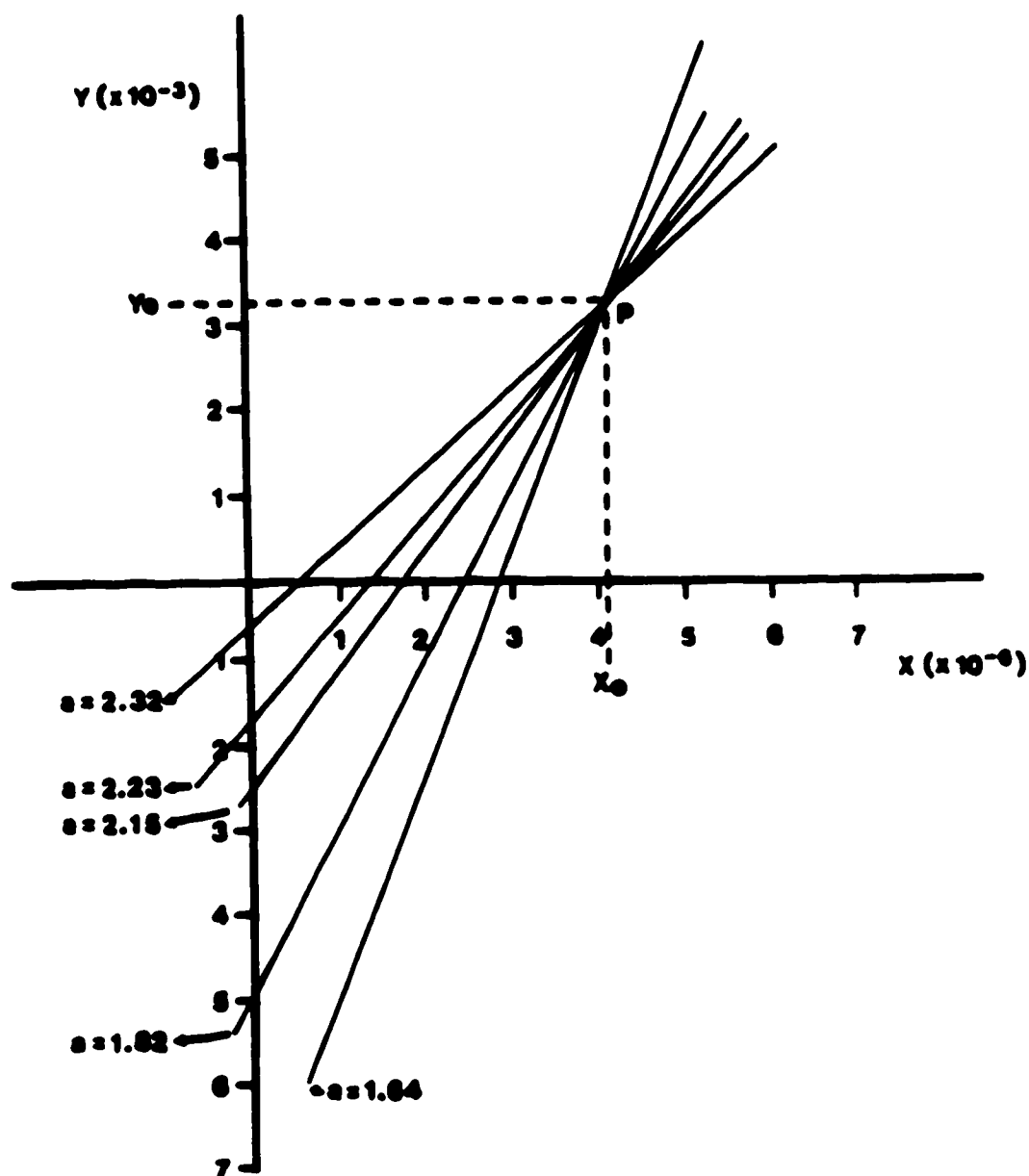


Figure 10. Illustration of the graphical solution for the determination of K_2 and K_3 using the values presented in Table 3. The common point of intersection, (X_0, Y_0) , is identified as P ; at this point the abscissa is equal to $K_2 K_3$, while the ordinate is equal to K_2 . Further details are presented in text.

where the contribution of H_3L is significant, a value of 0.0149 for K_1 was calculated for K_1 .

In a similar manner, the acid dissociation constants K_4 , K_5 , and K_6 were determined using potentiometric data at A values greater than 3. For the calculation of K_4 and K_5 , it was assumed that K_6 may be ignored because, as observed from Figure 8, it is sufficiently removed from the acid dissociation constants K_4 and K_5 which are overlapped. Between A values of 3 to 5 the final equation yields:

$$K_4 \{H (4-A) C + OH\} + K_4 K_5 \{(5-A) C + OH\} = H^2 \{(A-3) C - OH\} \quad [37]$$

The calculation of K_4 and K_5 was performed as before where the following x and y terms are defined:

$$x = H^2 \frac{AC - 3C - OH}{5C - AC + OH}$$

and

$$y = H \frac{AC - 3C - OH}{4C - AC - OH}$$

Using the above defined x and y values, Equation [37] may be rewritten as

$$y = K_4 + \frac{y}{x} K_4 K_5 \quad [38]$$

Using the data over the A range of 3 to 4.5, the common point of intersection, P, occurs at a point where the abscissa is equal to $K_4 K_5$, while the ordinate is equal to K_4 . The numerical values for x and y, as defined above, are tabulated

in Table 4; the plot for the graphical determination of K_4 and K_5 is shown in Figure 11. For this set of experimental data, K_4K_5 was equal to 1.45×10^{-17} while K_4 was equal to 5.77×10^{-9} ; the calculated K_5 is 2.51×10^{-8} . The last acid dissociation constant, K_6 was calculated using the complete equation which incorporates K_6 into equation [37], where A varies between 3 to 6 with the above predetermined values of K_4 and K_5 . A constant of 2.04×10^{-11} was obtained for K_6 . All six pK_n values obtained from Method 1 are summarized in Table 5.

3. Method 2

The second method used to determine the acid dissociation constants is that of Schwarzenbach (81,87). The derivation of the equations used in this method is identical to those used in Method 1. However, this method considers only the region between A values of 0 to 2 for the graphical determination of K_1 and K_2 , which are considered to occur simultaneously; K_3 is then determined algebraically from the predetermined values of K_1 and K_2 . The calculation of K_4 and K_5 , is also similar to Method 1. K_6 is significantly separated from K_5 , as seen by the inflection point where A equals 5 in Figures 8A and 8B, so that it may be considered individually using the following equation:

$$K_6 = \frac{AC - 5C + H - OH}{6C - AC - H + OH} (H) \quad [39]$$

Using the method of Schwarzenbach, the six pK_n values were determined to be 1.85, 2.49, 2.92, 8.11, 8.72, and 10.30 respectively. These are all tabulated in Table 5.

Table 4. Calculated x and y values for the determination of K_4 and K_5 using Method 1

A value	- x value ($\times 10^{-16}$)	- y value ($\times 10^{-8}$)
3.101	784.00	11.7
3.225	59.20	4.45
3.308	23.10	3.10
3.432	7.73	1.99
3.515	4.47	1.59
3.639	2.11	1.15
3.722	1.45	9.81
3.846	0.712	0.715
3.928	0.604	0.664
4.011	0.432	0.570
4.135	0.276	0.464
4.218	0.191	0.390
4.300	0.142	0.339
4.425	0.0861	0.267
4.507	0.0612	0.227
4.631	0.0356	0.175
4.714	0.0226	0.140
4.838	0.0105	0.0957
4.921	0.00611	0.0734
5.003	0.00304	0.0520
5.127	0.000907	0.0285
5.210	0.000438	0.0199
5.334	0.000161	0.0121

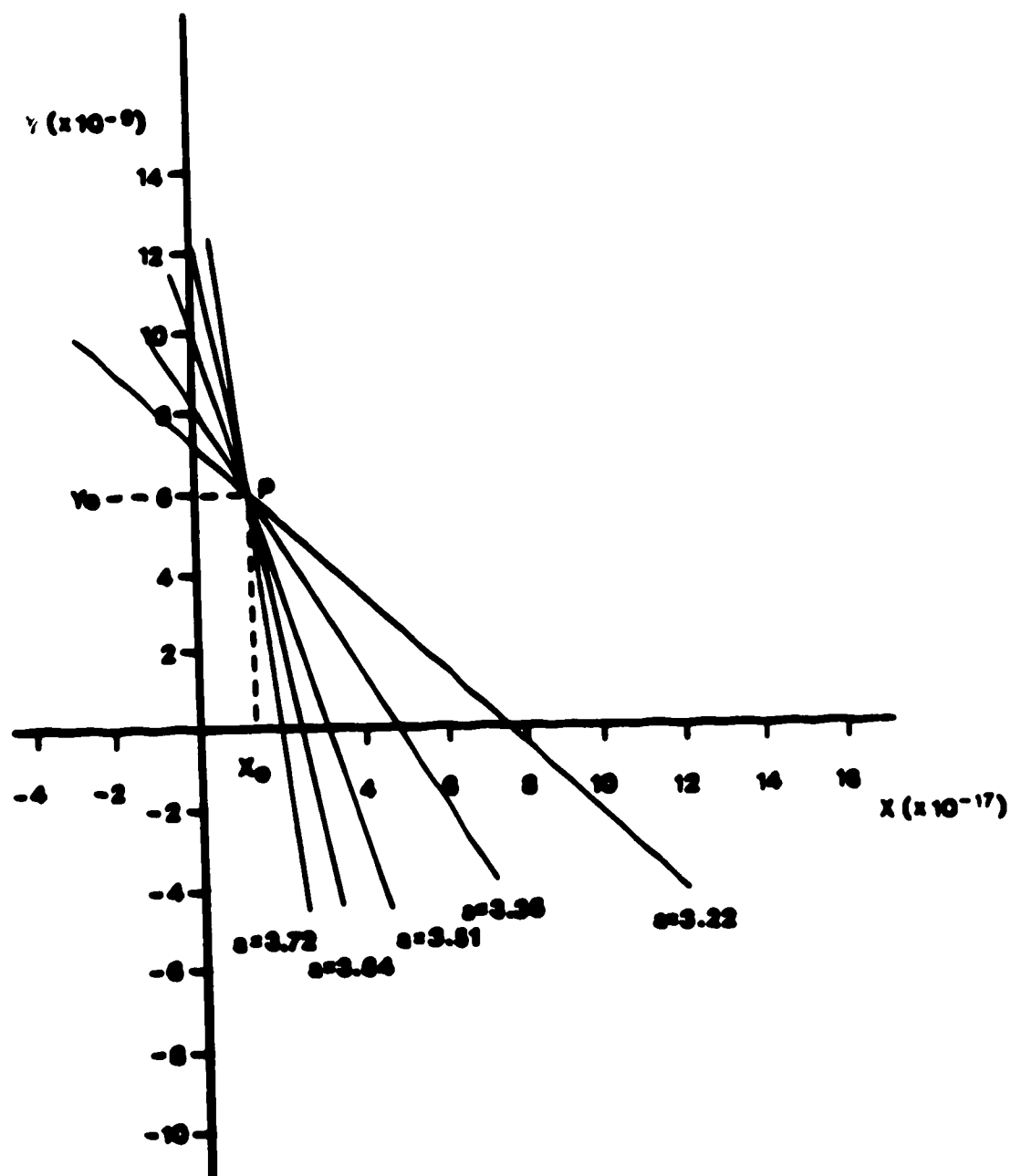


Figure 11. Illustration of the graphical solution for the determination of K_4 and K_5 . The common point of intersection, (X_0, Y_0) , is identified as P; at this point the abscissa is equal to $K_4 K_5$, while the ordinate is equal to K_4 . Further details are presented in text.

Table 5. Comparison of the six acid dissociation constants of TAHA obtained from the three different methods.

Method	pK ₁	pK ₂	pK ₃	pK ₄	pK ₅	pK ₆
1 (Wanninen)	1.826	2.508	2.884	8.138	8.760	10.690
2 (Schwarzenbach)	1.851	2.490	2.923	8.110	8.720	10.300
3 (Bjerrum)	1.861	2.482	2.883	8.11 ¹	8.81 ¹	10.31 ¹

¹ pK₄, pK₅, and pK₆ were estimated as described in the text.

4. Method 3

This method is that of Bjerrum (88-90) in which the acid-base chemistry of a ligand is treated in terms of successive association constants for the stepwise protonation reactions. The ligand TAHA will again be treated as two triprotic acids. For the derivation of the equations for a triprotic acid, H_3L , the following terms need to be defined:

A = central ligand

H = ion bound to central ligand; in this case the hydrogen ion

C_T = total ligand concentration

C_H = total concentration of free and bound protons

Bjerrum introduced the concept of the degree of formation \bar{n} , which is defined as the average number of hydrogen ions, bound to the central ligand:

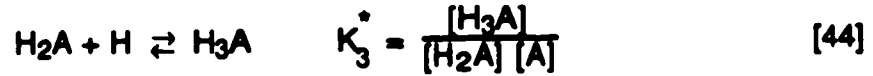
$$\bar{n} = \frac{\text{concentration of bound hydrogen ions}}{\text{concentration of ligand}} \quad [40]$$

From the potentiometric data, \bar{n} was calculated using Equation [41]:

$$\bar{n} = \frac{C_H - [H]}{C_T} \quad [41]$$

To relate \bar{n} to the acid dissociation constants, the following equations were derived.





$$K_1^* = \frac{1}{K_1}, \quad K_2^* = \frac{1}{K_2}, \quad K_3^* = \frac{1}{K_3} \quad [45]-[47]$$

where K_1^* , K_2^* , K_3^* are the acid association constants and K_1 , K_2 , and K_3 are the acid dissociation constants for the triprotic acid H_3A .

By definition, \bar{n} is equal to the following:

$$\bar{n} = \frac{C_{\text{H}} - \text{H}}{C_{\text{T}}} = \frac{\text{HA} + 2\text{H}_2\text{A} + 3\text{H}_3\text{A}}{\text{H}_3\text{A} + \text{H}_2\text{A} + \text{HA} + \text{A}} \quad [48]$$

By combining Equations [42] to [44] and removing common terms, Equation [49] is obtained:

$$\bar{n} = \frac{K_1^* [\text{H}] + 2K_1^*K_2^* [\text{H}]^2 + 3K_1^*K_2^*K_3^* [\text{H}]^3}{1 + K_1^* [\text{H}] + K_1^*K_2^* [\text{H}]^2 + K_1^*K_2^*K_3^* [\text{H}]^3} \quad [49]$$

Rearrangement of this equation yields

$$\bar{n} = (1 - \bar{n}) K_1^* [\text{H}] + (2 - \bar{n}) K_1^*K_2^* [\text{H}]^2 + (3 - \bar{n}) K_1^*K_2^*K_3^* [\text{H}]^3 \quad [50]$$

For A values greater than 1, the following approximation is valid:

$$\bar{n} = (1 - \bar{n}) K_1^* [H] + (2 - \bar{n}) K_1^* K_2^* [H]^2 \quad [51]$$

Equation [51] may be rearranged to give an equation for a straight line:

$$\frac{\bar{n}}{(1 - \bar{n}) [H]} = \frac{(2 - \bar{n}) [H] K_1^* K_2^*}{(1 - \bar{n})} + K_1^* \quad [52]$$

This equation is in the form of $y = x K_1^* K_2^* + K_1^*$ where

$$y = \frac{\bar{n}}{(1 - \bar{n}) [H]}$$

and

$$x = \frac{(2 - \bar{n}) [H]}{(1 - \bar{n})}$$

A plot of x versus y (Figure 12) yields a straight line with the y intercept equal to K_1^* and the slope equal to $K_1^* K_2^*$. Once K_1^* and K_2^* are calculated, the value of K_3^* can be calculated using Equation [50]. The slope and y intercept obtained using the data in Figure 8 were 2.402×10^5 and 773.98 respectively. The acid dissociation constants, pK_1 , pK_2 , and pK_3 were then calculated using Equations [45] to [47]; the results obtained were 1.86, 2.48 and 2.88 respectively, which are given in Table 5.

The formation curve (\bar{n} vs pH) for the dissociation of the carboxylate groups (A equals 0 to 3) is plotted in Figure 13. Table 6 is the tabulation of \bar{n} , A

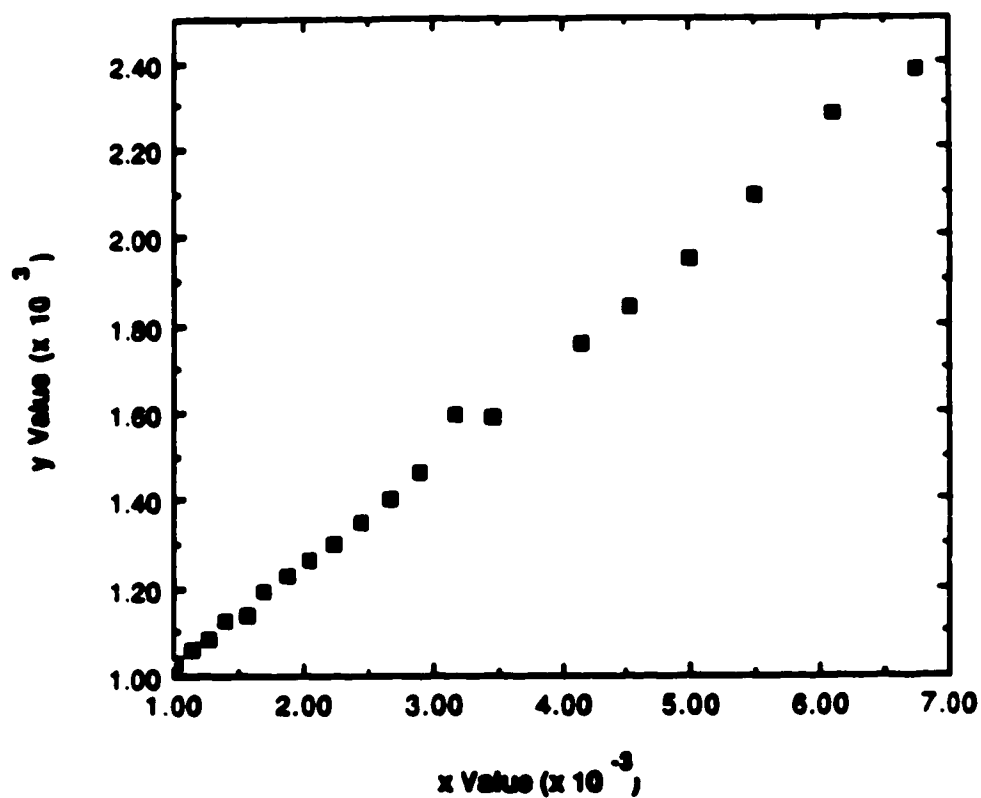


Figure 12. Straight line plot for the determination of the stepwise association constants K_1^* and K_2^* using the method of Bjerrum. The x value is equal to $(2 - \bar{n}) [H] / (1 - \bar{n})$ and the y value is equal to $\bar{n} / [H] (1 - \bar{n})$.

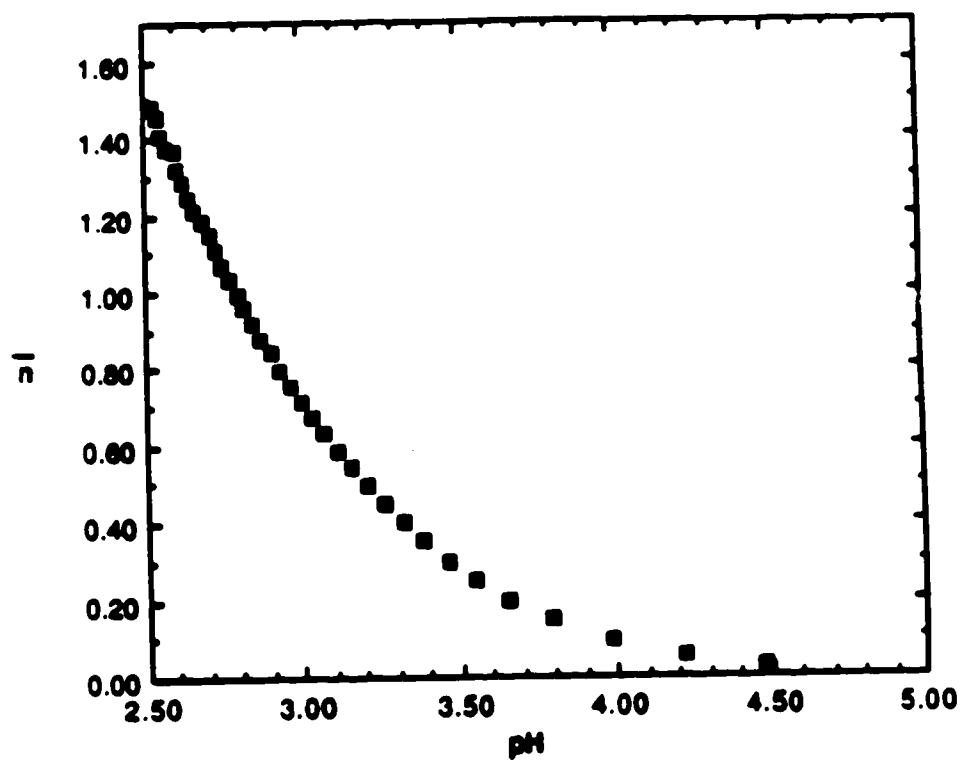
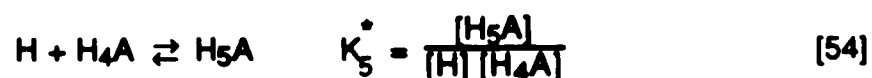
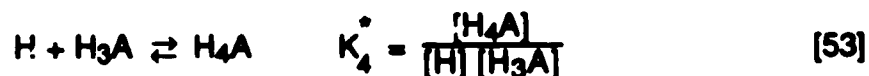


Figure 13. Formation curve, \bar{n} versus pH, for the dissociation of the carboxylate groups of TAHA; in this case the A value range is between 0 to 3 for a triprotic acid.

Table 6. Tabulation of experimentally determined \bar{n} values, along with the A values and pH's, for the determination of the first three acid dissociation constants using the method of Bjerrum.

A value	\bar{n}	pH
0.4135	1.481	2.53
0.8270	1.463	2.53
0.2068	1.407	2.55
0.4135	1.335	2.60
0.6203	1.245	2.64
0.8270	1.175	2.70
1.034	1.070	2.75
1.241	0.972	2.80
1.406	0.879	2.84
1.613	0.795	2.93
1.819	0.695	3.01
2.026	0.586	3.11
2.192	0.494	3.20
2.440	0.352	3.38
2.605	0.252	3.55
2.812	0.121	3.88
2.977	0.013	4.71

value, and pH, for this data. Figure 14 is the formation curve in which the ligand was considered as the hexaprotic acid H_6L . In the region where A is greater than 3 (at pH greater than 6), where there are three association constants, K_4^* , K_5^* , and K_6^* , the graph exhibits two distinct breaks. The first break corresponds to association of the fourth and fifth protons with the central ligand, which do not differ greatly in the magnitude of their association constants. The last break in Figure 14 corresponds to association of the last proton. In this region (where A is greater than 3), the first three acid association constants may be ignored. Calculation of the last three association constants uses the following equations:



The degree of formation, \bar{n} , as previously defined, is given by Equation [56]:

$$\bar{n} = \frac{H_4A + 2H_5A + 3H_6A}{H_3A + H_4A + H_5A + H_6A} \quad [56]$$

Corresponding acid dissociation constants K_4 , K_5 and K_6 are then calculated from the following equations:

$$K_4^* = \frac{1}{K_4}, \quad K_5^* = \frac{1}{K_5}, \quad K_6^* = \frac{1}{K_6} \quad [57]-[59]$$

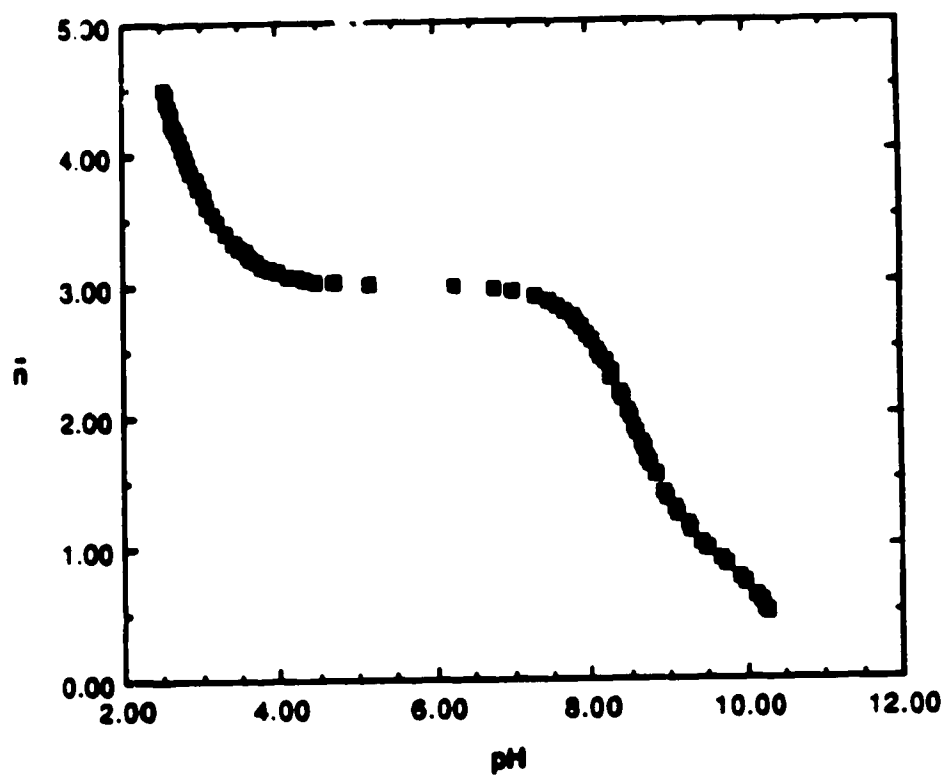


Figure 14. Formation curve, \bar{n} versus pH, in which TAHA is considered as an hexaprotic acid.

From the formation curve (Figure 14) initial estimates of K_4^* , K_5^* and K_6^* may be made by interpolation of half \bar{n} values. The equations involved in such a procedure are as follows: when $[H_4A] = [H_3A]$ the contribution of $[H_6A]$ and $[H_5A]$ is small and therefore may be ignored. Thus Equation [56] may be rewritten as

$$\bar{n} = \frac{H_4A}{H_4A + H_4A} = \frac{1}{2} \quad [60]$$

$$\bar{n} = 0.5$$

Therefore, in the formation curve, the pH where \bar{n} equals 0.5 is an approximation of K_4^* . Similarly, K_5^* is the pH at which \bar{n} equals 1.5 and K_6^* is the

pH at which \bar{n} equals 2.5. Using this estimation procedure values for pK_4 , pK_5 , and pK_6 obtained were 8.1, 8.8, and 10.2 respectively, which are tabulated in Table 5.

In the case for the formation curve of TAHA (Figure 14), the constants K_4^* and K_5^* are not sufficiently separated to arrive at good estimates; however estimates of K_6^* have less error. A more accurate calculation of the association constants is performed using a linear least squares treatment defined in Equation [52] for the calculation of K_4^* , K_5^* and K_6^* using Equations [53] and [55].

5. Discussion

The acid dissociation constants obtained using the three methods for a single set of potentiometric data are all summarized in Table 5. All three methods gave results within 0.03 for the calculation of pK_1 to pK_5 . There was more variation in the calculation of pK_6 .

Average values of pK_n in H_2O were calculated from three different potentiometric data sets; in D_2O , the average pK_n were calculated from two different potentiometric measurements. All potentiometric experiments were performed at 25.00 °C and a constant ionic strength of 0.1 M with KNO_3 in both H_2O and D_2O . The pK_n values reported and used in the remainder of this thesis are tabulated in Table 7.

Method 1, although tedious, gave reproducible pK_n values for all six acid dissociation constants from different data sets. Method 2, the method of Schwarzenbach, was generally used for the determination of pK_4 , pK_5 and pK_6 , which were then compared with values obtained from Method 1. It was found that there was some variation in the values obtained with the method of Bjerrum, depending on the number of data points which were used for the linear regression plots. For example, in Figure 12, the values calculated for the slope and y intercept were on the order of 10^5 and 700-800 respectively; as the number of experimental data points was randomly decreased, there was some variation in the slope and y intercept which resulted in differences in pK_n as large as 0.3 from a single set of experimental data (even though the correlation coefficient was always greater than 0.99). The method of Bjerrum gave good values for the calculation of the last three acid dissociation constants by linear regression analysis.

From Table 6 it is seen the value of the first \bar{n}_{calc} is 1.481 indicating that the first proton is completely dissociated when TAHA is dissolved under these conditions and hence very acidic ($K_1 = 0.0151$), and the second proton is approximately 50% ionized at this point, which is also seen from the distribution curves (Figures 15 and 16) of the ligand TAHA, both in H_2O and D_2O .

The distribution curves were calculated in the usual manner using the definition of the acid dissociation constants, K_n , as defined earlier and the term

Table 7. Acid dissociation constants for TAHA in H₂O and D₂O (25.00 °C, $\mu = 0.1 \text{ M KNO}_3$).

n	H ₂ O		D ₂ O		ΔpK_n^1
	K_n	pK_n (average)	K_n	pK_n (average)	
1	0.0151 0.0149 0.0150	1.820 ± 0.002	9.55×10^{-3} 9.48×10^{-3}	2.020 ± 0.003	0.200
2	3.02×10^{-3} 3.10×10^{-3} 3.07×10^{-3}	2.514 ± 0.006	2.40×10^{-3} 2.42×10^{-3}	2.620 ± 0.003	0.106
3	1.12×10^{-3} 1.23×10^{-3} 1.10×10^{-3}	2.94 ± 0.05	9.33×10^{-4} 8.51×10^{-4}	3.05 ± 0.04	0.11
4	6.60×10^{-9} 6.03×10^{-9} 6.61×10^{-9}	8.19 ± 0.04	4.79×10^{-9} 1.17×10^{-9}	8.33 ± 0.03	0.14
5	2.00×10^{-9} 2.19×10^{-9} 1.70×10^{-9}	8.72 ± 0.03	1.26×10^{-9} 1.17×10^{-9}	8.91 ± 0.03	0.19
6	4.07×10^{-11} 3.89×10^{-11} 3.55×10^{-11}	10.42 ± 0.06	4.90×10^{-12} 4.37×10^{-12}	11.33 ± 0.05	0.91

¹ see text

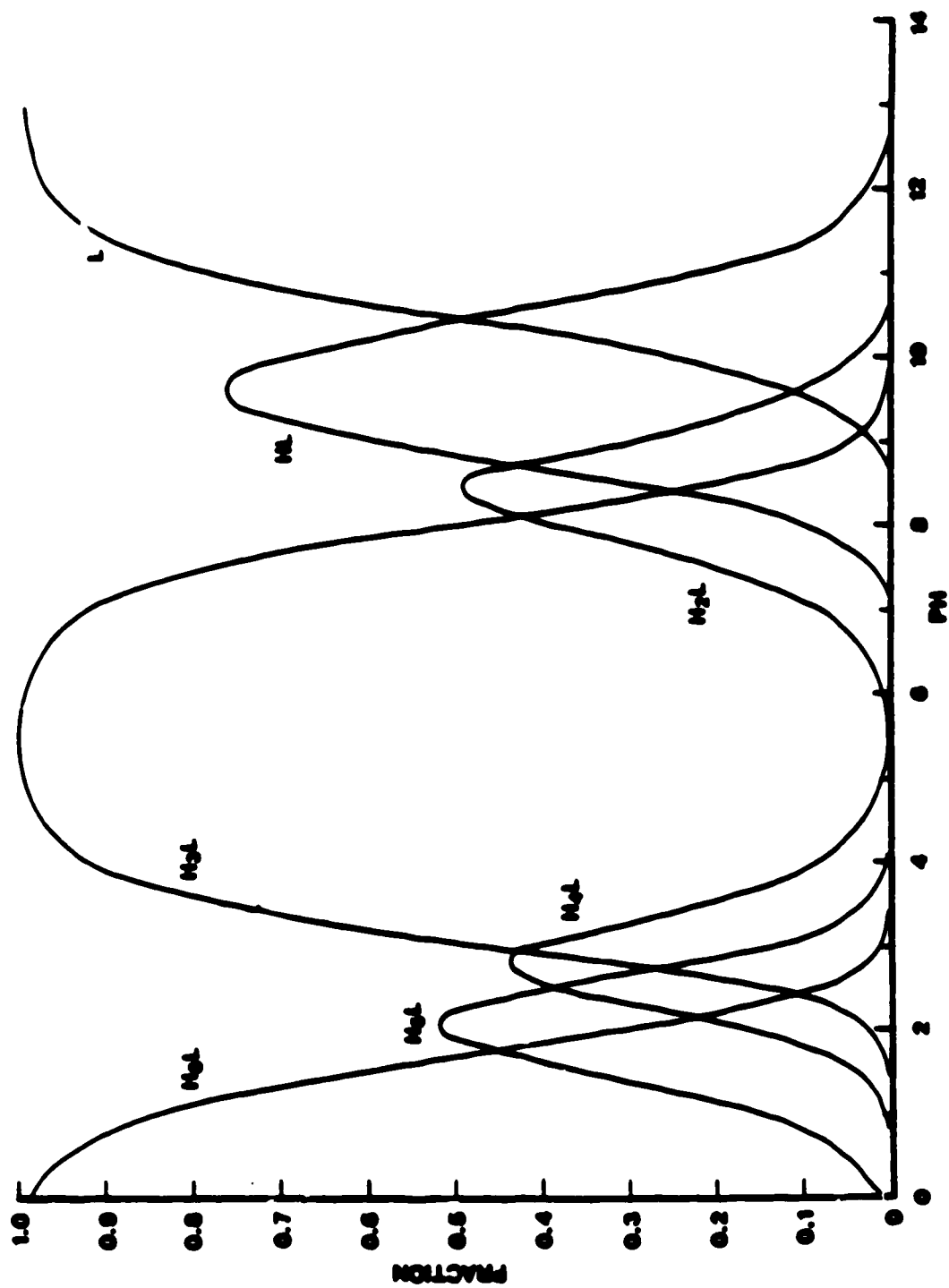


Figure 15. Distribution curve in H₂O at constant ionic strength and temperature ($\mu=0.1$ M KNO₃ and 25.00 °C).

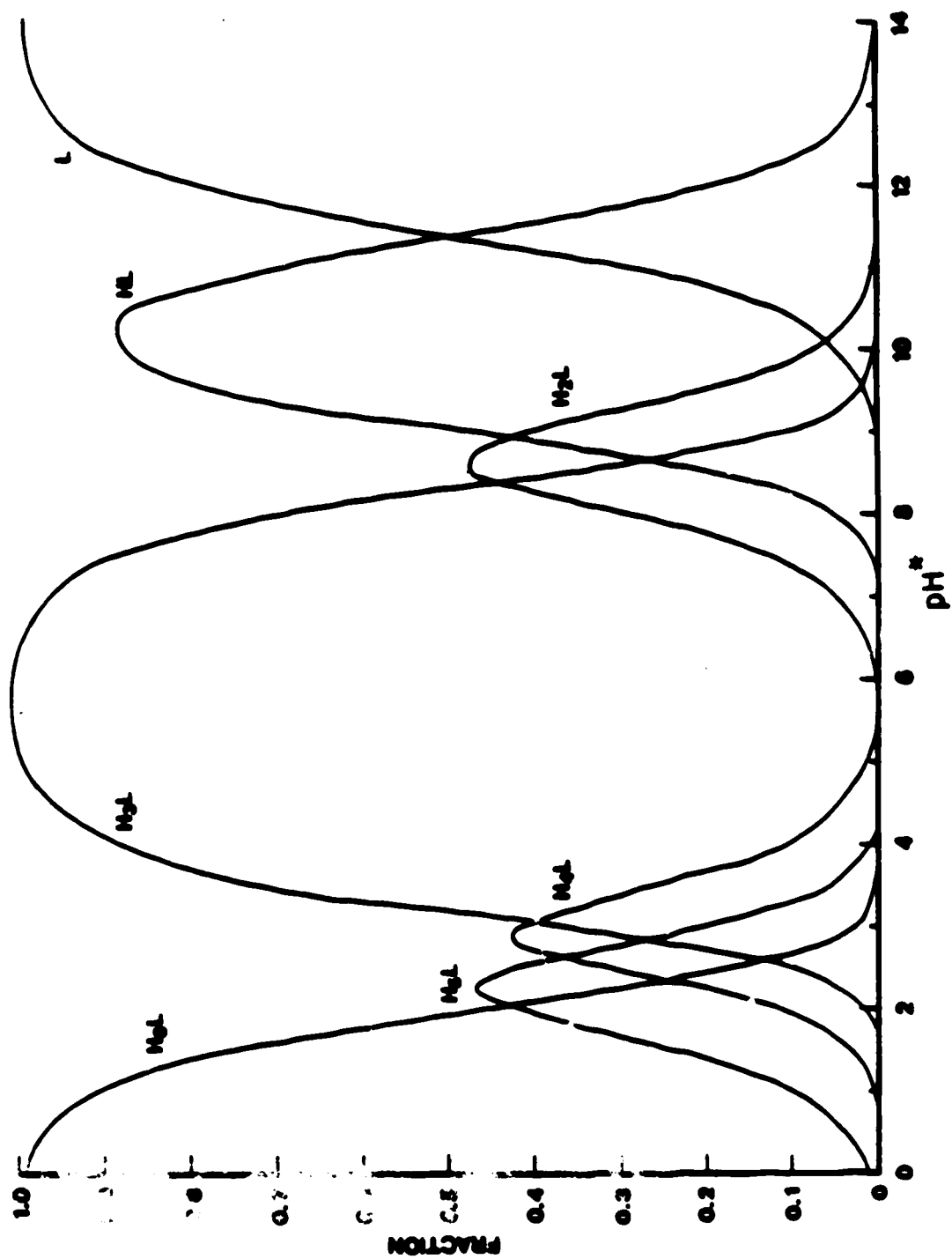


Figure 16. Distribution curve in D₂O at constant ionic strength and temperature ($\mu=0.1$ M KNO₃ and 25.00 °C).

L' which is defined as all species that contain TAHA. For all of the following equations, charges have been omitted for simplicity.

$$L' = H_6L + H_5L + H_4L + H_3L + H_2L + HL + L \quad [61]$$

$$L' = [L] + K_1 [H] + K_1 K_2 [H]^2 + K_1 K_2 K_3 [H]^3 + K_1 K_2 K_3 K_4 [H]^4 + K_1 K_2 K_3 K_4 K_5 [H]^5 + K_1 K_2 K_3 K_4 K_5 K_6 [H]^6 \quad [62]$$

The alpha (α) coefficients, or distribution coefficients, for a hexaprotic acid (H_6L) are then defined in the following equations:

$$\alpha_0 = \frac{[H_6L]}{L'} = \frac{[L]}{L'} \quad [63]$$

$$\alpha_1 = \frac{[H_5L]}{L'} = \frac{K_1 [H]}{L'} \quad [64]$$

$$\alpha_2 = \frac{[H_4L]}{L'} = \frac{K_1 K_2 [H]^2}{L'} \quad [65]$$

$$\alpha_3 = \frac{[H_3L]}{L'} = \frac{K_1 K_2 K_3 [H]^3}{L'} \quad [66]$$

.

.

.

$$\alpha_6 = \frac{[L]}{L'} = \frac{K_1 K_2 K_3 K_4 K_5 K_6 [H]^6}{L'} \quad [67]$$

As can be seen from Table 7, the corresponding pK_n values in D_2O are higher than those obtained in H_2O . This is due to two reasons. Firstly, the effect

is due to primary isotope effects which refers to the effect of substituting deuterium for the labile hydrogen atoms of the acid group. Secondly, the solvent isotope effect is involved, which refers to the effect of the medium on the acid-base equilibrium. These two effects are not distinguishable in the presence of exchangeable protons on the ligand and may be measured by a ΔpK value which is also tabulated in Table 7. The term ΔpK is defined as:

$$\Delta pK_n = pK_n(D_2O) - pK_n(H_2O) \quad [68]$$

The value of ΔpK_n is found to be dependent on the functional groups on the ligand: as a general rule, the effect is more pronounced for the ionization of amino groups than for that of the carboxylic acid groups.

In this work, the ΔpK 's for the first five acid dissociation constants were less than 0.20; however the ΔpK_n for the last acid dissociation constant (pK_6) is calculated to be 0.93, which indicates that the last proton from TAHA is less acidic in D_2O than in H_2O . Reid and Podanyi (91) have recently reported the same trend for the acid dissociation constants for glycine. The authors reported a ΔpK of 0.4 and 0.94 for the carboxylic and amino acid dissociation constants of glycine. Jameson *et al.* (92) have reported differences of a similar order of magnitude for several amines and phenols.

The acid dissociation scheme for the three carboxylate groups is shown schematically in Figure 17. If all the microscopic constants are assumed to be independent of each other, it can be calculated that the following relationships hold:

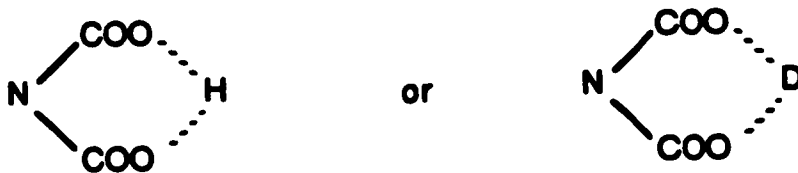
$$pK_1 \leq pK_2 - 0.47 \quad [69]$$

$$pK_2 \leq pK_3 - 0.47$$

[70]

Hence pK_1 must be ≤ 2.05 while pK_2 must be ≤ 2.48 (using the pK_n values in Table 7). It is seen that although the first relationship (Equation [69]) is valid, the second relationship (Equation [70]) is not. It is probable that the microscopic constants involved in H_5L^{-1} going to H_4L^{-2} are not independent. Since removal of a proton from a carboxylate group depends on the functional group as well as the environment in which the group is located (due to electrostatic interaction), it is possible that the H_5L^{-1} and H_4L^{-2} species have important intramolecular hydrogen bonding between adjacent carboxylate groups as has been described for EDTA (93) and TTHA (triethylenetetramine hexaacetic acid) (94).

Interactions such as



may be important in such a ligand. In addition, a carboxylic acid group which is surrounded by negative groups tends to be more weakly acidic.

The microscopic scheme for the amino groups is a more complex and will be discussed at a later point in this chapter.

C. 1H NMR Studies of the Acid/Base Chemistry of TAHA

1. Introduction

The following 1H NMR studies were performed on a Varian XL 400 spectrometer using a digital resolution of 0.33 Hz per point and a probe temperature of 25 °C. Typically 0.75 mL sample volumes were used. The

results presented in this section are a combination of three different types of ^1H NMR experiments.

In the first type of experiment a pH titration was performed in D_2O at constant ionic strength (0.1 M KNO_3) using a double-walled flow cell with the temperature held constant at $25.00 \pm 0.01 \text{ }^\circ\text{C}$. The TAHA concentration was approximately 3.0 mM for this and all other NMR experiments. A $750 \text{ }\mu\text{L}$ aliquot was removed for the NMR measurement at appropriate pH^* values; after the NMR measurement, the aliquot was returned to the titration vessel. The pH^* was then adjusted with standardized KOD for the next sample.

In the second type of experiment, the pH titration of approximately 3.0 mM TAHA was performed in the NMR tube (5 mm OD). The pH^* was measured using an Ingold semi-micro combination electrode (diameter 3 mm , length 180 mm) with an Ag/AgCl internal reference element that was immersed directly into the sample in the NMR tube.

When TAHA is dissolved, an initial pH^* of 2.8 is obtained for a solution with a concentration of 3.0 mM . A third titration under the same conditions as above was performed by adding DCl to obtain chemical shift versus pH^* data at lower pH^* values, where the lowest pH^* measured was 0.50 .

The protonation scheme of TAHA was elucidated from the chemical shifts of resonances for the T1, T2, and T3 methylene protons as a function of pH^* . Assignment of the T1, T2, and T3 methylene protons as well as the N1 and N2 nitrogen groups was given in Figure 6. Figures 18A to 18H are representative ^1H NMR spectra observed at pH^* values between 8.10 to 11.66 as TAHA was titrated at constant ionic strength ($\mu = 0.1 \text{ M KNO}_3$) and ambient temperature. Figure 19 is a plot of the chemical shift (ppm) of each resonance as a function of

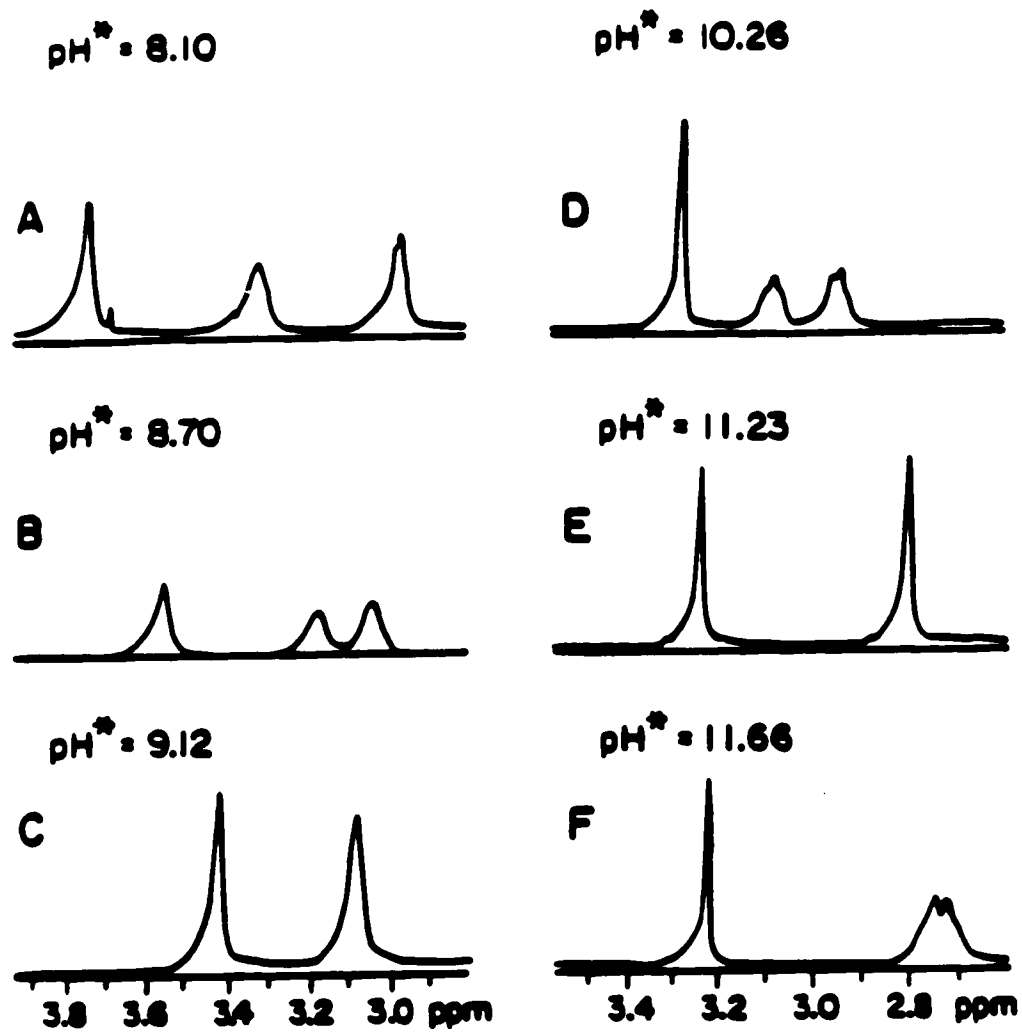


Figure 18. Representative ^1H NMR spectra of TAHA as a function of pH^* .

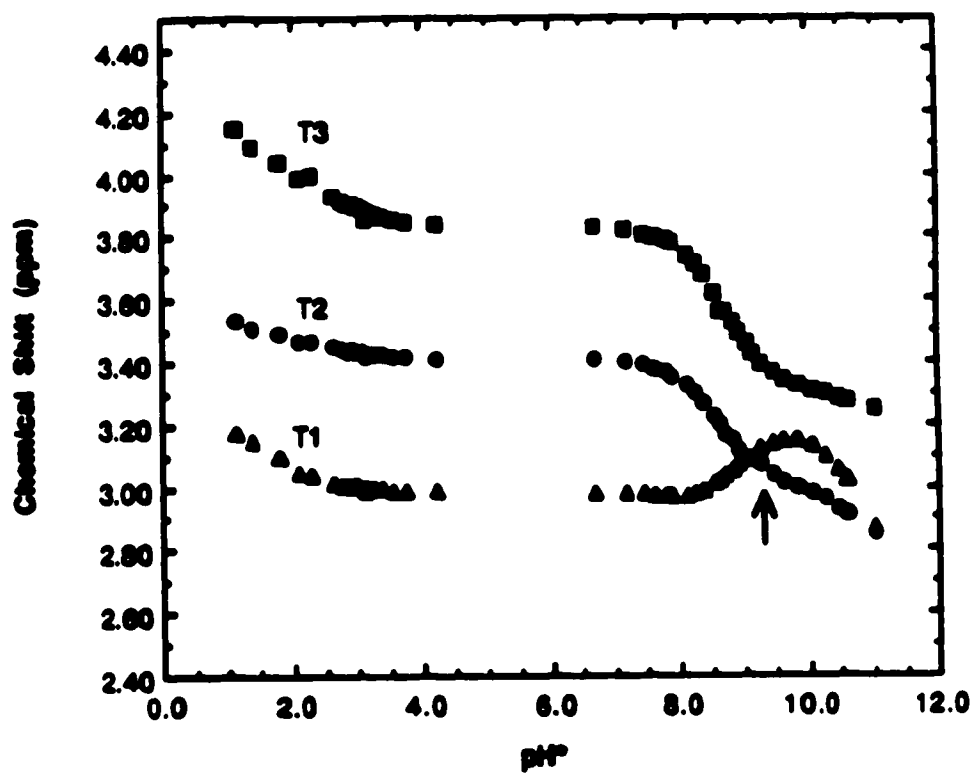


Figure 19. Chemical shift (ppm) versus pH* for the T1, T2 and T3 methylene proton resonances of TAHA. An arrow on the T2 curve indicates a distinct change in the slope of the curve as discussed in the text.

pH^* . In the case of the two triplets which are observed (see Figure 7), only the chemical shift of the central resonance is plotted. A coupling constant of 6.8 Hz was observed for both of the triplets.

Resonances were assigned to the various methylene protons in the following manner. At pH^* less than 3, the ligand, TAHA, has three resonances (Figures 7 and 18A), a singlet and two triplets in a ratio of 2.0:1.0:1.0. There are twice as many T3 methylene protons, therefore the singlet at 3.930 ppm (pH^* 2.91, Figure 18A) is assigned to the T3 methylene groups. Further evidence for this assignment is that, upon deprotonation of the carboxylate groups between pH^* 2.0 to 3.5, the chemical shift of the T3 resonance is most affected (largest slope in the T3 curve presented in Figure 19) due to its close proximity to the functional groups being titrated. Below pH^* 2.0 formation of H_7L^+ and H_8L^+ species occurs. As the pH^* was decreased to a pH^* of 0.5, there was no plateau in the chemical shift, nor was there precipitate present, indicating that the above protonated species exist as soluble cations.

Comparison of the chemical shifts as a function of pH^* in Figure 19 indicates that the resonance due to the singlet at 3.930 ppm (pH^* 2.91) is more affected by deprotonation of the carboxylic acid groups than the resonance at 3.438 ppm (pH^* 2.91); that is, the singlet exhibits a larger downfield shift as the carboxylic acid groups of TAHA are deprotonated in comparison to the change in the chemical shift of the resonance at 3.438 ppm, which is due to the methylene protons that are the next closest to the carboxylic groups (i.e. on the N2 nitrogen atom). The resonance at 3.002 ppm is for the T1 protons. The T1 protons are further removed from the carboxylic acid groups, and thus they are expected to be the least affected by the deprotonation of the carboxylic groups. On this basis, the triplet at 3.438 ppm was assigned to the T2 methylene protons. At pH^* values less than 1.8, there is a downfield shift of the resonance

for the T1 protons, indicating that protonation is occurring at the central nitrogen atom (N1 nitrogen) when species such as H_7L^+ or H_8L^{+2} are formed.

At pH 8.10, Figures 18A and 18B, the coupling for the triplets was not observed. The resonance due to the T1 methylene protons moves downfield while the resonance due to the T2 protons moves upfield (with respect to DSS) until they both overlap at pH* 9.00. Both resonances shift, then overlap, until approximately pH* 9.20 (Figure 18D). From pH* 9.2 to approximately pH* 9.6, the resonance from the T1 methylene protons continues to move downfield, in the opposite direction from the change in the chemical shift of the resonance from the T2 methylene protons. At pH* greater than 9.4 both resonances move upfield until they overlap once more between pH* 10.9 to pH* 11.4. At pH* greater than 11.6, the two resonances due to the T2 and T1 methylene protons begin to separate and move upfield at different rates; thus it was possible to identify each resonance by comparison of the relative rates of the change in chemical shift as a function of pH*. (i.e. by comparison of the $\Delta \text{ppm}/\Delta \text{pH}^*$ of each resonance).

In Figure 19, the curve which represents the chemical shift of the T2 methylene protons as a function of pH* indicates that after pH* 7.8 there is an upfield shift of the resonance for the methylene protons closest to the N2 nitrogen as the protons on these nitrogens become deprotonated. In this region there is a distinct change in the slope, as indicated by the arrow. The moles of KOH necessary to titrate each portion of the curve are equal to each other and represent the moles of base required to titrate one proton from TAHA. The first proton starts to be removed at pH* 7.8, while the second proton starts being removed at pH* 9.8. When approximately 97% of the first proton is removed, migration of a proton to the central nitrogen (the N1 nitrogen) atom occurs as indicated by the downfield shift in curve representing the behavior of the T3

methylene protons. The process of migration is essentially complete when the first proton from the N2 nitrogen groups is completely removed. During the pH^{*} region between 8.1 to 9.4, migration of a proton to the central nitrogen group occurs; this process is complete at pH^{*} 9.4. After pH^{*} 9.5 there is simultaneous deprotonation of the remaining two protons on the ligand: one proton on the N2 nitrogen and one proton on the central nitrogen atom.

Acid base chemistry is usually characterized by macroscopic ionization constants. The calculation of microscopic ionization constants of TAHA is more difficult due to the behavior of the protons on the amino groups as detailed below. For the calculation of microscopic constants, chemical shift versus pH^{*} data obtained from ¹H NMR measurements are especially useful because of the sensitivity of the chemical shift with respect to protonation/deprotonation at nearby functional groups.

However, for the ligand TAHA, individual microscopic constants can not be calculated from the chemical shift versus pH^{*} curves presented in Figure 19. The curve which is due to the T3 methylene protons closest to the carboxylate groups did not exhibit three inflection points as was expected. When the observed chemical shift and pH^{*} data were run through KINET the curve did not converge when treated as a triprotic acid. The curve due to the T2 methylene protons exhibited two inflection points, and did converge when treated as a diprotic acid. However, the methylene protons that give rise to this curve are in close proximity to the central nitrogen group, and therefore are affected by the migration and deprotonation behavior that occurs at this nitrogen atom. Hence the dissociation constants calculated from this curve (not presented) are not a true indication of the behavior of TAHA in D₂O. Likewise, the curve due to the T1 methylene protons that are closest to the central nitrogen atom are also affected by the deprotonation behavior occurring at the N2 nitrogen atoms and

therefore the calculation of acid dissociation constants were once again irrelevant.

Since the behavior of the ligand TAHA is very complex at the microscopic level, only qualitative information may be obtained from Figure 19.

The dissociation scheme of the amino groups with the labelled microscopic constants involved is schematically drawn in Figure 20. For simplicity, the carboxylate groups are not depicted in the figure. As can be seen from this figure, the migration of a proton from N2 nitrogen groups greatly complicates the dissociation scheme of the amino nitrogens. It is unlikely that $k_4 = k_4^M$, $k_5 = k_5^M$ and $k_6 = k_6^M$, (where the superscript 'M' represents migration from the appropriate nitrogen proton), since the processes of migration and deprotonation are completely different. For TAHA, migration of a proton to the central nitrogen atom is due to the increased basicity of this nitrogen relative to the N2 nitrogen groups. From the ^1H NMR studies, there was no evidence for the migration of a proton from a nitrogen atom to any of the carboxylate groups of TAHA.

Although migration has not generally been reported by ^1H NMR for polycarboxylate amino acids, Kula (96) has reported that, for the pentaprotic ligand DTPA, the migration of a proton between the central and end nitrogen groups does occur. In the case of DTPA, if the ligand is titrated from a high pH to a low pH value, the first protonation ($\text{p}K_5 = 10.45$) occurs on the central nitrogen; the second protonation ($\text{p}K_4 = 8.53$) occurs on one of the end nitrogen groups. At this time the proton from the central nitrogen group migrates to the other end nitrogen group. The net result is that the two end nitrogens are completely protonated. The third protonation ($\text{p}K_3 = 8.53$) then occurs on the central nitrogen. In the case of the ligand DTPA it is easier to understand the

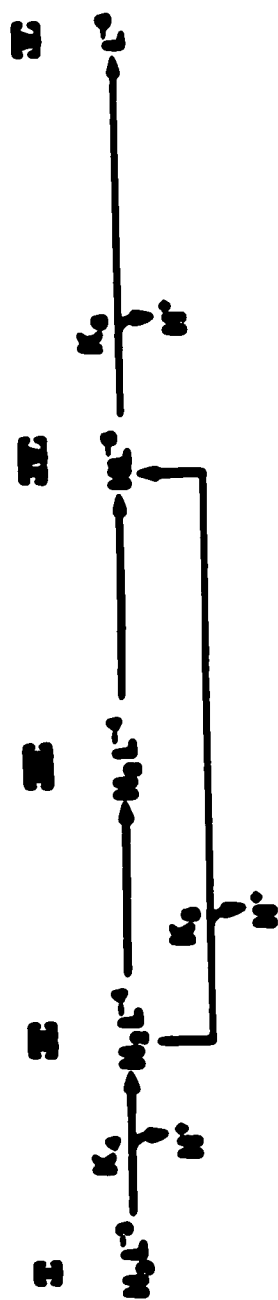
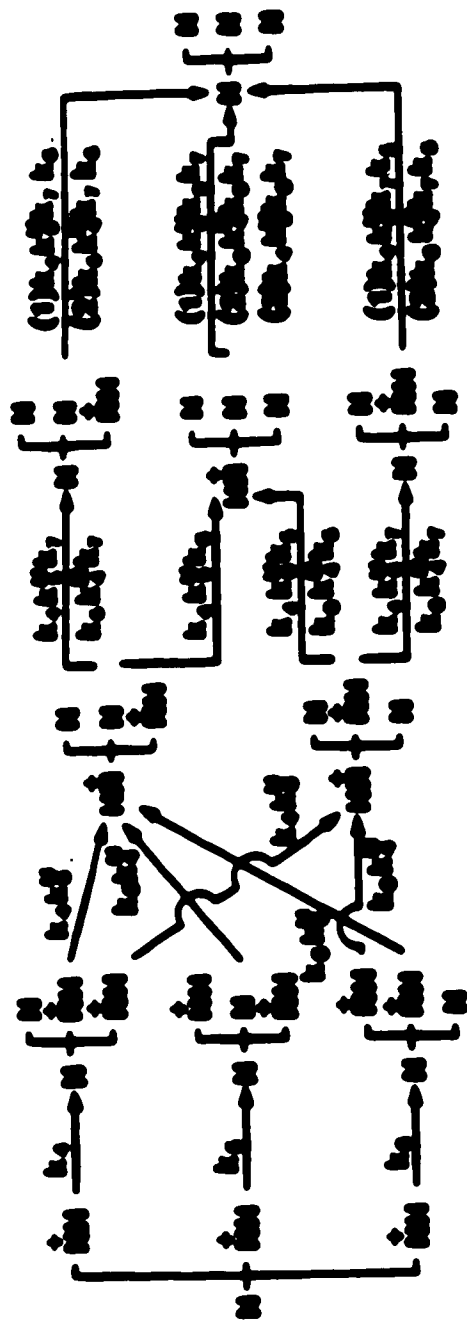


Figure 20. A schematic of the microscopic dissociation constants of TAHA amino groups. The deprotonation steps indicated by k_4 , k_5 , and k_6 , are for the removal of a proton as species II. For simplicity the microscopic constants denoted as k_{ab} represent the dissociation of the proton from group b after the association of the proton from group a occurred in a previous step. The macroscopic constants K_1 , K_2 , and K_3 for TAHA, are shown at the bottom. Each species of TAHA, (H_3L^+ , H_2L^+ , HL^+ , and L^+) are given by the Roman symbols I to V respectively. The superscript 'M' for k_3 is for the migration of the appropriate proton of the N2 nitrogen atom to the central, or N1 nitrogen atom.

migration process in terms of electrostatic interactions.

From Figure 20, there are two different H_2L^{-4} species possible. The first type is labeled as species II and has two protons present on two of the three N2 nitrogens, while the second, labeled as species III, has one proton on the N2 nitrogen, and the other proton on the central nitrogen group. After one proton is removed from the amino groups of TAHA, migration of a proton may be more favorable due to the minimization of the electrostatic interactions present and due to the increased basicity of the central nitrogen atom. From the chemical shift versus pH^* curves (Figure 19), the last two protons present on TAHA are simultaneously removed to give the totally deprotonated TAHA molecule, labeled as species V in Figure 20.

D. Summary

Protonation sites and conformations of aminopolycarboxylic acids in aqueous solutions have been studied extensively, especially for ligands such as EDTA, EDTA analogues, and DTPA. For ligands that have more than six acid dissociation constants (e.g. TTHA, TAHA), conformation studies of the ligand are not so well characterized (95). The acid dissociation constants and protonation schemes are important in the study of the complexation of these ligands with metal ions.

Since TAHA is compared with different ligands in this section, some common ligands along with their pK_n values are tabulated in Appendices 4A and 4B for reference.

The ability of a ligand to strongly complex to a metal depends partly on the presence of groups through which a metal may coordinate, such as carboxylate ions or amino groups. Using the nomenclature of Schwarzenbach

(97), the following equations may be defined:

$$\alpha^* = \frac{1}{\alpha_6} \quad [71]$$

where α_6 was defined in Equation [67] and

$$K_{ML}^C = \frac{K_{ML}}{\alpha^*} = K_{ML} \alpha_6 \quad [72]$$

where K_{ML}^C is the conditional or effective formation constant and K_{ML} is the thermodynamic stability constant.

On a simple level the ligand TAHA may be compared to other ligands on the basis of α^* or the acid dissociation constants. Figure 21A is a plot of α^* versus pH for the ligands TAHA, EDTA, and DTPA, while Figure 21B is the same plot for the hexaprotic acids TAHA, TTHA, and TAPHA. As can be seen from Figure 21A, the α^* value of TAHA is always higher than that of EDTA which is higher than that of DTPA up to pH 9.0. However, it is seen

from the plots in Figure 21B, that the values of α^* for TAHA and TTHA are very similar. If only this data were considered, it would indicate that formation constants for metal-ligand complexes of both TAHA and TTHA would be of the same order of magnitude. Figures 21A and 21B do not, however, consider the ability of the ligand to take up a proton in acidic solutions, or of the metal to add a hydroxyl group in alkaline solutions when the metal-ligand complex is formed. These figures only indicate possible similarities between TAHA and TTHA in regard to the acid dissociation constants.

Calculation of metal-ligand stability constants using TAHA as the complexing agent, and comparison of calculated K_{ML} values for some of the

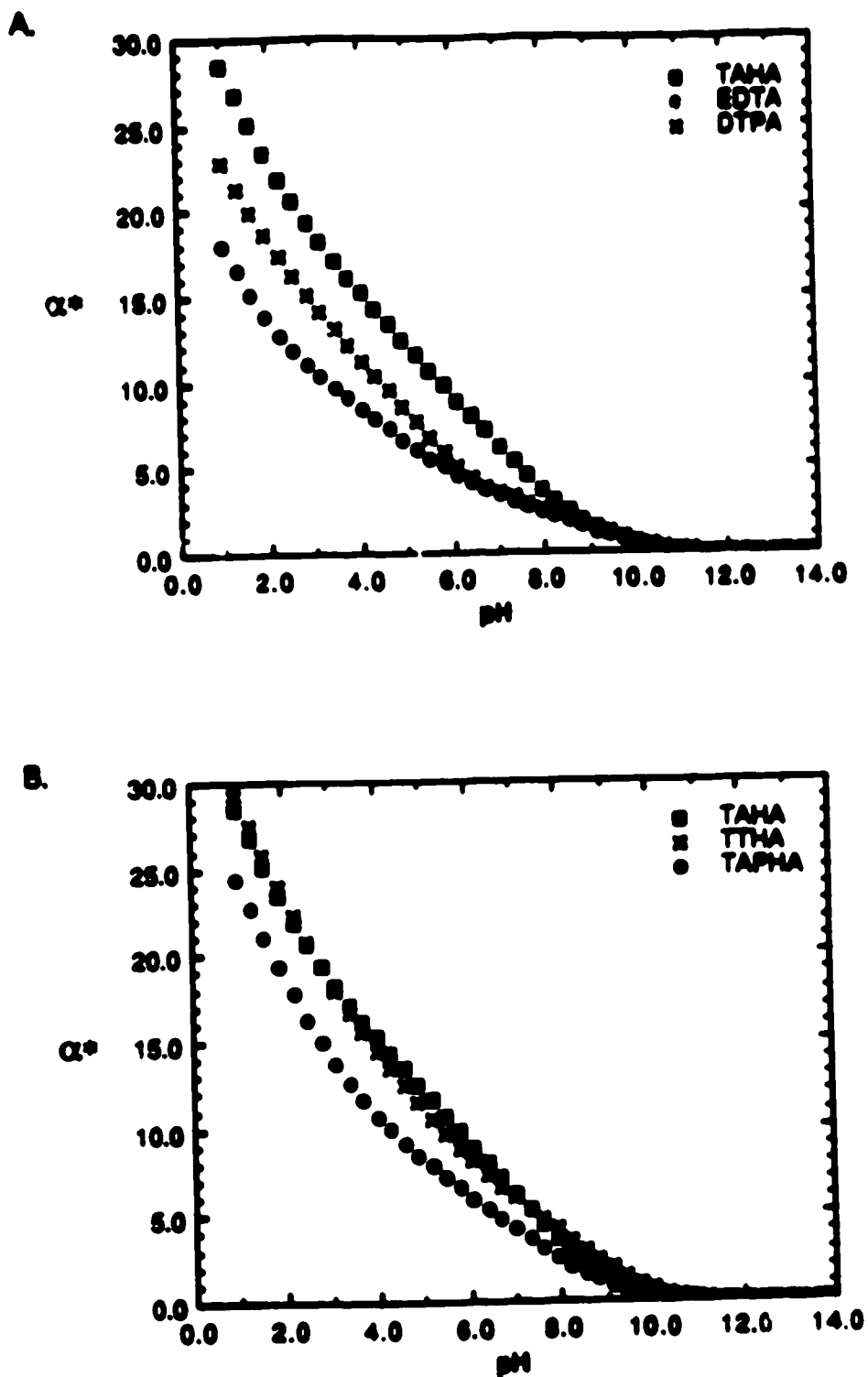


Figure 21. Comparison of TAHA with other ligands using α^* versus pH plots; the term α^* is defined as $\alpha^* = [\alpha_6]^{-1}$. The ligands are identified in the legends.

ligands tabulated in Appendix 4 will be presented in the following chapter which will present the results of the interaction of TAHA with a variety of metals.

IV. METAL BINDING STUDIES

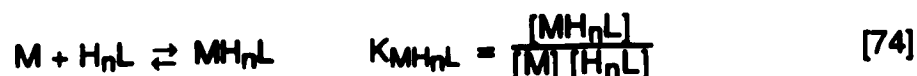
A. Introduction

In the previous chapter the ligand tris(2-aminoethyl)amine hexaacetic acid, TAHA, has been characterized in terms of its acid-base chemistry (calculation of acid dissociation constants), melting point, decomposition, solubility, and protonation/deprotonation behavior. This ligand has 10 coordination sites, hence it can potentially form strong complexes with divalent and trivalent metal ions. The potential for high stability constants with a variety of metals is due to the "chelate effect". Hence, metal complexes of multidentate ligands, such as EDTA, DTPA, TTHA and TAHA, are of higher stability than monodentate complexes. The relative strength of the chelate complex generally increases with an increase in the number of rings which are formed, provided that the stereochemical requirements are met. This may be illustrated by the ligand DTPA which has been shown, by x-ray analysis, to be an octadentate complex (25,26) with the gadolinium ion. The net result of this is that the stability of metal-ligand complexes is enhanced as the ligand "wraps" itself around the metal ion. Corresponding changes in enthalpy and entropy upon chelation have been well characterized and tabulated in the literature (30).

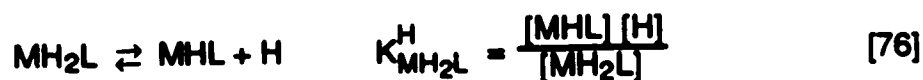
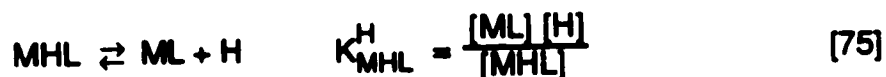
In this chapter, metal-TAHA complexes were studied to determine their stability. Complexes of the metal ions mercury (Hg^{+2}), lanthanum (La^{+3}), and calcium (Ca^{+2}) were studied by three different methods: the pH titration, the pHg method, and by ^1H NMR as described in Chapter II. The results will be given in detail in the following sections. Complexes of TAHA with several other metal ions were also studied, results of which are presented in the last section of this chapter.

The following symbols, equilibria, and definitions will be used for the remainder of this chapter. In all cases, M refers to the trivalent or divalent metal ion, L to the ligand TAHA, and K to the thermodynamic stability constant unless otherwise stated. All charges are omitted for simplicity.

The stability constants for the metal-TAHA complexes can be defined in general terms as follows:



where n may equal 1, 2 or 3. In Equation [74], the α_n of TAHA, as previously defined in Equations [63] to [67], are used in the calculation of $[H_nL]$. The acid dissociation constants for protonated metal TAHA complexes are denoted as K^H and defined as:

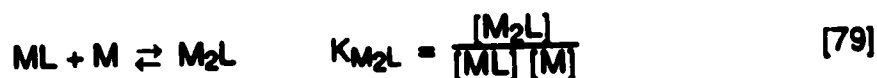


Using the definition of the acid dissociation constants K_5 and K_6 and Equations [73], [75] and [76], the following two relationships may be derived:

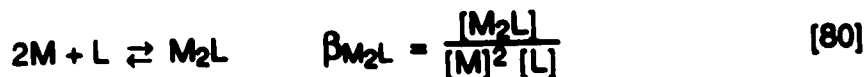
$$K_{ML} = \frac{K_{MHL}^H K_{MH_2L}^H}{K_6} \quad [77]$$

$$K_{MHL} = \frac{K_{MH_2L}^H K_{MH_2L}}{K_5} \quad [78]$$

Polynuclear complexes are defined as



and



where β_{M_2L} is the overall formation constant and equal to

$$\beta_{M_2L} = K_{ML} K_{M_2L} \quad [81]$$

For the remainder of this thesis, the above equations will be referred to with the general symbol M usually replaced with the metal ion studied.

B. Mercury

1. Potentiometric Studies

Mercury generally forms quite stable metal ligand complexes. It has a coordination number of two, four, or six depending on the ligand and has been shown to form polynuclear complexes with several ligands such as TTHA (98).

In Figure 22, data from potentiometric pH titrations for various ratios of Hg^{+2} :TAHA are presented. The pH is plotted as a function of the A value which is defined in the usual manner as moles of base added per mole of TAHA present. The first curve corresponds to the pH titration TAHA alone at a concentration of 1.89 mM. This curve exhibits a sharp inflection point at an A

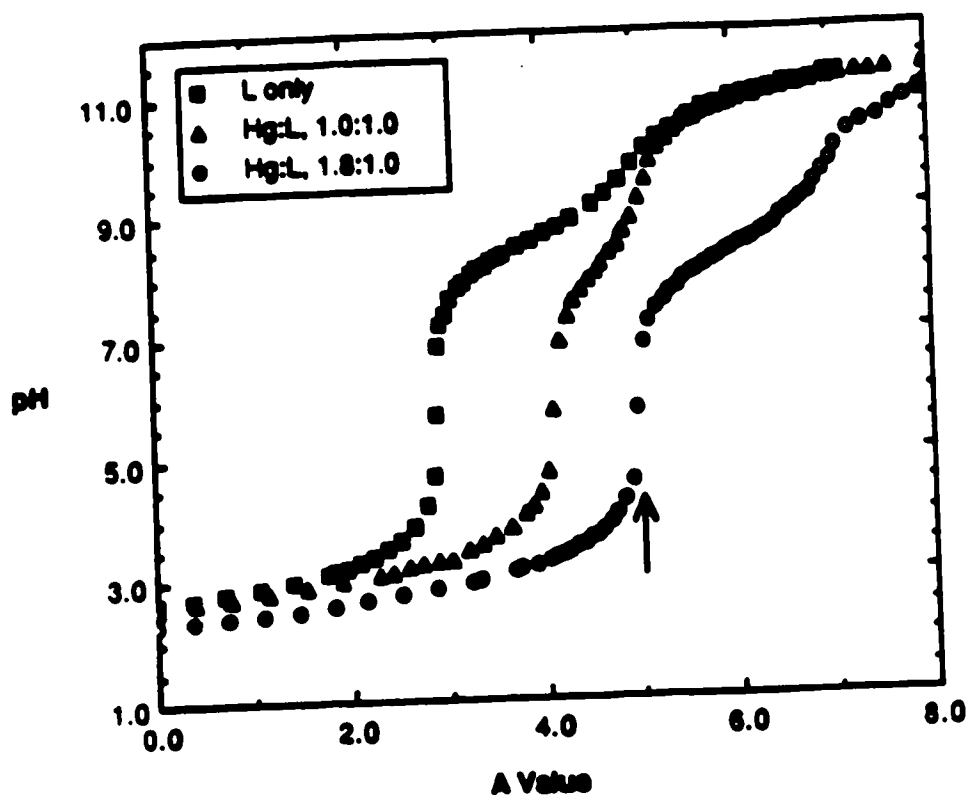


Figure 22. Titration curves of pH versus A value for the mercury-TAHA system at various concentrations; the L represents the ligand TAHA. The arrow on the Hg⁺²:TAHA curve in a 1.8:1.0 ratio represents the pH at which total dissolution occurred. All titrations were performed at constant ionic strength and temperature ($\mu=0.1$ M KNO₃ and 25.00 °C).

value of 3, corresponding to the titration of three carboxylic acid protons; at this point there are three protons remaining on the nitrogen atoms which are then titrated from A values 3 to 6. The second curve in Figure 22 is the pH titration curve for a solution of Hg^{+2} :TAHA in a ratio of 1.0:1.0 (1.28 mM Hg^{+2} , 1.37 mM TAHA). This curve is initially displaced to lower pH values when compared to that of TAHA alone, due to the displacement of protons from the ligand upon complexation with mercury. There is a shallow buffer region between A values of 2 and 4; at an A value of 4 there is a sharp inflection point up to pH 6. This type of behavior is usually characteristic of the formation of stable protonated complexes such as $\text{HgH}_2\text{L}^{-2}$. Between A values of 4 to 5 the curve is similar to a simple acid dissociation curve where one proton is titrated according to the following equilibrium:



Between A values of 5 to 6, HgL^{-4} is formed by titration of the proton from HgHL :



When the A value is greater than 6 it is possible that hydroxyl complexes such as $\text{HgL}(\text{OH})_n$ form.

The last curve in Figure 22 is the pH titration curve for a solution containing Hg^{+2} :TAHA at a ratio of 1.8:1.0 (2.79 mM Hg^{+2} , 1.57 mM TAHA). This curve is displaced to lower pH values (from both of the other two curves) at the start of the titration, as expected, when protons are displaced from the ligand by formation of metal complexes. This curve parallels the curve in which the Hg^{+2} :TAHA ratio was 1.0:1.0 until an A value of 4 is reached; at a value of 5

there is a distinct inflection point. During the titration of this solution a fine white insoluble powder was present until a pH of approximately 5.2 (corresponding to an A value of 4.20). The point at which total dissolution occurred is indicated by an arrow on the curve presented in Figure 22.

To obtain further information regarding the composition of the insoluble product, the complex was purified at pH 1.50 and pH 3.20 by a procedure similar to that described in Chapter III for TAHA. The powder was dried and sent for elemental analysis (Galbraith Laboratories, Inc.). The elemental analysis for the sample purified at pH 1.50 was: C, 18.12%; H, 3.03%; N, 4.91%; and O, 24.30%, while the elemental analysis for the sample purified at pH 3.20 was: C, 17.81%; H, 2.13%; N, 4.65%; and O, 24.08%. When the solid material was tested for the presence of potassium by the addition of HClO_4 , the test was negative, indicating that the solid was not a potassium salt. It was therefore assumed that the only other atom present in the complex was mercury; with this assumption the per cent mercury was calculated as 49.64% and 51.33% for the samples at pH 1.50 and pH 3.20, respectively. Comparison of relative ratios of C/Hg and N/Hg indicate that the complex was of the stoichiometry Hg_3L , rather than the $\text{Hg}_2\text{H}_2\text{L}$ form. However, the %H and %O data indicate that the complex was not the trinuclear complex Hg_3L . It is possible that the Hg_3L complex precipitated in a hydrated form and/or in a dimer/polymer combination.

As mentioned earlier, titration curves similar to the curve in which the $\text{Hg}^{+2}:\text{TAHA}$ ratio was 1.0:1.0 are commonly interpreted as indicating the presence of protonated metal-ligand species. However, Harju and Ringbom (98-100) have stated that in their work with the hexaprotic ligand TTHA that the pH titration curves must be interpreted with caution. In their studies of metal-TTHA complexes, they observed, for a M:L ratio of 1:1, a marked buffer region between A values of 2 to 5 that was due to the presence of binuclear complexes

in acidic solutions *rather than* the formation of stable protonated complexes. These authors have observed that formation of 1:1 and 2:1 complexes of mercury TTHA occur in solutions in which the ratio of $\text{Hg}^{+2}:\text{TTHA}$ is 1:1. The complex which predominates depends largely on the experimental conditions and especially on the pH of the solution.

An attempt to investigate the possibility of the formation of bimetal mercury complexes with the ligand TAHA was made using the method of Harju (98). This method involved using the pHg Method for the titration of a solution containing a 1:1 ratio of $\text{Hg}^{+2}:\text{TAHA}$ (1.05 mM Hg^{+2} , 1.03 mM TAHA). Analysis of the pHg results was performed as follows: combining Equation [73] for the formation of HgL and Equation [79] for the formation of Hg_2L , Equation [84] is obtained after elimination of the common species HgL :



Using the relation defined in Equation [81] the following approximation is valid:

$$\frac{1}{K_{\text{HgL}}} \cdot \frac{1}{K_{\text{Hg}_2\text{L}}} = \frac{[\text{Hg}^{+2}]^2 [\text{L}]}{[\text{Hg}_2\text{L}]} = \frac{1}{\beta_{\text{Hg}_2\text{L}}} \quad [85]$$

$$[\text{Hg}^{+2}]^2 = (\beta_{\text{Hg}_2\text{L}})^{-1} \quad [86]$$

which assumes that all the ligand TAHA is complexed in the form Hg_2L (i.e. concentration of HgL is negligible) and where $\beta_{\text{Hg}_2\text{L}}$ is defined as the overall formation constant for the formation of the mercury bimetal complex. When no other interfering reactions occur, the overall formation constant, $\beta'_{\text{Hg}_2\text{L}}$, may be defined as:

$$[\text{Hg}^{+2}]^2 = (\beta'_{\text{Hg}_2\text{L}})^{-1} \quad [87]$$

The term $\beta'_{\text{Hg}_2\text{L}}$ is the overall formation constant where the superscript " ' " indicates that the protonation of the ligand TAHA has not been considered for this reaction. For Equation [87] to be valid there are several requirements. It assumes that there are no other interfering ligand present and that α_{HgL} is close to zero. The term α_{HgL} is defined in Equation [88]:

$$\alpha_{\text{HgL}} = \frac{[\text{HgL}]}{[\text{HgL}] + 2[\text{Hg}_2\text{L}] + [\text{Hg}]} \quad [88]$$

When the acid dissociation constants are considered, Equation [86] may be written as

$$[\text{Hg}^{+2}]^2 = \frac{\alpha_6}{\beta_{\text{Hg}_2\text{L}}} \quad [89]$$

where α_6 is the fraction of totally deprotonated TAHA, as defined in Equation [67].

Calculation of $\beta_{\text{Hg}_2\text{L}}$ and $\beta'_{\text{Hg}_2\text{L}}$ using Equation [87] and Equation [89] was performed from the experimentally determined potentials, from which the concentration of free mercury ions was calculated using the Nernst equation, and α_6 was calculated from the pH and the acid dissociation constants. Values of $[\text{Hg}^{+2}]$, $\beta_{\text{Hg}_2\text{L}}$ and $\beta'_{\text{Hg}_2\text{L}}$ for one set of experimental data are presented in Table 8. The pH dependence of $\beta_{\text{Hg}_2\text{L}}$ and $\beta'_{\text{Hg}_2\text{L}}$ as calculated using the above method is presented in Figure 23. From this figure, the value of the logarithm of $\beta'_{\text{Hg}_2\text{L}}$ increases linearly with pH, which is expected since the acid dissociation constants were not considered. However, the value of $\beta_{\text{Hg}_2\text{L}}$

Table 8. Tabulation of $[\text{Hg}^{+2}]$ and the overall formation constants, $\beta'_{\text{Hg}_2\text{L}}$ and $\beta_{\text{Hg}_2\text{L}}$, for the bimetal complex $\text{Hg}_2(\text{TAHA})^{-2}$.

pH	pHg	$\log \beta'_{\text{Hg}_2\text{L}}$	$\log \beta_{\text{Hg}_2\text{L}}$
2.30	10.759	21.517	42.945
2.36	10.931	21.862	43.003
2.44	11.103	22.207	42.970
2.54	11.276	22.552	42.882
2.66	11.483	22.965	42.753
2.83	11.759	23.517	42.637
3.11	12.241	24.483	42.514
3.19	12.379	24.758	42.507
3.28	12.586	25.172	42.626
3.38	12.690	25.379	42.484
3.50	12.862	25.724	42.412
3.65	13.103	26.207	42.419
3.86	13.483	26.966	42.504
4.23	14.000	28.000	42.408
4.74	14.793	29.586	42.436
6.19	17.138	34.276	42.762
7.19	19.655	39.310	44.861
7.64	20.172	40.345	44.662
7.88	20.345	40.690	44.391
8.12	20.483	40.966	44.102
8.54	20.586	41.172	43.446
9.66	21.207	42.414	43.220
10.20	22.000	44.000	44.390
10.47	22.448	44.897	45.146
10.63	22.655	45.310	45.495
10.80	22.965	45.931	46.064
10.96	23.207	46.413	46.510
11.09	23.345	46.690	46.763
11.30	23.621	47.241	47.288

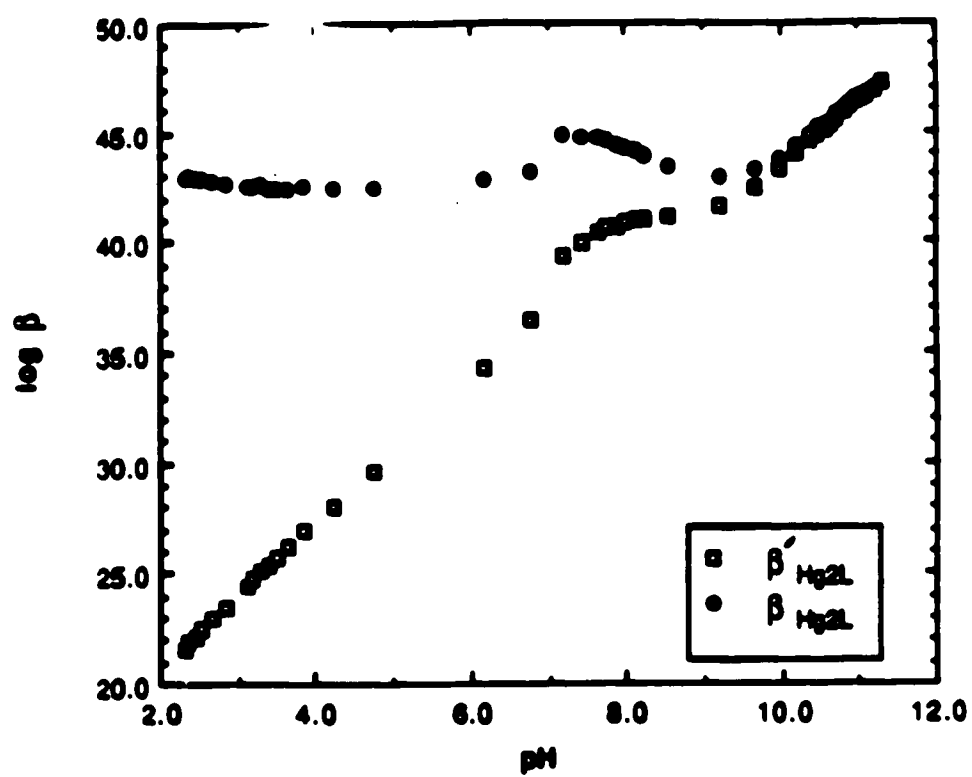


Figure 23. Plot of logarithm of $\beta'_{\text{Hg}_2\text{L}}$ and $\beta_{\text{Hg}_2\text{L}}$ as a function of pH. For details see text.

calculated from Equation [89] is constant between pH 3.11 to 6.20. This implies that formation of protonated binuclear complexes does occur in this particular solution of Hg^{+2} :TAHA ratio of 1:1. An average value of 42.5 ± 0.1 for the logarithm of $\beta_{\text{Hg}_2\text{L}}$ was obtained (a variation of 0.1 is small compared to the magnitude of the large formation constant calculated). This value is comparable to a value of 39.1 obtained for the $\text{Hg}_2(\text{TTHA})^{-2}$ complex reported by Harju(98). Schmidt and Reiley (65) have also reported the formation of an insoluble $\text{Hg}(\text{EDTA})$ complex which forms the soluble $\text{Hg}_2(\text{EDTA})^{-2}(\text{OH})$ at a pH of approximately 7.0; above this pH the complexes decomposes into HgO and $\text{Hg}(\text{EDTA})(\text{OH})^{-3}$.

At pH values less than pH 3.0 it is expected that protonated binuclear complexes such as $\text{Hg}_2\text{H}(\text{TAHA})^{-1}$ and $\text{Hg}_2\text{H}_2(\text{TAHA})$ may form to a small extent since the logarithm of $\beta_{\text{Hg}_2\text{L}}$ seems to increase slightly from pH 3.1 to 2.2 with a total variation of 0.5. This value is small when looking at the overall magnitude of the number considered (1×10^{42}) although due to the low variation of the logarithm of $\beta_{\text{Hg}_2\text{L}}$ values obtained, the small variation of 0.5 may be significant.

When formation of the protonated mercury-ligand complexes $\text{Hg}_2\text{H}(\text{TAHA})^{-1}$ and $\text{Hg}_2\text{H}_2(\text{TAHA})$ was included in the above model, the experimental data did not fit the theoretical model. It is possible that the high overall formation of Hg_2L in this experiment prevented the formation of monoprotonated mercury-TAHA complexes in large concentrations. However, the formation of bimetal mercury-TAHA complexes appears to contradict other pHg and ^1H NMR results. At this point the validity of the bimetal complexes is uncertain. It can be said that it is possible that $\text{Hg}_2(\text{TAHA})^{-2}$ complexes do form under certain conditions as indicated by the calculations presented in Table 8 and discussed above. It is also possible that a very complex equilibrium

involving Hg_2L , HgHL , HgH_2L , and $\text{Hg}_2\text{H}_2\text{L}$ occurred under this particular set of experimental conditions. The fact that a pH independent overall formation constant ($\beta_{\text{Hg}_2\text{L}}$) was calculated for this set of experimental data using the method of Harju (98), who reported such complexes with the hexaprotic ligand TTHA, may be fortuitous. Although this data has some contradictions with other potentiometric results, I feel that the *formation of bimetal mercury-TAHA complexes under certain experimental conditions cannot be ruled out* for several reasons: Firstly, as will be presented at a later point in this chapter, the formation of mixed metal complexes such as $\text{MM}'\text{L}$, where one of the metals is mercury, is indicated. Secondly, the presence of unidentified resonances observed by ^1H NMR may be due to the presence of small concentrations of bimetal mercury-TAHA complexes. The exact conditions under which these complexes form merits further study.

After pH 8.2 both curves in Figure 23 exhibit a 'dip'. Formation of other aqueous species such as hydroxyl binuclear ($\text{Hg}_2\text{L}(\text{OH})_n$) or mononuclear ($\text{HgL}(\text{OH})_n$) complexes would make Equations [87] and [89] invalid. These species may start forming in small concentrations after pH 8.0.

The formation of both homonuclear (M_2L) and heteronuclear ($\text{MM}'\text{L}$), binuclear complexes has been observed for ligands whose coordination sites that are available for binding become higher than the coordination number on the metal ion. Ligands such as DTPA (101), EDTA (65), TTHA (98), and TAPHA (102) (where TAPHA is the nonadentate ligand, triaminopropane hexaacetic acid), have been studied for their ability to form binuclear complexes. However, most of the metals studied are transition metals and alkaline earth metals (i.e. there is little information regarding the formation of Hg_2L and Hg_3L type complexes, and even less on mixed metal ligand complexes).

Figure 24 shows potential-pH diagram obtained by using the pHg method for a solution of $\text{Hg}^{+2}:\text{L}$ in a ratio of 1.0:1.60. Curve A is the experimental potential for a solution containing 1.189 mM Hg^{+2} and 1.968 mM TAHA. Curve B is the upper potential limit calculated for the mercury indicating electrode as a function of pH using Equation [22]. pHg values calculated from the potentials on the left axis using Equation [7] are given on the right y axis. For potential-pH diagrams of mercury in the presence of excess ligand, Schmidt and Reilley (65) have reported that deviations at both low ($\text{pH} < 4$) and high pH ($\text{pH} > 8$) were observed due to the formation of HgHL^{-1} and $\text{HgL}(\text{OH})^{-2}$ where L denotes EDTA. There are other reports (64) of deviations at pH values less than 3.0 due to the formation of protonated species of HgL and deviations at pH values greater than 8.0 to 10.0 due to hydroxyl HgL species, where the L represents ligands such as HEDTA, EGTA and DTPA (the nomenclature and acid dissociation constants of these ligands are presented in Appendix 4). In the present work, only slight deviations at pH values less than 3.0 were observed for all the metals studied, including the lanthanides, some transition metals, and mercury. For the majority of the calculations, experimental data in this region were not used for the calculation of formation constants. Very little deviation was observed at a high pH value (i.e., $\text{pH} > 11.0$) for the mercury-TAHA system.

Concentrations calculated from the experimental data presented in Figure 24 are tabulated in Table 9. Column 1 is the experimentally obtained pH. Column 2 is $[\text{Hg}^{+2}]$ calculated using the Nernst equation as defined by Equation [7]. As seen from this column, the concentration of free mercury ions is very small (i.e. $[\text{Hg}^{+2}]$ is always less than $1 \times 10^{-12} \text{ M}$), which indicates that all of the mercury is complexed. Column 3 is the concentration of mercuric hydroxide, $\text{Hg}(\text{OH})^{+}$, calculated with the following equation, using a value of

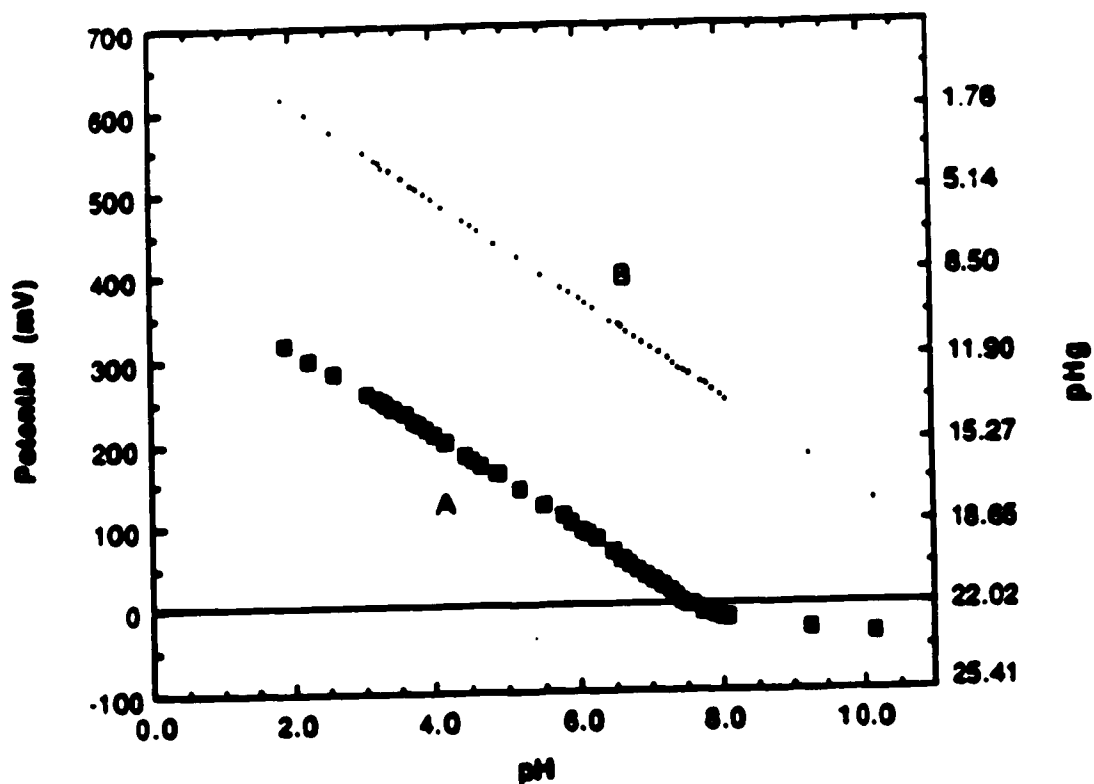


Figure 24. Potential-pH diagram for a solution in which the Hg^{+2} :TAHA ratio is 1.00:1.60. The total concentration of Hg^{+2} and TAHA is 1.189 mM and 1.968 mM respectively for curve A. Curve B represents the theoretical upper potential limit at the mercury indicating electrode. The right y axis represents the calculated pHg values.

Table 9. Tabulation of the concentrations of various mercury containing species, Hg^{+2} , $\text{Hg}(\text{OH})^+$, and $\text{Hg}(\text{TAHA})^{-4}$, and conditional formation constants, as a function of pH. The results presented in this table are for a solution in which $[\text{Hg}^{+2}]$ and $[\text{TAHA}]$ were 1.189 mM and 1.968 mM respectively.

pH	$[\text{Hg}^{+2}]$	$[\text{Hg}(\text{OH})^+]$	$[\text{HgL}]$	$[\text{L}]$	$\text{Log } K_{\text{HgL}}^c$
1.89	6.08×10^{-12}	4.72×10^{-14}	1.12×10^{-3}	8.70×10^{-4}	11.33
2.23	1.39×10^{-12}	2.34×10^{-14}	1.12×10^{-3}	8.70×10^{-4}	11.97
2.56	3.69×10^{-13}	1.35×10^{-14}	1.12×10^{-3}	8.70×10^{-4}	12.54
3.02	5.71×10^{-14}	5.94×10^{-15}	1.12×10^{-3}	8.70×10^{-4}	13.35
3.24	2.25×10^{-14}	3.90×10^{-15}	1.12×10^{-3}	8.70×10^{-4}	13.76
3.40	1.21×10^{-14}	3.00×10^{-15}	1.12×10^{-3}	8.70×10^{-4}	14.03
3.69	3.47×10^{-15}	1.71×10^{-15}	1.12×10^{-3}	8.70×10^{-4}	14.57
3.87	1.59×10^{-15}	1.18×10^{-15}	1.12×10^{-3}	8.70×10^{-4}	14.91
4.1	4.59×10^{-16}	6.53×10^{-16}	1.12×10^{-3}	8.70×10^{-4}	15.45
4.40	1.55×10^{-16}	3.93×10^{-16}	1.12×10^{-3}	8.70×10^{-4}	15.92
4.69	5.62×10^{-17}	2.42×10^{-16}	1.12×10^{-3}	8.70×10^{-4}	16.36
4.87	2.58×10^{-17}	1.90×10^{-16}	1.12×10^{-3}	8.70×10^{-4}	16.70
5.16	5.89×10^{-18}	8.52×10^{-17}	1.12×10^{-3}	8.70×10^{-4}	17.34
5.52	1.34×10^{-18}	4.44×10^{-17}	1.12×10^{-3}	8.70×10^{-4}	17.98
5.89	2.43×10^{-19}	1.90×10^{-17}	1.12×10^{-3}	8.70×10^{-4}	18.72
6.04	1.21×10^{-19}	1.31×10^{-17}	1.12×10^{-3}	8.70×10^{-4}	19.03
6.24	4.74×10^{-20}	8.16×10^{-18}	1.12×10^{-3}	8.70×10^{-4}	19.43
6.49	1.37×10^{-20}	4.18×10^{-18}	1.12×10^{-3}	8.70×10^{-4}	19.97
6.63	6.78×10^{-21}	2.89×10^{-18}	1.12×10^{-3}	8.70×10^{-4}	20.28
6.82	2.66×10^{-21}	1.75×10^{-18}	1.12×10^{-3}	8.70×10^{-4}	20.68
7.05	1.05×10^{-21}	1.18×10^{-18}	1.12×10^{-3}	8.70×10^{-4}	21.09
7.27	3.53×10^{-22}	6.55×10^{-19}	1.12×10^{-3}	8.70×10^{-4}	21.56
7.44	1.50×10^{-22}	4.12×10^{-19}	1.12×10^{-3}	8.70×10^{-4}	21.93
7.59	9.40×10^{-23}	3.65×10^{-19}	1.12×10^{-3}	8.70×10^{-4}	22.14
7.80	4.67×10^{-23}	2.94×10^{-19}	1.12×10^{-3}	8.70×10^{-4}	22.44
8.09	3.16×10^{-23}	3.92×10^{-19}	1.12×10^{-3}	8.70×10^{-4}	22.61
9.22	1.24×10^{-23}	2.07×10^{-18}	1.12×10^{-3}	8.70×10^{-4}	23.02

$10^{10.1}$ for K_{HgOH} (30):



$$K_{\text{Hg}(\text{OH})} = \frac{[\text{Hg}(\text{OH})^+]}{[\text{Hg}^{+2}] [\text{OH}^-]} \quad [91]$$

where $[\text{Hg}^{+2}]$ is the value obtained from the mercury electrode potential and $[\text{OH}^-]$ is calculated using Equation [92]:

$$K_w = [\text{OH}^-][\text{H}^+] \quad [92]$$

where $K_w = 1.0 \times 10^{-14}$ and $[\text{H}^+]$ was calculated from the experimentally measured pH. The solution remained clear over the pH range studied indicating that correction for the neutral species, $\text{Hg}(\text{OH})_2$, was not necessary. Since all the mercury is complexed to TAHA, as indicated by the low Hg^{+2} concentration (see Table 9), conditional formation constants, K_{HgL}^c , were calculated at each pH value using the following equation:

$$K_{\text{HgL}}^c = \frac{[\text{HgL}]}{[\text{Hg}^{+2}] [\text{L}]_f} \quad [93]$$

where HgL represents the total concentration of $\text{Hg}(\text{TAHA})^{-4}$ species and $[\text{L}]_f$ represents the total concentration of unbound ligand. The term $[\text{L}]_f$ was calculated using the following equations:

$$[\text{HgL}] = C_{\text{Hg}} \quad [94]$$

and

$$[L]_f = C_L - C_{Hg} \quad [95]$$

where C_L and C_{Hg} represent the total concentration of TAHA and Hg^{+2} present in solution. The above Equations assume that all the mercury is bound as the mononuclear complex (HgL) in solution. Substitution of the calculated $[HgL]$ and $[L]_f$ values, together with the measured $[Hg^{+2}]$, into Equation [93] gives a value for K_{HgL}^C at any given pH. $[HgL]$ and $[L]_f$ for this experiment are tabulated in column 4 and column 5 of Table 9 respectively. The logarithms of K_{HgL}^C at each pH value were calculated using equation [93] and are tabulated in column 6.

In Figure 25 there are two plots of logarithm of K_{HgL}^C versus pH for solutions in which excess TAHA is present ($Hg^{+2}:L$ is approximately 1:2). The two plots in this figure are from two duplicate runs. The open squares are results obtained from a solution in which the Hg^{+2} and TAHA concentrations were 1.189 mM and 1.968 mM respectively, while the darkened circles are the results obtained from a ten-fold dilution of the Hg^{+2} and TAHA concentrations (0.104 mM Hg^{+2} , 0.2095 mM TAHA). As seen from Figure 25, the calculated logarithm of K_{HgL}^C obtained from two separate experiments in which the total concentration of mercury and TAHA present differed by a factor of ten, gave identical calculated values for K_{HgL}^C , as determined by the pHg method. From these plots and the tabulated values presented in Table 9, it is obvious that TAHA complexes of mercury ions are extremely stable, even at low pH values. At the lowest pH value (pH 1.89), a value of 11.33 for logarithm of K_{HgL}^C is

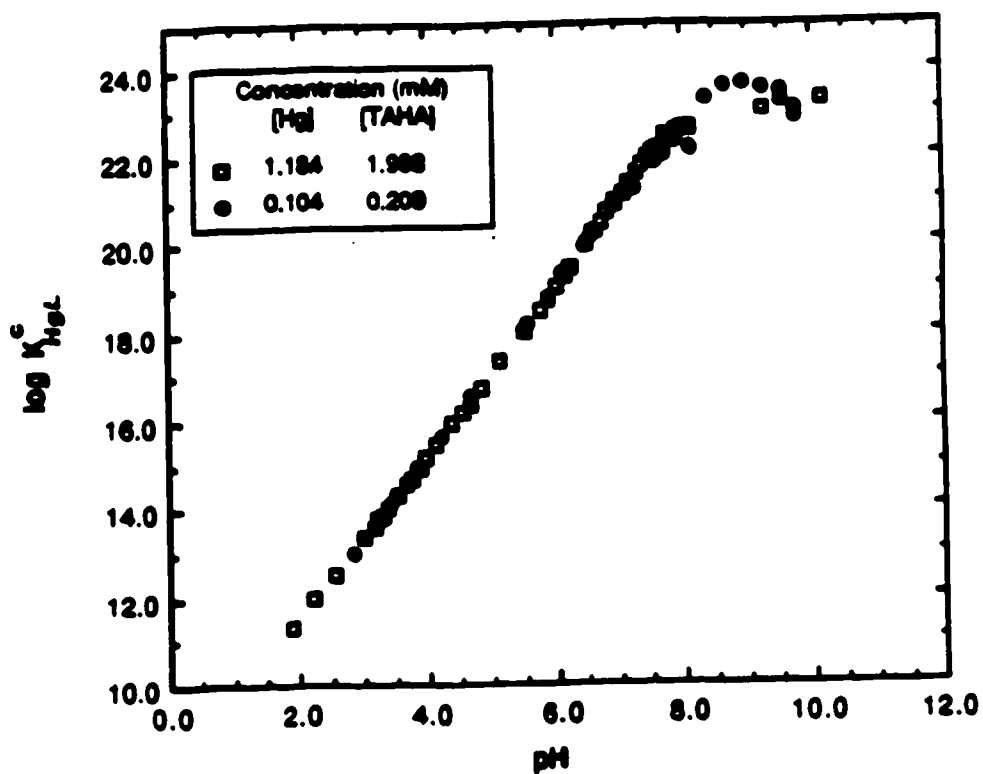


Figure 25. Plot of K_{HgL}^c as a function of pH for duplicate runs of Hg⁺²:TAHA in a ratio of 1.0:2.0. The darkened circles represent data obtained for a ten fold dilution in concentration in comparison with the open squares.

obtained. The potential (and therefore the concentration of free mercury) is pH independent at pH values greater than 11.0 where the ligand is totally deprotonated (see Figure 22). At high pH values, because the ligand is in the totally deprotonated form (TAHA⁻⁶), the stability constant K_{HgL} may be extrapolated; such extrapolation from these experimental results gave a logarithm of K_{HgL} value of 23.59 ± 0.02 ; for a separate experiment, a value of 23.60 ± 0.01 was obtained using the above method. For the calculation of pH-independent formation constants, different models which assumed the formation of different protonated and non-protonated mercury-TAHA complexes were considered. The model which best fit the experimental results assumed the formation of the mononuclear species $\text{HgH}_2\text{L}^{-2}$ and HgHL^{-3} species in the pH range 2.8 to 5.2. For the calculation of the stability constants for these two protonated complexes it was assumed that these species were dominant from approximately pH 3.0 to 5.0. The triprotonated and diprotonated mercury-TAHA complexes occur in the buffer region where A varies from 3 to 6 (pH also varies from 3 to 6). However when the formation of the complex $\text{HgH}_3\text{L}^{-1}$ was incorporated into the above model, linear regression analysis of such a model did not fit the experimental results. Although such pH titration curves are usually indicative of the number of protons remaining on the metal-ligand complex, they must be interpreted with some degree of caution. As stated earlier, Harju (98) has reported that marked buffer regions may be interpreted as due to the formation of stable protonated mononuclear complexes or due to the presence of other complexes such as bimetal complexes.

The following equations describe the calculation of $K_{\text{HgH}_2\text{L}}$ and K_{HgHL} using the $K_{\text{HgL}}^{\text{C}}$ values obtained from the pHg data:

$$K_{\text{HgL}}^c = \frac{[\text{total bound HgL species}]}{[\text{Hg}^{+2}] [\text{L}]_f} \quad [96]$$

$$K_{\text{HgL}}^c = \frac{([\text{HgH}_2\text{L}] + [\text{HgHL}])}{[\text{Hg}^{+2}] [\text{L}]_f} \quad [97]$$

By substitution for $[\text{HgHL}]$ and $[\text{HgH}_2\text{L}]$ using Equation [74], Equation [97] may be written in the following manner:

$$K_{\text{HgL}}^c = \frac{K_{\text{HgH}_2\text{L}} [\text{Hg}^{+2}] [\text{H}_2\text{L}] + K_{\text{HgHL}} [\text{Hg}^{+2}] [\text{HL}]}{[\text{Hg}^{+2}] [\text{L}]_f} \quad [98]$$

Using the acid dissociation constant, K_5 , to substitute for $[\text{H}_2\text{L}]$, and eliminating the common term $[\text{Hg}^{+2}]$, equation [98] becomes

$$K_{\text{HgL}}^c = \frac{K_{\text{HgH}_2\text{L}} [\text{HL}] [\text{H}]}{K_5 [\text{L}]_f} + \frac{K_{\text{HgHL}} [\text{HL}]}{[\text{L}]_f} \quad [99]$$

The term $[\text{HL}]$ may be calculated using the species distribution coefficient, α_5 (α_{HL}), as defined in the previous chapter:

$$\alpha_{\text{HL}} = \alpha_5 = \frac{[\text{HL}]}{[\text{L}]_f}$$

Equation [99] may be rewritten as

$$K_{\text{HgL}}^c = \frac{K_{\text{HgH}_2\text{L}} [\text{H}]}{K_5} \alpha_5 + K_{\text{HgHL}} \alpha_5 \quad [100]$$

and can be rearranged into an equation for a straight line in the form $y = mx + b$:

$$\frac{K_{\text{HgL}}^{\text{C}}}{[\text{H}] \alpha_5} = \frac{K_{\text{HgH}_2\text{L}}}{K_5} + K_{\text{HgHL}} \frac{1}{[\text{H}]} \quad [101]$$

where

$$x = \frac{1}{[\text{H}]}$$

and

$$y = \frac{K_{\text{HgL}}^{\text{C}}}{[\text{H}] \alpha_5}$$

The slope of a plot of $(K_{\text{HgL}}^{\text{C}} (\alpha_5[\text{H}])^{-1})$ versus $([\text{H}])^{-1}$ is equal to K_{HgHL} , while the y intercept is equal to $K_{\text{HgH}_2\text{L}}(K_5)^{-1}$. A linear regression analysis was performed on the data between the pH range 2.8 to 5.2 for the calculation of the slope and y intercept. A plot of Equation [101] and its best fit line is presented in Figure 26. Once the values were obtained for $K_{\text{HgH}_2\text{L}}$ and K_{HgHL} , the constant $K_{\text{HgH}_2\text{L}}^{\text{H}}$ was calculated using equation [64]. The values obtained for $K_{\text{HgH}_2\text{L}}$, K_{HgHL} , and $K_{\text{HgH}_2\text{L}}^{\text{H}}$ for duplicate runs, and the average stability constants along with the correlation coefficient for the best fit line, are tabulated in Table 10.

It must be noted that for the average stability constants reported in Table 10 the formation of bimetal complexes were not incorporated into the above model. As discussed earlier, when such complexes were included in the derivation, curved plots were obtained rather than linear plots. All possible equilibria at all pH ranges were considered; that is, calculation of the formation of $\text{Hg}_2\text{H}_2\text{L}^{-2}$, $\text{HgH}_3\text{L}^{-1}$, $\text{Hg}_2\text{HL}^{-2}$ and HgHL^{-3} over several pH ranges and A

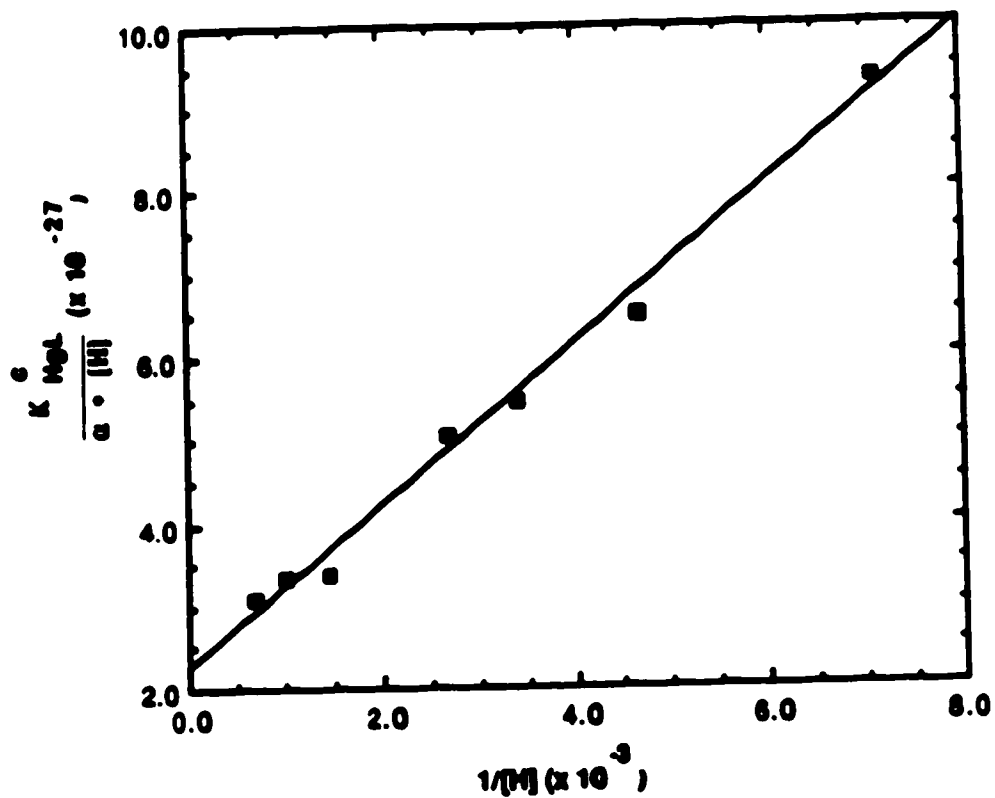


Figure 26. Plot of the linear regression analysis for the calculation of $K_{H_2H_2L}$ and $K_{H_2H_2L}$ using Equation [101]. The symbols represent experimental data points while the straight line represents the best fit line.

Table 10. Tabulation of stability constants for protonated mercury-TAHA complexes (25 °C, μ = 0.1 M KNO₃).

pH Independent Range	K_{HgHL}	$K_{\text{HgH}_2\text{L}}$	$K_{\text{HgH}_2\text{L}}^{\text{H}}$	Correlation Coefficient
3.02 to 5.16 ¹	7.01×10^{23}	5.76×10^{18}	2.30×10^{-4}	0.991
2.80 to 4.69 ²	9.73×10^{23}	4.41×10^{18}	4.17×10^{-4}	0.999
average	8.37×10^{23}	5.09×10^{18}	3.24×10^{-4}	
log K	23.92 ± 0.1	18.71 ± 0.08	-3.38 ± 0.2	

¹ 1.1840 mM Hg²⁺, 1.9680 mM TAHA

² 0.1040 mM Hg²⁺, 0.2095 mM TAHA

values was attempted. All such attempts were unsuccessful; when such theoretical models were analyzed with the experimental $K_{\text{HgL}}^{\text{C}}$ and pH (Figure 25), curved plots rather than the expected linear plots were always obtained. The values given in Table 10 are the results from the model that best fit the experimentally obtained conditional formation constants presented in Figure 25. As will be discussed below, it is assumed that these values are the right order of magnitude when compared with other mercury-ligand complexes.

As can be seen from Table 10 and Figure 26, the correlation coefficient for the best fit line is greater than 0.99 for both of the duplicate runs, indicating a good fit between the experimental data and the model which included the formation of the monoprotonated and diprotonated mercury-TAHA complexes. The two values for $K_{\text{HgH}_2\text{L}}$ (7.01×10^{23} and 9.73×10^{23}) are in good agreement with each other, especially in light of the fact that the concentration of the total mercury ion and TAHA present in solution had a ten-fold difference between the duplicate runs. Likewise, the two values for K_{HgHL} (5.76×10^{18} and 4.41×10^{18}) are also in good agreement with each other. Standard deviations for the logarithm of the stability constant of metal-ligand complexes often have variations between ± 0.1 to ± 1.0 (30); the standard deviations reported in Table 10 (± 0.08 and ± 0.1) are therefore quite low. There is a much higher standard deviation in the calculation of $K_{\text{HgH}_2\text{L}}^{\text{H}}$ (2.30×10^{-4} and 4.17×10^{-4}) between duplicate runs. This may be due partly to the fact that calculation of this constant involved a division between two very large numbers (K_{HgHL} and $K_{\text{HgH}_2\text{L}}$). Therefore, the error may be greatly magnified when the acid dissociation constant, $K_{\text{HgH}_2\text{L}}^{\text{H}}$, is calculated.

The logarithm of K_{HgHL} values for various monoprotonated mercury-ligand complexes are compared in Table 11. Values for $K_{\text{HgH}_2\text{L}}$ were not

Table 11. Comparison of the logarithm of K_{HgHL} values for various monoprotated mercury-ligand complexes (25.00 °C, $\mu = 0.1$ M KNO_3)

Ligand	H_nL	$\log K_{HgHL}$	ΣpK_n
EDTA ¹	H_4L	14.47	21.01
EGTA ¹	H_4L	16.56	22.98
EEDTA ¹	H_4L	16.15	22.96
DTPA ¹	H_5L	20.19	27.90
TAHA ²	H_6L	23.92	34.54
TTHA ¹	H_6L	21.90	35.28

¹ Reference 30

² This work, duplicate runs (see Table 10)

obtained for some of these ligands, or the values which were obtained were at different ionic strengths and/or different temperatures, hence comparisons of K_{HgH_2L} values for different ligands are not presented. For comparison purposes, the sums of the pK values (ΣpK 's) for each ligand is also reported in this table.

A plot of the logarithm of K_{HgHL} versus the sum of pK's (ΣpK 's) will give a straight line when all factors that influence the stability of the metal ligand complex, such as the nature of the metal ion, the number of rings formed upon chelation to the metal, and the size of the ring formation, is equal (103). Deviations from a straight line indicate that factors other than the ones mentioned above are also important. Bjerrum (104) has also pointed out that the deviations from this relationship could be accounted for on the basis of steric considerations. A plot of the logarithm of K_{HgHL} versus ΣpK 's for various ligands is presented in Figure 27. All of the ligands plotted have four to six carboxylate groups and several nitrogen atoms available for binding. Although there is no best fit straight line that can be drawn with a high degree of correlation, it is interesting to note the difference between TTHA and TAHA. Although the structures of these two compounds are very different, they both have six carboxylate groups and four nitrogen groups, and as shown in Figure 21, plots of α^* versus pH of these two hexaprotic ligands imply that stability constants of metal-ligand complexes would be similar in magnitude (as discussed in the previous chapter). The logarithm of K_{HgHL} is higher for TAHA even though the ΣpK 's were lower in comparison to TTHA. This may be partly due to the fact that the N2 nitrogens are more involved in binding with TAHA than the nitrogen atoms of TTHA. From these results it seems that the mercury ion in the $HgHL$ species is held more tightly by TAHA than by TTHA. This may

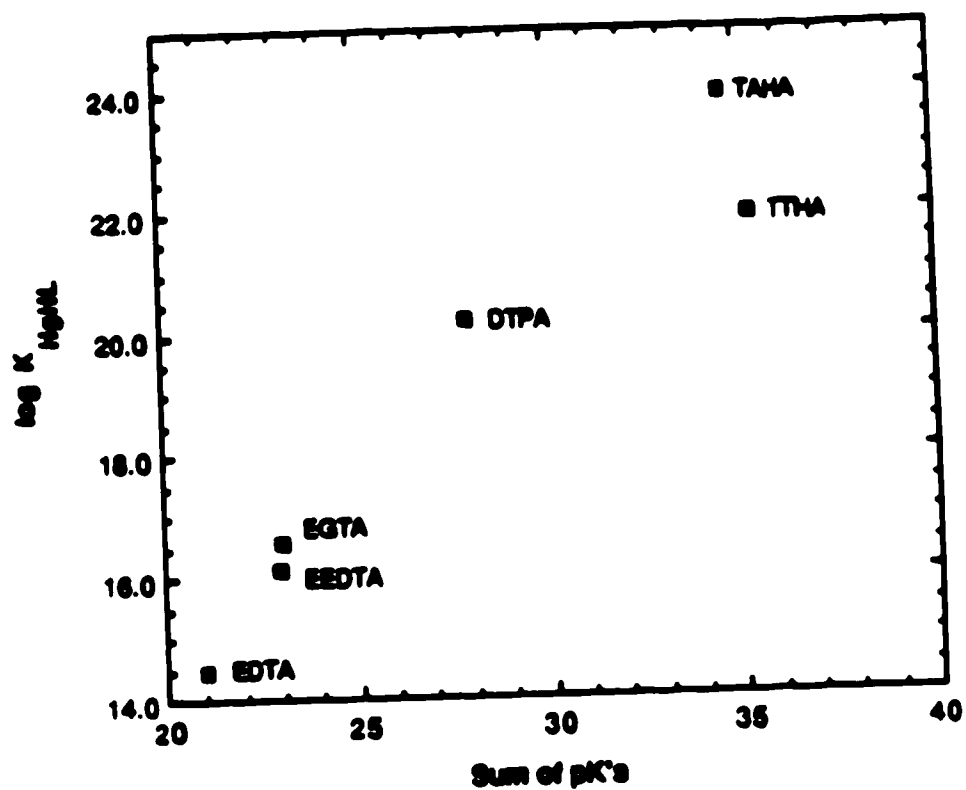


Figure 27. Plot of the logarithm of K_{HgHL} versus sum of $pK's$ ($\sum pK's$) for several mercury-ligand complexes.

in part also be due to differences in steric effects and the location of differences in steric effects and the location of the coordinating sites of TAHA and TTHA.

2. ^1H NMR Studies

To further characterize the mercury-TAHA system a D_2O solution of Hg^{+2} and TAHA, at a ratio of 1.06:1.0 (5.64 mM Hg^{+2} and 5.32 mM TAHA), was titrated with standardized KOD at a constant ionic strength of 0.1 M made with KNO_3 . Samples were withdrawn as the pH^* was varied, and ^1H -NMR spectra were measured. The titration was performed from a pH^* range of 2.07 to 11.81. All ^1H NMR spectra were obtained under the conditions described in Chapter II.

Figure 28 is a spectrum obtained at pH^* 4.62; the spectrum has been expanded in order to present a typical ^1H NMR spectrum obtained in the pH^* range 4.26 to 7.09, and also to explain the identification of the methylene protons of TAHA in the ^1H NMR binding studies of mercury with TAHA. Assignment of resonances to the T3, T2, and T1 methylene protons from TAHA bound to mercury was done by observation of chemical shift as a function of pH^* , relative intensities, and actual deconvolution results. In this figure, each resonance is labeled from 1 to 7 and will be referred to in this manner for the remainder of this section, i.e. the most downfield resonance will be referred to as peak 1 while the most upfield resonance will be referred to as peak 7. Identification of the spectrum in Figure 28 is as follows. Peak 1 at 3.801 ppm and peak 4 at 3.132 ppm are identified as resonances due to the T2 methylene protons; peak 2 at 3.469 ppm and peak 3 at 3.351 ppm are due to the resonances of the T3 methylene protons, and peak 5 at 2.985 ppm, peak 6 at 2.945 ppm and peak 7 at 2.841 ppm are all due to the resonances from the T1 methylene protons of TAHA which are complexed to mercury. A summary of the above information is given in Table 12. Also presented in this table are the

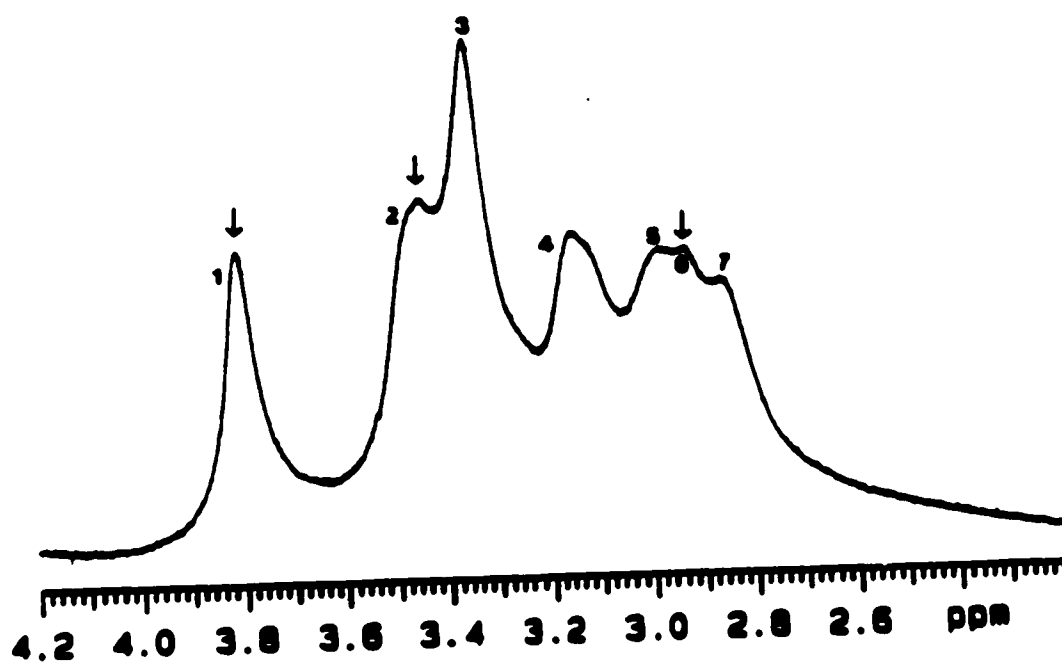


Figure 28. Typical ¹H NMR spectrum for a 1.0:1.0 solution of Hg⁺²:TAHA (1.06 mM Hg⁺², 5.32 mM TAHA) obtained in the pH⁺ range 4.26 to 7.09. Each resonance is labelled from 1 to 7, where peak 1 is the most downfield resonance.

Table 12. Tabulation of the chemical shift, linewidth, and assignment of each resonance observed in the ^1H NMR spectrum for the mercury-TAHA system (Figure 28).

Peak Label	Chemical Shift (δ , ppm)	Methylene Protons	$W_{1/2}$ (Hz)
1	3.801	T2	39.34
2	3.469	T3	61.44
3	3.351	T3	48.07
4	3.132	T2	76.71
5	2.985	T1	60.54
6	2.945	T1	24.34
7	2.845	T1	79.73

linewidths at half-height ($W_{1/2}$) for the spectrum in Figure 28. Typical linewidths obtained by deconvolution of data in the pH^* range 3.24 to 7.10 varied from 40-80 Hz.

Representative ^1H NMR spectra measured as a function of pH^* are presented in Figures 29A to 29E. The spectrum measured at a pH^* 2.07 exhibits three resonances which have a ratio for the T3:T2:T1 of 2.0:1.0:1.0 which is the theoretical ratio of TAHA in solution; however the chemical shifts of these resonances are very different from those of the free TAHA. It is assumed that in spectrum 28A different protonated mercury-TAHA species (HgH_nL) are in fast exchange with each other at these low pH^* values. The shift of the three resonances in spectrum 29 as the pH^* is changed is indicated by the arrows in Figures 29B to 29E.

The spectra obtained between pH^* 3.2 to 3.6 were very noisy and very broad, and none of the resonances could be clearly distinguished due to the appearance of a "large hump". The resonances in the pH^* range 3.25 to 5.50 were very complex due to the presence of broad and overlapped resonances (see spectra 28, 29B and 29C). In this region, there are seven different resonances and deconvolution output for data from this region provided useful information which will be discussed in more detail later.

After pH^* approximately 7.3 (spectrum 29D) three broadened resonances are again observed. These resonances become narrower as the pH^* is raised to 9.43 indicating that there is again fast exchange among the different mercury-TAHA species present at high pH values.

The ligand TAHA has 12 T3-type protons, 6 T2-type protons and 6 T1-type protons. In any given spectrum the ratio of all resonances due to the T3 methylene protons should be twice that of the resonances due to either T2 or T1 methylene protons. Also the ratio of total resonance intensities from each

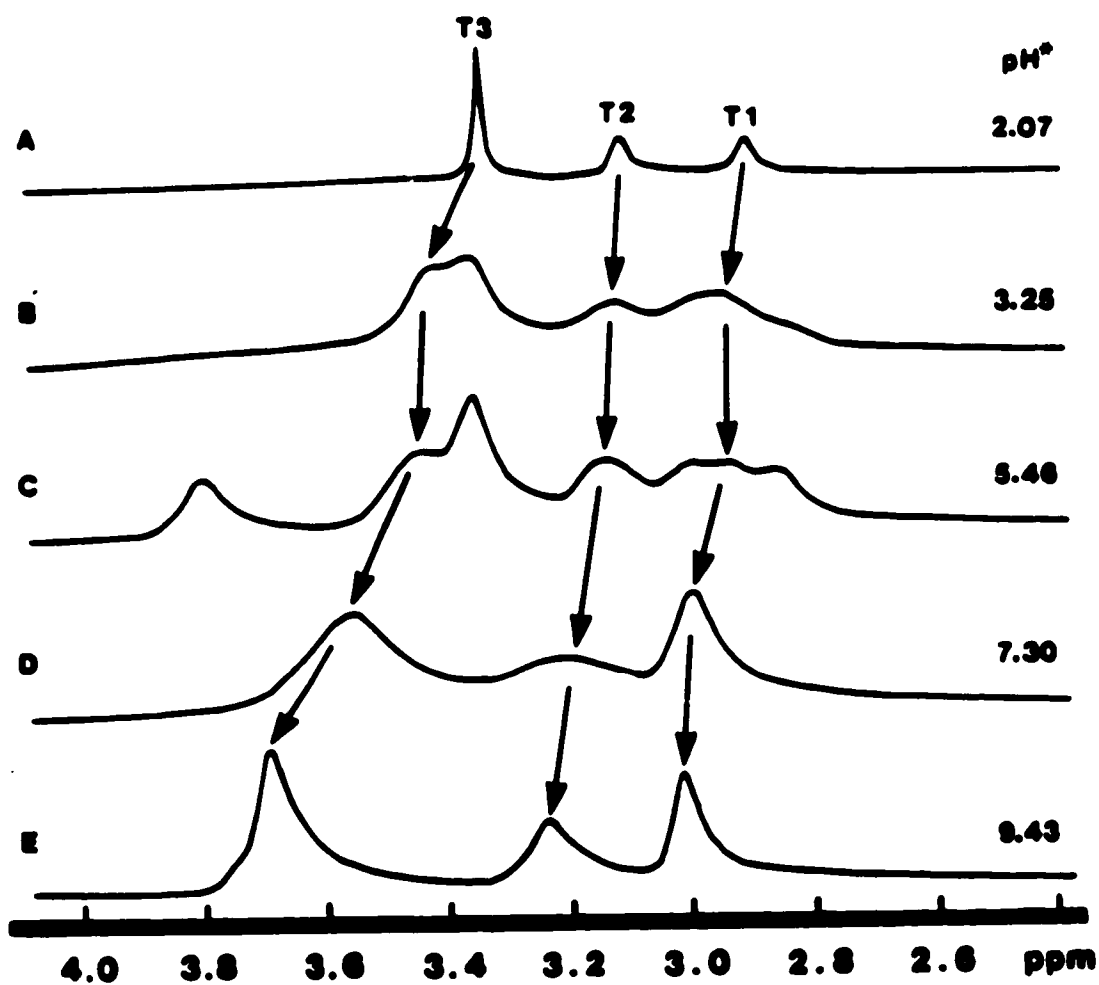


Figure 29. ^1H NMR spectra for a 1.0:1.0 solution of Hg^{+2} :TAHA (1.06 mM Hg^{+2} , 5.32 mM TAHA), as a function of pH^* .

different proton should remain constant at any given pH*. This was studied for spectra similar to that presented in Figures 28 and 29C, where the areas for each resonance were obtained from deconvolution of the data. The next several figures will present the trends observed from the relative ratios or the fractions of two of the three methylene protons of TAHA as a function of pH* in order to confirm the assignment of each resonance of bound TAHA given in Table 12.

Figure 30 is a comparison of the fraction of the total intensity of all resonances due to the T3 and T1 methylene protons of TAHA. Curve 1, which is the fraction of the T3 methylene protons, $T3/(T3+T1)$, has a theoretical value of 0.66 while curve 2, which is the fraction of the T1 methylene protons, $T1/(T3+T1)$, has a theoretical value of 0.33. Both curves should remain constant since all resonances arising from the T3 and T1 protons remain constant regardless of the type of complex(es) formed. As can be seen from Figure 30, curves 1 and 2 are constant, however, the average fraction of resonances due to the T3 methylene groups (curve 1) is 0.6 while the average fraction of resonances due to the T1 methylene protons is 0.4. This may be due to two factors: firstly, an experimental error or a systematic error in the curve fitting that was not detected, or secondly, it may be due to resonances that are under the broad resonances observed in Figure 28. The latter is more likely since as three separate resonances due to the T1 methylene protons are observed, there should be three separate resonances due to the T3 methylene protons. As only two resonances from the T3 methylene protons are observed, the third resonance may be beneath the broad resonance that is observed for the T2 methylene protons. This is further illustrated by Figure 31 which depicts the fraction of the total intensity of all the resonances due to the T3 and T2 methylene protons. As can be seen from this figure, the relative fraction of

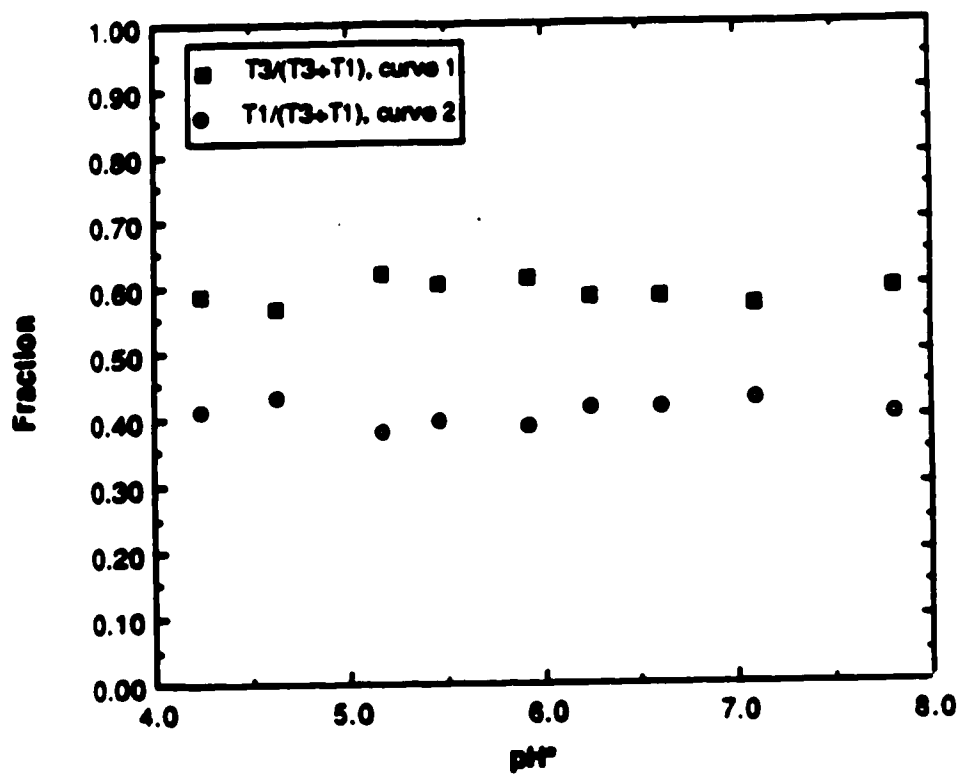


Figure 30. Comparison of ^1H NMR resonances due to the T1 and T3 methylene protons of TAHA complexed to mercury as a function of pH^* . The circles represent the fraction of the total intensity of T1 methylene resonances, while the squares represent the fraction of total intensity of T3 methylene resonances.

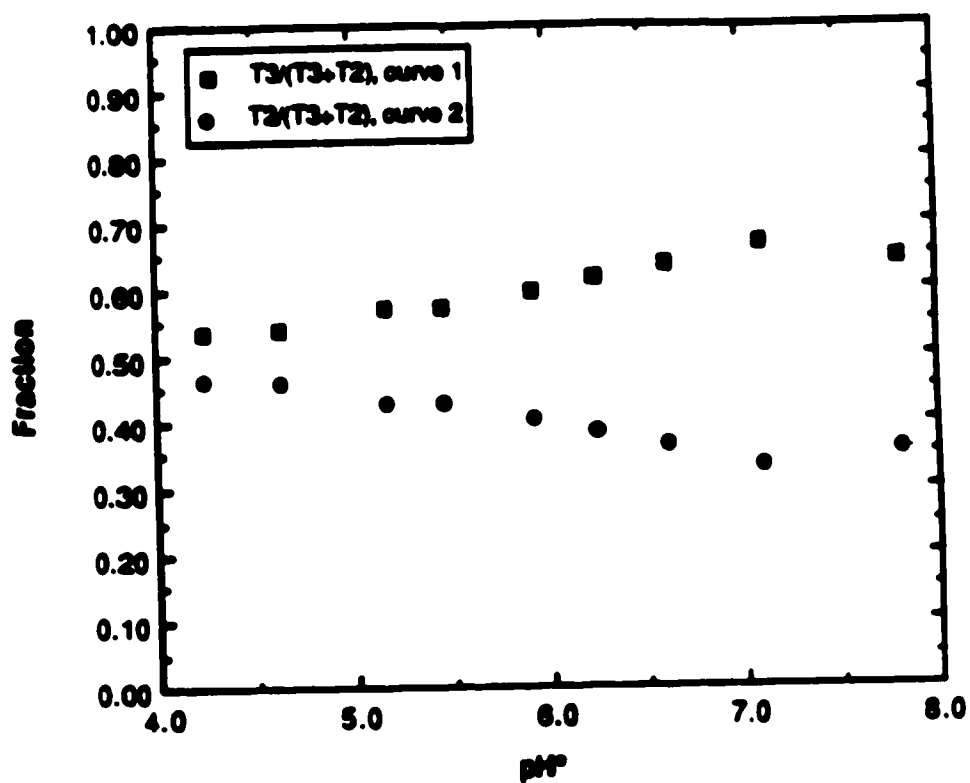


Figure 31. Comparison of the ^1H NMR resonances due to T2 and T3 methylene protons of TAHA complexed to mercury, as a function of pH^* . The circles represent the fraction of total intensity of T2 methylene resonances, while the squares represent the fraction of total intensity of T3 methylene resonances.

resonances due to the T3 methylene protons, $T3/(T3+T2)$, represented in curve 1 seems to increase with a corresponding decrease in the fraction of resonances due to the T2 methylene protons, $T2/(T3+T2)$, presented in curve 2. At pH* 7.1 the fraction of the resonances due to the T3 methylene protons is 0.64 while the fraction of the resonances due to the T2 methylene protons is 0.33. This approaches the theoretical ratios of 0.66 and 0.33 respectively. At a lower pH* (4 to 6) the presence of protonated species such as HgH_nL , which become deprotonated as the pH* is raised may account for this type of behavior.

Both Figures 30 and 31 indicated the possibility of small resonances in the range 3 to 4 ppm where there is a broad envelope. These resonances may be in fast exchange with the resonances from the T3 and T2 methylene protons of bound TAHA, arising from different mercury complexes of TAHA that may be present only in very low concentrations.

The fraction of the total intensity due to the resonances giving rise to the T2 and T1 methylene groups should be equal since they are both due to six protons. Similar plots of the relative fractions of resonances from the T2 and T1 methylene protons were close to the theoretical ratio of 0.5 between pH* 6.0 to 7.0. However, the relative resonances due to the T2 protons decreased from pH* 6.0 to 7.0 (figure not shown).

In Figure 28, there are two resonances, at 3.801 ppm and 3.132 ppm (peak 1, Figure 28), due to the T2 methylene protons. These assignments were made by observation of the behavior of these two resonances as a function of pH*. It appeared that the resonance at 3.132 ppm increased in intensity (i.e. area) as the resonance at 3.801 ppm decreased. Figure 32 illustrates this point more clearly. After pH* 5.0 it is seen that the relative fraction of peak 4

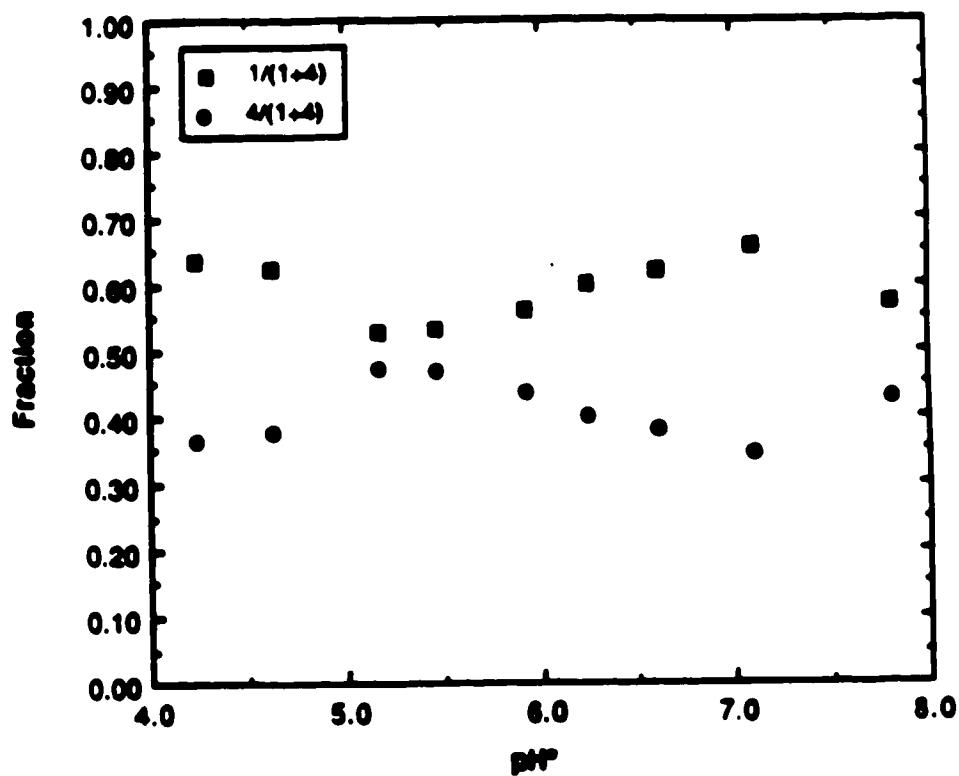


Figure 32. Comparison of the two ^1H NMR resonances, assigned as peak 1 and peak 4 in Figure 28, due to the T2 methylene protons of TAHA complexed to mercury. The circles represent the fraction of total intensity of peak 4, while the squares represent the fraction of total intensity of peak 1.

increases with pH^* while the relative fraction of peak 1 decreases with pH^* . Because of this trend, it appears that since the relative area of peak 1, Figure 32 decreases as pH^* increases, the resonance which gives rise to the peak must be more protonated than the resonance which gives rise to peak 4. Below pH^* 4.0 the curve fitting of the spectra was difficult because peak 1 appeared as a very broad hump, and deconvolution results in this region were questionable.

A plot of the chemical shift of each of the seven resonances (labeled in Figure 28 as peaks 1 to 7) as a function of pH^* , is presented in Figure 33. The chemical shift dependence of free or unbound TAHA obtained under identical experimental conditions is also presented for comparison purposes. There are several important points that can be observed from this figure. At pH^* values less than 4.0, peak 2 (due to the bound T3 methylene protons of TAHA) has a chemical shift versus pH^* behavior quite similar and to that of the free T3 methylene protons of TAHA. This confirms that the resonance labeled as peak 2 is indeed due to the methylene protons closest to the carboxylate groups. By similar analysis it is confirmed that peak 4 (due to the T2 bound methylene protons of TAHA) is less affected by the deprotonation of the carboxylate groups; therefore, the identification of the bound T2 methylene protons of TAHA as being the next closest group to the carboxylate group, is correct, i.e. these protons are next to the N2 nitrogen atoms. Likewise, peak 6 (due to the bound T3 methylene protons of TAHA) is the least affected by the deprotonation at the carboxylate groups, hence they are next to the N1 or central nitrogen atom. Both curves due to peaks 2 and 4 of the mercury TAHA complex mimic the corresponding curves for the T3 and T2 curves of the unbound TAHA, however they are displaced upfield due to the binding with the mercury ion. These results also indicate that all of the six carboxylate groups are not bound to the mercury ion when complexation occurs.

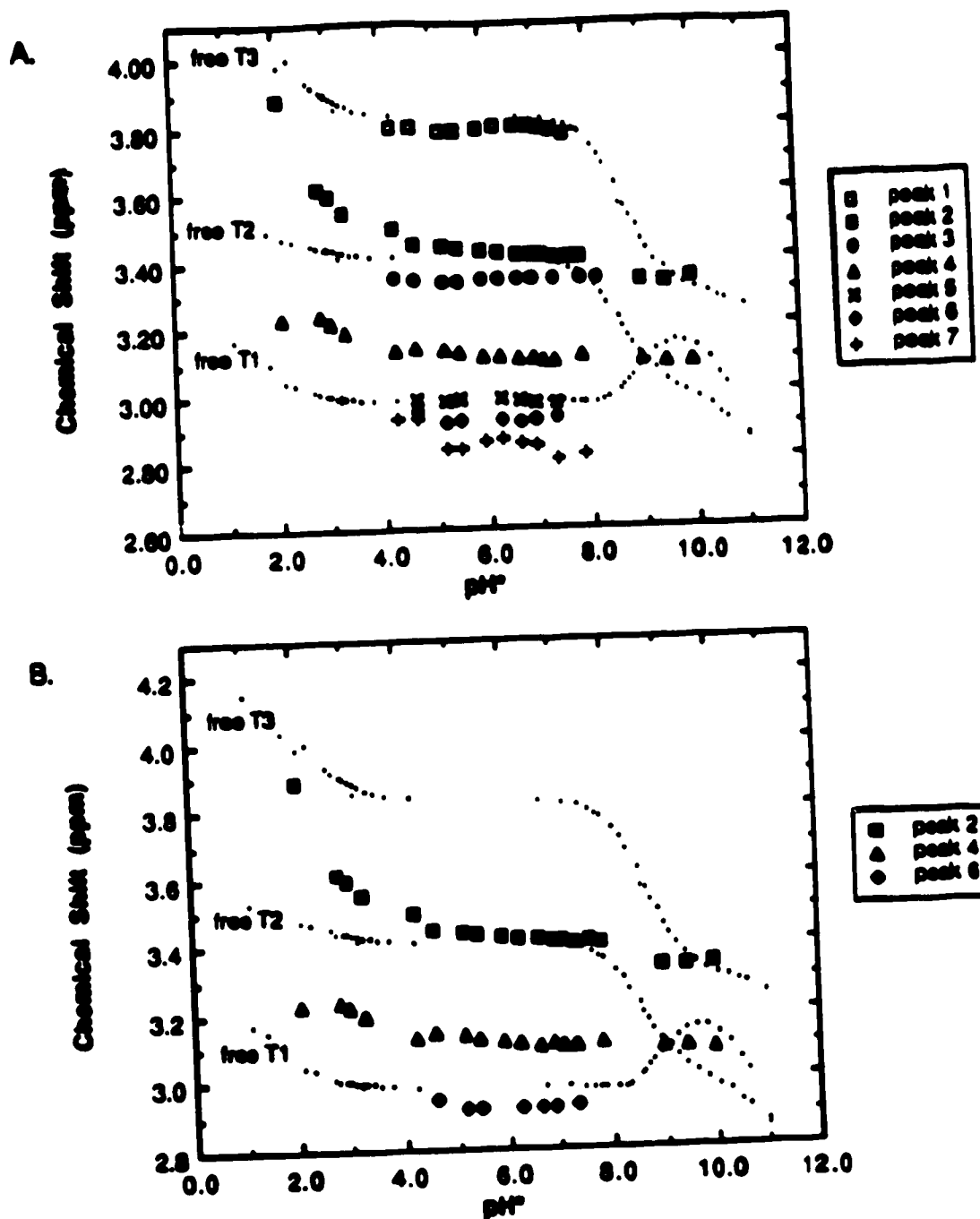


Figure 33. Chemical shift (ppm) as a function of pH^* for the mercury-TAHA system. Assignments of peaks 1 to 7 are presented in Figure 28. The chemical shift dependence of the resonances for free TAHA is also presented. The chemical shift dependence of peaks 2 and 6, due to the T3 methylene protons and peak 4, due to the T2 methylene protons of TAAHA are replotted in 33B for clarity.

Between pH* 7.5 and 10.0 peaks 4 and 6 do not have the deprotonation/migration behavior which is observed for free TAHA in solution. The chemical shifts of both of these peaks remain constant as a function of pH*, although there appears to be a slight downfield shift for the peak 2 which implies that there is something occurring at the N2 nitrogen atoms in this pH* range. If there were a proton(s) present on the N2 nitrogens, it would be reflected in a much more pronounced change in the chemical shift of peak 4. The slight downfield shift of the T3 methylene protons may be due to the rearrangement of the mercury-TAHA complex. This assumes that all three of the carboxylate protons were titrated prior to pH* 4.0 which seems reasonable when looking at the magnitude of the change in chemical shift of the peak 2 curve between the pH* range 2.0 to 4.0 and considering the acid dissociation behavior of carboxylate groups of free TAHA as described in the previous chapter.

The above results indicate that, in a 1.0:1.0 solution of Hg^{+2} :TAHA, there is a definite interaction of the mercury ion with the N2 nitrogen atoms and perhaps with the central nitrogen atom. In this pH* range the potentiometric (see Figure 22) A value varies from 4 to 5, indicating that there is two protons present on the mercury TAHA complex at pH* 7.5. At this time the exact location of the proton is uncertain.

It seems unlikely that only the nitrogen atoms are involved in the mercury-TAHA complexes since there are a maximum of six available carboxylate coordination sites; it is probable that there are interactions with some of the carboxylate groups for all possible mercury-TAHA complexes formed.

Such behavior of the ligand TAHA is not unreasonable. Hagen *et al.* (105) have reported that coordination of the tetra anion of EDTA to metal ions

occurs by means of relatively strong bonds to the nitrogen sites and weaker bonds to the carboxylate group site.

At no time in the ^1H NMR experiments was ^1H - ^{199}Hg coupling observed for the mercury-TAHA system. This is likely due to "exchange decoupling." The ^{199}Hg couplings in ^1H NMR are difficult to observe and are usually very broad, especially at high field strengths, due to chemical shift anisotropy. Recently, Ried and Podanyi (91) have reported that they have observed ^1H - ^{199}Hg coupling constants for the Hg^{+2} -glycine system through a heteroatom. The authors have stated that "to their knowledge, such coupling has not previously been observed." If this coupling was present, it may not have been observed due to the presence of broad and overlapped resonances (see Figure 27). If it is assumed that no coupling is observed, the mercury-nitrogen bonds and the mercury-oxygen bonds, can be said to have short lifetimes on the NMR time scale. This would be indicated in a relatively simple ^1H NMR spectrum due to internal averaging; the spectra obtained (Figures 28 and 29) may be due to "simple ^1H NMR spectra" from several different mercury-TAHA species which results in the observation of a single overlapped spectrum at any given pH^* .

Excess $\text{Hg}(\text{NO}_3)_2$ was added to one of the samples so that a permanent precipitate was present (the Hg^{+2} :TAHA ratio was 2.7:1.0). The final pH^* of this solution was 1.52. The ^1H NMR spectrum of this sample is presented in Figure 34A. The three resonances observed were at 3.821 ppm, 3.253 ppm and 3.039 ppm. This spectrum is similar to that in Figure 29A except that all the resonances are slightly shifted downfield due to the lower pH^* of this solution. The precipitate is probably due to the trinuclear complex Hg_3L as described earlier. Enough carbonate-free KOD was added to this sample to barely dissolve the precipitate present. The final pH^* was approximately 5.2 (see Figure 34B). The resulting spectrum is quite complex but seems similar to those

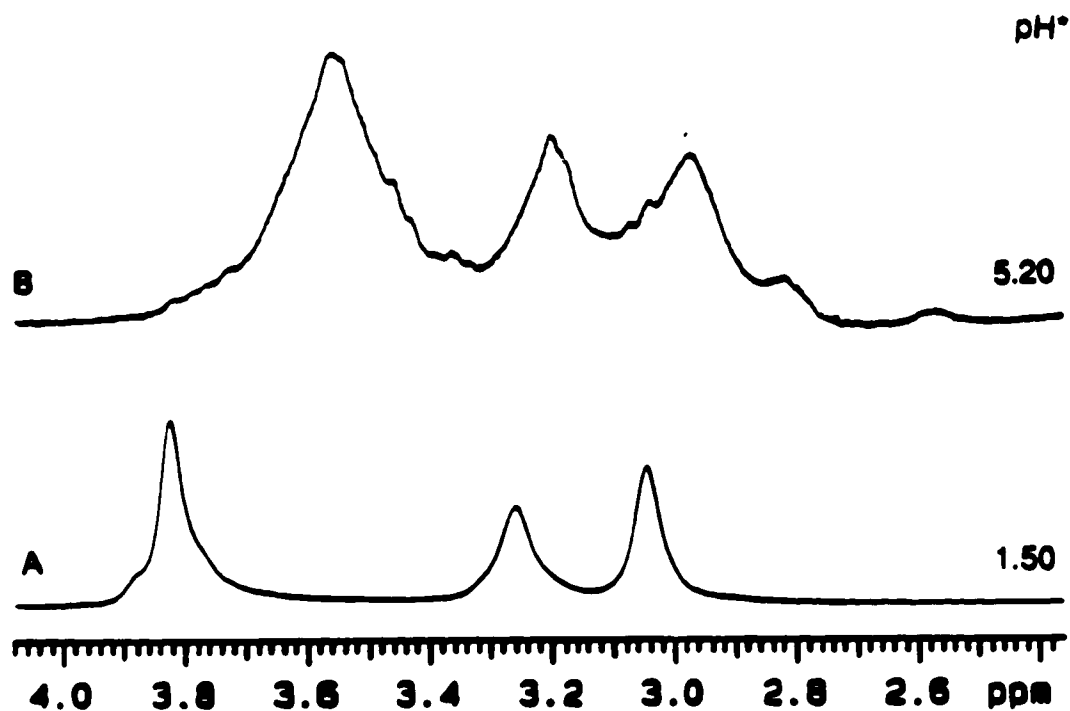


Figure 34. ^1H NMR spectra of a sample in which the Hg^{+2} :TAHA ratio is 2.7:1.0; A. In the presence of precipitate. B. After the precipitate was completely dissolved by the addition of carbonate free KOD.

obtained in Figure 29 (B and C). Comparison with the curve for the Hg^{+2} :TAHA ratio of 1.8:1.0 presented in Figure 22 indicates that at $\text{pH}^* 5.2$ there is at least one proton present in the complex. Since the exact structure of the precipitate is unknown (see results from the elemental analysis presented in Chapter III), that is, whether the trinuclear complex is in a polymer or dimer form, the structure of the dissolved species remains uncertain after the present study .

The pH^* region between 4.24 to 7.20 was curve fitted by the deconvolution program provided by the Varian software. Although the results of deconvolution of the mercury-TAHA system were not utilized for the calculation of stability constants, such results were later used for the calculation of formation constants for other metal-TAHA complexes. It was therefore necessary to determine the reproducibility, precision and any systematic errors present in the program as well as to make comparisons with earlier NMR computer fitting programs that are well documented in the literature (72-74).

As stated in Chapter II, the numerical output provided by the Varian deconvolution program includes the frequency of each resonance, its height, linewidth ($W_{1/2}$), the integral of the area of the resonance, as well as an indication of the goodness of fit, as measured by χ^2 . After the iteration is complete a plot of the original spectrum, the calculated spectrum, and each of the component lines is obtained. A typical plot is presented in Figure 35A which is a spectrum obtained for a sample at $\text{pH}^* 5.17$. The total number of iterations necessary for convergence was 29 and the final χ^2 obtained was 4425. The deconvolution output in Figure 35B was obtained under identical parameter settings, except that the input parameters stated that there were a total of eight resonances present in the original spectrum. Figure 35B converged after 42 iterations and had a final χ^2 of 10562, which is 2.4 times larger than the χ^2

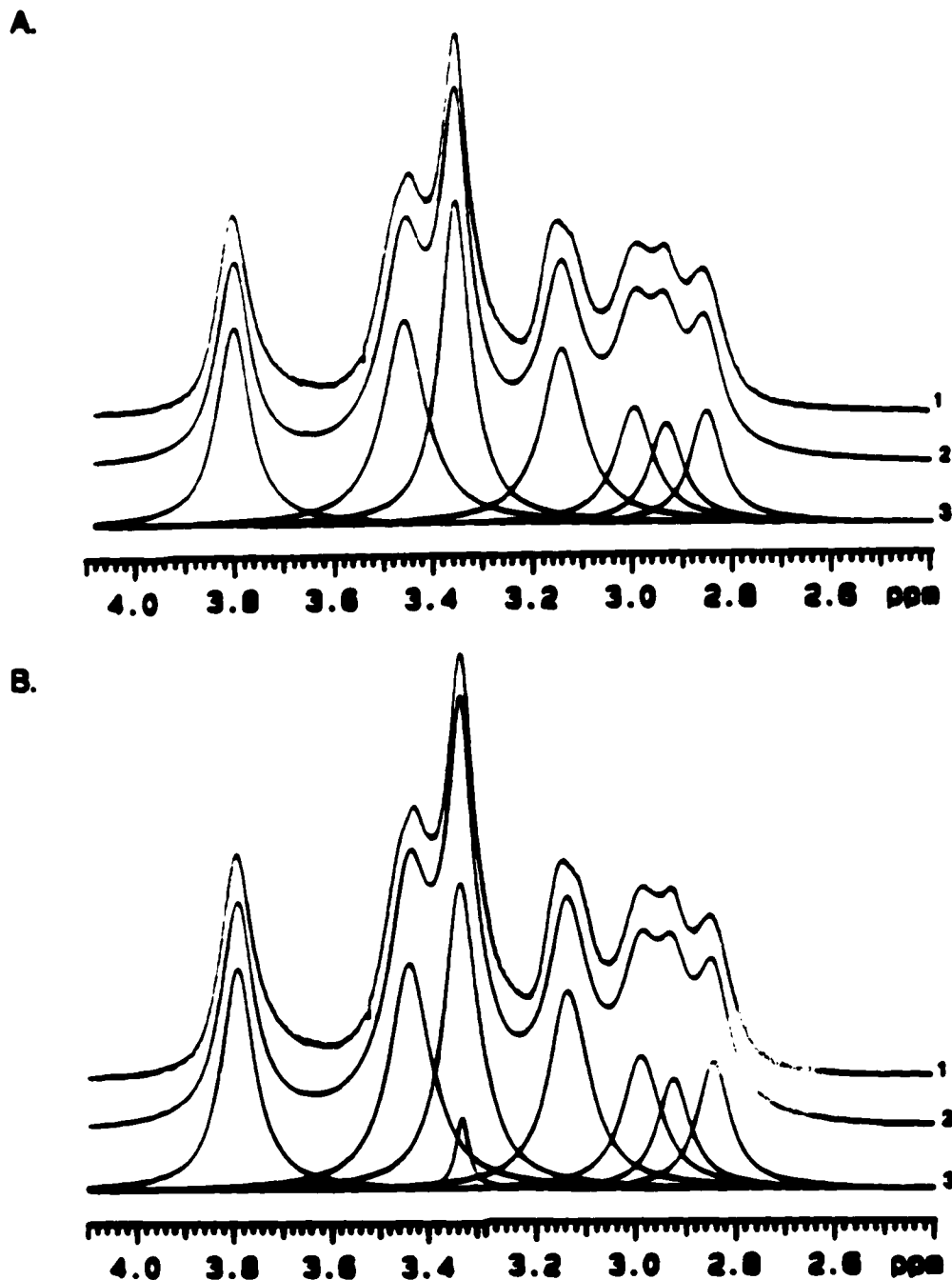


Figure 35. Deconvolution output of a 1.0:1.0 ratio of Hg^{+2} :TAHA at $\text{pH}^* 5.17$. Curve 1 is the original spectrum, curve 2 is the calculated spectrum, and curve 3 is the plot of each individual component in the spectrum. A. Input parameters indicate that the total number of resonances present is seven. B. Input parameters indicate that the total number of resonances is eight.

obtained for Figure 35A.

The numerical output of the curve fitted spectra in Figures 35A and 35B is presented in Table 13. Comparing these results, it should be noted that there is a small peak at 3.343 ppm that is at the same chemical shift as the large resonance labelled peak 3 (Figure 28). The presence of an additional small peak in curve fitted spectra may be due to several causes as stated by Keller *et al.* (74) in their study of problems associated with the original DECOMP NMR curve fitting program.

If a curve fitting program is allowed to fit too many peaks to an observed spectrum an additional small peak may be observed in an attempt to fit the noise, hence the extra peak may be observed at any frequency but it will be on the order of the magnitude of the noise. This is not very likely in this case since the measured signal to noise ratio for the spectra presented in Figure 35 was approximately 200. Another possibility is that an additional small peak is due simply to initially assigning two resonances too close to each other in the input parameters. In this case the algebraic sum of the intensities of the two peaks will be equal to the true intensity. Thus, the following ratios should be equal:

from Figure 35A

$$\text{peak } \left\{ \frac{3}{1+2+3+4+5+6+7} \right\} \quad [102]$$

and from Figure 35B

$$\text{peak } \left\{ \frac{3+4}{1+2+3+4+5+6+7+8} \right\} \quad [103]$$

Table 13. Numerical output of deconvolution results shown in Figures 35A and 35B for a solution in which the ratio of Hg^{+2} :TAHA is 1.0:1.0. The frequency, height, linewidth, and integral are internally consistent within each spectrum.

Line	Frequency (ppm)	Height (mm)	Linewidth (Hz)	Integral (mm²)
From Figure 35A				
1	3.790	34.43	40.27	1386.30
2	3.446	35.55	51.38	1826.47
3	3.343	56.32	36.40	2050.16
4	3.129	30.57	49.85	1523.93
5	2.984	20.12	45.87	922.75
6	2.919	17.25	40.42	697.47
7	2.840	19.38	38.23	740.69
From Figure 35B				
1	3.790	38.37	39.62	1520.00
2	3.446	39.01	50.47	1968.92
3	3.343	12.32	16.14	198.87
4	3.343	52.84	41.60	2198.25
5	3.129	34.11	48.78	1663.73
6	2.984	22.83	47.15	1076.23
7	2.919	18.80	39.74	747.04
8	2.840	21.84	39.40	860.24

where the numbers 1 to 7 and 1 to 8 refer to the frequency of the resonance so identified in Table 13. The ratios obtained from equations [102] and [103] are 0.224 and 0.234, respectively. Because both of the ratios are similar, it was assumed that this was the cause of the additional peak observed in Figure 35B. This also indicates that, although the process of curve fitting very broad and overlapped spectra such as those obtained for ^1H NMR studies of the mercury TAHA complex, may give seemingly different results, these results can be considered both consistent and reproducible for use in the calculation of stability constants.

Because many of the lines in the original spectra were broad, the ratios of the final numerical results such as those presented in Table 13 did not change as the digital resolution was decreased to include a wider spectral window to be curve fitted in order to accommodate the peak tailing. Such comparisons which cut off tails of the peaks was necessary to see if a flat baseline was necessary, especially in light of the fact that the deconvolution program performed an automatic linear baseline correction, to obtain reproducible numerical outputs from ^1H NMR deconvolution. This was especially important in the mercury-TAHA studies since it was necessary to curve fit several resonances and there was considerable tailing at both ends of the spectral window.

3. Summary

Figure 36 summarizes all possible equilibria which may be involved in the mercury-TAHA system. The formation constants of $\text{Hg}(\text{OH})^+$ and $\text{Hg}(\text{OH})_2$ are known (30), and the acid dissociation constants of TAHA have been calculated. At no time was the formation of hydroxyl species such as $\text{Hg}(\text{OH})^+$ and $\text{Hg}(\text{OH})_2$ detected. Formation constants of HgHL^{-3} and $\text{HgH}_2\text{L}^{-2}$ as well as

$K_{\text{HgH}_2\text{L}}^{\text{H}}$ have been obtained from pHg measurements in the presence of excess TAHA (Table 10). The results obtained and reported in Table 10 seem to be comparable to literature values obtained for other protonated mercury complexes (Figure 27). The calculation of HgL^{-4} was possible from the experimentally determined $K_{\text{HgL}}^{\text{C}}$ at high pH values where TAHA is totally deprotonated. The presence of Hg_3L type species is indicated by elemental analysis, although the exact nature of this species is uncertain, i.e. it is not known if a dimer or polymerization type of reaction was responsible for the trinuclear mercury-TAHA complex that occurs.

Calculation of $\beta_{\text{Hg}_2\text{L}}$ according to the method of Harju (98) was attempted and a pH independent constant representing the overall formation constant was calculated; the validity of these results is uncertain at this time as was discussed, although their validity cannot be completely ruled out due to the complex nature of the interaction of the mercury ion with TAHA. The formation of such homonuclear bimetal complexes did not fit the experimental data when it was incorporated into the models utilized for the calculation of the formation of other mercury-TAHA complexes from other potentiometric and ^1H NMR results. These data are included for the purpose of elaborating on the complexity of the behavior of the mercury ion with TAHA. The possibility of the formation of bimetal complex under the specific experimental conditions is of interest from the chemical point of view and has been reported for the hexaprotic ligand TTHA (98). To characterize the degree of formation of the Hg_2L (and Hg_3L) species as well as the specific conditions to which this occurs (i.e. ionic strength, molar ratio) would prove to be fascinating.

An experiment was attempted to see if a mixed $(\text{Hg}(\text{TAHA})\text{Ca})^{-2}$ would form according to the method of Schmidt and Reilley (65). This involved a pH

titration of equimolar concentrations of $\text{Hg}^{+2}:\text{Ca}^{+2}:\text{TAHA}$. The pH versus A value curve was similar to that obtained for a $\text{Hg}^{+2}:\text{TAHA}$ solution in a 1.0:1.0 ratio (Figure 22) however, the buffer region and the inflection point was slightly displaced to the right. Attempts to calculate HgLCa and $\text{HgLCa}(\text{OH})$, where L denotes TAHA, using mass balance equations were unsuccessful. This may be due in part to the complex behavior of Hg^{+2} with TAHA. Addition of another metal would be a further complication until the HgL complexation with TAHA is fully characterized. The formation of $\text{MM}'\text{L}$ types of complexes was studied with a variety of metals (La^{+3} , Zn^{+2} , Pb^{+2}). Although the results indicated the formation of $\text{HgM}'\text{L}$ complexes, where M' represents the second metal, calculation of the stability constants were all unsuccessful. It is possible that the mixed metal ligand complexes were in the form of $\text{HgM}'(\text{OH})_n$. Such calculations were also attempted but they too were unsuccessful. At the present time one can only say that homonuclear and heteronuclear bimetal complexes involving mercury as one of the metals do occur although the exact nature of these complexes is unknown and requires further study.

The interaction of mercury ion (II) with the nitrogen and carboxylate groups of TAHA has been briefly discussed in the section on ^1H NMR studies. Although ^1H NMR curve fitting results provided useful information, comparison of these results with potentiometric results and treatment of the data using different models, including the formation of protonated or non-protonated mononuclear complexes and dinuclear complexes, were unsuccessful. It is possible that other equilibria was involved and unaccounted for.

It was possible to calculate conditional formation constants (K_{HgL}^C) which are used later in this thesis for the calculation of the equilibrium and formation constants of several other metal-TAHA complexes.

Hydroxyl mercury-TAHA complexes such as $\text{HgL}(\text{OH})_n$ did not appear to form, although their formation cannot be completely ruled out.

Overall, it appears that the interaction of the mercury ion with the ligand TAHAs is very complex involving many different equilibria. Although the interaction of mercury and the hexaprotic ligand TAHAs has some interesting chemistry, to fully characterize this system would require much more work. Some possible experiments which may provide further interesting light on this area will be briefly described in the last chapter of this thesis.

C. Lanthanum

1. Potentiometric Studies

The lanthanides (or rare earth metals) exhibit similar chemical and physical properties, with lanthanum often being considered as prototypical. All the lanthanides have partially filled 4f orbitals with the trivalent ion, La^{+3} , having the same electronic configuration as the noble gas xenon. The rest of the lanthanides (cerium to lutetium, with atomic numbers from 58 to 71) differ only in the number of 4f electrons; however these electrons play little part in chemical bonding. The increasing nuclear charge from La to Lu causes a progressive contraction of the atomic and ionic radii and, since the binding of ligands by lanthanide ions is largely ionic, the stability constants increase from La to Lu, with the exception that a "gadolinium break" is often observed.

The stability constants of lanthanide complexes with many aminopolycarboxylic acids, such as EDTA (30), HEDTA (106), DTPA (101,106), and TTHA (98), have been reported.

In this section, results from studies to determine the formation constants of lanthanum-TAHAs complexes will be presented. Studies involving the other lanthanides will be discussed in Section E of this chapter.

Figure 37 presents the pH versus A value data from the titration of TAHAs

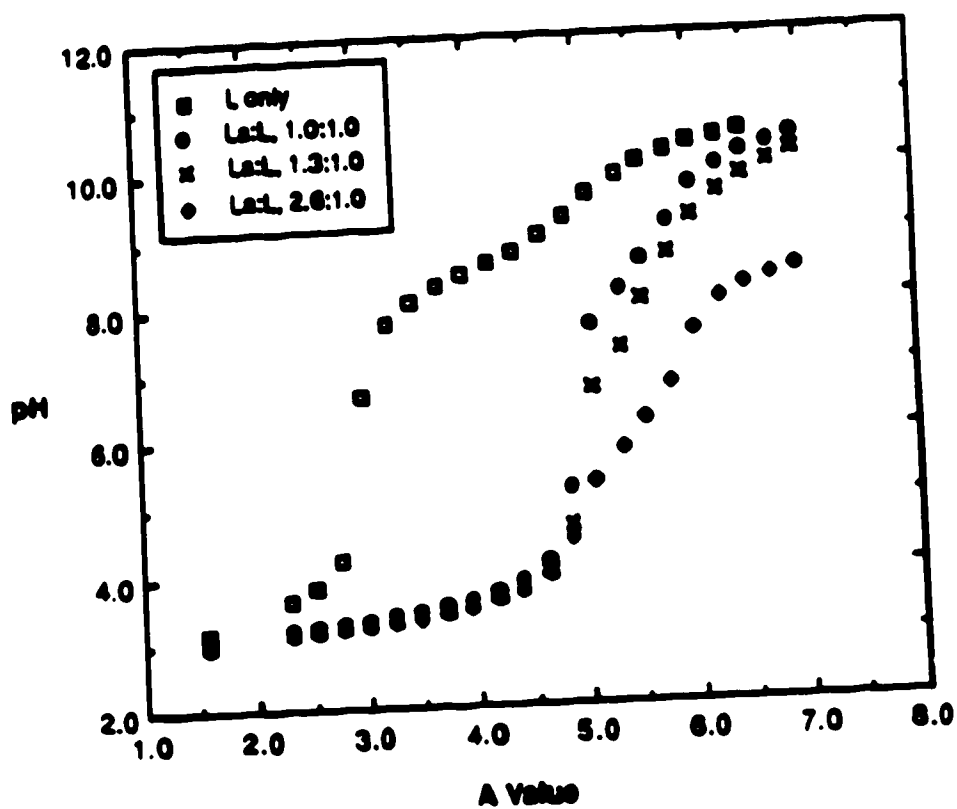
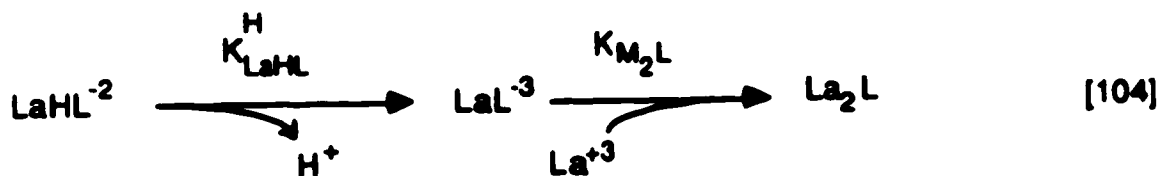


Figure 37. Titration curves of pH versus A value for the lanthanum-TAHA system in various concentrations; L represents the ligand TAHA. All titrations were performed at constant ionic strength and temperature ($\mu=0.1$ M KNO_3 and 25.00°C).

in the presence of various concentrations of La^{+3} . For comparison, the pH titration curve of free TAHA is also presented. This curve exhibits the usual sharp inflection at an A value of 3. The second curve is data from a titration of La^{+3} :TAHA at a ratio of 1.0:1.0 (0.782 mM La^{+3} , 0.748 mM TAHA). This curve exhibits a sharp inflection point at an A value of 5 indicating the presence of the protonated species LaHL^{-2} . In the buffer region where A is between 4 and 5, the monoprotonated complex LaHL^{-2} and diprotonated complex $\text{LaH}_2\text{L}^{-1}$ are in equilibrium. Between A values of 5 to 6 the monoprotonated complex is deprotonated to form LaL^{-3} according to the equilibria presented in Equation [75] where, in this case M, represents La^{+3} . The second curve is data from the titration of La^{+3} :TAHA at a ratio of 1.3:1.0 (0.976 mM La^{+3} , 0.748 mM TAHA) which mimics the previous curve. However the sloping buffer region between A values of 5 to 6 is displaced further to the right (i.e. to higher A values). The last curve presents the data from a titration in which the La^{+3} :TAHA ratio is 2.6:1.0 (1.96 mM La^{+3} , 0.748 mM TAHA). Here the buffer region between A values of 5 to 6 is even further displaced and the curve appears to flatten when A is greater than 6. It is assumed from these curves that, in the presence of excess metal, formation of the bimetal complex occurs according to equilibria defined in Equation [79]. In this case, LaHL^{-2} is deprotonated to form LaL^{-3} , which in turn reacts with excess La^{+3} present in solution to form La_2L . The presence of excess metal would force the equilibria in Equation [104] to the right.



At no time during the titrations was precipitation of the neutral bimetal complex (La_2L) or any other species observed. Calculation of $K_{\text{LaHL}}^{\text{H}}$ was performed using the method of Schwarzenbach (87). A calculated value of 8.58 ± 0.09 was obtained for the constant $\text{p}K_{\text{LaHL}}^{\text{H}}$ from four different pH values. This method involved treating the dissociation of LaHL^{-2} as a simple monoprotic acid over the range where A varies from 5 to 6.

Figure 38 presents the experimental potential-pH diagram obtained using the pHg method for a solution in which the $\text{Hg}^{+2}:\text{La}^{+3}:\text{TAHA}$ ratio was 1.0:2.0:2.0. The exact concentrations used for curve C were 0.951 mM Hg^{+2} , 2.00 mM La^{+3} and 1.99 mM TAHA. Curve A represents the potential-pH diagram obtained from a titration of the mercury-TAHA complex in the presence of excess TAHA. Curve B is the theoretical upper potential limit at the Hg indicating electrode. The data from curves A and B have been discussed in detail in the previous section.

As described in Chapter II, the stability constant of a metal-complex (K_{ML}) may be determined by using the pHg method and Equation [18] which defines $[\text{Hg}^{+2}]$ for a given solution; $[\text{Hg}^{+2}]$ is calculated from the experimentally measured potential and the Nernst equation (Equation [7]); the stability constant K_{LaL} is then calculated using the stability constant K_{HgL} , which was previously calculated, and Equation [19]. This calculation uses the potential obtained in a pH independent region of the titration curve.

As seen from curve C in Figure 38, the potential between the pH range 3.30 to 4.60 is pH independent. Prior to pH 3.0, the potential increases as the pH decreases, in a manner which is identical to mercury in the presence of excess TAHA. Prior to this pH, La^{+3} does not complex to the ligand, as is verified by ^1H NMR studies which will be presented in section 2.

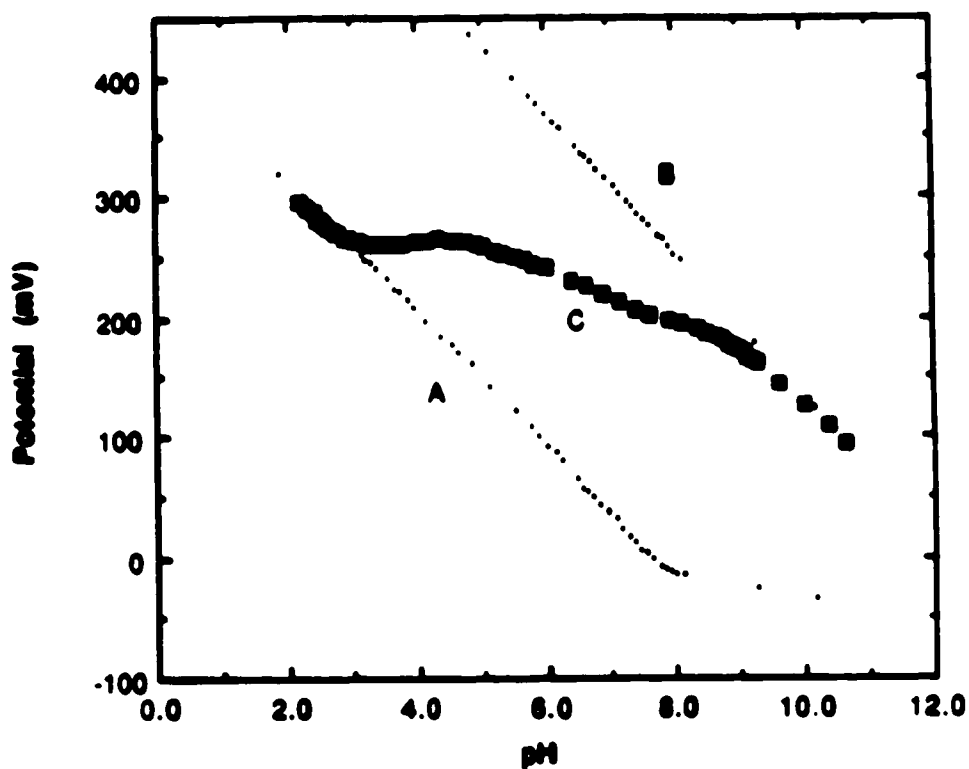


Figure 38. Potential-pH diagram (curve C) for a solution in which the ratio of $\text{Hg}^{+2}:\text{La}^{+3}:\text{TAHA}$ is 1.0:2.0:2.0. The total concentrations of Hg^{+2} , La^{+3} , and TAHA, are 0.951 mM, 2.00 mM, and 1.99 mM respectively. Curve A represents the potential-pH dependence of the mercury-TAHA system while curve B represents the theoretical upper potential limit at the mercury indicating electrode.

Table 14 has concentrations calculated for the experimental data from curve C presented in Figure 38. Column 1 is the pH obtained experimentally while column 2 is the $[\text{Hg}^{+2}]$ calculated by using the Nernst equation defined in equation [7]. Column 3 is the $[\text{OH}^-]$ calculated from K_w and the pH. The concentrations of $[\text{Hg}(\text{OH})^+]$ and $[\text{La}(\text{OH})^{+2}]$ were calculated by Equation [91] using stability constants of $K_{\text{HgOH}} = 1 \times 10^{10.1}$ (30) and of $K_{\text{LaOH}} = 1 \times 10^{4.57}$ (30). The concentration of $[\text{La}_2(\text{OH})^{+5}]$ was calculated by using a stability constant of $1 \times 10^{4.2}$ (30) for the following equation

$$K_{\text{La}_2\text{OH}} = \frac{[\text{La}_2\text{OH}^{+5}]}{[\text{La}^{+3}]^2 [\text{OH}^-]} \quad [105]$$

The concentration of $[\text{La}^{+3}]$ was calculated assuming that all the ligand TAHA is complexed to Hg^{+2} and La^{+3} ; the concentration of La^{+3} which is present in excess was then calculated from the mass balance relationships. The concentrations of Hg^{+2} , $\text{Hg}(\text{OH})^+$, $\text{La}(\text{OH})^{+2}$, and $\text{La}_2(\text{OH})^{+5}$ are tabulated in columns 2, 4, 5, and 6 respectively in Table 14. As can be observed the concentrations of all of these ionic species are very small between the pH range 3.0 to 9.2. Therefore, these species are not forming under the experimental conditions in which the data for curve C was obtained. As observed from curve C in Figure 38, the potential drops markedly after a pH of 5.0; this type of decrease in a potential-pH diagram is often due to a decrease in the stability constant of hydroxyl complexes of the chelate. This type of behavior is similar to that reported by Schmidt and Reilley (65) at pH values greater than 8.0 for the alkaline earth metals (Mg^{+2} , Sr^{+2} , and Ba^{+2}) with the ligand EDTA. Such behavior has also been characterized by Holloway and Reilley (64) for HEDTA at pH 7.2 using the same metals. Both EDTA and HEDTA exhibited a deviation

Table 14. Tabulation of various species (ML and $ML(OH)_n$ complexes) as a function of pH for the pHg data, for a solution in which the ratio of $Hg^{+2} : La^{+3} : TAHA$ is 1.0 : 2.0 : 2.0.

pH	$[Hg^{+2}]$	$[OH^-]$	$[La_2(OH)^{+5}]$	$[La(OH)^{+2}]$	$[Hg(OH)^{+}]$
3.05	1.24×10^{-13}	1.12×10^{-11}	1.67×10^{-13}	3.94×10^{-10}	1.75×10^{-14}
3.38	8.43×10^{-14}	2.41×10^{-11}	3.60×10^{-13}	8.49×10^{-10}	2.56×10^{-14}
3.58	7.80×10^{-14}	3.80×10^{-11}	5.68×10^{-13}	1.34×10^{-9}	3.73×10^{-14}
3.70	7.80×10^{-14}	5.02×10^{-11}	7.50×10^{-13}	1.77×10^{-9}	4.93×10^{-14}
3.99	7.80×10^{-14}	9.68×10^{-11}	1.45×10^{-12}	3.41×10^{-9}	9.50×10^{-14}
4.14	7.80×10^{-14}	1.37×10^{-10}	2.05×10^{-12}	4.83×10^{-9}	1.35×10^{-13}
4.57	7.80×10^{-14}	3.70×10^{-10}	5.52×10^{-12}	1.30×10^{-8}	3.63×10^{-13}
4.84	8.43×10^{-14}	6.90×10^{-10}	1.03×10^{-11}	2.43×10^{-8}	7.32×10^{-13}
5.51	4.89×10^{-14}	3.22×10^{-9}	4.81×10^{-11}	1.14×10^{-7}	1.98×10^{-12}
5.71	3.58×10^{-14}	5.12×10^{-9}	7.64×10^{-11}	1.80×10^{-7}	2.31×10^{-12}
5.99	2.25×10^{-14}	8.87×10^{-9}	1.32×10^{-10}	3.13×10^{-7}	2.51×10^{-12}
6.22	1.30×10^{-14}	1.65×10^{-8}	2.47×10^{-10}	5.82×10^{-7}	2.71×10^{-12}
6.54	6.47×10^{-15}	3.44×10^{-8}	5.14×10^{-10}	1.21×10^{-6}	2.80×10^{-12}
6.84	3.21×10^{-15}	7.00×10^{-8}	1.05×10^{-9}	2.47×10^{-6}	2.83×10^{-12}
7.13	1.59×10^{-15}	1.35×10^{-8}	2.01×10^{-9}	4.75×10^{-6}	2.71×10^{-12}
7.36	1.00×10^{-15}	2.30×10^{-7}	3.43×10^{-9}	8.09×10^{-6}	2.89×10^{-12}
7.55	6.27×10^{-16}	3.59×10^{-7}	5.36×10^{-9}	1.26×10^{-5}	2.83×10^{-12}
7.79	4.25×10^{-16}	6.18×10^{-7}	9.23×10^{-9}	2.18×10^{-5}	3.31×10^{-12}
7.96	3.11×10^{-16}	9.08×10^{-7}	1.36×10^{-8}	3.20×10^{-5}	3.56×10^{-12}
8.14	2.28×10^{-16}	1.40×10^{-6}	2.09×10^{-8}	4.92×10^{-5}	4.01×10^{-12}
8.32	1.95×10^{-16}	2.09×10^{-6}	3.12×10^{-8}	7.36×10^{-5}	5.14×10^{-12}
8.82	1.05×10^{-16}	6.68×10^{-6}	9.98×10^{-8}	2.36×10^{-4}	8.82×10^{-12}
9.25	4.12×10^{-17}	1.77×10^{-5}	2.64×10^{-7}	6.22×10^{-4}	9.16×10^{-12}

in the potential pH diagrams of HgL in the presence of excess L due to the formation of HgL(OH) species. When the authors used a correction factor to account for the decrease in the concentration of HgL due to the formation of HgL(OH) in Equation [18] for each metal studied, the result was an increase in the region over which the potential was independent of pH for all the alkaline earth metals. However, the formation of the Hg(TAHA)(OH)⁻⁵ complex was not observed in the previous section (see Figure 23), therefore the decrease in potential as a function of pH observed in curve C of Figure 38 cannot be due to a hydroxyl mercury-TAHA complex. The formation constant of LaL(OH) in the absence of mercury was determined using the method of Gupta and Powell (107). This method involves titration of a solution containing La⁺³ and TAHA in a ratio of 1.0:1.0 with carbonate-free standardized KOH. Whether the reaction mechanism is regarded as the substitution of an hydroxyl ion for a water molecule coordinated to the complex, or as titration of a proton from a coordinated water molecule, is immaterial. The calculation of the formation constant K_{LaL(OH)} was attempted using the following equation:

$$K_{LaL(OH)} = \frac{([OH^-]_E - [OH^-])}{(C_{LaL} - [OH^-]_E + [OH^-]) [OH^-]_w} \quad [106]$$

where the terms in the above equation are defined as follows:

$[OH^-]_E$ = the concentration of hydroxyl ions that would have resulted had no association occurred considering the amount of base which had been added.

$[OH^-]$ = concentration of hydroxyl ions obtained from the pH measurement.

C_{LaL} = concentration of the lanthanum-TAHA complex in either a protonated or non-protonated form.

All pH measurements were performed at a constant ionic strength of 0.1 M with KNO_3 , at ambient temperature. From potentiometric measurements (Figure 37), the A value is greater than 6 when the pH is approximately 9.5. The above calculations were performed between pH 9.5 to 10.5, where protonated species of lanthanum-TAHA are not present. Solutions with various concentrations of base added were allowed to equilibrate for a maximum of seven days, with pH measurements performed periodically. It was found that the complex $LaL(OH)^{-4}$ did not appear to form under these conditions up to a final pH of 11. Hence, it is unlikely that the formation of $LaL(OH)^{-4}$ occurred under the experimental conditions from which the data in Figure 38 was collected. The method of Gupta and Powell (107) was used to determine the formation of $M(TAHA)(OH)_n$ complexes for all of the rare earth metals studied in this work; for these metals, the results were identical to those obtained for the lanthanum-TAHA complex. Another possibility for the decrease in potential in curve C after pH 5.0 may be the formation of mixed metal ligand complexes of the type $HgL(La)$. Considering the complexity of the interaction of Hg^{+2} with the ligand TAHAs, and previous experimental data, which suggests that the formation of mixed complexes such as $HgLCa^{-2}$ are possible, the formation of $HgLLa^{-1}$ mixed complexes is a reasonable possibility. From the potential-pH diagram presented in curve C of Figure 38, an equilibrium constant K_{eq}^{La} may be calculated for an exchange reaction as defined in Equation [13] which is rewritten below for this system:



where L represents TAHA. The equilibrium constant $K_{\text{eq}}^{\text{La}}$ for the above reaction is defined as

$$K_{\text{eq}}^{\text{La}} = \frac{[\text{Hg}^{+2}][\text{LaL}^{-3}]}{[\text{HgL}^{-4}][\text{La}^{+3}]} \quad [108]$$

which may be written in terms of the conditional formation constants for LaL^{-3} ($K_{\text{LaL}}^{\text{C}}$) and HgL^{-4} ($K_{\text{HgL}}^{\text{C}}$):

$$K_{\text{eq}}^{\text{La}} = \frac{K_{\text{LaL}}^{\text{C}}}{K_{\text{HgL}}^{\text{C}}} \quad [109]$$

The concentrations of LaL^{-3} , HgL^{-4} , and La^{+3} were calculated from the initial concentrations present assuming that all the TAHA is bound, which is reasonable since the total metal concentration is twice the total ligand concentration. The concentration of Hg^{+2} present is calculated from the electrode potential using the Nernst equation.

A plot of $-\log K_{\text{eq}}^{\text{La}}$ ($\text{p}K_{\text{eq}}^{\text{La}}$) versus pH is presented in Figure 39. The increase in $\text{p}K_{\text{eq}}^{\text{La}}$ in the pH range of 2.0 to 3.0 is probably due to the presence of protonated mercury-TAHA complexes as explained earlier; from the ^1H NMR studies protonated lanthanum-TAHA complexes were not observed in this pH region. Between pH 3.3 to 4.6 the $\text{p}K_{\text{eq}}^{\text{La}}$ is constant as would be expected from Figure 38, since this is the region where the potential is pH independent. There are two plots in Figure 39 which are both superimposable up to pH 9.8. The first

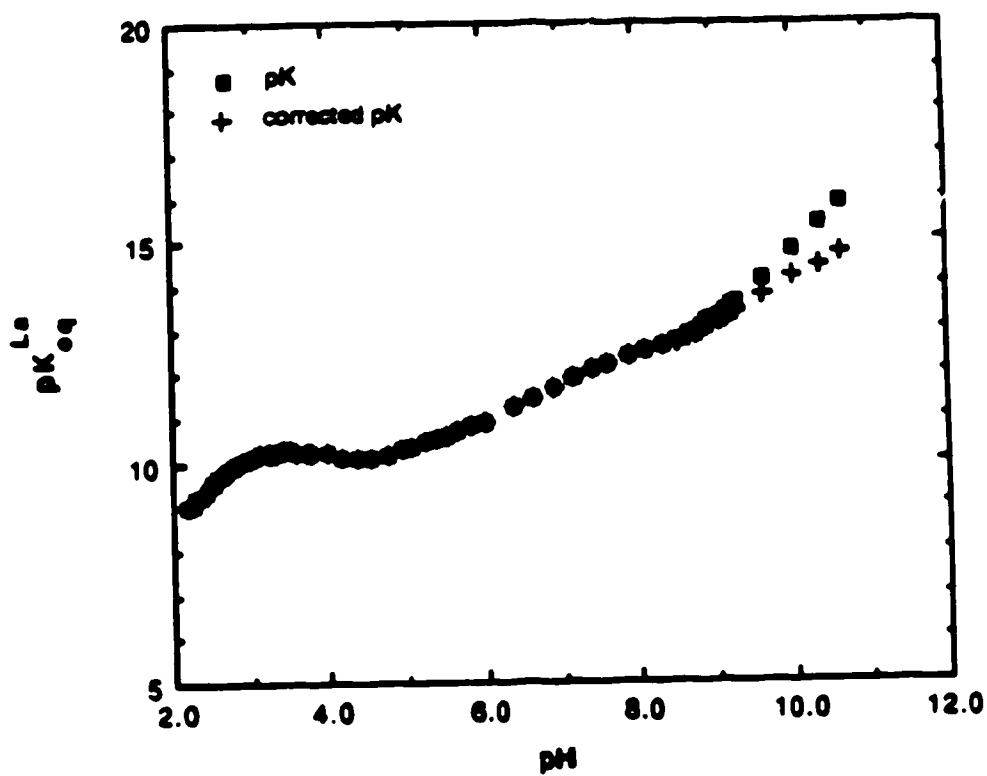


Figure 39. Plot of pK_{eq}^{La} versus pH. The square symbols represent the uncorrected pK_{eq}^{La} values, while the crosses represent pK_{eq}^{La} values that have been corrected for the formation of $La(OH)^{+2}$.

plot, labeled pK_{eq}^{La} (identified as pK in legend) is the plot without the correction for the formation of $La(OH)^{+2}$ which has a K_{LaOH} of $1 \times 10^{4.53}$ at an ionic strength of 0.1 M (30). The second plot, labeled corrected pK_{eq}^{La} (identified as corrected pK in legend) is the plot where there was a correction applied to Equation [108] for the presence of $La(OH)^{+2}$ using α_{La} as defined below:

$$\alpha_{La} = \frac{[La^{+3}]}{[La^{+3}] + [La(OH)^{+2}]} \quad [110]$$

Equation [110] may be rewritten with the incorporation of $K_{La(OH)}$ and collection of the common term $[La^{+3}]$ as follows:

$$\alpha_{La} = \frac{1}{1 + (K_{LaOH}) ([OH^-])} \quad [111]$$

Figure 40 is the plot of the logarithm of K_{La}^C as a function of pH. K_{La}^C was calculated using Equation [109] with K_{HgL}^C obtained from a separate experiment (see Figure 25). The two plots, labeled $\log K_{LaL}^C$ and corrected $\log K_{LaL}^C$ (identified as log K and corrected log K respectively in the legend) are with and without the correction applied for formation of $La(OH)^{+2}$. In the pH region from 3.0 to 4.0 a pK_{eq}^{La} value of 10.20 with a variance of 0.07 is obtained from 20 data points ($n = 20$). For a duplicate run similar results to those presented in Figures 38, 39, and 40 were obtained for a duplicate run ($pK_{eq}^{La} = 10.15$ with a variance of 0.02, $n = 11$). The average value of pK_{eq}^{La} is 10.18 ± 0.03 for the two duplicate runs.

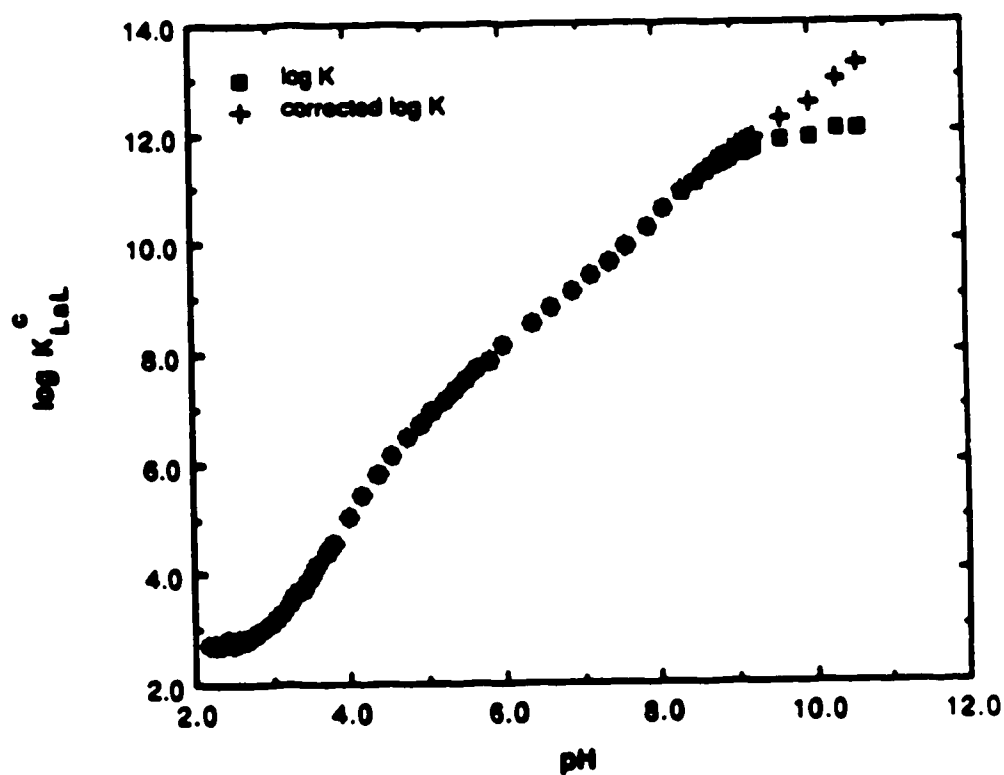


Figure 40. Plot of the logarithm of K_{LaL}^C as a function of pH. The square symbols represent the uncorrected $\log K_{LaL}^C$ values while the crosses represent logarithm K_{LaL}^C values that have been corrected for the formation of $La(OH)^{+2}$.

2. ^1H NMR Studies

A solution of La^{+3} :TAHA in a 1.02:1.00 ratio (4.36 mM La^{+3} , 4.224 mM TAHA) was titrated with KOD in D_2O at a constant ionic strength of 0.1 M with KNO_3 . This solution was titrated with pH^* increments of approximately 0.1 pH^* units from 3.09 to 4.24, which is the pH^* range over which the pH titration indicated that the protonated species LaHL^{-2} and $\text{LaH}_2\text{L}^{-1}$ form. Results obtained from this ^1H NMR study proved to be useful for the calculation of the constants K_{LaHL} and $K_{\text{LaH}_2\text{L}}$ along with the conditional formation constants as will be detailed later. Figure 41 is a spectrum obtained at pH^* 3.09. As in the case of ^1H NMR studies with mercury and TAHA, the individual peaks will be identified from 1 to 8, as depicted in Figure 41. The chemical shift (ppm) of all eight resonances as well as the chemical shift (ppm) for the three resonances due to free TAHA are plotted as a function of pH in Figure 42. As before, resonances will be referred to as due to the T3, T2, and T1 methylene protons from free and bound TAHA. Resonances labeled as peak 1 (the singlet at 3.895 ppm, Figure 41), peak 4 (the middle resonance of the triplet centered at 3.462 ppm, Figure 41) and peak 6 (the middle resonance of the triplet centered at 3.008 ppm, Figure 41) are due to the T3, T2, and T1 methylene protons of the free TAHA as can be observed by the identical pH-chemical shift behavior as depicted in Figure 42A. As is clear from both Figures 41 and 42A, resonances due to the free TAHA are clearly observed at pH 3.09.

The resonances labeled peak 7 and peak 8 are due to the T1 methylene protons, while resonances labeled peak 3 and peak 5 are due to the T2 methylene protons of the bound complex. The resonance labeled peak 2 is unidentified and will be discussed in more detail later. Table 15 tabulates the above information.

Representative ^1H NMR spectra measured at several pH^* values are

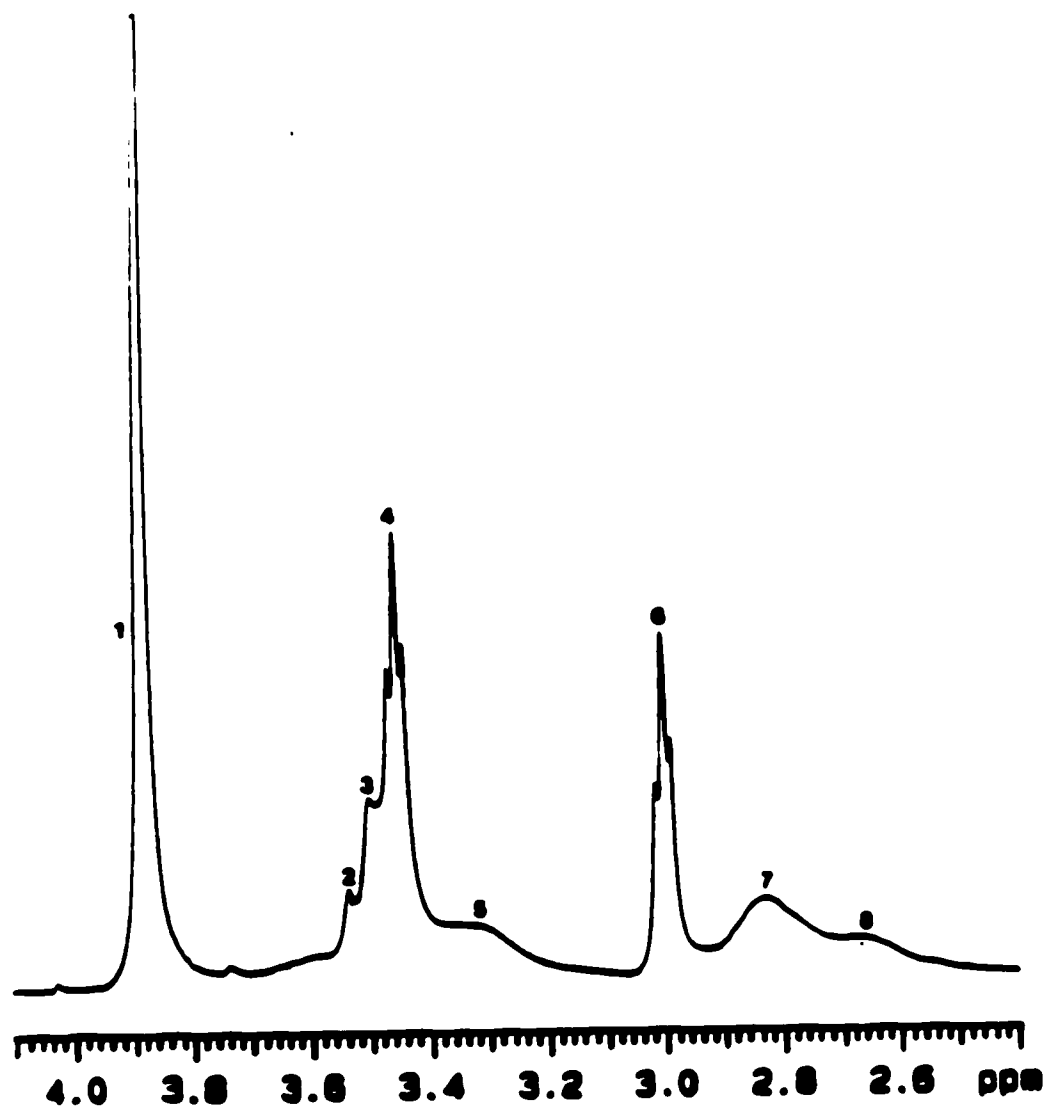


Figure 41. ^1H NMR spectrum at pH* 3.09 for the lanthanum-TAHA system. Each resonance observed is labelled peaks 1 through 8.

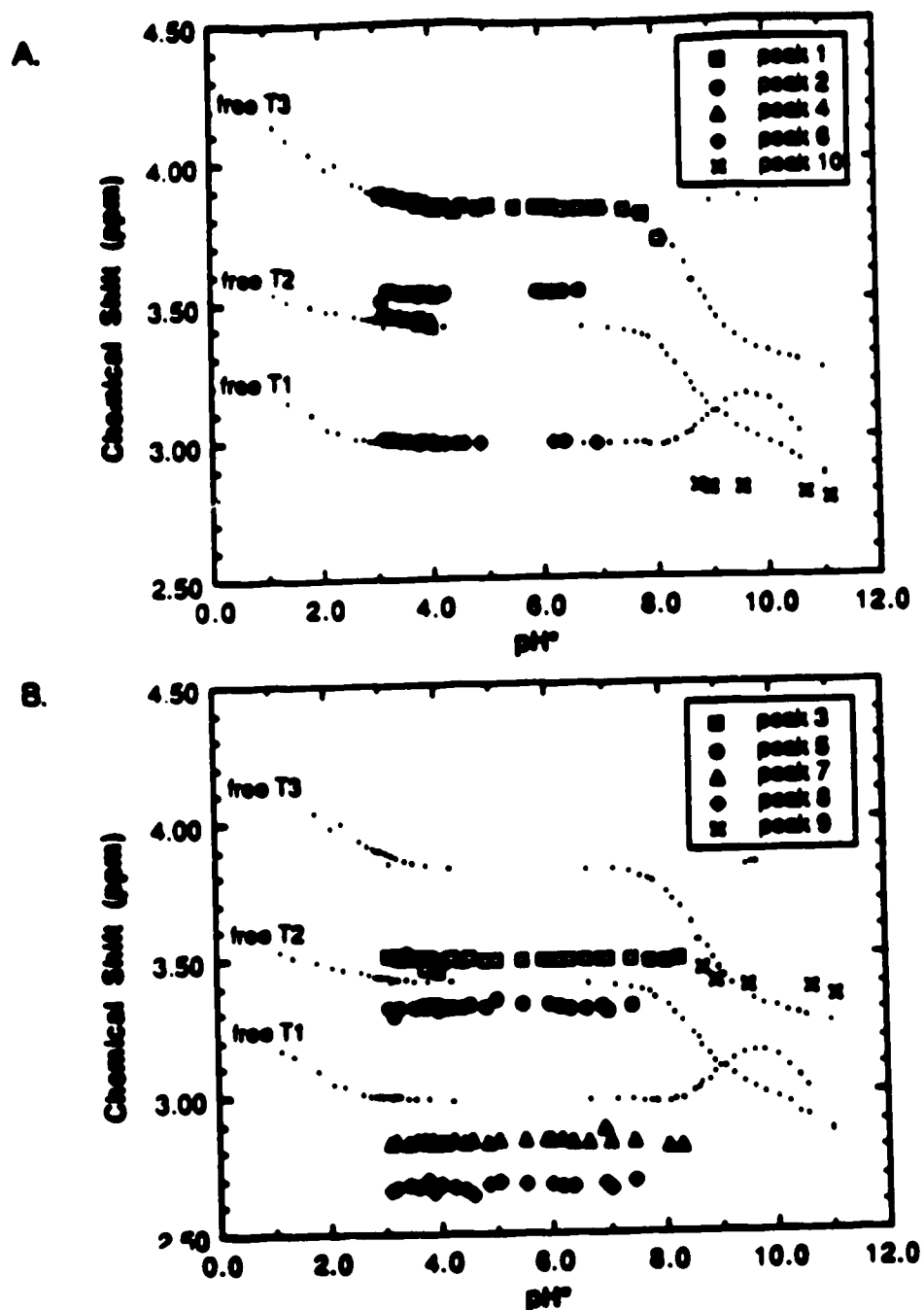


Figure 42. Chemical shift (ppm) as a function of pH^* for the lanthanum-TAHA system. Assignment of peaks 1 through 8 are presented in Figure 41, while assignments of peaks 9 and 10 are presented in Figure 45B. The chemical shift dependence of the resonances due to free TAHA is also presented for comparison.

Table 15. Summary of all the ^1H NMR resonances observed for the lanthanum-TAHA system as well as assignment of the complex giving rise to each resonance.

Peak Label	Chemical Shift (δ, ppm)	Methylene Protons	Species
1	3.895	T3	free TAHA
2	3.540	?	?
3	3.508	bound T2	$\text{LaH}_2\text{L} \cdot 1$
4	3.468	T2	free TAHA
5	3.324	bound T2	$\text{LaHL} \cdot 2$
6	3.008	T1	free TAHA
7	2.833	bound T1	$\text{LaH}_2\text{L} \cdot 1$
8	2.667	bound T1	$\text{LaHL} \cdot 2$

shown in Figure 43. Spectra A, B, and C are for pH^* 3.55, 3.83, and 4.24 respectively.

Deconvolution of the region between 2.4 ppm to 3.6 ppm gave integrals for all the resonances present in this frequency range (see Figures 41). The fractions of the total intensity of peak 7 ($7/(7+8)$) and peak 8 ($8/(7+8)$) are plotted as a function of pH^* in Figure 44. As observed, the relative area of peak 7 decreases as the pH^* increases: thus the species giving rise to peak 7 is more protonated than the species giving rise to peak 8. In this case the resonance labeled as peak 7 is due to $\text{LaH}_2\text{L}^{-1}$ while the resonance labeled as peak 8 is due to LaHL^{-2} ; from changes in the intensities of resonances as a function of pH^* . It was concluded that $\text{LaH}_2\text{L}^{-1}$ also gives rise to peak 3 while LaHL^{-2} gives rise to peak 5. Identification of all species which give rise to the eight resonances is given in the last column of Table 15.

Another ^1H NMR titration of a solution with a La^{+3} and TAHA ratio of 1.00:0.98 (4.387 mM La^{+3} , 4.494 mM TAHA) was performed over the pH^* range 3.00 to 11.00. Some representative spectra are presented in Figure 45. The spectrum presented in Figure 45A is similar to those presented in Figures 41 and 43; what is important to note about these spectra is that at approximately pH^* 7.50, all resonances begin to overlap and after pH^* 8.30 only two resonances are observed. These two resonances are labelled as peak 9 and peak 10 in the spectrum presented in Figure 45F; and are due to fast exchange between all different species present at high pH^* . The chemical shift (ppm) of these two resonances as a function of pH^* is plotted in Figure 42 with the resonances previously assigned as peaks 1 through 8.

^1H NMR spectra for the pH^* region 3.09 to 4.24 (see Figures 42 and 43) provided information for the calculation of formation constants of $\text{LaH}_2\text{L}^{-1}$ and LaHL^{-2} . For these calculations, integrals of the resonances were obtained

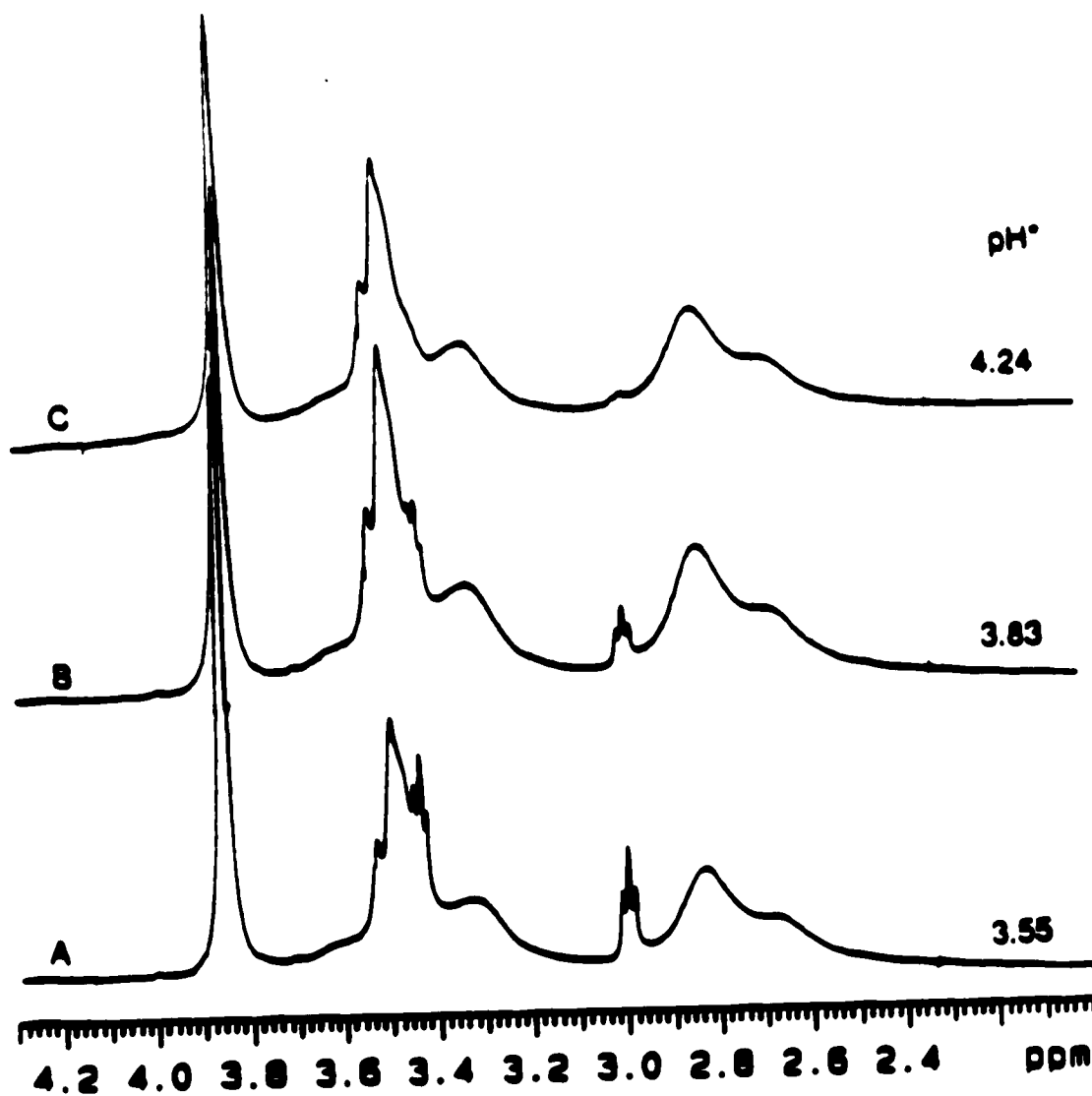


Figure 43. Representative ^1H NMR spectra as a function of pH^* in the range 3.55 to 4.24 for the lanthanum-TAHA system. The total concentration of La^{+3} and TAHA was 4.367 mM and 4.224 mM respectively (ratio of La^{+3} :TAHA is 1.02:1.00).

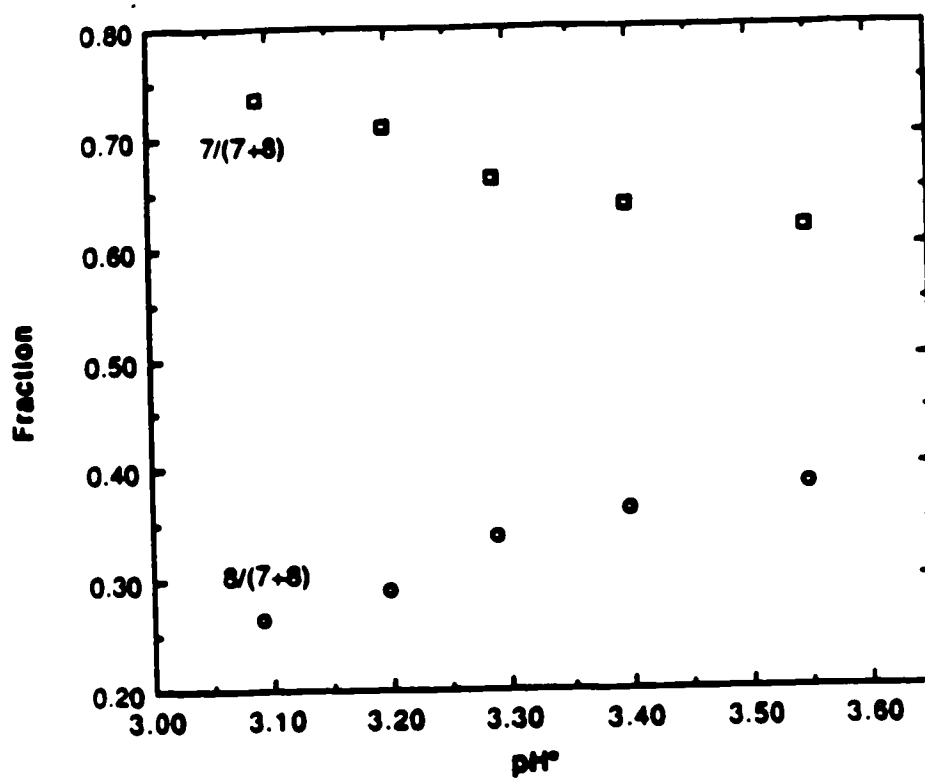


Figure 44. Fraction of the total intensity of peaks 7 and 8, assigned in Figure 41, as a function of pH. The circles represents the fraction of the total intensity of peak 8, while the squares represents fraction of the total intensity of peak 7.

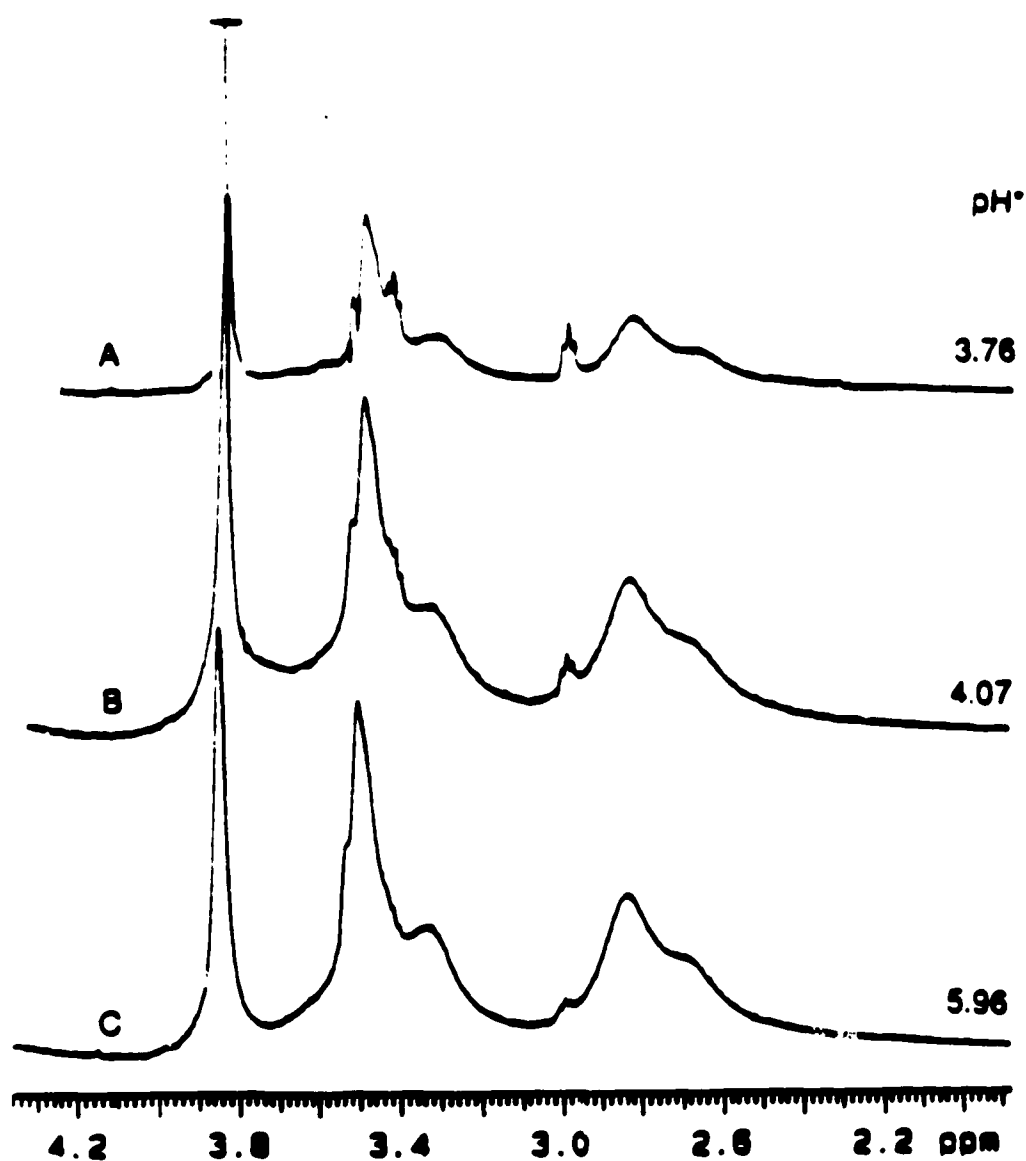


Figure 45. Representative ^1H NMR spectra as a function of pH* in the range 3.76 to 9.52 for the lanthanum-TAHA system. The total concentrations of La^{+3} and TAHA were 4.387 mM and 4.494 mM respectively (ratio of La^{+3} :TAHA is 1.00:0.98).

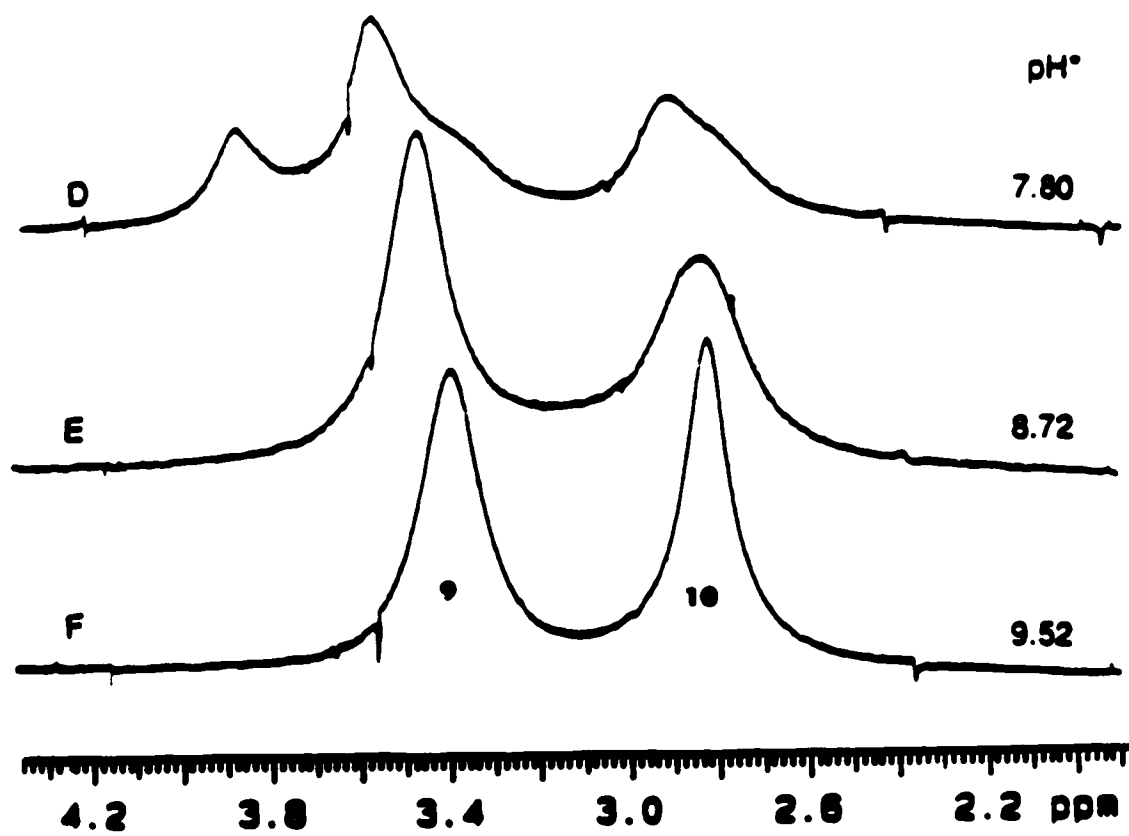


Figure 45. (continued).

by curve fitting the original spectrum by the deconvolution program.

Spectra in which the resonance due to the free TAHA, and the resonances due to LaHL^{-2} and $\text{LaH}_2\text{L}^{-1}$ clearly were observed (i.e. Figures 41, 43A and 43B) were curve fitted via deconvolution of the data in the frequency range from 2.40 to 3.2 ppm; the frequency range from 3.20 to 3.70 was not used due to the large degree of overlap of all the resonances which were observed.

Figure 46 shows typical output from the deconvolution calculations, in this case using the spectrum presented in Figure 43A at $\text{pH}^* 3.55$. Curve 1 is the original spectrum, curve 2 is the final calculated spectrum, and curve 3 refers to the calculated spectrum for each of the components present in the original spectrum. In this case, convergence was reached in 43 iterations with a final χ^2 of 696. Visually the calculated spectrum appears to be a good representation of the resonances present in the original spectrum. For all spectra which were curve fitted, a digital resolution of 0.39 Hz per point was maintained and χ^2 varied between 200 to 700.

Two formation constants are defined below:

$$K_1^c = \frac{[\text{LaH}_2\text{L}^{-1}]}{[\text{La}^{+3}] [\text{L}^{-6}]_f} \quad [112]$$

$$K_2^c = \frac{[\text{LaHL}^{-2}]}{[\text{La}^{+3}] [\text{L}^{-6}]_f} \quad [113]$$

where $[\text{La}^{+3}]$ represents the total free metal and $[\text{L}^{-6}]_f$ represents the total free TAHA in solution.

Since all the resonances present in Figure 46 are for methylene groups closest to the central nitrogen, the relative ratios of integrals will give the fraction of free TAHA, the fraction bound as $\text{LaH}_2\text{L}^{-1}$ and the fraction bound as LaHL^{-2} .

Frequency (ppm)	Height (mm)	Linewidth (Hz)	Integral (mm ²)	Species (T1 methylene protons)
3.014	12.83	3.31	42.51	free TAHA
3.000	23.87	4.82	114.99	free TAHA
2.986	12.25	4.42	54.13	free TAHA
2.832	21.41	63.63	362.21	LaH ₂ L ⁻¹
2.675	9.19	93.89	863.10	LaHL ⁻²

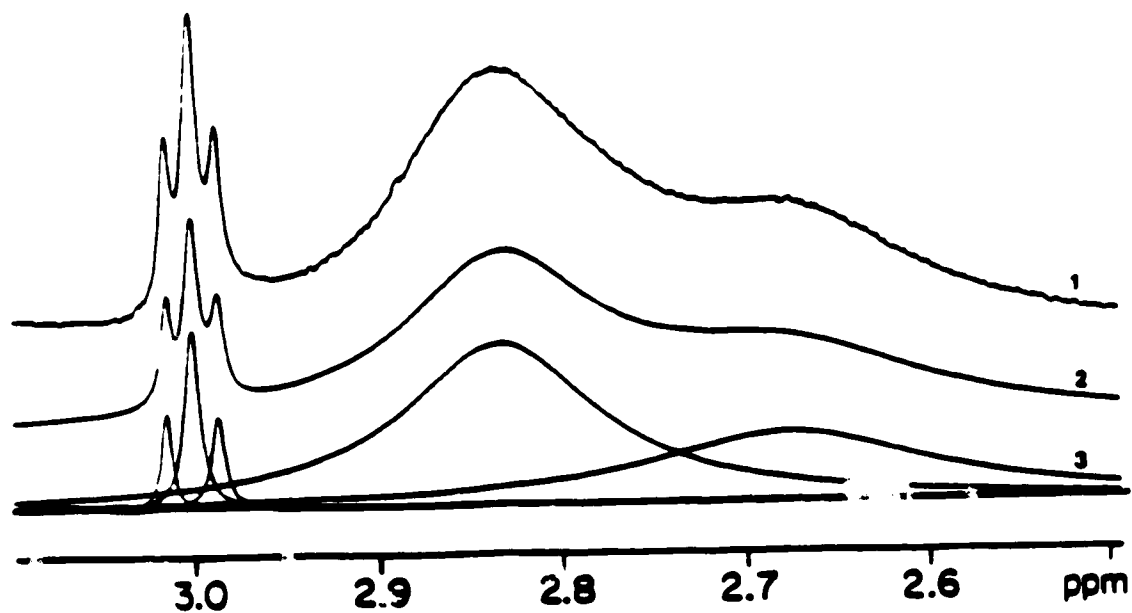


Figure 46. Deconvolution output of a 1.0:1.0 ratio of La³⁺:TAHA at pH* 3.55. Curve 1 is the original spectrum, curve 2 is the calculated spectrum, and curve 3 is the plot of each individual component in the spectrum. The numerical results obtained and the species giving rise to each resonance are tabulated above.

From the usual mass balance relationships, the concentrations of $\text{LaH}_2\text{L}^{-1}$, LaHL^{-2} , La^{+3} , and L_1 may then be obtained knowing the initial total concentrations of lanthanum and ligand in solution. These concentrations are then substituted into Equations [112] and [113] to calculate the formation constants as a function of pH^* . Figure 47 is a plot of $\log K^c$ versus pH^* for each of the conditional constants defined above. Both the K^c values increase linearly in the pH^* range 3.0 to 3.8. From the above formation constants, the pH independent constants $K_{\text{LaH}_2\text{L}}^D$ and K_{LaHL}^D were calculated using the following

equations:

$$K_{\text{LaH}_2\text{L}}^D = \frac{[\text{LaH}_2\text{L}^{-1}]}{[\text{La}^{+3}][\text{H}_2\text{L}^{-4}]} \quad [114]$$

$$K_{\text{LaHL}}^D = \frac{[\text{LaHL}^{-2}]}{[\text{La}^{+3}][\text{HL}^{-5}]} \quad [115]$$

The superscript "D" denotes that these experiments were performed in D_2O rather than H_2O . The concentrations of H_2L and HL were calculated using the acid dissociation constants to calculate α_4 ($\alpha_{\text{H}_2\text{L}}$) and α_5 (α_{HL}) as defined previously in Chapter III. The logarithm of K_{LaHL}^D had little variation from pH^* 3.09 to 3.70; an average value of 1 ± 0.1 ($n=10$) was obtained and is tabulated in Table 16. There was more variation in the calculation of the logarithm of $K_{\text{LaH}_2\text{L}}^D$ especially at pH^* values greater than 3.5; an average value of 8.6 ± 0.2 ($n=6$) was obtained for the logarithm of $K_{\text{LaH}_2\text{L}}^D$. The variation observed for the calculation of $K_{\text{LaH}_2\text{L}}^D$ may be due partly to inaccuracies in the calculation of the integral of the T1 resonance for LaH_2L , that is, the large tailing of this resonance combined with the fact that the concentration of LaH_2L

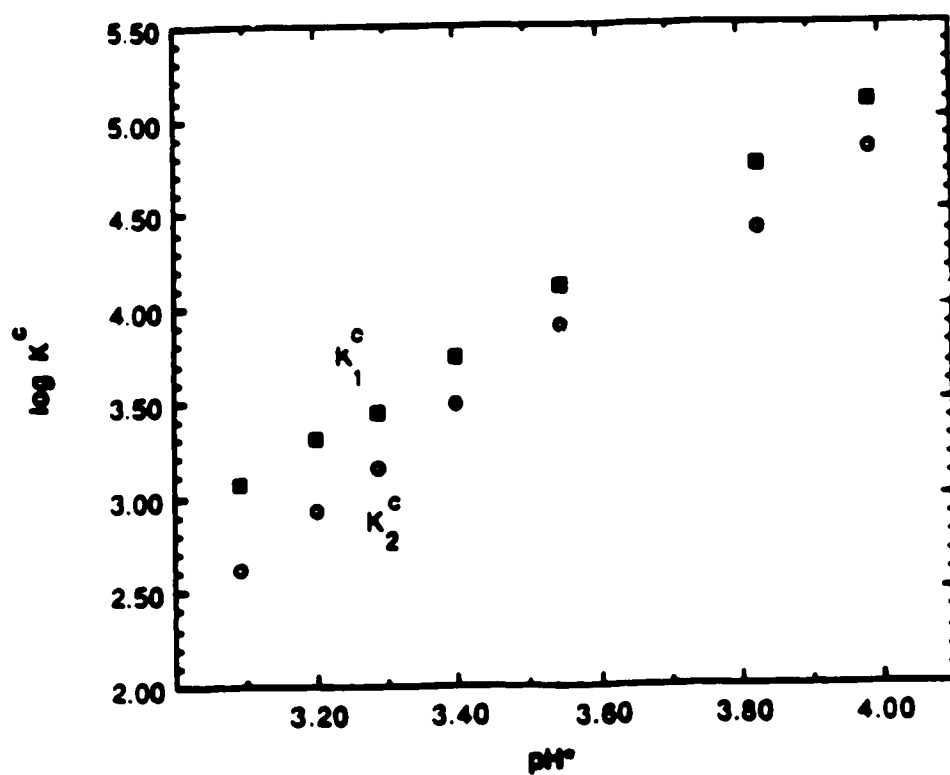


Figure 4.7 Plot of conditional formation constants for $\text{LaH}_2\text{L}^{-1}$, (K_1^c), and LaHL^{-3} , (K_2^c), as a function of pH^* .

Table 16. Tabulation of the stability constants for the lanthanum-TAHA system ($\mu = 0.1 \text{ M KNO}_3$, 25°C).

Constant	Definition	Number of Runs (N)	log K
K_{LaL}	$\frac{[\text{LaL}^{-3}]}{[\text{La}^{+3}][\text{L}^{-6}]}$	2	16.06 ± 0.02
$K_{\text{La}_2\text{L}}$	$\frac{[\text{La}_2\text{L}]}{[\text{LaL}^{-3}][\text{La}^{+3}]}$	2	6.16 ± 0.03
$\beta_{\text{La}_2\text{L}}$	$\frac{[\text{La}_2\text{L}]}{[\text{La}^{+3}]^2[\text{L}^{-6}]}$	2	22.22 ± 0.01
$K_{\text{LaH}_2\text{L}}^{\text{D} \dagger}$	$\frac{[\text{LaH}_2\text{L}^{-1}]}{[\text{La}^{+3}][\text{H}_2\text{L}^{-4}]}$	2	8.6 ± 0.2
$K_{\text{LaHL}}^{\text{D}}$	$\frac{[\text{LaHL}^{-2}]}{[\text{La}^{+3}][\text{HL}^{-5}]}$	2	13.1 ± 0.1
$K_{\text{LaHL}}^{\text{H} \ddagger}$	$\frac{[\text{LaL}^{-3}][\text{H}^{+}]}{[\text{LaHL}^{-2}]}$	2	8.57 ± 0.09
$K_{\text{LaHL}}^{\text{H(La)}}$	$\frac{[\text{La}_2\text{L}][\text{H}^{+}]}{[\text{LaHL}^{-2}][\text{La}^{+3}]}$	2	-3.21 ± 0.09
$K_{\text{LaH}_2\text{L}}^{\text{H}}$	$\frac{[\text{LaHL}^{-2}][\text{H}^{+}]}{[\text{LaH}_2\text{L}^{-1}]}$	2	-4.37 ± 0.03

† the superscript "D" refers to constants obtained in D_2O at a constant ionic strength of 0.1 M KNO_3 .

‡ the superscript "H" refers to a deprotonation equilibrium.

decreases with increasing pH^* may have a more significant effect on the calculated value of $K_{\text{LaH}_2\text{L}}^{\text{D}}$ than for the value of $K_{\text{LaHL}}^{\text{D}}$. The value of the stability constant obtained for $K_{\text{LaHL}}^{\text{D}}$ is considered both accurate and reproducible from the results obtained; however the constant $K_{\text{LaH}_2\text{L}}^{\text{D}}$ may in fact be slightly higher than that given in Table 16.

Calculation of K_{LaL} as defined by Equation [73] was obtained using Equation [77]. A value for the acid dissociation constant K_8^{D} ($1 \times 10^{-11.34}$) was obtained for a solution of TAHA in D_2O ; the value K_{LaHL} ($1 \times 10^{13.1}$) was obtained from ^1H NMR studies. The value of $K_{\text{LaHL}}^{\text{H}}$ used was from aqueous solutions ($1 \times 10^{-8.61}$); this value may be slightly higher for corresponding D_2O solutions, therefore the value K_{LaL} calculated may be slightly lower than that reported here. A value of 16.06 was obtained for logarithm of K_{LaL} . The overall formation constant logarithm of $\beta_{\text{La}_2\text{L}}$ was calculated using Equation [81] to be 22.22.

Using Equation [78], the $\text{p}K_{\text{LaH}_2\text{L}}^{\text{H}}$ was calculated as being 4.37. For this calculation, the acid dissociation constant $K_{\text{LaH}_2\text{L}}^{\text{H}}$ was again obtained from aqueous solutions while K_5^{D} and $K_{\text{LaH}_2\text{L}}^{\text{D}}$ were obtained in D_2O solutions, both at a constant ionic strength. All of the above stability constants are tabulated in Table 16.

The constants $K_{\text{LaH}_2\text{L}}^{\text{H}}$ and K_{LaL} may be slightly different than the values reported in Table 16 due to one of the constants used in Equations [77] and [78] being obtained from aqueous pH titrations rather than from pH titrations in D_2O . However, the general magnitude of the constants reported in Table 16 can be considered to be valid.

Overall, the stability constants of lanthanum complexes with other ligands (e.g. the hexaprotic ligand TTHA) seem comparable to the values reported in Table 16. It was expected that the value of K_{LaL} for TAHA would be on the same order of magnitude as for DTPA ($1 \times 10^{19.48}$) or TTHA ($1 \times 10^{22.22}$) (30). However, the value for K_{LaL} for TAHA is lower than was expected, probably due to the value obtained for the constant $pK_s(H,LaHL)$. Usually values obtained for pK_{LaHL}^H with other ligands such as TTHA are much lower (98).

A plot of logarithm of K_{LaHL} for various complexes versus the sum of the acid dissociation constants (ΣpK 's) is presented in Figure 48. For the calculation of ΣpK 's for TAHA, the acid dissociation constants used were for D_2O solutions, because the stability constant, K_{LaHL} , was obtained in D_2O , while for the rest of the ligands, the ΣpK 's were obtained for aqueous solutions (30). This plot simply indicates the trend observed; the significance of such plots was explained in the previous section.

Excess La^{+3} was added to four of the 1H NMR samples of La^{+3} :TAHA in a ratio of 1.0:1.0 to give a final ratio of 2.3:1.0. The pH^* of these solutions was measured using a micro-combination glass electrode that was inserted directly into the NMR tube. The spectra obtained are presented in Figures 49A and 49B. In Figure 49A, resonances for the methylene groups closest to the carboxylate functional groups (the bound T3 methylene protons) are plotted as a function of pH^* . Figure 49B shows the 2.4 to 3.8 ppm region (where the bound T1 and T2 methylene protons are observed) for the same spectra. The notation in these spectra is the same as the previous notation, except that the extra resonance at 3.90 ppm (pH^* 2.98, spectrum A in Figure 49A) will be referred to as peak 11.

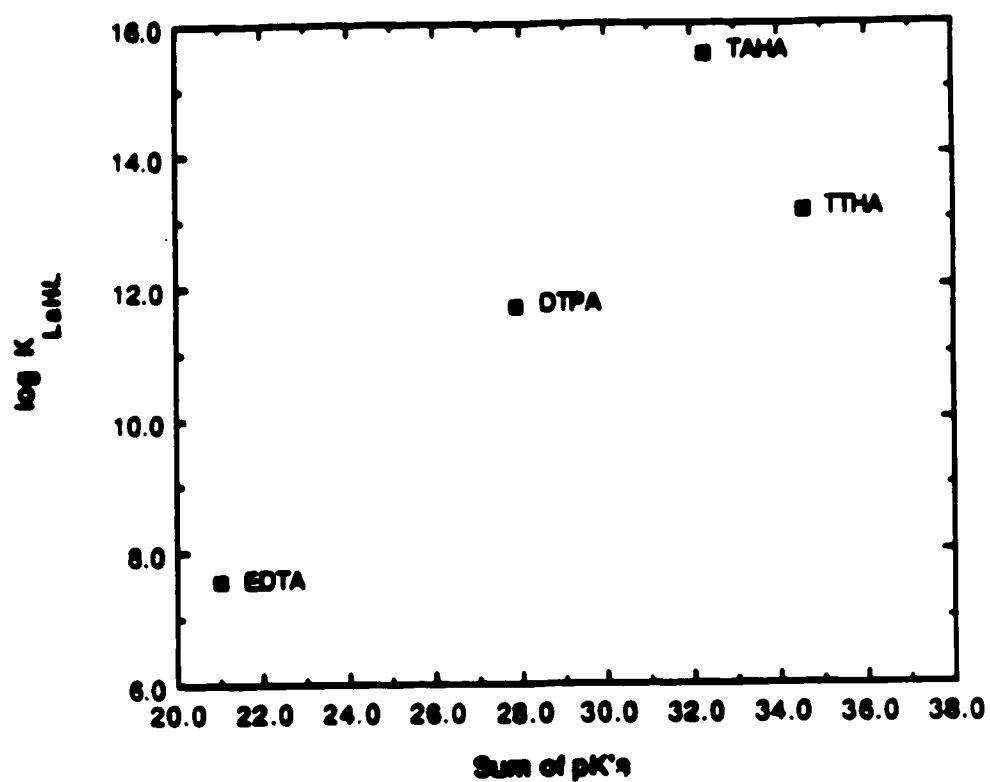


Figure 48. Plot of the logarithm of K_{LaHL} versus the sum of $pK's$ ($\sum pK's$) for several lanthanum-ligand complexes.

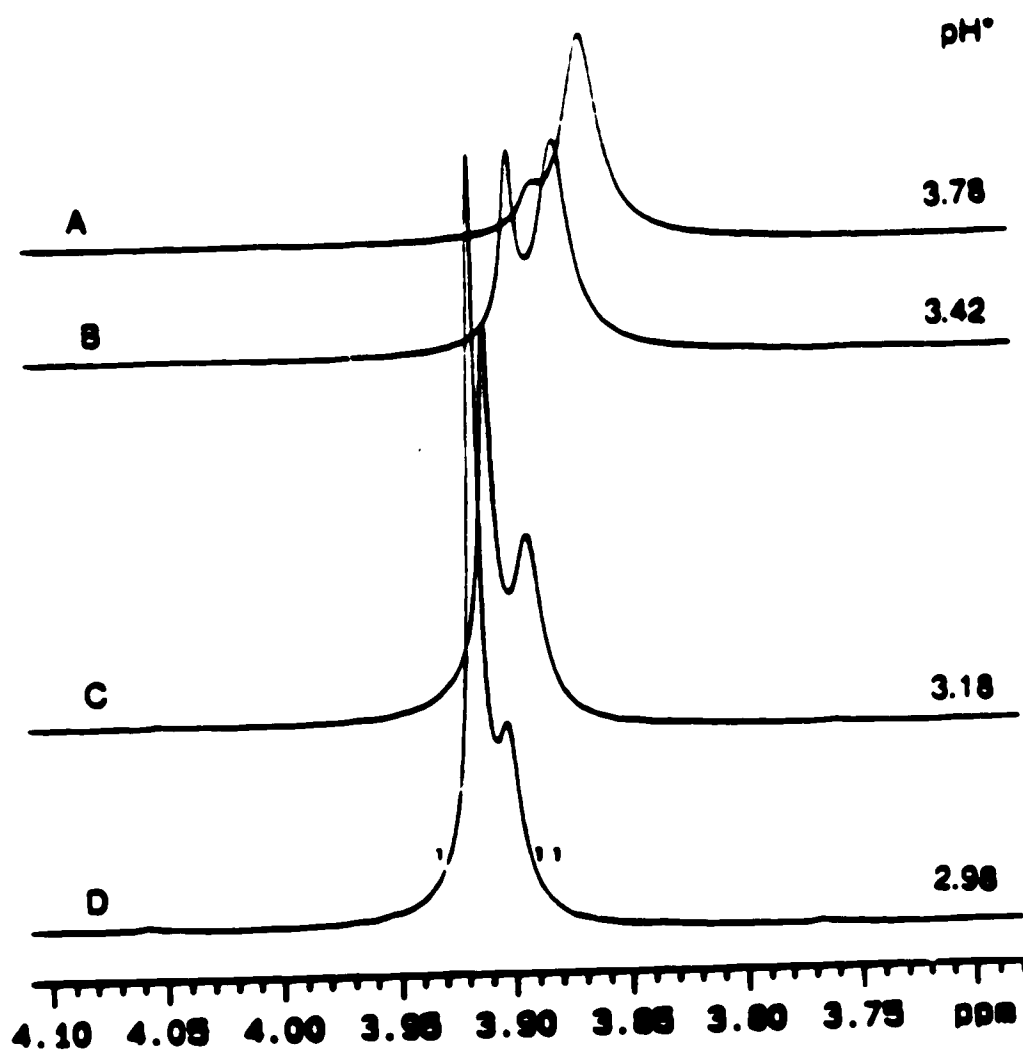


Figure 49. ^1H NMR spectra in which the final $\text{La}^{+3}:\text{TAHA}$ ratio was 2.3:1.0, plotted as a function of pH° . A. Chemical shift (ppm) range is 3.70 to 4.10, depicting the region in which bound T3 methylene protons are observed.

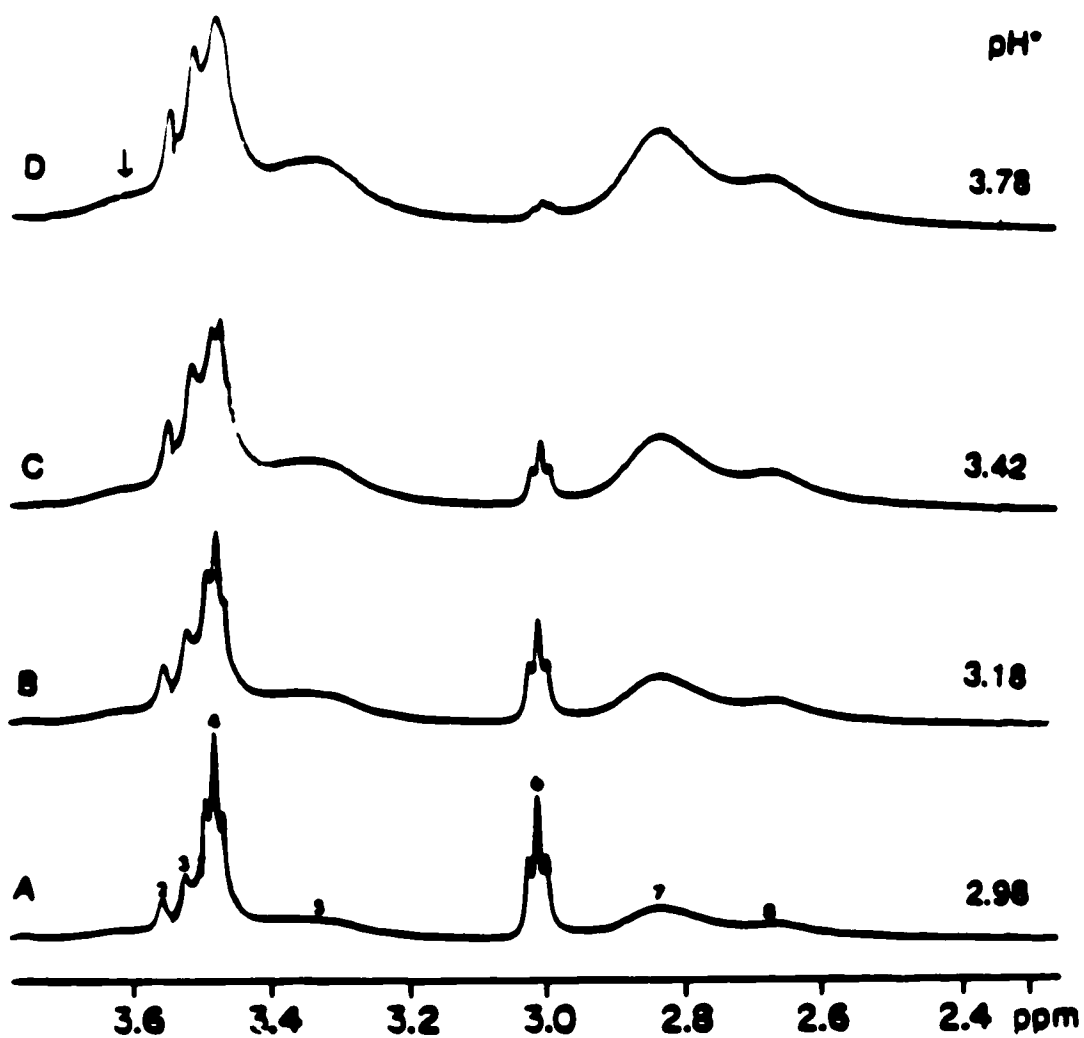


Figure 49. (continued). B. Chemical shift (ppm) range is 2.40 to 3.80, depicting the bound T1 and T2 methylene protons. Assignment of the peaks from 2 to 8 is as presented in Figure 41.

There are several things to note about these spectra. Firstly, the resonance at 3.900 ppm grows in intensity and the resonance at 3.914 ppm decreases in intensity as pH^* is increased (Figure 49A). This implies the presence of a new species, perhaps the formation of a binuclear complex such as La_2L . However, when the pH^* value is converted to pD values, the pD range is 3.37 to 4.18. Comparison with the pH titration of a 2.6:1.0 ratio of La^{+3} :TAHA (Figure 37) indicates that this is the sloping buffer region in which protonated species of the complex LaL exist. Observation of the resonances at 2.835 ppm (peak 7) which are due to LaH_2L and the resonance at 2.667 ppm (peak 8) which is due to LaHL (at pH^* 2.98) indicate that these resonances also increase in intensity as the resonance at 3.900 ppm increases. This implies that peak 11 for the methylene protons is due to the bound protonated species which perhaps are in fast exchange. However, results presented later indicate that there is only one species which gives rise to this resonance.

Another possibility, as proposed by Harju (98), is the formation of binuclear species in this region. For a species La_2L , the first La^{+3} may interact more strongly with the nitrogen groups present which would allow for the available carboxylate groups to interact with a second metal ion. If this were the case, then the methylene protons closest to the carboxylate group would be the most affected hence a new resonance would be observed (such as La_2L).

Other points of interest in these spectra are as follows. The unidentified resonance previously labeled as peak 2 in Figure 41 appears to grow in intensity together with the resonance labelled peak 11 when the pH^* is increased. This seems to again imply the presence of a new species such as La_2L in the presence of excess La^{+3} . Also there appears to be an increase in a small hump, as indicated by the arrow, as the pH^* is raised from 2.98 to 3.78. This "hump" is real and appears to increase; the species giving rise to this

broad resonance is uncertain.

Figure 50 is the chemical shift (ppm) versus pH^* plot of all the resonances observed in which the $\text{La}^{+3}:\text{TAHA}$ ratio was 2.3:1.0 (Figures 49A and 49B). As seen from Figure 50, all resonances are pH^* independent in the region where complex formation occurs. The frequency, integral, and $W_{1/2}$ values obtained from deconvolution of the chemical shift region presented in Figure 49A are tabulated in Table 17. As indicated from the last column, and as is obvious from Figure 49A, the percent of free TAHA decreases from 59.1% to 8.2% from spectrum A to spectrum D indicating that in the presence of excess La^{+3} , more TAHA is bound as the pH^* is raised from 2.98 to 3.78.

Since there appeared to be no visual difference in spectra A to D in Figure 49B between 2.4 to 3.2 ppm, it was attempted to calculate the stability constants $K_{\text{LaH}_2\text{L}}^{\text{D}}$ and $K_{\text{LaHL}}^{\text{D}}$ using the same resonances and the same method as described earlier. The logarithms of $K_{\text{LaH}_2\text{L}}^{\text{D}}$ and $K_{\text{LaHL}}^{\text{D}}$ were calculated to be 8.3 ± 0.3 and 12.7 ± 0.2 respectively. These values are on the same order of magnitude as those reported in Table 16.

The conditional formation constants, K_1^{C} and K_2^{C} , calculated using Equations [112] and [113] have the same trend and magnitude as that presented in Figure 47 (figure not shown).

It was attempted to decrease the exchange rate to the slow exchange limit for the sample in which the $\text{La}^{+3}:\text{TAHA}$ ratio was 2.3:1.0 at $\text{pH}^* 3.42$ (spectrum C in Figures 49A and 49B), by decreasing the sample temperature. The behavior of the two resonances at 3.897 and 3.877 ppm as a function of temperature is presented in Figure 51; the results are summarized in Table 18 (resonance identification, temperature and the $W_{1/2}$). At high temperatures (spectrum F at 69.0°C and spectrum E at 62.4°C), the resonances are in the

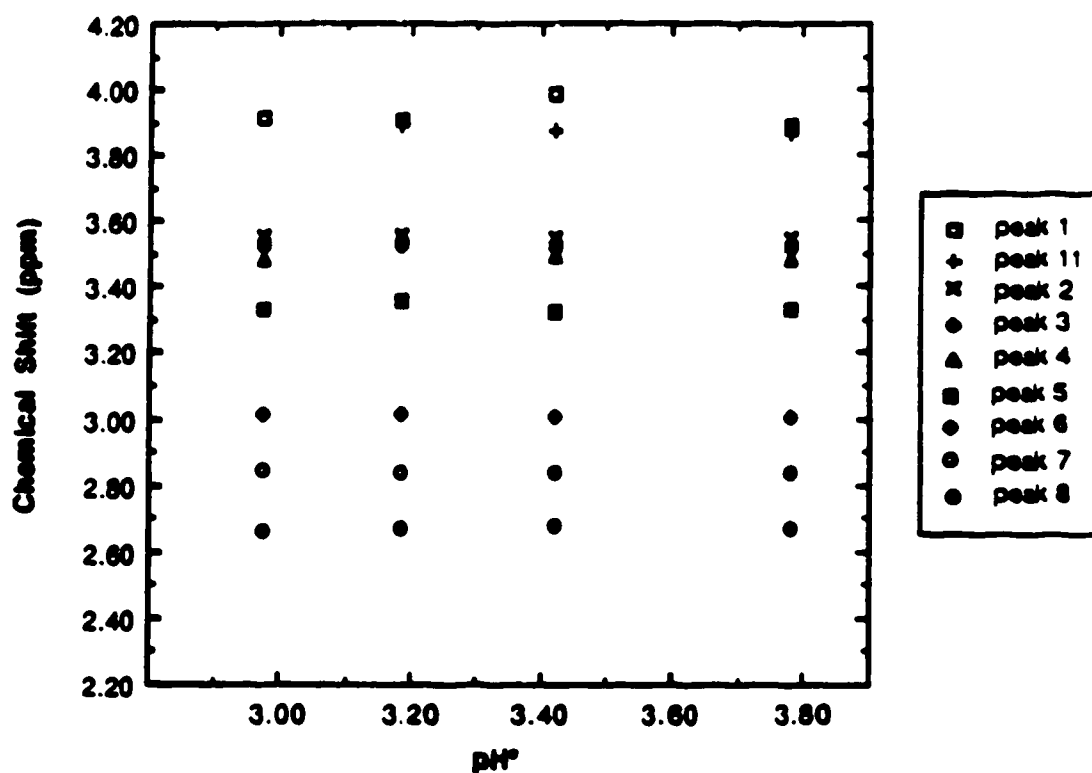


Figure 50. Plot of chemical shift (ppm) versus pH^* of all ^1H NMR resonances in which the $\text{La}^{+3}:\text{TAHA}$ ratio was 2.3:1.0. Identification of peaks 1 to 8 are presented in Figure 41, while peak 11 is assigned in Figure 49A.

Table 17. Tabulation of pH*, chemical shifts, linewidths, and relative integrals for the two ^1H NMR resonances labelled as peak 1 and peak 11 in Figure 49A.

Curve	pH*	δ (ppm)	$W_{1/2}$ (Hz)	Relative Integral	Percent
		peak 1 peak 11	peak 1 peak 11	peak 1 peak 11	of peak 1
A	2.98	3.914	2.67	129.54	59.1
		3.900	7.59	89.71	
B	3.18	3.910	3.43	80.96	45.6
		3.890	8.14	96.66	
C	3.42	3.897	3.66	42.33	27.1
		3.877	8.34	114.10	
D	3.78	3.887	3.66	11.191	8.2
		3.864	8.34	125.193	

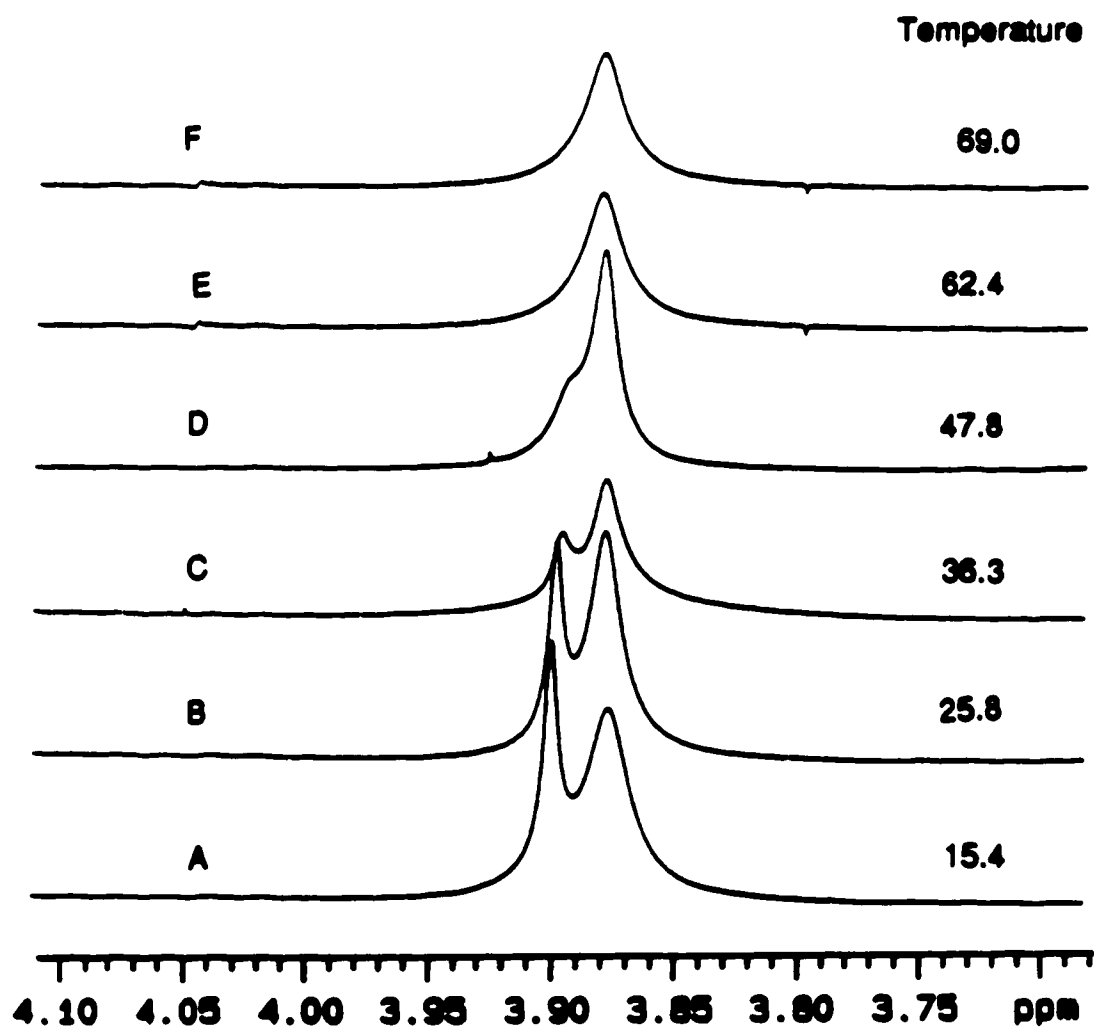


Figure 51. Representative ^1H NMR spectra of as a function of temperature in which the $\text{La}^{+3}:\text{TAHA}$ ratio was 2.3:1.0.

Table 18. Summary of effect of change in temperature on peak half widths as shown in Figure 51 (note that a line broadening function of 0.3 Hz was applied to all spectra).

Spectrum	Temperature (°C)	W _{1/2} (Hz)	
		peak 1	peak 11
A	15.37	5.0	12.3
B	25.80	5.0	8.5
C	36.26	5.6	7.7
D	47.81		6.9
E	62.42	10.1 ¹	
F	69.00	14.7 ¹	

¹ The value of W_{1/2} given is for the single resonance observed at this temperature

fast exchange region and only a single, exchange averaged resonance is observed. As the temperature is decreased, the exchange rate decreases and two resonances are observed (spectrum B at 25.8 °C and spectrum A at 15.4 °C). Calculation of exchange rates is best performed in the intermediate exchange region (spectra B, C, or D); however, in order to calculate exchange rates, the frequency and $W_{1/2}$ must be known in the absence of exchange. It was not possible to decrease the probe temperature (with flowing air) to values less than 15.4 °C, hence a spectrum could not be obtained in the slow exchange limit. Therefore the exchange rate could not be measured for any of the species present.

After the stability constants for the complexes $\text{La}(\text{TAHA})^{-3}$, $\text{LaH}(\text{TAHA})^{-2}$ and $\text{LaH}_2(\text{TAHA})^{-1}$ were determined, it was attempted to use these values to estimate the stability constant for the bimetal complex La_2L as defined in Equation [79] from the 2.62:1.00 pH titration curve presented in Figure 37. These calculations assumed that all the TAHA is bound, an assumption which ^1H NMR studies showed to be valid within this pH region in the presence of excess metal. The calculations were performed using the following equations where charges are omitted for simplicity.

$$C_{\text{La}} = [\text{LaHL}] + [\text{LaL}] + 2 [\text{La}_2\text{L}] + [\text{La}] \quad [116]$$

$$C_{\text{L}} = [\text{LaHL}] + [\text{LaL}] + [\text{La}_2\text{L}] \quad [117]$$

$$T_{\text{OH}} = \frac{(\text{M}_{\text{OH}})(V_{\text{OH}})}{(V_{\text{OH}} + V_{\text{i}})} \quad [118]$$

$$T_{\text{H}} = \text{H} + \text{LaHL} \quad [119]$$

The terms C_{La} and C_L are the total concentrations of La^{+3} and TAHA present in solution respectively. The term T_{OH} is the total concentration of the base added while M_{OH} and V_{OH} are the molarity and volume of the titrant KOH added. The symbol V_i is the initial volume of the solution. The term T_H is the total concentration titratable hydrogen which can also be defined by the following equation:

$$T_H = 6C_L - T_{OH} \quad [120]$$

A value of 6.16 ± 0.05 ($n=4$) for the logarithm of K_{La_2L} was obtained; the overall formation constant β_{La_2L} is then calculated to be $1 \times 10^{22.22}$. The dissociation constant $K_{LaHL}^{H(La)}$, which is defined below, was calculated to be $1 \times 10^{-3.21}$ when the A value of the solution was greater than 5 (and the pH of the solution was also greater than 5):



The calculated values of K_{La_2L} , K_{LaHL}^H and $K_{LaHL}^{H(La)}$ are tabulated in Table 16, along with the stability constants calculated from 1H NMR studies. From the above calculations it appears that the presence of excess metal such as La^{+3} effectively displaces the proton from $LaHL^{-2}$ to form La_2L .

3. Summary

Of all the rare earth metals studied, the interaction of La^{+3} with TAHA appeared to be the most well behaved regarding the results obtained from pH titrations and the pHg method at various ratios of La^{+3} :TAHA. The formation of

mixed metal ligand complexes such as HgLLa or $\text{HgLLa}(\text{OH})_n$ may be possible. This type of interaction was implied in potentiometric titrations of solutions in which the ratio of $\text{Hg}^{+2}:\text{La}^{+3}:\text{TAHA}$ was 1.0:1.0:1.0. As discussed earlier, formation constants could not be calculated, partly due to the complexity of the interaction of the mercury ion with TAHA which has not yet been fully characterized. ^1H NMR spectra obtained for this system were much simpler than those obtained for the mercury-TAHA system; however, there is an unidentified resonance (peak 2, Figure 41) which may be due to the presence of small concentrations of the binuclear complex present when the $\text{La}^{+3}:\text{TAHA}$ ratio is 1.0:1.0. Between the pH range 2.0 to 12.0 there was no precipitate formed due to the formation of the neutral complex La_2L . The formation of hydroxyl complexes such as $\text{LaL}(\text{OH})_n$ was not indicated even at very high pH values.

All the stability constants calculated for this system are tabulated in Table 16 while all possible equilibria present in the lanthanum-TAHA system are depicted in Figure 52.

D. Calcium

Calcium, an alkaline earth metal, has an important biological role. The divalent ion Ca^{+2} plays an important role in many body processes and its concentration in body fluids is maintained within narrow limits by two hormones: the parathyroid hormone, which helps keep the concentration of calcium in the cellular and extracellular fluids constant despite the large variations in the calcium intake and excretion, and the calcitonin hormone, which lowers the

concentration of calcium in plasma. Both these hormones have opposing actions which maintain $[Ca^{+2}]$ levels at the required level. Such regulation is important considering the broad scope of the function of calcium in the body: it controls the permeability and electric properties of cell membranes. It is important in bone composition, it is necessary in blood clotting and finally it is necessary for muscle contraction (108).

Because of the biological importance of calcium ions and because this work was originally undertaken to study the use of TAHA as a potential contrast agent, it was necessary to characterize the interaction of this ligand with Ca^{+2} via potentiometric and 1H NMR studies. In this section the interaction of Ca^{+2} with the ligand TAHA is presented.

1. Potentiometric Studies

Figure 53 presents a plot of pH versus the A value for the ligand TAHA in the presence of Ca^{+2} . The first curve is the titration of TAHA alone, which exhibits the usual inflection point at an A value of 3; the other two curves are duplicate pH titrations for a solution of Ca^{+2} :TAHA in a ratio of 0.97:1.0 (0.6765 mM Ca^{+2} , 0.6735 mM TAHA). From these curves it is observed that no complexation occurs until approximately pH 6.0, where the A value is 3. At A values less than 3, all three curves are identical, indicating that the pH is determined by the ligand and that there is no complexation in this pH region. The displacement of the plateau region to a lower pH after an A value of 3 when both TAHA and Ca^{+2} are present is indicative of the relatively weak calcium-TAHA binding. Between A values of 3 to 5 there is a shallow buffer region due to the presence of protonated complexes such as CaH_nL where n is 2 or 3. Between the A values of 5 to 6 the pH rises as the complex $CaHL^{-3}$ is deprotonated to form CaL^{-4} . A value for K_{CaHL}^H as

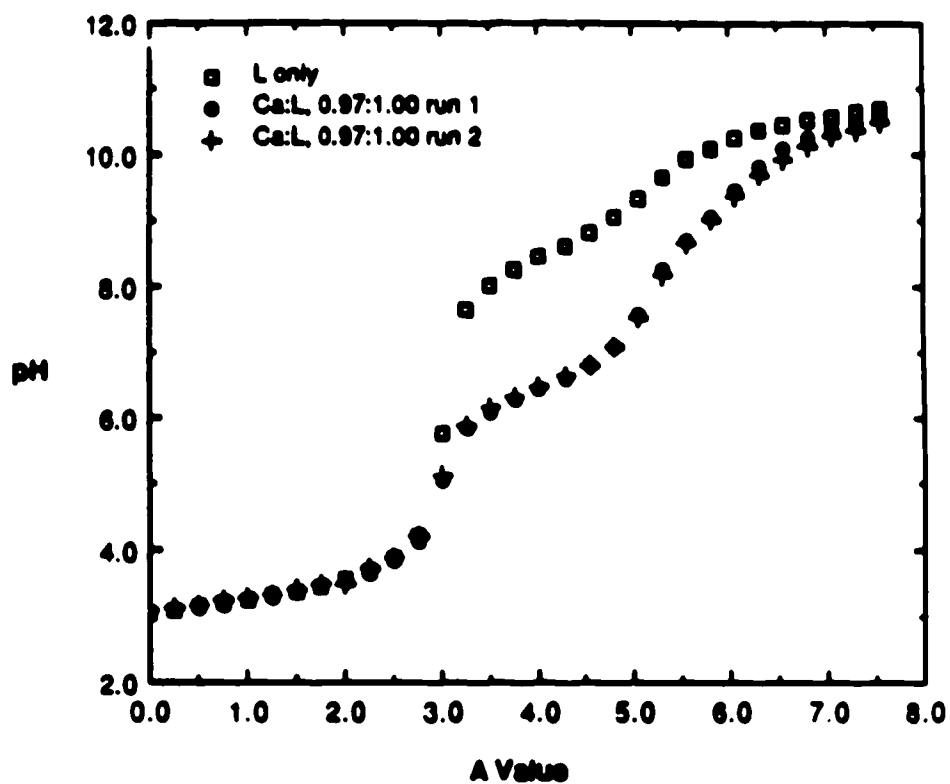


Figure 53. Titration curves of pH versus A value for the calcium-TAHA system at various concentrations; L represents the ligand TAHA. All titrations were performed at constant ionic strength and temperature ($\mu=0.1$ M KNO_3 and 25.00°C).

defined in Equation [75] was calculated using the method of Schwarzenbach as described in the previous section. For two duplicate runs K_{CaHL}^H was calculated to be 2.45×10^{-9} and 2.19×10^{-9} . The value is given in Table 19.

In Figure 54 are plotted pHg data for a solution of $Hg^{+2}:Ca^{+2}:TAHA$ in which the ratio is 1.0:2.0:2.1 (0.9578 mM Hg^{+2} , 1.9586 mM Ca^{+2} , 2.002 mM TAHA). Curve A represents the potential-pH dependence for the mercury-TAHA system while curve B represents the theoretical upper potential limit at the mercury indicating electrode. Before pH 6.0 the curve is identical to the potential-pH diagram of the mercury-TAHA system. Between pH 6.0 to 6.5 there is a dip in the potential-pH diagram. In this region equilibrium was reached very slowly, taking two to three hours during which the potential increased slowly as the pH remained constant. After pH 7.0 potential measurements were recorded after the potential had been stable for at least thirty minutes. As observed from this curve there are two pH independent regions, the first between pH 7.0 to 8.0 (labelled as region C), and the second between pH 10.0 to pH 11.0 (labelled as region D). From the experimental data in Figure 54 the pK_{eq}^{Ca} and K_{CaL}^C were calculated using Equations [108] and [109]: these formation constants are presented as open squares in Figure 55. The lines represent the curves corrected for the formation of $Ca(OH)^+$ which has $K_{Ca(OH)}$ of $1 \times 10^{0.64}$ (30); as seen from this figure formation of $Ca(OH)^+$ does not occur. The calculated pK_{eq}^{Ca} in the pH range 7.08 to 7.99 was 15.51 ± 0.03 and the pK_{eq}^{Ca} calculated in the pH range 10.09 to 10.87 was 17.97 ± 0.01 .

In a duplicate run, where equilibrium had not been attained (i.e. it was assumed that the potential measured after a few minutes was the equilibrium

Table 19. Tabulation of the stability constants calculated for the calcium-TAHA system (25.00 °C, $\mu=0.1$ M KNO₃).

Constant	Definition	Number of Runs (N)	log K
K_{CaL}^D	$\frac{[CaL^{-4}]}{[Ca^{+2}][L^{-6}]}$	2	8.32 ± 0.02
K_{CaHL}^D	$\frac{[CaHL^{-3}]}{[Ca^{+2}][HL^{-5}]}$	2	6.56 ± 0.02
$K_{CaH_2L}^D$	$\frac{[CaH_2L^{-2}]}{[Ca^{+2}][H_2L^{-4}]}$	2	4.75 ± 0.02
K_{CaHL}^H	$\frac{[CaL^{-4}][H^+]}{[CaHL^{-3}]}$	2	-8.65 ± 0.05
$K_{CaH_2L}^{H(D)}$	$\frac{[CaHL^{-3}][H^+]}{[CaH_2L^{-2}]}$	2	-7.10 ± 0.03

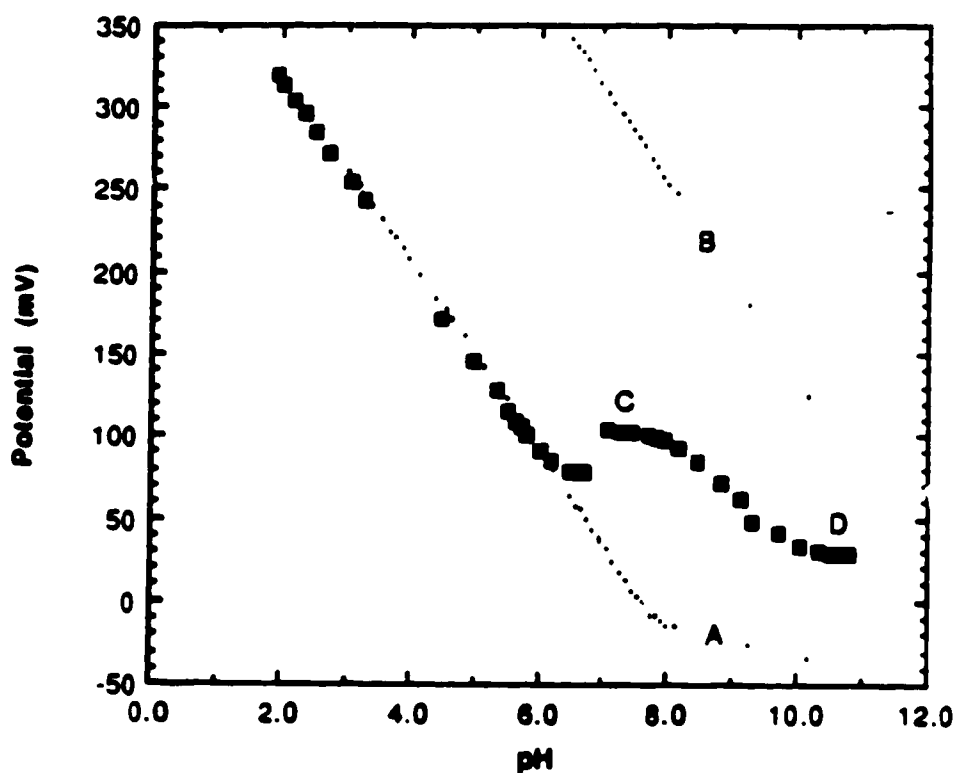


Figure 54. Potential-pH diagram for a solution in which the ratio of $\text{Hg}^{+2}:\text{Ca}^{+2}:\text{TAHA}$ is 1.0:2.0:2.0. The total concentration of Hg^{+2} , Ca^{+2} , and TAHA is 0.9578 mM, 1.959 mM, and 2.00 mM respectively. Curve A represents the potential-pH dependence of the calcium-TAHA system while curve B represents the theoretical upper potential limit at the mercury indicating electrode. Two plateau regions labelled 'C' and 'D' are observed.

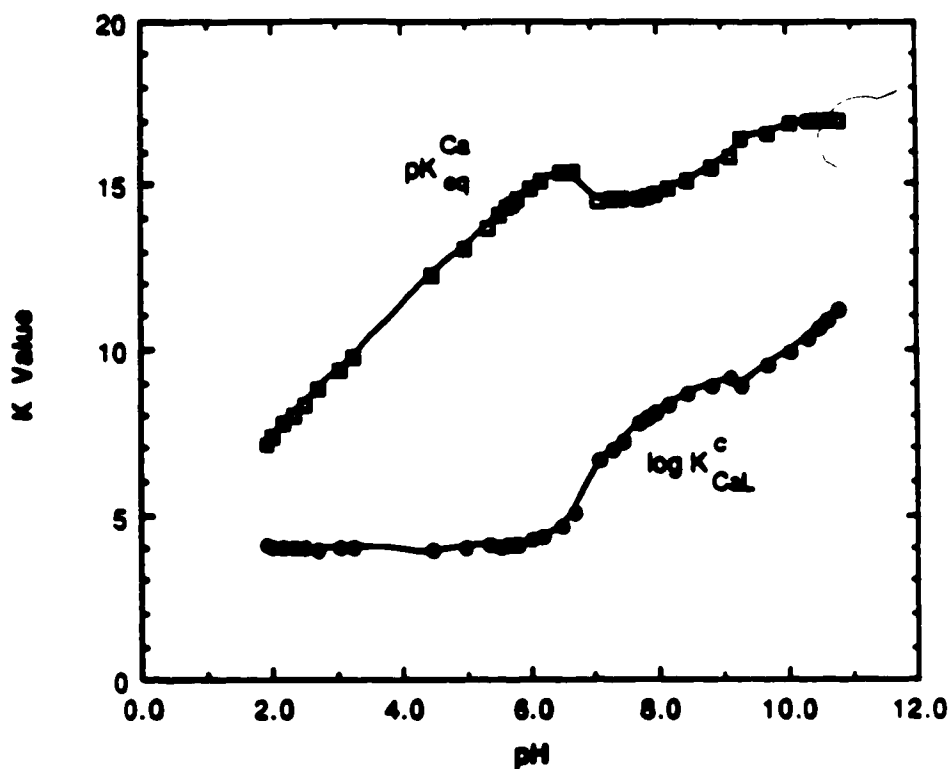


Figure 55. Plot of pK_{eq}^{Ca} and logarithm of K_{CaL}^C as a function of pH. The symbols represent data that has not been corrected for the formation of $Ca(OH)^+$, while the lines represent the calculated pK_{eq}^{Ca} and logarithm of K_{CaL}^C , after the correction for $Ca(OH)^+$ has been applied.

potential as was true for all other metals), the calculated pK_{eq}^{Ca} values were lower by approximately 1 pK_{eq} unit in both potential pH independent regions.

The first equilibrium constant calculated for the pH range 7.0 to 8.0 is probably, due to the exchange reaction defined by Equation [13] while the second equilibrium constant is probably due to the association of hydroxyl ion(s) to calcium-TAHA complexes such as $CaL(OH)_n$. This is based on the fact that approximately 0.08 mM KOH was required to raise the pH by 0.2 units after pH 10.0; this is approximately *10-fold* more KOH than was required prior to pH 10.

2. 1H NMR Studies

1H NMR studies of Ca^{+2} :TAHA gave useful information regarding the complexation behavior of Ca^{+2} in the presence of TAHA. Figure 56 is a representative 1H NMR spectra as a function of pH* for a solution of Ca^{+2} :TAHA in a 1.08:1.00 ratio (3.7100 mM Ca^{+2} , 3.4900 mM TAHA). Between pH* 5.92 to 7.11 resonances due to both free and bound TAHA were observed which is expected since the potentiometric titrations indicated that no complex formation occurred prior to pH 6 (pH* 6.4). Resonances at 3.238 ppm and 2.640 ppm in spectrum A are due to the T3 and T1 methylene protons of bound TAHA respectively and are identified by the two arrows in spectrum F of Figure 57. The singlet at 3.819 ppm in spectrum A is due to the free T3 methylene protons. The assignment of the T3 methylene protons of bound TAHA was identified by decreasing the temperature and hence the exchange rate between overlapping resonances observed in the 1H NMR spectra for a sample at pH* 6.91; the spectra as a function of temperature are presented in Figure 57. Spectrum C was taken at 25.8 °C: the resonances at 3.226 ppm and 2.641 ppm are for the T3 and T1 methylene protons of bound TAHA while those at 3.391 and

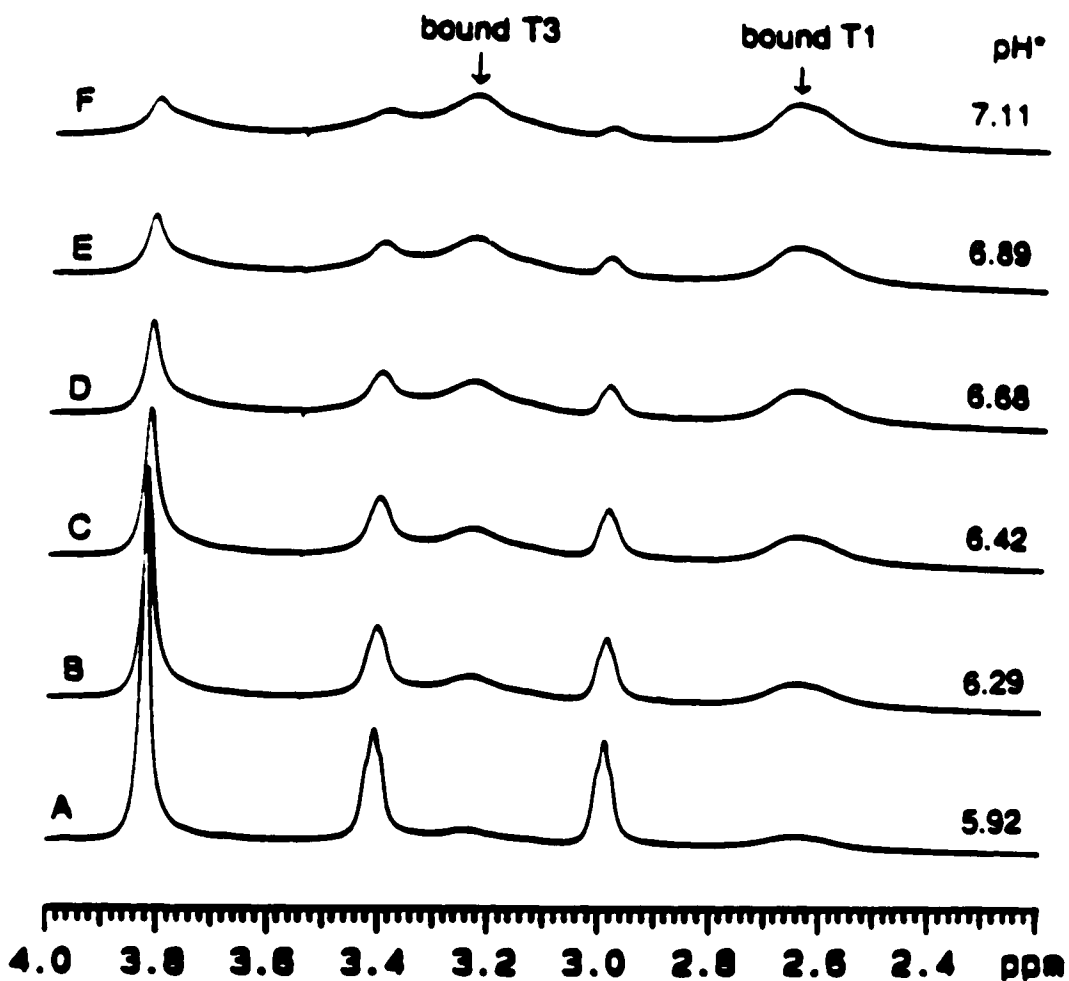


Figure 56. Representative ^1H NMR spectra as a function of pH^* for the calcium-TAHA system. The total concentration of Ca^{+2} and TAHA was 3.710 mM and 3.490 mM respectively (ratio of Ca^{+2} :TAHA is 1.08:1.00). The resonances due to the free and bound T1 and T3 methylene protons of TAHA are labelled.

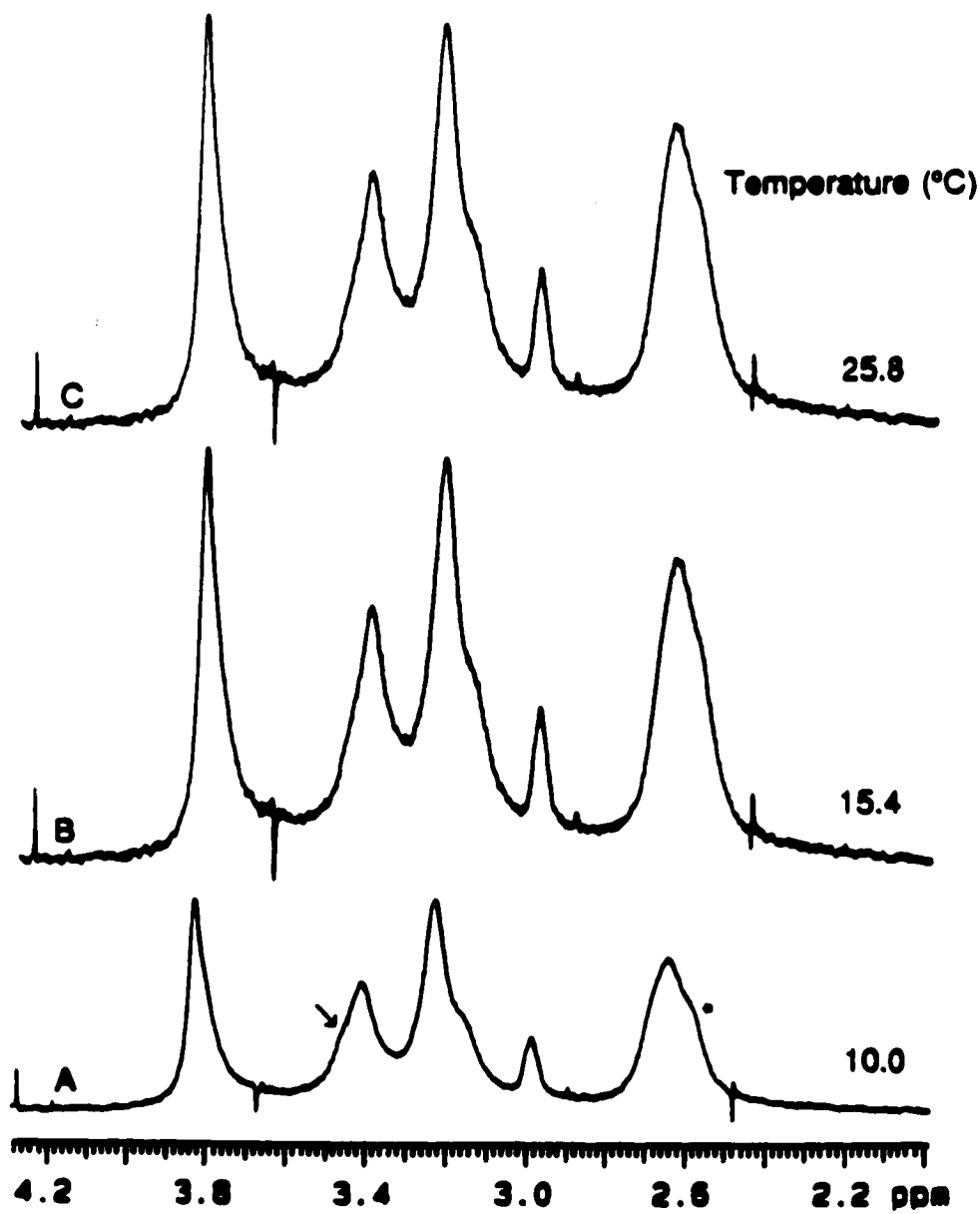


Figure 57. Representative ^1H NMR spectra of as a function of temperature in which the Ca^{2+} :TAHA ratio was 1.08:1.00 at pH* 6.91. For details see text.

2.978 ppm are due to the T2 and T1 methylene protons of free TAHA. In spectrum A, taken at 10.0 °C; the resonances due to the T3 and T1 methylene protons of bound TAHA have a shoulder due to the formation of two different complexes. The resonance at 3.404 ppm which appears to be due solely to the T2 methylene protons of free TAHA (by comparison with Figure 57A) has a slight shoulder as marked by an arrow. The singlet at 3.822 ppm does not appear to be any different than the singlet in spectrum C taken at 25.8 °C, therefore it is unlikely that this resonance is due to overlapping species. Examination of the spectrum in Figure 57A indicates that the resonance at 2.650 ppm has a slight shoulder which is marked by a star. This figure also indicates that the single resonances due to bound TAHA are due to two overlapping complexes. Comparison with the pH titration curves for this pH region indicates that the complexes $\text{CaH}_2\text{L}^{-2}$ and CaHL^{-3} are formed.

Between pH* 7.5 to 8.3, all resonances begin to overlap for a 1.08:1.00 solution of Ca^{+2} :TAHA (spectra not shown). After pH* 8.4, two broad resonances were observed which was due to different complexes present in fast exchange; the spectra in this region are similar to those presented for the lanthanum-TAHA system (Figure 45, spectra E and F). After pH* 9.5 both resonances begin to sharpen as the fast exchange region is reached.

If the exchange rate is decreased for a sample at pH* 10.10, the overlapping resonances begin to separate as the intermediate exchange region is approached; this is illustrated by the spectra presented in Figure 58. The broad resonance at 2.679 ppm at 25.8° (spectrum C) separates into three resonances at 2.930 ppm, 2.724 ppm, and 2.589 ppm. The resonance at 2.930 ppm appears to be due to free TAHA present in solution.

The chemical shift versus pH* for the titration of Ca^{+2} :TAHA in a 1.08:1.00 ratio is presented in Figure 59. The resonances due to the free and

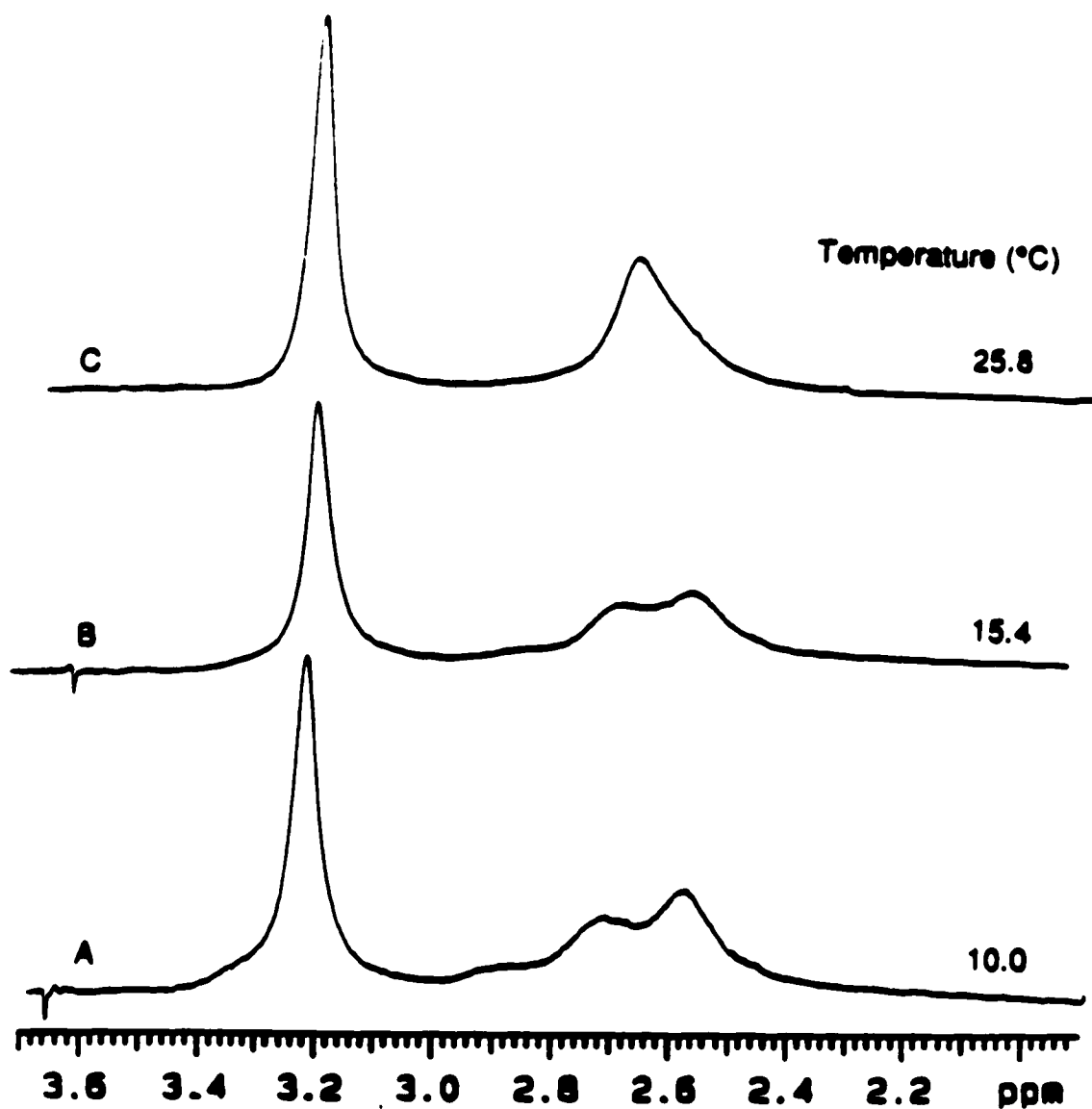


Figure 58. Representative ^1H NMR spectra of as a function of temperature in which the Ca^{+2} :TAHA ratio was 1.08:1.00 at pH* 10.10. For details see text.

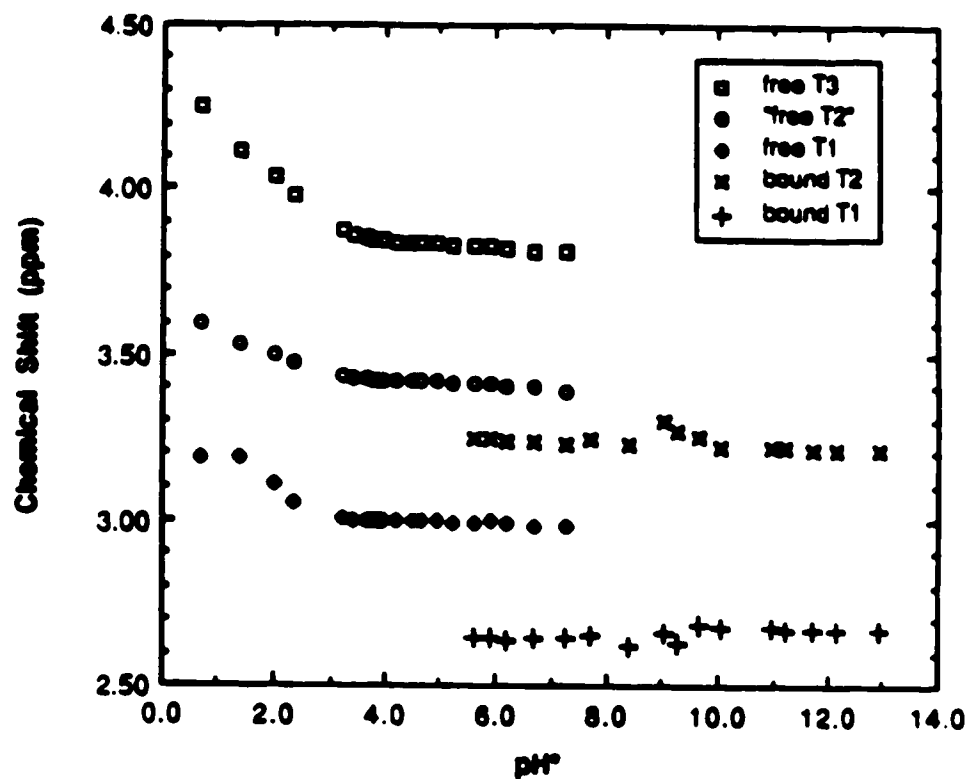


Figure 59. Chemical shift (ppm) versus pH* for the titration of Ca²⁺:TAHA in a ratio of 1.08:1.00. Identification of each resonance has been discussed in the text.

bound TAHA are labeled in the legend (the legend assigns the resonance at 3.226 ppm (pH* 6.91) to "free T2" although in light of the above discussion it must be noted that at ambient temperature there may be small degree of overlap).

For the 2.4 ppm to 3.5 ppm region in the pH* range 5.9 to 7.1, all the ^1H NMR spectra were curve fitted for the calculation of stability constants, $K_{\text{CaH}_2\text{L}}^{\text{D}}$ and $K_{\text{CaHL}}^{\text{D}}$. A typical curve fitted spectrum is presented in Figure 60 for the calcium-TAHA system at pH* 6.17. The original spectrum and the calculated spectrum are labeled as curves 1 and 2 respectively, while curve 3 represents the plot of each of the individual components. The numerical output obtained from the curve fitting program is also presented at the top of this figure. For all spectra that were curve fitted, a digital resolution of 0.195 Hz per point was maintained, the χ^2 varied from 100 to 600 and convergence was usually reached between 20 to 40 iterations. From the total areas obtained, the fraction of TAHA free and bound was calculated. From this the total concentration of free TAHA ($[\text{L}]_{\text{f}}$), the total concentration of free Ca^{+2} , $[\text{Ca}^{+2}]_{\text{f}}$, and the total concentration of the bound species were calculated from mass balance relationships. From the above values, a conditional formation constant, $K_{\text{CaL}}^{\text{C}}$ was calculated using the following equation:

$$K_{\text{CaL}}^{\text{C}} = \frac{[\text{Total Bound Complex}]}{[\text{Ca}^{+2}]_{\text{f}} [\text{L}]_{\text{f}}} \quad [122]$$

where the total bound complex represents all of the calcium bound as $\text{CaH}_2\text{L}^{-2}$ and CaHL^{-3} . This is also confirmed by the potentiometric results presented in Figure 53 for the pD range in which the above $K_{\text{CaL}}^{\text{C}}$ was calculated. A plot of the logarithm of $K_{\text{CaL}}^{\text{C}}$ as a function of pH* is presented in Figure 61; as

Frequency (ppm)	Height (mm)	Linewidth (Hz)	Integral (mm ²)	Species (T1 methylene protons)
3.000	24.02	8.19	196.82	free TAHA
2.987	44.77	9.64	431.64	free TAHA
2.973	30.51	13.03	397.48	free TAHA
2.934	16.64	72.31	1203.07	bound TAHA

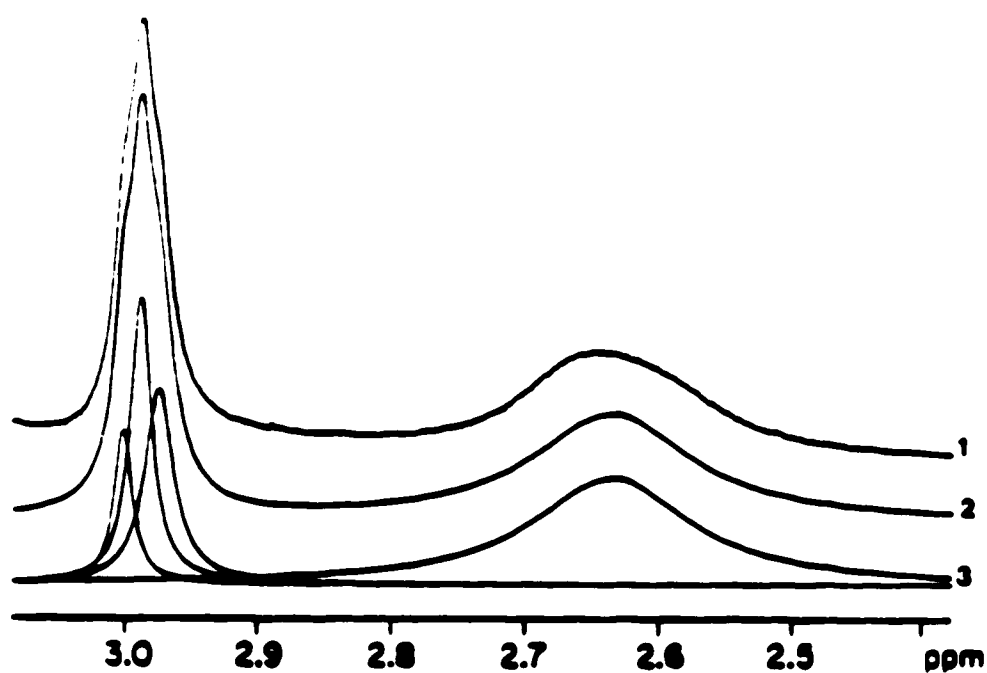


Figure 60. Deconvolution output of a 1.08:1.00 ratio of Ca^{+2} :TAHA at pH 6.17. Curve 1 is the original spectrum, curve 2 is the calculated spectrum, and curve 3 is the plot of each individual component in the spectrum. The numerical results obtained and species giving rise to each resonance are tabulated above.

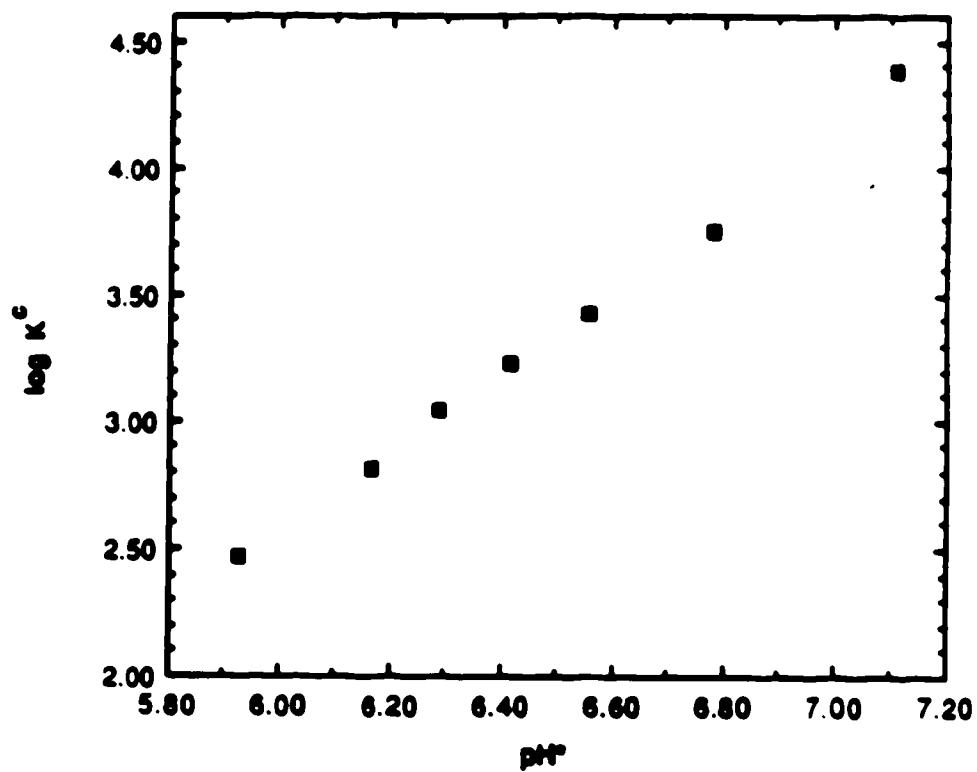


Figure 61. Plot of the logarithm of K_{CaL}^C (K^C), versus pH^* for the calcium-TAHA system.

expected, in this pH* range K_{CaL}^C increases linearly with pH*.

Equation [122] may be rewritten in the following manner:

$$K_{CaL}^C = \frac{[CaH_2L^{-2}] + [CaHL^{-3}]}{[Ca^{+2}]_f [L^{-6}]_f} \quad [123]$$

Using the definitions of $K_{CaH_2L}^D$ and K_{CaHL}^D as defined in Equation [74] for aqueous solutions, Equation [123] may be rearranged as (neglecting charges):

$$K_{CaL}^C = (K_{CaH_2L}^D) \frac{[H_2L]}{[L]_f} + (K_{CaHL}^D) \frac{[HL]}{[L]_f} \quad [124]$$

(where the superscript "D" again refers to experiments performed in D₂O).

Now defining

$$\alpha_4 = \alpha_{H_2L} = \frac{[H_2L]}{[L]_f}$$

and

$$\alpha_5 = \alpha_{HL} = \frac{[HL]}{[L]_f}$$

and substitution into Equation [124], gives after rearrangement, Equation [125]:

$$K_{CaL}^C = (K_{CaH_2L}^D) (\alpha_4) + (K_{CaHL}^D) (\alpha_5) \quad [125]$$

which may be rearranged into the form $y = mx + b$ for a straight line:

$$\frac{K_{CaL}^C}{\alpha_4} = (K_{CaHL}^D) \frac{\alpha_5}{\alpha_4} + K_{CaH_2L}^D \quad [126]$$

A linear regression analysis of a plot where

$$x = \frac{\alpha_5}{\alpha_4}$$

and

$$y = \frac{K_{CaL}^C}{\alpha_4}$$

will give a slope equal to K_{CaHL}^D and a y intercept equal to $K_{CaH_2L}^D$. Figure 62 presents the experimental data as well as the best fit line for the pH* range 5.9 to 7.11 in which linear regression was performed using Equation [126]. The stability constants $K_{CaH_2L}^D$ and K_{CaHL}^D obtained were 5.64×10^4 and 3.67×10^6 respectively, with a correlation coefficient of 0.98 for the best fit line presented in Figure 62. These values are tabulated in Table 19. Calculation of the stability constant for the triprotonated species, $K_{CaH_3L}^D$ was attempted using the 1H NMR data. It was found that the concentration of the bound species in the pH* region of interest (pH range 5.0 to 5.7) was very low. Large errors in the curve fitting of these very broad resonances gave very high χ^2 values (approximately 2000). This translated into extremely large errors for the linear least square calculation of $K_{CaH_3L}^D$ using the above procedure.

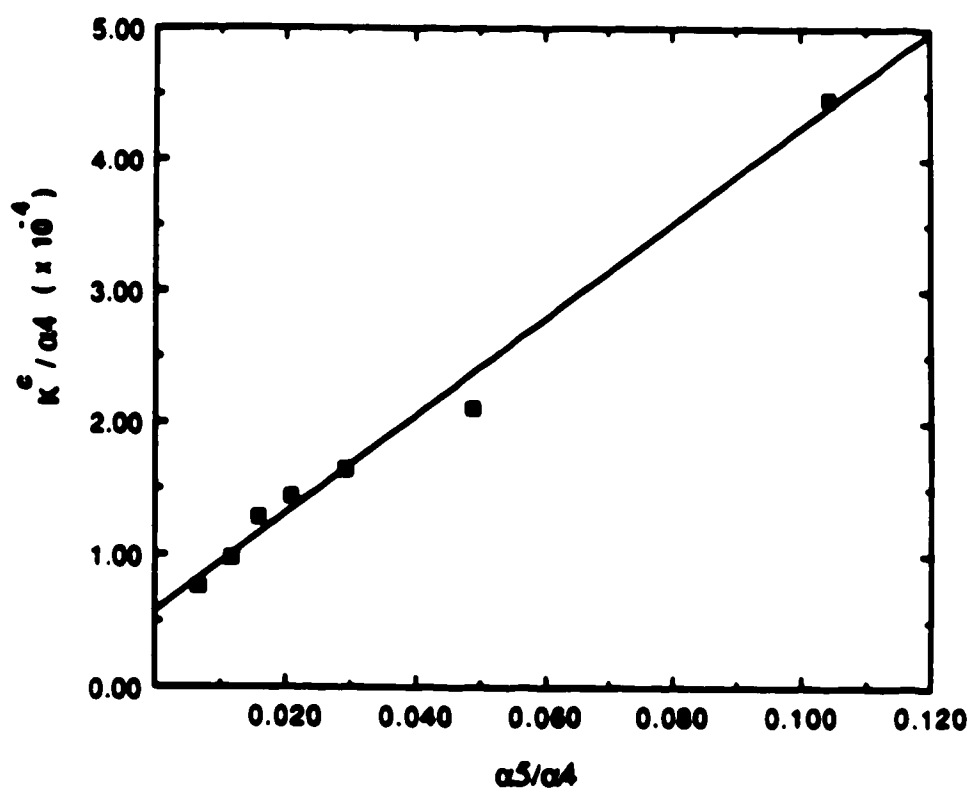


Figure 62. A plot of the linear regression analysis from which the calculation of the formation constants K_{CaHL}^D and $K_{\text{CaH}_2\text{L}}^D$ was performed as described in text.

The symbols represent calculated data points while the line represents the best fit line.

The constant $K_{CaH_2L}^H$ (denoted as $K_{CaH_2L}^{H(D)}$ in Table 19) was calculated using Equation [64] with the acid dissociation constants K_5 obtained from a D_2O solution ($pK_5 = 8.91$); a value of 7.98×10^{-8} was obtained for the constant $K_{CaH_2L}^H$ which is also given in Table 19.

The stability constant K_{CaL} was calculated using Equation [77] and $K_{CaH_2L}^H$ and K_6 previously calculated from aqueous solutions. It was assumed that K_{CaHL}^D would be of the same order of magnitude in aqueous solutions in which the ionic strength and temperature were identical. A value of 2.11×10^8 was calculated for K_{CaL} (see Table 19).

No stability constants were calculated at high pH^* values for two reasons. Firstly, Figure 58 showed small concentrations of free TAHA which could not be observed at $25.8^\circ C$ hence the concentration of free TAHA (if any) and calcium-TAHA species would have to be estimated if the above method were utilized, and secondly the exact nature of the calcium TAHA complexes were unknown (i.e. $CaL(OH)_n^{(-n-4)}$).

For some of the 1H NMR studies the Ca^{+2} :TAHA ratio was increased to 2.35:1.0 (8.21 mM Ca^{+2} , 3.49 mM TAHA). The 1H NMR spectra measured were similar to those observed in Figure 56 except that there was more bound TAHA at each given pH^* . The presence of binuclear complexes was not indicated.

3. Summary

Several stability constants for the calcium-TAHA system are summarized in Table 19. Comparison of K_{CaL} with various other ligands is reported in Table 20. As can be seen, all ligands, including TAHA, tend to form relatively weak complexes with calcium, and they are all within the range of 1×10^8 to 1×10^{11} .

It is possible that mixed metal complexes such as $HgL(Ca)$ form, as was discussed earlier. Since TAHA has ten available coordination sites, it would be

Table 20. Tabulation of the logarithm of K_{CaL} for various ligands (25.00 °C, $\mu=0.1$ M KNO_3).

Ligand	H_nL	log K_{CaL}
EDTA ¹	H_4L	10.61
EGTA ¹	H_4L	10.86
EEDTA ¹	H_4L	9.96
DTPA ¹	H_5L	10.75
TAHA ²	H_6L	8.32
TTHA ¹	H_6L	9.89

¹ Reference 30

² This work

possible to form mixed complexes of calcium and mercury as has been observed for EDTA by Reilley and Schmidt (65). Also complexes such as $\text{CaL}(\text{OH})_n^{(-n-4)}$ cannot be ruled out at the present time, especially at high pH values. It was not attempted to look for aqua complexes such as $\text{CaL}(\text{H}_2\text{O})_n^{-4}$.

The types of equilibria involved (and may be involved in this system) are similar to those of the mercury-TAHA system (Figure 36).

E. Other Metals Studied

1. The Rare Earth Metals

Complexation of TAHAs by ten other rare earth metals besides La^{+3} was studied using the pHg method. These were the trivalent metal ions of praseodymium (Pr^{+3}), neodymium (Nd^{+3}), samarium (Sm^{+3}), europium (Eu^{+3}), gadolinium (Gd^{+3}), terbium (Tb^{+3}), dysprosium (Dy^{+3}), holmium (Ho^{+3}), erbium (Er^{+3}), and ytterbium (Yb^{+3}). The potential-pH diagrams for each of these metals are presented in Figure 63; the initial concentrations of Hg^{+2} , M^{+3} , and TAHAs are tabulated in Table 21. The curves labeled A and B are for the titration of the mercury in the presence of excess TAHAs and the theoretical upper potential limit at the mercury electrode respectively, as described earlier, and presented here for comparison purposes. All of the metals except Eu^{+3} exhibited a potential decrease as the pH was raised after pH 5.0, as was observed for lanthanum; europium however exhibited a potential decrease after pH 4.1. In general, of all the rare earth ions studied, La^{+3} was the best behaved in terms of the large pH independent potential region observed (approximately two pH units; see Figure 38).

For all these metal ions, the calculation of $\text{ML}(\text{OH})_n$ species was attempted using the method of Gupta and Powell (107) as described previously;

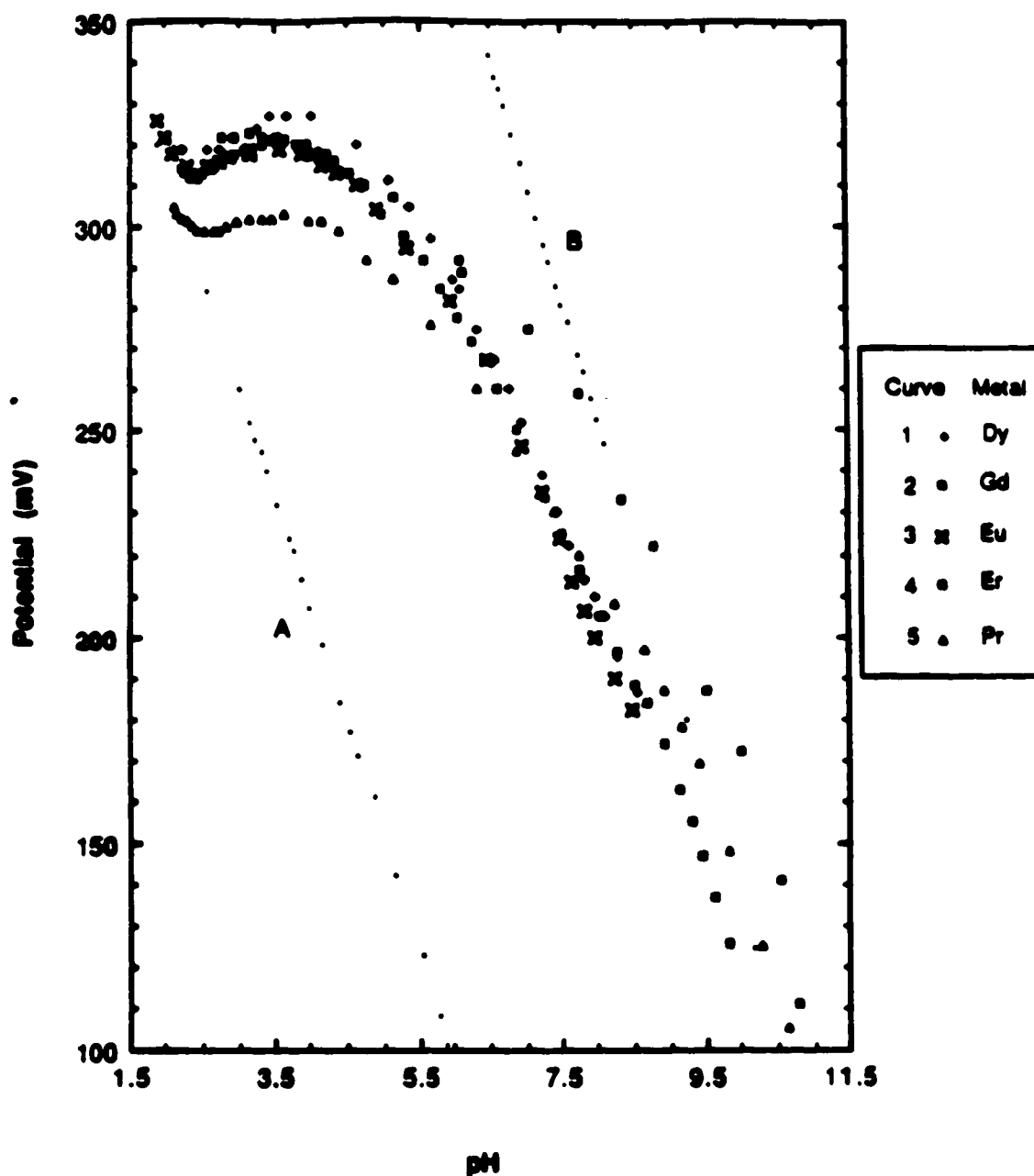


Figure 63. Potenti-pH diagrams for solutions in which the ratio of $\text{Hg}^{+2}:\text{M}^{+3}:\text{TAHA}$ is 1.0:2.0:2.0, where M^{+3} represents the trivalent rare earth metal ion. Curve A represents the potential-pH dependence of the metal-TAHA system while curve B represents the theoretical upper potential limit at the mercury indicating electrode.

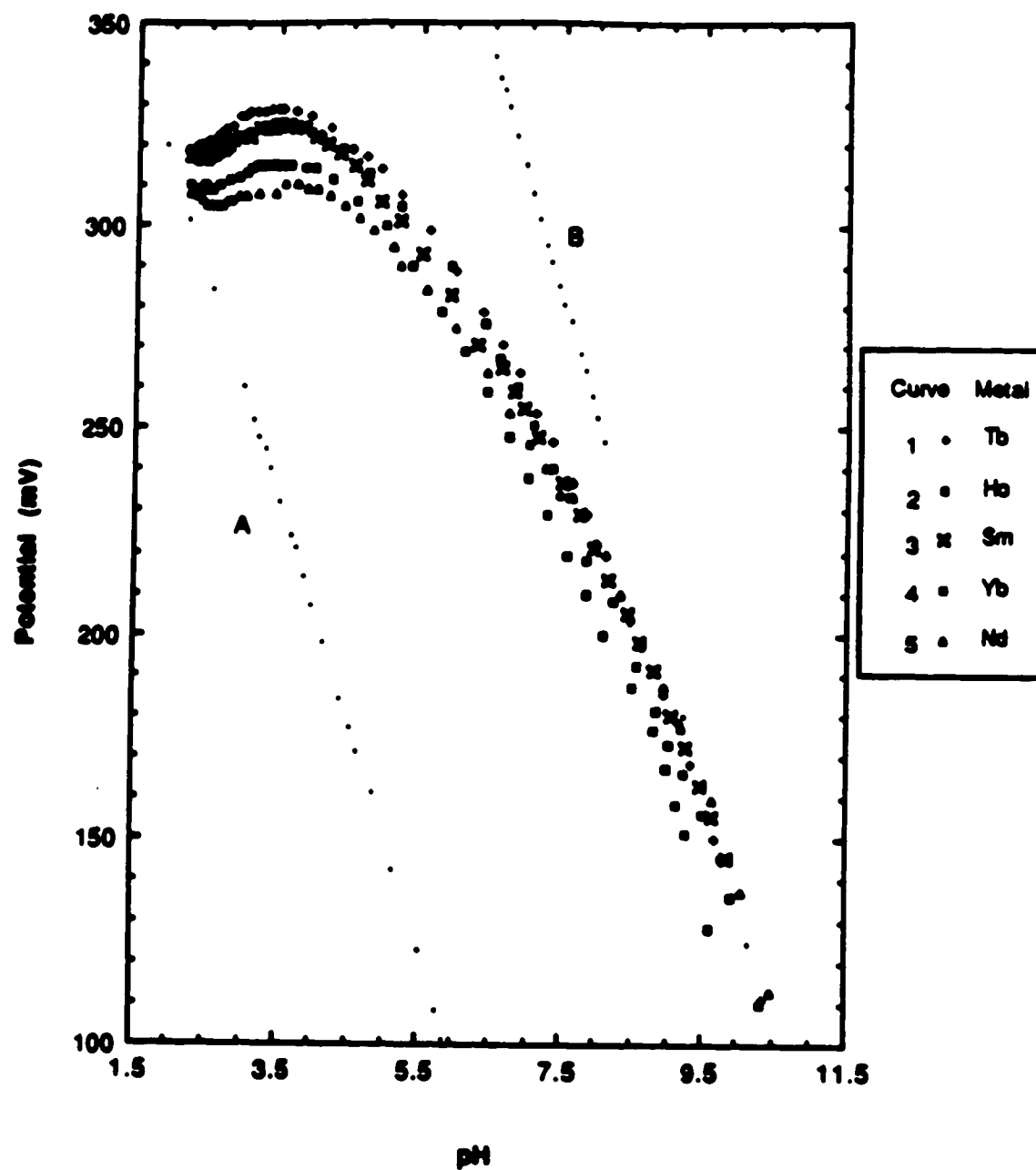


Figure 63. (continued).

Table 21. Tabulation of initial concentrations used for potential-pH diagrams presented in Figure 65.

Metal	Concentration (mM)		
	Hg⁺²	M⁺³	TAHA
Eu	0.597	0.978	1.065
Gd	0.597	1.220	1.065
Dy	0.597	1.003	1.065
Er	0.968	1.983	1.942
Sm	0.968	1.982	1.942
Ho	0.968	2.004	1.942
Tb	0.968	2.015	1.942
Yb	0.968	1.955	1.942
Nd	0.968	2.065	1.942
Pr	0.968	2.026	1.942

and in all cases the presence of such species was not indicated.

Calculation of the equilibrium constant (K_{eq}^M) for the exchange reaction between the mercury-TAHA complex and the metal-TAHA was performed using Equation [108] as described in section C of this chapter. From the calculated K_{eq}^M values, the conditional formation constant (K_{ML}^C) was calculated at each pH using Equation [108]. Figures 64A to 64J are the plots of pK_{eq}^M and $\log K_{ML}^C$ as a function of pH for each metal (labelled as pK and log K respectively, in the legend). Correction for the formation of $M(OH)_n$, as defined by Equations [110] and [111] was applied for each metal; the corresponding corrected formation constants, K_{eq}^M and K_{ML}^C , which are labelled as pK corrected and log K corrected respectively in the legend in Figure 64, are also plotted as a function of pH. Comparison of all four plots for each metal ion indicate that a deviation between the corrected and uncorrected formation constants occurred at pH values greater than 9.0. Since the stability constant for $M(OH)^{+2}$ (where M represents the rare earth metal) is generally quite low (on the order of 1×10^4 to 1×10^6), the corresponding alpha term was generally around 1.0; thus, such species do not form in these solutions. The stability constant for $Hg(OH)^+$ is $1 \times 10^{10.1}$ (30) and it was shown from previous results that $Hg(OH)^+$ also does not form at these pH values. The other possibility is the formation of mixed metal ligand species such as $HgML$ or $HgML(OH)_n$. Although the results are inconclusive at this time, some general qualitative statements may be made. Figure 65 is a plot of the potential versus pH and millimoles of base added versus pH for the titration of holmium-TAHA system using the pHg method. The millimoles of base added represents the total concentration of free acid titrated from the stock $Hg(NO_3)_2$ solution (which was initially dissolved in acid) and therefore was

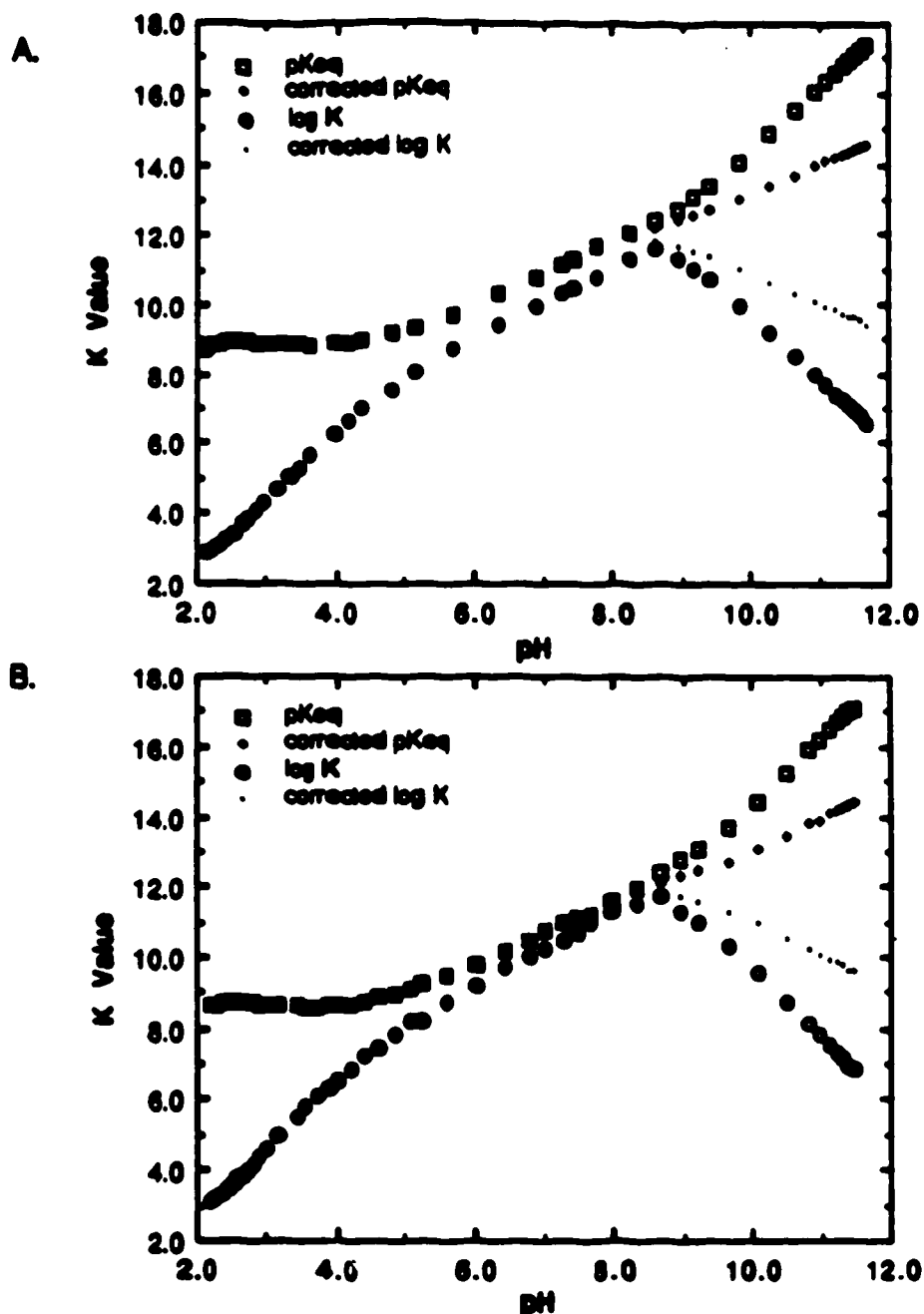


Figure 64. Plot of pK_{eq}^M and logarithm of K_{WL}^C as a function of pH. Formation

constants that are corrected and uncorrected for the formation of the metal hydroxyl species, $(M(OH)_n)^{m-n}$ are plotted as defined in the legend.

- | | | |
|-------------------------------|------------------------------|----------------------------|
| A. Praseodymium (Pr^{+3}) | B. Neodymium (Nd^{+3}) | C. Samarium (Sm^{+3}). |
| D. Europium (Eu^{+3}). | E. Gadolinium (Gd^{+3}). | F. Terbium (Tb^{+3}). |
| G. Dysprosium (Dy^{+3}). | H. Holmium (Ho^{+3}). | I. Erbium (Er^{+3}). |
| J. Ytterbium (Yb^{+3}). | | |

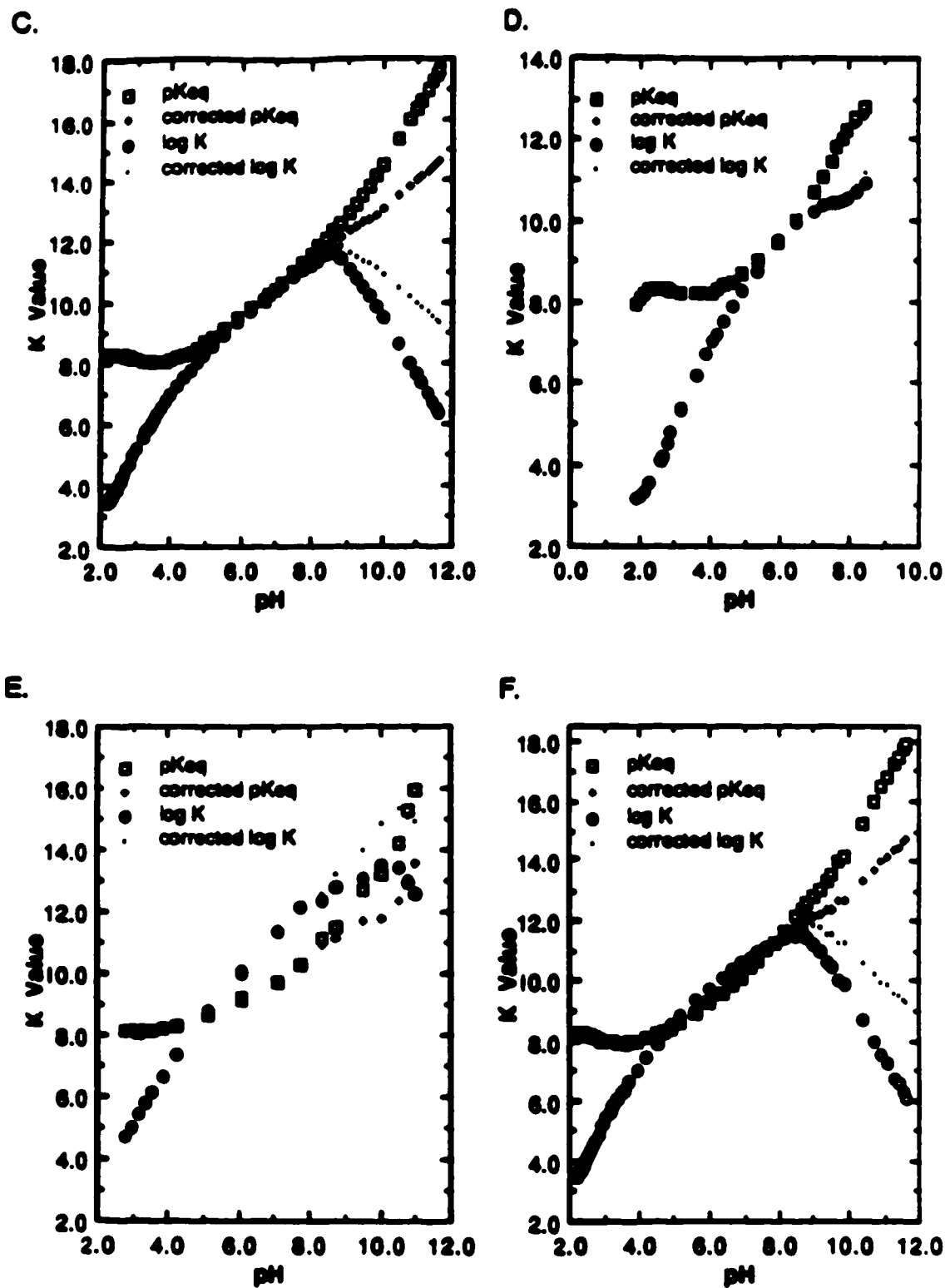


Figure 64. (continued).

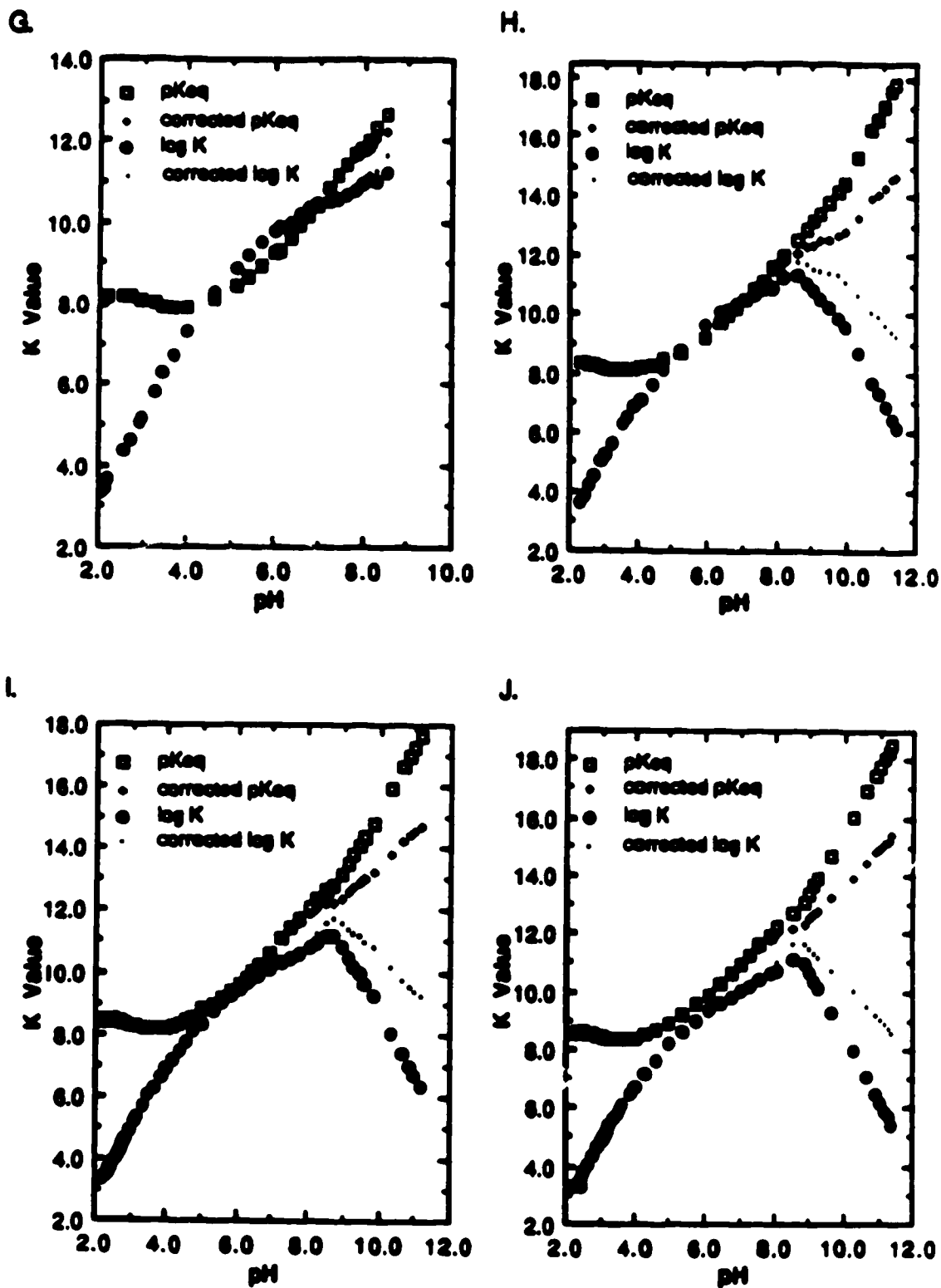


Figure 64. (continued).

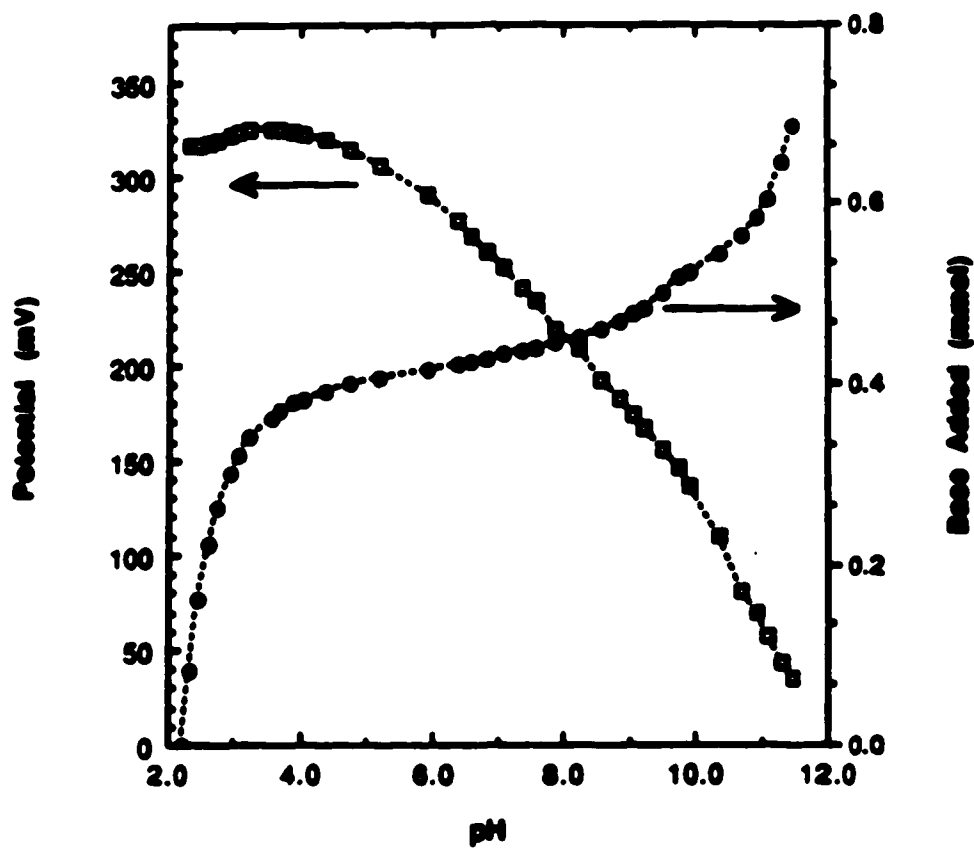


Figure 65. Potential-pH diagram (left y axis) and mmoles base added (right y axis) versus pH for the holmium-TAHA system.

present at the start of the titration, as well as the acid which is liberated when complexation to the metal occurs. As stated earlier, the potential drops after pH 5.0; at this time the mmoles of base added per pH unit increases significantly, which implies that association of hydroxyl ions with a complex occurs; since the formation of $\text{HgL}(\text{OH})_n$ and $\text{ML}(\text{OH})_n$ do not occur, formation of the mixed ligand complex $\text{HgLHo}(\text{OH})_n$ is a very likely possibility.

For all the plots in Figure 64, the $\text{pK}_{\text{eq}}^{\text{M}}$ is constant between approximately pH 2.5 to 4.5 while the $\log K_{\text{ML}}^{\text{C}}$ increases as a function of pH up to pH 9.0. All the pHg experiments were performed in duplicate, using different concentrations of Hg^{+2} , M^{+3} , and TAHA, while maintaining a constant ionic strength of 0.10 M with KNO_3 . The internal variation of $\text{pK}_{\text{eq}}^{\text{M}}$ from individual titrations was low, usually from 0.01 to 0.06 for ten to twenty data points in the region in which the potential was pH independent. It is therefore assumed that the calculated $\text{pK}_{\text{eq}}^{\text{M}}$ values are a good indication of the exchange reaction in which the rare earth metal displaces mercury from the $\text{Hg}(\text{TAHA})^{-4}$ complex. The calculated $\text{pK}_{\text{eq}}^{\text{M}}$ values for each metal are shown in Table 22 along with the atomic number (Z), ionic radius (\AA), and the potential-pH independent region. The average between the two runs is tabulated in the last column of this table. The $\text{pK}_{\text{eq(av)}}^{\text{M}}$ is plotted as a function of atomic number (Z) in Figure 66, and as a function of ionic radius (\AA) in Figure 67. From the definition of $\text{pK}_{\text{eq}}^{\text{M}}$, it can be said that the larger the $\text{pK}_{\text{eq}}^{\text{M}}$, the less effective the metal is in displacing the mercury ion from the mercury-ligand complex. This is observed in Figure 66: $\text{pK}_{\text{eq}}^{\text{M}}$ decreases sharply from La^{+3} (Z = 57) to Sm^{+3} (Z = 62); after Tb^{+3} (Z = 65) $\text{pK}_{\text{eq}}^{\text{M}}$ increases slightly. This behavior is reflected in Figure 67. The largest variation in the calculation of $\text{pK}_{\text{eq}}^{\text{M}}$ shown in Table 22 is for Eu^{+3} (Z = 63) due to the difficulty in obtaining a stable and relatively large pH independent region;

Table 22. Tabulation of pK_{eq}^M and the potential-pH independent region for various rare earth metals with TAHA.

Atomic Number	Metal	Ionic Radius (Å) (ref. 109)	pH Independent Range	Number of Runs (± variance) (N)	pK_{eq}^M (± variance)	pK_{eq}^M (average)
57	La	1.016	3.0 - 4.0	5	10.18 ± 0.03 10.20 ± 0.07	10.19 ± 0.04
59	Pr	1.013	2.0 - 4.2	3	8.88 ± 0.04 8.91 ± 0.04	8.89 ± 0.02
60	Nd	0.995	2.2 - 4.0	3	8.68 ± 0.05 8.72 ± 0.04	8.70 ± 0.03
62	Sm	0.984	2.6 - 4.3	3	8.14 ± 0.07 8.09 ± 0.04	8.12 ± 0.04
63	Eu	0.950	2.6 - 4.1	3	8.26 ± 0.05 8.40 ± 0.06	8.33 ± 0.01
64	Gd	0.938	2.5 - 4.3	4	8.15 ₉ ± 0.03 8.16 ₂ ± 0.06 8.19 ± 0.05	8.17 ± 0.02
65	Tb	0.923	2.6 - 4.3	3	8.00 ± 0.10 7.99 ± 0.06	8.00 ± 0.01
66	Dy	0.908	2.0 - 3.3	3	8.09 ₁ ± 0.06 8.03 ₅ ± 0.06	8.06 ± 0.04
67	Ho	0.894	3.0 - 4.4	7	8.16 ± 0.06 8.36 ± 0.04	8.26 ± 0.14
68	Er	0.881	3.0 - 4.0	3	8.23 ± 0.04 8.32 ± 0.05	8.28 ± 0.06
70	Yb	0.858	3.0 - 4.3	3	8.40 ± 0.04 8.74 ± 0.07	8.57 ± 0.24

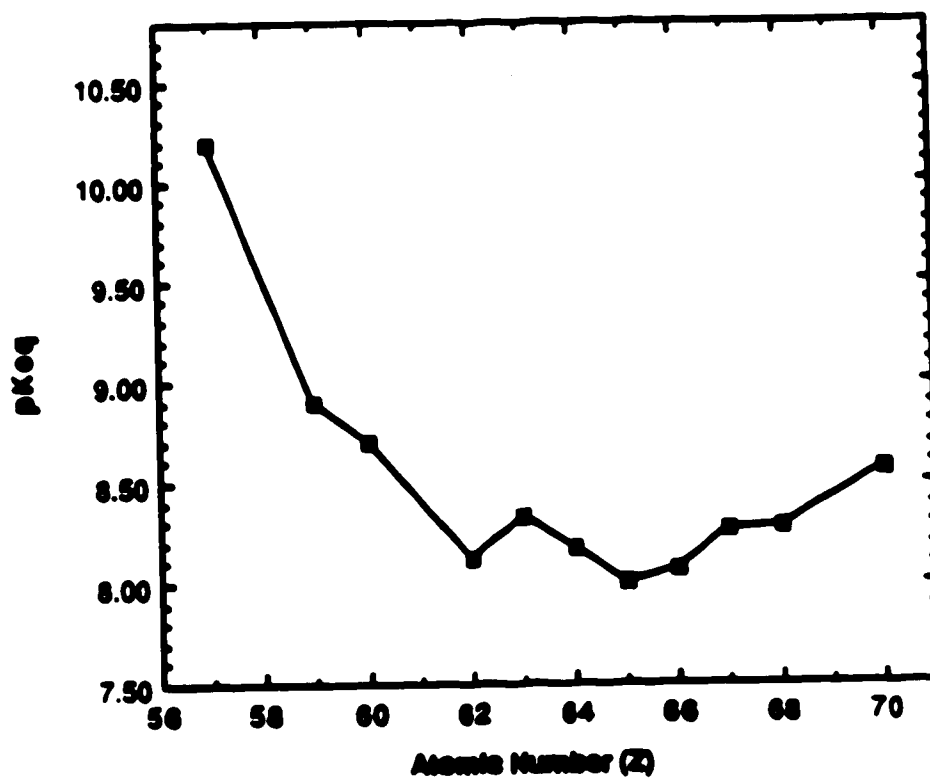


Figure 66. Plot of $pK_{eq(av)}^M$ versus atomic number (Z) for the interaction of the rare earth metals with TAHA.

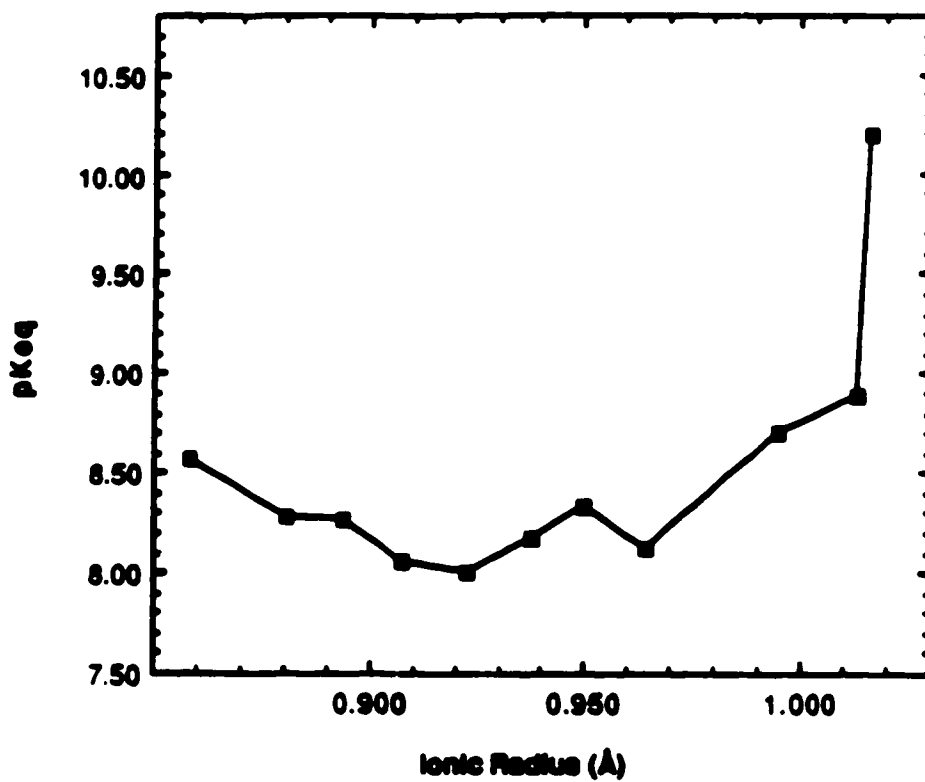


Figure 67. Plot of $pK_{eq(av)}^M$ versus ionic radius (\AA) for the interaction of the rare earth metals with TAHA.

therefore the calculation of pK_{eq}^{Eu} had the largest variation between the duplicate runs.

2. Other Metals

The aqueous chemistry of the cadmium-TAHA complex was studied by potentiometric titrations. The titration of TAHA in the presence of various concentrations of Cd^{+2} is presented in Figure 68. The first curve is for the titration of free TAHA and exhibits the usual inflection point at an A value of 3. The second curve is the titration of Cd^{+2} :TAHA in a ratio of 1.0:1.0 (0.4322 mM Cd^{+2} , 0.4275 mM TAHA). This curve is similar to the titration of Hg^{+2} :TAHA in a ratio of 1.0:1.0 (Figure 22) which exhibits a sharp inflection point at an A value of 5 indicating the presence of the monoprotonated complex. The last curve is the titration of Cd^{+2} :TAHA in a 1.9:1.0 ratio (0.8300 mM Cd^{+2} , 0.4322 mM TAHA); as expected this curve is displaced to slightly lower pH values due to the liberation of protons as more TAHA is complexed to the metal. In this curve, a buffer region between A values of 5 to 6 is observed; after A values greater than 6, the titration curves of TAHA in the presence of cadmium plateau at approximately the same pH as the curve for the titration of TAHA only. The 1.9:1.0 curve indicates that at a pH greater than 8.0, all six protons are displaced as Cd^{+2} complexes to the ligand. Such behavior would indicate that in the presence of excess Cd^{+2} , CdL^{-4} and perhaps Cd_2L^{-2} complexes exist in this region. Between A values of 5 to 6, an equilibrium between the above complexes and the monoprotonated Cd-TAHA complexes is present.

Figure 69 is the potential-pH diagram of several different metals including Cd^{+2} and Zn^{+2} . The concentrations of Hg^{+2} , M^{+2} , and TAHA are tabulated in Table 23; the atomic number (Z), ionic radius (Å), potential-pH independent region and the calculated pK_{eq}^M are tabulated in Table 24. As

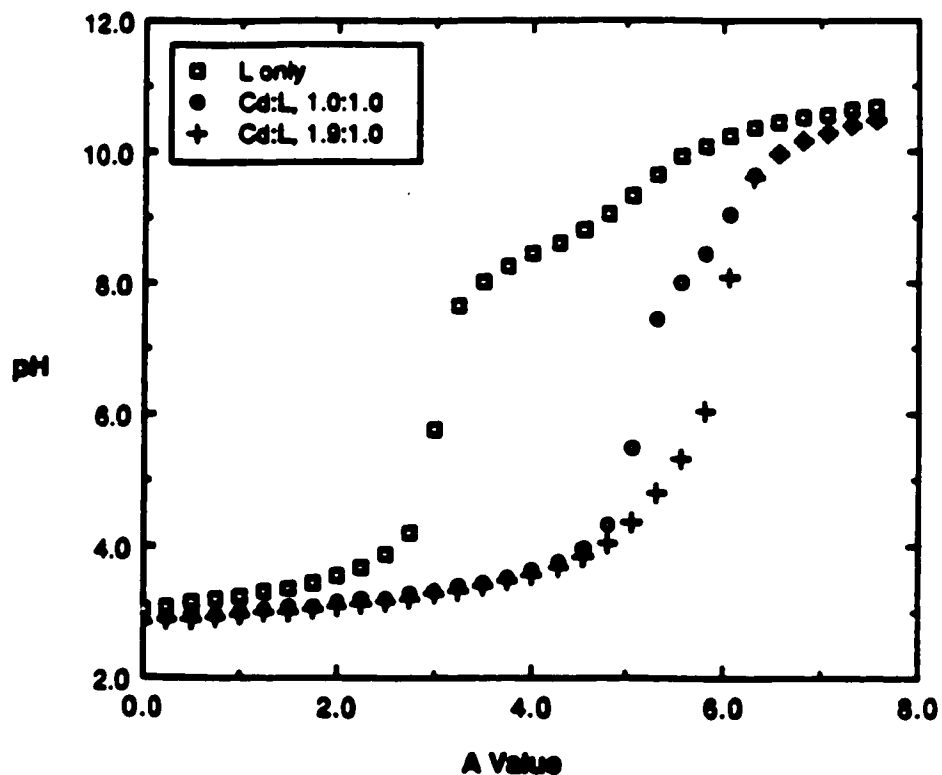


Figure 68. Titration curves of pH versus A value for the cadmium-TAHA system at various concentrations; L represents the ligand TAHA. All titrations were performed at constant ionic strength and temperature ($\mu=0.1$ M KNO_3 and 25.00°C).

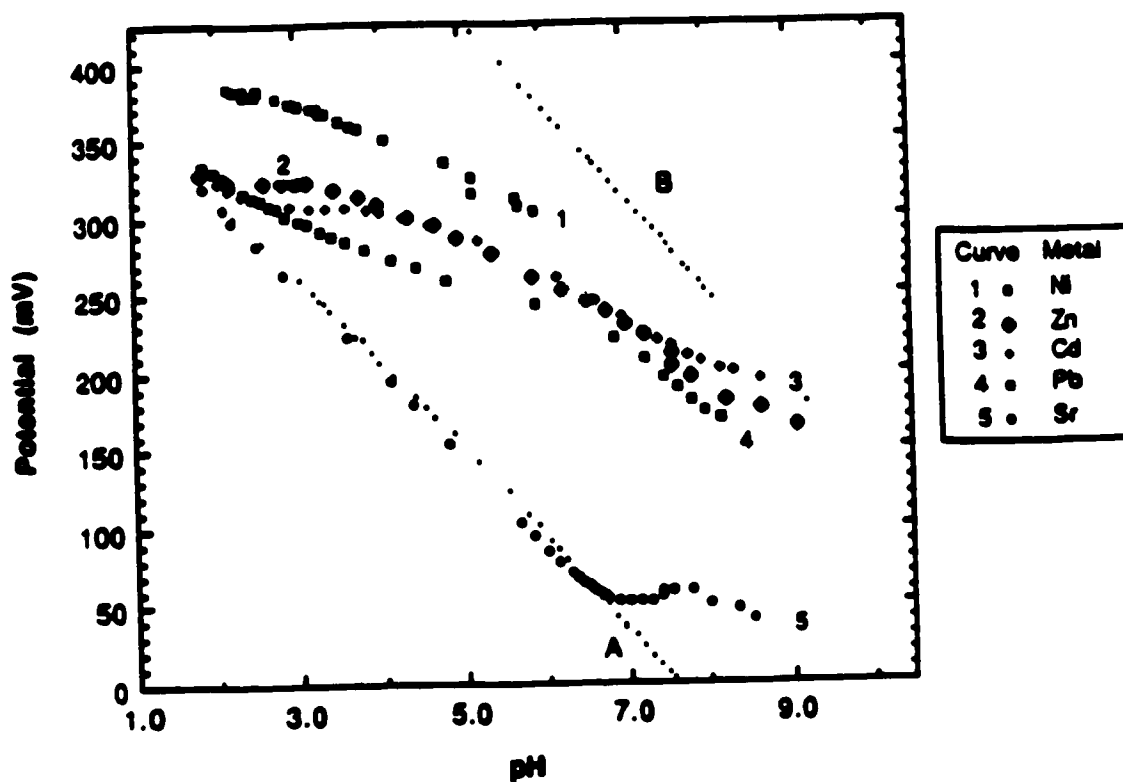


Figure 69. Potential-pH diagram for a solution in which the ratio of $\text{Hg}^{+2}:\text{M}^{+m}:\text{TAHA}$ is 1.0:2.0:2.0; the divalent metal ions are tabulated in the legend. Curve A represents the potential-pH dependence of the metal-TAHA system while curve B represents the theoretical upper potential limit at the mercury indicating electrode.

Table 23. Tabulation of concentrations used for potential-pH diagrams presented in Figure 69.

Metal	Concentration (mM)		
	Hg ⁺²	M ⁺²	TAHA
Cd	0.958	2.033	2.001
Zn	0.958	1.970	2.001
Pb	0.958	2.034	2.001
Sr	0.958	1.999	2.002
Ni	1.002	1.850	1.820

Table 24. Tabulation of pK_{eq}^M and the potential-pH independent region for various metals with TAHA.

Atomic Number	Metal	Ionic Radius (Å) (ref. 109)	pH Independent Range	Number of Runs (N)	pK_{eq}^M (average)
30	Zn	0.74	2.2 - 3.2	3	8.04 ± 0.02
38	Sr	1.12	6.6 - 8.0	3	17.09 ± 0.10
48	Cd	0.97	3.0 - 4.0	3	8.51 ± 0.20
82	Pb	1.20	4.5 - 5.5	4	10.31 ± 0.40

observed, the pH region over which the potential is independent for Cd^{+2} is from pH 3.0 to 4.0 while for Zn^{+2} it is between 2.2 and 3.2. This figure indicates that the complexes of TAHA with zinc are stronger than those with cadmium, which is reflected in the $\text{pK}_{\text{eq}}^{\text{M}}$ values of 8.04 and 8.51 respectively (Table 24) .

This is unusual as CdL complexes (where L is DTPA or TTHA) are often stronger than the corresponding ZnL complexes (30). However CdL (where L is HEDTA) complexes are of lower stability than the corresponding ZnL complexes, while the stabilities of Cd^{+2} and Zn^{+2} complexes with EDTA are of the same order of magnitude (30). The plots of pK_{eq} and $\log K_{\text{ML}}^{\text{C}}$ (corrected and uncorrected for the formation of metal hydroxyl species) are presented in Figure 70A for cadmium-TAHA complex, and Figure 70B for zinc-TAHA complex.

A pH titration of a solution of $\text{Hg}^{+2}:\text{Zn}^{+2}:\text{TAHA}$, where the concentrations of Hg^{+2} , TAHA, and Zn^{+2} were approximately 1 mM, was performed to observe the possible formation of mixed complexes involving these two metals. Between pH 7.0 to 9.0 a shallow buffer region was observed, with a precipitate forming at pH 9.4. The nature of the precipitate is unknown, although it may be $\text{Zn}(\text{OH})_2$ which has an overall formation constant of $1 \times 10^{11.1}$ at 25 °C and zero ionic strength (30).

Nickel, a group VIII element, exhibited unusual and unexpected interactions with TAHA. The potential-pH diagram (Figure 69) was the highest observed for all the metals studied *including* the rare earth elements. Complexation occurred at very low pH values (pH less than 2.5) before the potential began to drop with increasing pH. Three such runs, using different concentrations of Hg^{+2} , Ni^{+2} , and TAHA was studied using the pHg method. In

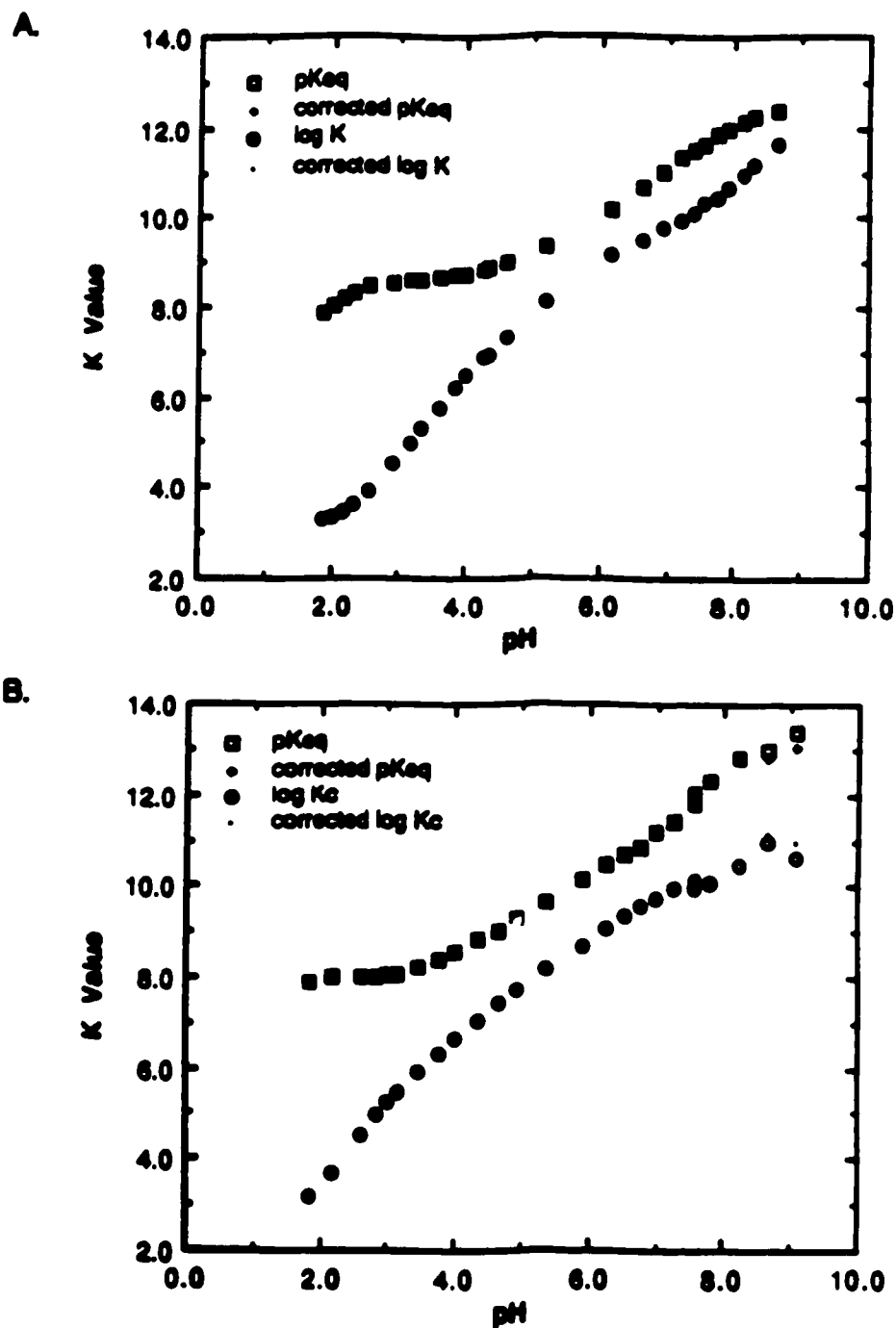


Figure 70. Plot of pK_{eq}^M and logarithm of K_{ML}^C as a function of pH. Formation constants which are both corrected and uncorrected for the formation of the metal hydroxyl species, $(M(OH)_n)^{m-n}$, are plotted as defined in the legend. A. Cadmium (Cd^{+2}), B. Zinc (Zn^{+2}).

all cases a constant ionic strength of 0.1 M was maintained with KNO_3 . The initial concentrations of each species in the titration vessel are given in Table 25A, along with calculated $\text{pK}_{\text{eq}}^{\text{Ni}}$ values. Table 25B tabulates the concentration of HgL , NiL , and Ni^{+2} present in solution assuming that all the TAHA is bound to either mercury or nickel and that only mononuclear complexes are formed. Run two was performed under the usual concentrations for these types of studies while in run one the concentration of each species present was decreased by a factor of ten. In run three the upper potential limit at the mercury electrode was extended by changing the concentrations of each species appropriately (see Table 25B) which allowed for the determination of higher stability constants at the same measured concentration of free Hg^{+2} when no side reactions are occurring. The plot of $[\text{HgL}]$ versus $\text{pK}_{\text{eq}}^{\text{Ni}}$ presented in Figure 71 is linear. This implies that the exchange reaction in which nickel ion displaces the mercury is independent on the concentration of HgL present in the solution. The chemistry of the Hg^{+2} , Ni^{+2} , and TAHA appears to be unusual in that they seem to behave quite differently from all other metals that were studied. This type of behavior appears to be somewhat unusual and further study of the interaction of nickel with TAHA merits study.

A pH titration of Ni^{+2} :TAHA in a ratio of 1.15:1.0 (0.5350 mM Ni^{+2} , 0.4650 mM TAHA) with standardized carbonate-free KOH is plotted in the usual manner in Figure 72. An inflection point at A equal to five indicates the presence of NiHL^{-3} which is deprotonated as the A value is increased from 5 to 6. The presence of protonated metal-TAHA complexes did not previously result in the linear dependence of $\text{pK}_{\text{eq}}^{\text{M}}$ and HgL ; the significance of the above results is uncertain at this time.

Table 25. Tabulation of the concentrations of various species for the nickel-TAHA system.

A. -----

Run	Initial Concentrations (mM)			pK _{eq} (± variance)
	Hg ⁺²	Ni ⁺²	TAHA	
1	0.492	1.088	0.984	5.862 ± 0.03
2	1.002	1.850	1.820	6.037 ± 0.06
3	0.090	10.680	9.022	5.710 ± 0.10

B. -----

Run	Initial Concentrations (mM)			pK _{eq} (± variance)
	HgL	NiL	Ni ⁺²	
1	0.492	0.492	0.595	5.862 ± 0.03
2	1.002	0.818	1.032	6.037 ± 0.06
3	0.090	8.932	1.748	5.710 ± 0.10

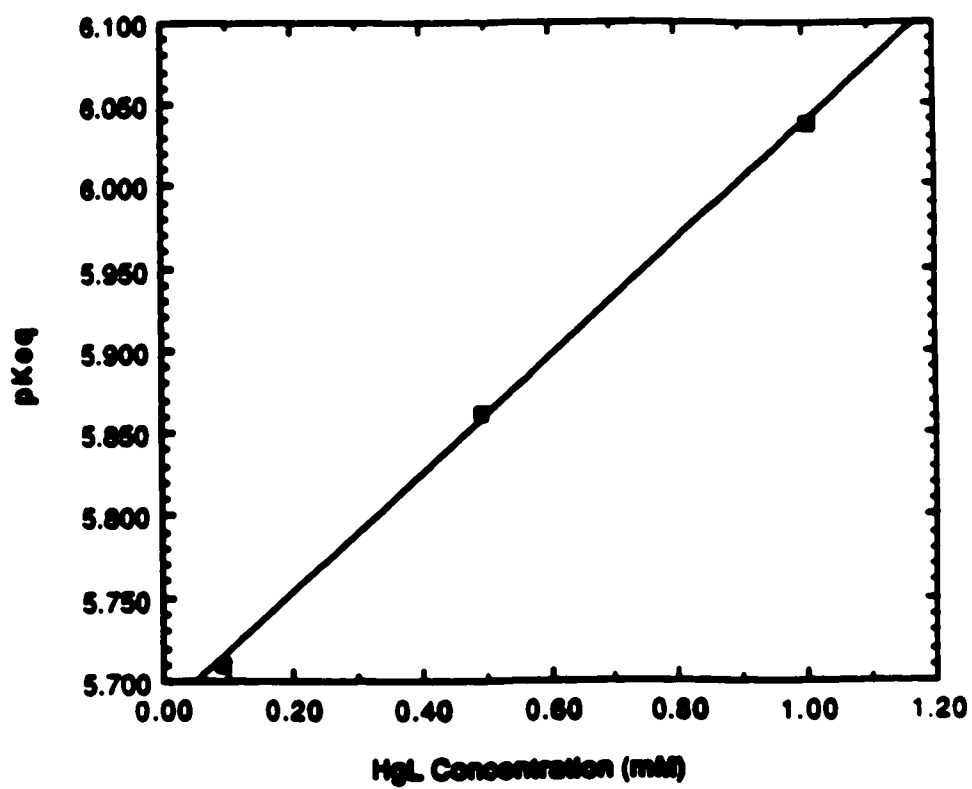


Figure 71. Plot of $[HgL]$ versus pK_{eq}^{Ni} .

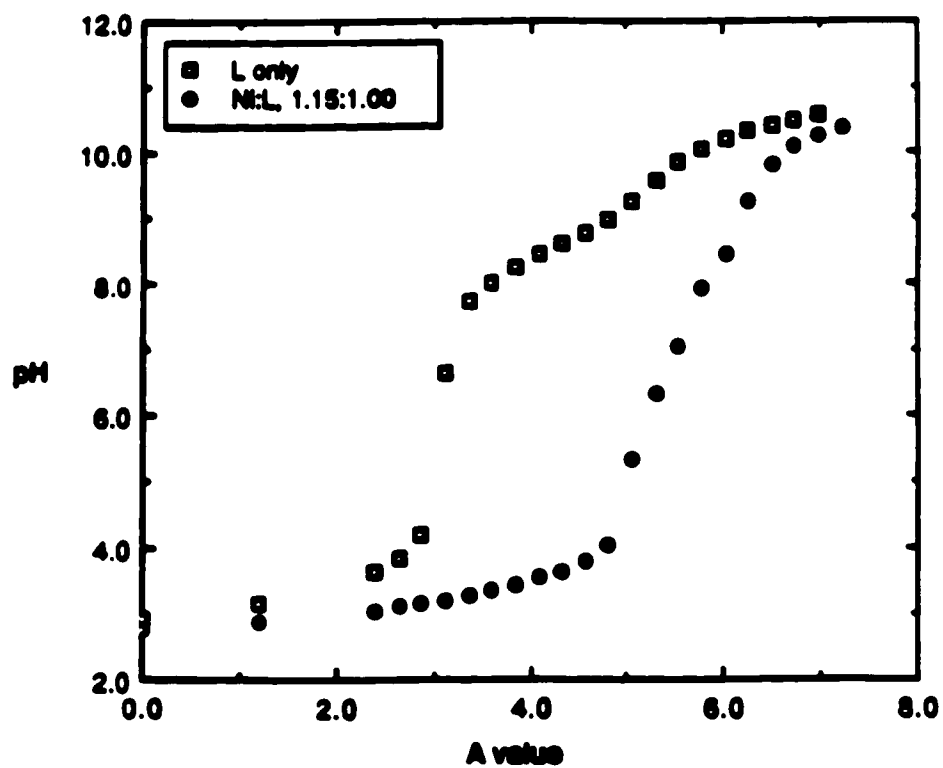


Figure 72. Titration curves of pH versus A value for the nickel-TAHA system at various concentrations; L represents the ligand TAHHA. All titrations were performed at constant ionic strength and temperature ($\mu=0.1$ M KNO_3 and 25.00°C).

In a similar manner a solution of $\text{Hg}^{+2}:\text{Ni}^{+2}:\text{TAHA}$ in a 1.0:1.0:1.0 ratio (the concentration of each species being 1.0 mM) was titrated to observe the formation of possible mixed metal complexes (data not presented). In this titration, it was observed that between pH 7.0 to 9.0 the pH of the solution dropped approximately 0.90 pH units as the solution was allowed to sit until equilibrium had been reached (about 30 minutes). This implies that free hydroxyl ions are being removed from the solution. Since this type behavior had not been observed previously, it is possible that formation of a $\text{HgLNi}(\text{OH})_n$ species occurred and that the equilibrium was attained very slowly. Under these conditions it is doubtful that $\text{Ni}(\text{OH})^+$ formed due to the low stability constant of $1 \times 10^{3.7}$ (30) for this complex.

In Figure 69 the potential-pH diagrams of Pb^{+2} and Sr^{+2} are also presented. Lead exhibited a potential-pH independent region between 4.5 to 5.5 in which the $\text{pK}_{\text{eq}}^{\text{Pb}}$ calculated was 10.31. Strontium, which forms very weak complexes with most ligands, has a potential-pH independent region between 6.6 to 8.0 in which a $\text{pK}_{\text{eq}}^{\text{Sr}}$ value of 17.1 was obtained. The $\text{pK}_{\text{eq}}^{\text{M}}$ and $\log K_{\text{ML}}^{\text{C}}$ (uncorrected and corrected for the formation of the metal hydroxyl species) of these two metals is plotted in Figure 73A (lead) and Figure 73B (strontium). For both these metals the formation of $\text{M}(\text{OH})_n$ species was not observed at any pH. Studies in which the formation of $\text{HgLSr}(\text{OH})_n$ was attempted revealed results which were similar to HgLCa results discussed earlier. As with the HgLCa data, such formation constants could not be calculated using mass balances equations.

3. Summary

The interaction of the metal ions of mercury, lanthanum and calcium were studied in depth by potentiometric and ^1H NMR methods. Several

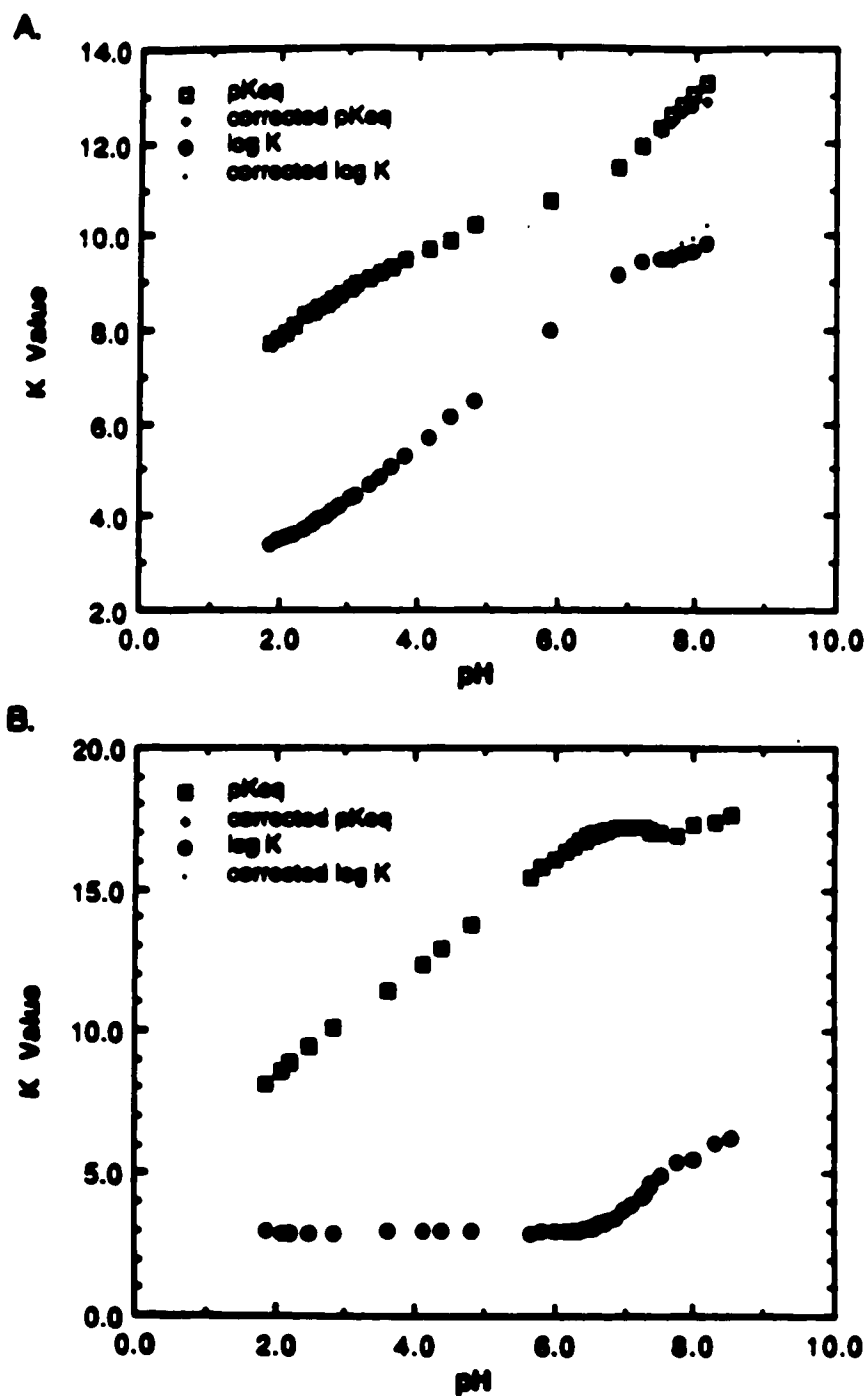


Figure 73. Plot of pK_{eq}^M and logarithm of K_{PbL}^C as a function of pH. Formation constants which are corrected and uncorrected for the formation of the metal hydroxyl species, $(M(OH)_n)^{m-n}$, are plotted as defined in the legend. A. Lead (Pb^{+2}). B. Strontium (Sr^{+2})

other metals including the lanthanide series were studied by potentiometric methods (both by pH titrations and the pHg method). The calculated K_{eq}^M values are tabulated in Tables 22 and 24; the variances presented in these tables is quite low. The results presented in the figures and tables of this section indicated that the interaction of TAHA with these metals is very complex.

The holmium-TAHA interaction indicates the formation of $HgLHo(OH)_n$ complexes. The hydroxyl mixed metal complex did not appear to form with the other rare earth metal, although this possibility cannot be ruled out: such species may have formed in aqueous solutions, however their concentrations may be too low to be detected by the methods used in this work. For the lanthanide series, there was no observation of the "gadolinium break" which is often observed for chelates.

The behavior of nickel was uncharacteristic of other nickel-ligand complexes reported in the literature and has been discussed.

Of the other metals studied, the behavior of TAHA with the cobalt ion is again quite complex. Formation of mixed metal ligand and mononuclear bimetal complexes are indicated, however calculations of the corresponding formation constants using mass balance and electroneutrality equations could not be made. Models that were tried for the calculation of the corresponding formation constants via linear regression analysis, which considered various equilibria within various pH ranges, failed to collaborate with the experimental potentiometric results and therefore at times only qualitative information was obtained.

V. DISCUSSION

The interactions of the metal ions mercury(II), lanthanum(III), and calcium(II) with the hexaprotic ligand TAHA have been studied in depth by both potentiometric and ^1H NMR methods; the stability constants were calculated and are tabulated in Tables 10, 16, and 24 respectively. As well, equilibrium constants ($\text{pK}_{\text{eq}}^{\text{M}}$) for the interaction of the metal ions of the lanthanide series and several other metal ions with the ligand TAHA are tabulated in Tables 22 and 24 respectively.

During the characterization of TAHA it was found that while the metal-TAHA interaction was very complex, this ligand also presented very interesting and challenging behavior in aqueous solution. Of particular interest was the formation of mixed metal ligand complexes; although these formation constants were not calculated in this study due to the complexity of the interaction of TAHA with the metal ions, this area definitely merits further study. Mixed metal ligand complexes, both homonuclear and heteronuclear, have not been well characterized for other chelates, due partly to their complexity.

^1H NMR proved to be a useful tool for studying the metal-TAHA interaction and provided information that would otherwise not have been obtained from potentiometric methods. Further studies using ^{113}Cd NMR, similar to those reported by Jensen *et al.* (110) and Keller *et al.* (111), would provide a useful insight into metal TAHA interactions. Observation of the cadmium nuclei would help to determine which and how many nitrogen and carboxylic atoms were coordinated to the metal ion of the $\text{Cd}(\text{TAHA})^{-3}$ complex. Experiments in which displacement of the mercury ion with the cadmium-TAHA

complex is studied would also be beneficial; in this case either the ^{113}Cd or ^{199}Hg nuclei could be observed as a function of time.

Synthesis and study of this ligand was originally undertaken because of its potential use in MRI as a contrast agent. TAHA has a total of ten coordination sites available for binding to divalent or trivalent metal ions; it was therefore thought that metal-TAHA complexes would be highly stable, that is, comparable to or equal to $\text{Gd}(\text{DTPA})^{-2}$ which is currently used in clinical studies. However the stability constants of metal-TAHA complexes were found to be significantly lower than those of metal-DTPA complexes including the complex $\text{Gd}(\text{DTPA})^{-2}$. The complexity of the interaction of TAHA with the metals studied *may* make this ligand unsuitable as a contrast agent ligand, however it is necessary to further study the behavior of metal-TAHA complexes in vitro. Future in vitro experiments to characterize the interaction of $\text{Gd}(\text{TAHA})^{-3}$ in serum and tissue cultures would be very necessary in the assessment of the potential of this complex as a contrast agent for MRI. As well in vivo (animal studies) would be required to determine the interaction of metal-TAHA complexes in a living system; studies involving rate of excretion, toxicity in rats (LD_{50}), and enhancement of tissue contrast would be necessary in order to establish the use of TAHA as a useful ligand for MRI.

Information as to the in vivo behavior of $\text{Gd}(\text{TAHA})^{-3}$, as well as other metal-TAHA complexes, is necessary in order to determine whether the presence of these complexes disrupts the delicate biological balance, and if so, what is the exact nature of the disruption. Since mixed metal complexes can be formed, it would be necessary to determine whether the presence of metal-TAHA complexes would remove important metals/ions from the body; for example, it would be necessary to look at the extent of the formation of $\text{Gd}(\text{TAHA})(\text{OH})_n$.

REFERENCES

1. R.B. Lauffer, Chem. Rev., 87(2), 901 (1987).
2. C.E. Swenberg and E.G. Meovius, "Magnetic Resonance Imaging and Contrast Enhancement" in Imaging Techniques in Biology and Medicine, C.E. Swenberg and J.J. Conklin, eds., Academic Press Inc., San Diego, California, 1988.
3. M.H. Mendonca and P.C. Lauterbur, Biol. Trace Elem. Res., 13, 229 (1987).
4. S. Ratkovic, Farm. Vestn. (Ljubljana), 28(3), 195 (1987).
5. D.H. Carr, Mag. Res. Imaging, 3, 17 (1985).
6. M.D. Ogan and R.C. Brasch, "Contrast Agents in NMR Imaging" in Annual Reports in Medicinal Chemistry, vol 20, D.M. Bailey, ed., Academic Press Inc., Orlando, Florida, 1985.
7. S.H. Koenig and R.D. Brown III, Mag. Res. Med., 1, 478 (1984).
8. J.A. Koutcher, R.B. Lauffer, and T. L. Brady, J. Nucl. Med., 25, 506 (1984).
9. T.F. Budinger and P.C. Lauterbur, Science, 226, 288 (1984).
10. B.L. Engelstad and R.C. Brasch, "Pharmaceutical Development for Magnetic Resonance Imaging" in Biomedical Magnetic Resonance, T.L. James and A.R. Margulis, eds., Radiology Research and Education Foundation., San Francisco, 1984.
11. R.M. Baum, Chem. and Eng. News, Oct. 31, p.18 (1988).
12. M. Mendonca-dias, M. Helena, E. Gaggelli, and P.C. Lauterbur, Semin. Nucl. Med., 13(4), 364 (1983).

13. V. M. Runge, C.M. Lukehart, C.L. Partain, and A.E. James Jr., *Am. J. Roentgenol.*, 141, 1209 (1983).
14. M.A. Mendonca-dias, E. Gaggelli, and P. Lauterbur, *Semin. Nucl. Med.*, 12, 364 (1983).
15. R. C. Brasch, *Radiology*, 147, 781 (1983).
16. H.J. Weinmann, R.C. Brasch, W.R. Press, and G.E. Wesbey, *Am. J. Roentgenol.*, 142, 619 (1984).
17. A. Najafi, E.G. Amparo, and R.F. Johnson Jr., *J. Labelled Compd. Radiopharm.*, 24(9), 1131 (1987).
18. S. Sanjay, D.D. Stark, T.J. Brady, J. Wittenberg, and J.T. Ferrucci Jr., *Am. J. Roentgenol.*, 147, 357 (1986).
19. U. Schmied, M.D. Ogan, M.E. Moseley, and R.C. Brasch, *Am. J. Roentgenol.*, 147, 1263 (1986).
20. V.M. Runge, J.Clanton, A. Jeffrey, A.C. Price, C.J. Wehr, W.A. Herzer, C.L. Partain, and A.E. James Jr., *Mag. Res. Imaging*, 3(1), 43 (1985).
21. G. Strich, K. Gerber, and R.A. Slutsky, *Mag. Res. Imaging*, 3(1), 37 (1985).
22. G. Strich, P.L. Hagan, K.H. Gerber, and R.A. Slutsky, *Radiology*, 154, 723 (1985).
23. R.A. Slutsky, T. Peterson, G. Strich, and J.J. Brown, *Radiology*, 154(3), 733 (1985).
24. E.J. Goldstein, K.R. Burnett, G.L. Wolf, J. Wortman, P. Joseph, and S. Sen, *Physiol. Chem. Phys. and Med. NMR.*, 17, 113 (1985).

25. E.J. Goldstein, K.R. Burnett, J.R. Hansell, J. Casaia, J. Dizon, B. Farrar, D. Gelburn, and G. Wolf, *Physiol. Chem. Phys. and Med. NMR.*, 16, 97 (1984).
26. H. Gries and H. Miklautz, *Physiol. Chem. Phys. and Med. NMR.*, 16, 105 (1984).
27. V.M. Runge, J.A. Clanton, A.C. Price, W.A. Herzer, C.J. Wehr, C.M. Lukehart, C.L. Partain, and A.E. James Jr., *Physiol. Chem. Phys. and Med. NMR.*, 16, 113 (1984).
28. R.C. Brasch, H.J. Weinmann, and G.E. Wesbey, *Am. J. Roentgenol.*, 142, 625 (1984).
29. D.H. Carr, J. Brown, G.M. Bydder, H.J. Weinmann, U. Speck, D.J. Thomas, and I.R. Younget, *Lancet*, 1(8375), 484 (1984).
30. A.E. Martell and R.M. Smith, Critical Stability Constants, Plenum Press, New York N.Y., 1977.
31. C. Curtet, C. Bourgoin, J. Bohy, J.C. Saccaulini, P. Thedrez, S. Akoka, C. Tellier, and J.F. Chatalrady, *Int. J. Cancer*, (Supplement 2), 126 (1988).
32. Y. Manabe, C. Longley, and P. Furmanski, *Biochim. Biophys. Acta.*, 883(3), 460 (1986).
33. R.B. Lauffer, T.J. Brady, R. D. Brown III, C. Bosglin, and S.H. Koenig, *Mag. Res. Med.*, 3(4), 541 (1986).
34. R. Lauffer, B. Randell, and T.J. Thomas, *Mag. Res. Imaging*, 3(1), 11 (1985).
35. R.C. Lyon, P.J. Faustino, J.S. Cohen, A. Katz, and D. Colcher, *Mag. Res. in Med.*, 4, 24 (1987).

36. N.J. Patronas, J. S. Cohen, R.H. Knop, A.J. Dwyer, D. Colcher, J. Lundy, F. Momex, P. Hambright, M. Sohn, and C.E. Myers, *Cancer Treat. Rep.*, 70(3), 391 (1986).
37. P. Marzola and S. Cannistroro, *Physiol. Chem. Phys. and Med. NMR.*, 19, 279 (1987).
38. G. Kabalka, E. Buonocore, K. Hubner, T. Moss, N. Norley, and L.Huang, *Radiology*, 163(1), 255 (1987).
39. R.C. Gamble, P. Schmidt, and P. Gardner, *Eur. Pat. Appl.* EP 160552 A2 Nov. 6 1985.
40. J.C. Gore, H.D. Sostman, and V.J. Caride, *J. Microencapsulation*, 3(4), 251 (1986).
41. D.H. Carr, *Physiol. Chem. Phys. and Med. NMR.*, 16, 137 (1984).
42. H.J. Weinmann, R.C. Brasch, W.R. Press, and G.E. Wesbey, *Am. J. Roentgenol.*, 142, 619 (1984).
43. H.J. Weinmann, M. Laniado, and W. Mutzel, *Physiol Chem. Phys. and Med. NMR.*, 16, 167 (1984).
44. D.H. Carr, J. Brown, G.M. Bydder, R.E. Steiner, H.J. Weinmann, U. Speck, A.S. Hall, and I.R. Young, *Am. J. Roentgenol.*, 143, 215 (1984).
45. M. Laniado, H.J. Weinmann, W. Schorner, R. Felix, and U. Speck, *Physiol. Chem. Phy. and Med. NMR.*, 16, 157 (1984).
46. C. Claussen, M. Laniado, E. Kazner, W. Schorner, and R. Felix, *Neuroradiology*, 27, 164 (1985).
47. R. Felix, W. Schorner, M. Laniado, H.P. Niendorf, C. Claussen, N. Fiegler, and H. Speck, *Radiology*, 156, 680 (1985).

48. W. Schorner, R. Felix, M. Laniado, *Fortschr. Rontgenstr.*, 140, 493 (1984).
49. W. Schorner, R. Felix, C. Claussen, W. Flegler, E. Kazner, H.P. Niendorf, *Fortschr. Rontgenstr.*, 141, 511 (1984).
50. D.D. Stark, R. Weissleder, G. Ellzondo, P.F. Hahn, S. Saini, L.E. Todd, J. Wittenberg, and J.T. Ferrucci, *Radiology*, 168, 297 (1988).
51. A.D. Sherry, PCT. Int. Appl. WO 86/2352 A1 24 April 1986 16pp (Appl. 85/US2014).
52. M. Magerstadt, O.A. Gansow, M.W. Martin, D. Colcher, L. Baltzer, R.H. Knop, M.E. Gilton, and M. Naegle, *Mag. Res. Med.*, 3(5), 808 (1986).
53. W.P. Cacheris, S.K. Nickle, and A.D. Sherry, *Inorg. Chem.*, 26, 958 (1987).
54. C.F.G.C. Gerraldes, A.D. Sherry, R.D. Brown III, and S.H. Koenig, *Mag. Res. Med.*, 3, 242 (1986).
55. R.H. Knop, J.A. Frank, A.J. Dwyer, M.E. Gilton, M. Naegle, M. Schrader, J. Cobb, O. Gansow, M. Magerstadt, M. Brechbiel, L. Baltzer, and J.L. Dopman, *Comput. Assist. Tomogr.*, 11, 35 (1987).
56. A.I. Vogel, Textbook of Quantitative Inorganic Analysis 4th edition, Longman Inc., New York, 1978.
57. C.N. Reilley, R.W. Schmidt, and D.W. Lamson, *Anal. Chem.*, 50(5), 953 (1958).
58. S.J. Lyle M.D. and M. Rahman, *Talanta*, 10, 1177 (1963).
59. R. Bates, Determination of pH: Theory and Practice, 2nd edition, John Wiley and Sons, Inc., 1973.

60. R.D. Durst, Standard Reference Materials, Analytical Chemistry Division, Institute for Materials Research, National Bureau of Standards.
61. H.A. Laitinen and W.E. Harris, Chemical Analysis: An Advanced Text and Reference, 2nd edition, McGraw- Hill, Inc., 1975.
62. R.G. Bates, *Anal. Chem.*, **40**(6), 28A (1968).
63. C.H. Reilley and R.W. Schmid, *Anal. Chem.*, **30**(5), 947 (1958).
64. J.H. Holloway and C.N. Reilley, *Anal. Chem.*, **32**(2), 249 (1960).
65. R.W. Schmid and C.N. Reilley, *J. Am. Chem. Soc.*, **78**(5), 5513 (1956).
66. J.E. Powell and J.L. Mackey, *Inorgan. Chem.*, **1**(2), 418 (1962).
67. W.M. Latimer, Oxidation Potentials, 2nd edition, Prentice-Hall, Inc., 1952.
68. A.L. Van Geet, *Anal. Chem.*, **40**(14), 2227 (1968).
69. D.S. Ralford, C.L. Fisk, and E.D. Becker, *Anal. Chem.*, **51**(2), (1979).
70. P. Plateau and M. Gueron, *JAACS.*, **104**, 7310 (1982).
71. J.K.M. Sanders and B.K. Hunter, Modern NMR Spectroscopy: A Guide for Chemists, Oxford University Press, 1987.
72. W.H. Press, B.P. Flannery, S.A. Teukolsky, and W.T. Vetterling, Numerical Recipes: The Art of Scientific Computing, Cambridge University Press, New York, 1986.
73. P. Diehl, H. Kellerhals, and E. Lustig, "Computer Assistance in the Analysis of High Resolution NMR Spectra" in NMR: Basic Principles and Progress, vol 6, P. Diehl, E. Fluck, and R. Kosfeld, eds., Springer-Verlag New York, 1972.

74. W.D. Keller, T.R. Lusebrink, and C.H. Sederholm, J. Chem. Phys., 44(2), 782 (1966).
75. J.L. Dye and V.A. Nicely, J. Chem. Ed., 48(7), 443 (1971), Supplement Program No. 00000485.
76. W.E. Wentworth, J. Chem Ed., 42(2), 96 (1965).
77. W.E. Wentworth, J. Chem. Ed., 42(2), 162 (1965).
78. J. Pitha and R.N. Jones, Can. J. Chem., 44, 3031 (1966).
79. M.J. Powel, Computer Journal, 7, 155 (1964).
80. J.C. Moore, USA Patent 2,239,617, Serial No. 270,911. April 22 1941.
81. G. Schwarzenbach and H. Ackermann, Helv. Chim. Acta., 31, 1029 (1948).
82. D. Chapman, D.R. Lloyd, and R.H. Prince, J.Chem. Soc. (London), 688, 3645 (1965).
83. W.J. Blaedel and H.T. Knight, Anal. Chem., 26(4), 741 (1954).
84. S. Brewer, Solving Problems in Analytical Chemistry, John Wiley and Sons, 1980.
85. E. Wanninen, Suomen. Kemistilehti., B28, 136 (1958).
86. D.R. Ryskiewich, Acid Dissociation Constant Diethylenetriamine-pentaacetic Acid and the Stability Constants of Some of its Metal Complexes, Dissertation, New York University, July 1956.
87. G. Schwarzenbach, A. Willi, and R.O. Bach, Helv. Chim. Acta., 30, 1303 (1947).

88. J. Bjerrum, Metal Amine Formation in Aqueous Solution. Theory of Reversible Step Reactions, Copenhagen, P. Haase and Son, 1957.
89. H. Irving (Ms.) and H.S. Rossotti, J. Chem. Soc., (London), No. 680, 3397(1953).
90. J.C. Sullivan and J.C. Hindman, J. Am. Chem. Soc., 74, 6091 (1952).
91. R.S. Reid and B. Podanyi, J. Inorg. Biochem., 32, 183 (1988).
92. R.F. Jameson, G. Hunter, and T. Kiss, J. Chem. Soc. Perkin Trans. II, 1105 (1980).
93. M.J.L. Tillotson and L.A.K. Staveley, J. Chem. Soc., (London), No 722, 3613 (1958).
94. P. Leykeman and A.E. Martell, Inorg. Chem., 18(5), 1284 (1979).
95. E.J. King, "Acid-Base Equilibria" in International Encyclopedia of Physical Chemistry and Chemical Physics, Topic 15, vol. 4, E.A. Guggenheim, J.E. Mayer, F.C. Tompkins, eds. in chief, New York, Pergamon Press, Inc., 1965.
96. R.J. Kula, Proton Nuclear Magnetic Resonance Studies of Ethylenediaminetetraacetic Acid and its Metal Complexes, Dissertation, University of California (Riverside), June 1964.
97. G. Schwarzenbach and H. Flaschka, Complexometric Titrations, 2nd edition, translation , Richard Clay (The Chaucer Press), Ltd., Bungay, Suffolk, (Great Britan), 1969.
98. L. Harju, Anal. Chim. Acta., 50, 475 (1970).
99. L. Harju and A. Ringbom, Anal. Chim. Acta., 49, 221 (1970).
100. L. Harju and A. Ringbom, Anal. Chim. Acta., 49, 205 (1970).

101. S. Chabereck, A.E. Frost, M.A. Doran, and N.J. Bricknell, *J. Inorg. Nucl. Chem.*, 11, 184 (1954).
102. F.Y. Moriguchi, M. Miyazaki, and K. Ueno, *Bull. of Chem. Soc. of Japan*, 41(6), 1344 (1968).
103. A.E. Martell and M. Calvin, *Chemistry of the Metal Chelate Compounds*, 1st edition, Prentice-Hall, Inc., New York, 1952.
104. J. Bjerrum, *Chem. Rev.*, 46, 381 (1950).
105. R. Hagen, J.P. Warren, D.H. Hunter, and J.D. Roberts, *J. Am. Chem. Soc.*, 95(17), 5712 (1973).
106. F.P. Spedding, J.E. Powell, and E.J. Wheelwright, *J. Am. Chem. Soc.*, 78, 34 (1956).
107. A.K. Gupta and J.E. Powell, *Inorg. Chem.*, 1(4), 955 (1962).
108. C.A. Keele and E. Neil, *Samson Wright's Applied Physiology*, 12th edition, Oxford University Press, 1971.
109. *CRC Handbook of Chemistry and Physics*, 66th edition, R.C. Weast, ed., CRC Press, Boca Raton, Florida, 1986. p. F-164.
110. C.F. Jensen, S. Deshmukh, H.J. Jakobsen, R.R. Inners, and P.D. Ellis, *J. Am. Chem. Soc.*, 103, 3659 (1981).
111. A.D. Keller, T. Drakenberg, R.W. Briggs, and Ian M. Armitage, *Inorg. Chem.*, 24, 1170 (1985).

APPENDIX 1

Sample subroutine for KINET used for the calculation of the acid dissociation constants for a triprotic acid using pH versus volume of titrant. This subroutine calculates the dissociation constants of a triprotic acid from pH versus volume of titrant added.

```
IMPLICIT REAL *8(A-H,-Z)
COMMON ZZZZZ, KNOOUNT, 1999, ITAPE, 1998, JTAPE, 1997, IWT,
      1996.LAP

C 1994, XINCR, NOPT, 1993, NOVAE, 1992, NOUNK, 1991, X, U,
C ITMAX,1990, WTX, TSY, I, 889, AV, RESID, IAR, 1888, EPS, ITYP,
C 1887, XX, RXTYP, DX11, FOP, FO, FU, P, ZL, TO, EIGVAL, XST, T, DT, L,
C 1886, M, 1885, JJJ, 1884, Y, DY, VECT, NCEST, 1880, CONST

      DIMENSION X (5,200), U(20), WTX (5,200), XX(5), FOP (200), FO (200),

C  FU (200), P (20,21), VECT (20,21), ZL (200), TO (20), EIGVAL (20),
C  XST(200), Y (10), DY (10), CONST (20)

      GOTO (2,3,4,5,1), ITYP
1     CONTINUE
      ITAPE=5
      JTAPE=6

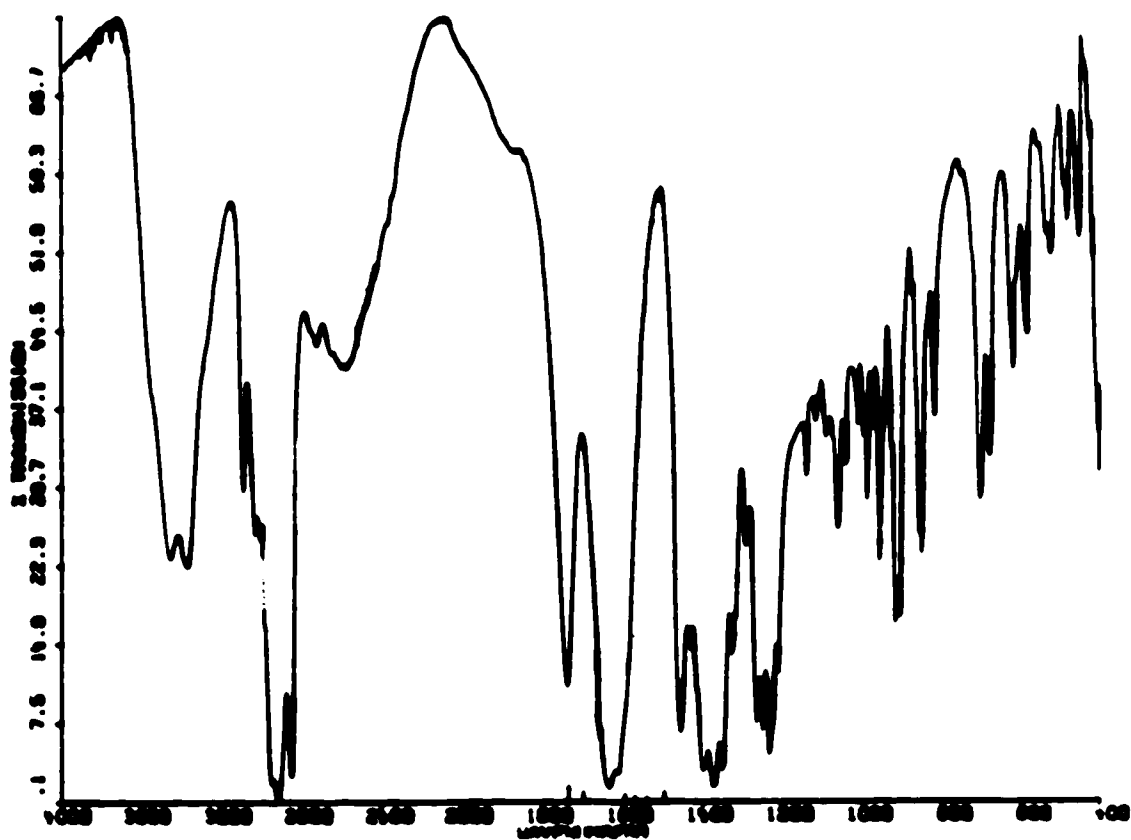
C  INSERT NOUNK AND NOVAR ASSIGNMENTS HERE

      NOVAR=4
      NOUNK=3
      RETURN
2     CONTINUE
      XK1=U(1)
      XK2=U(2)
      XK3=U(3)
      XN=XX(1)
      AA=XX(2)
      BB=XX(3)
      CC=XX(4)
      AAA=AA*U(1)
      BBB=BB*U(2)
      CCC=CC*U(3)
      DD=AAA+BBB+CCC
      YCALC=DD
      RESID=YCALC-XX(1)
      RETURN
```

3 CONTINUE
4 CONTINUE
5 CONTINUE
RETURN
END

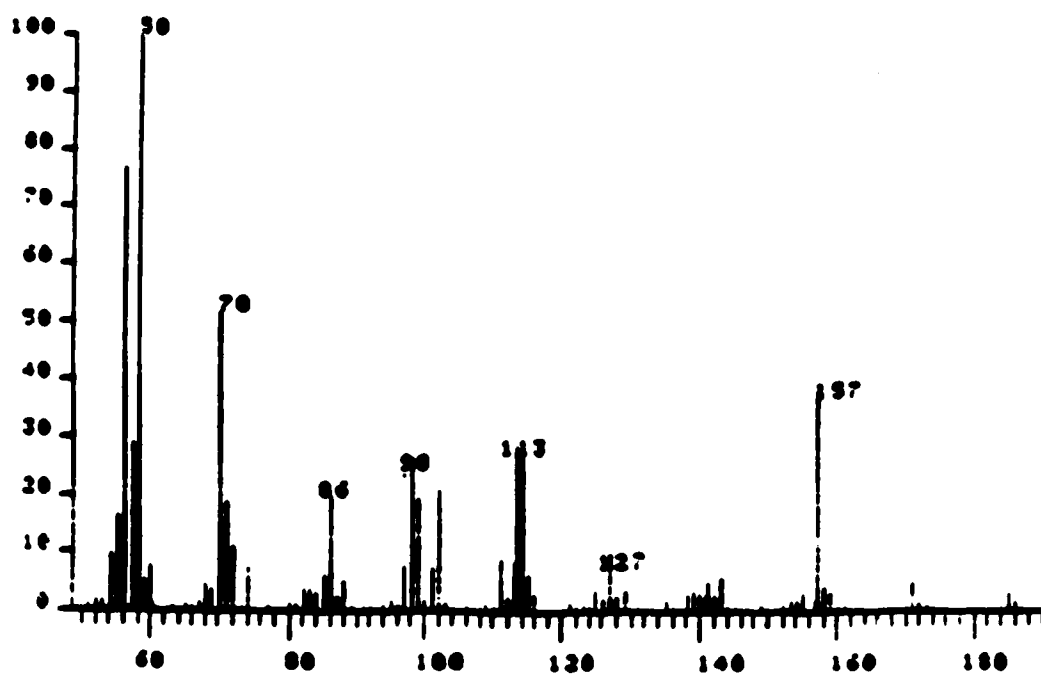
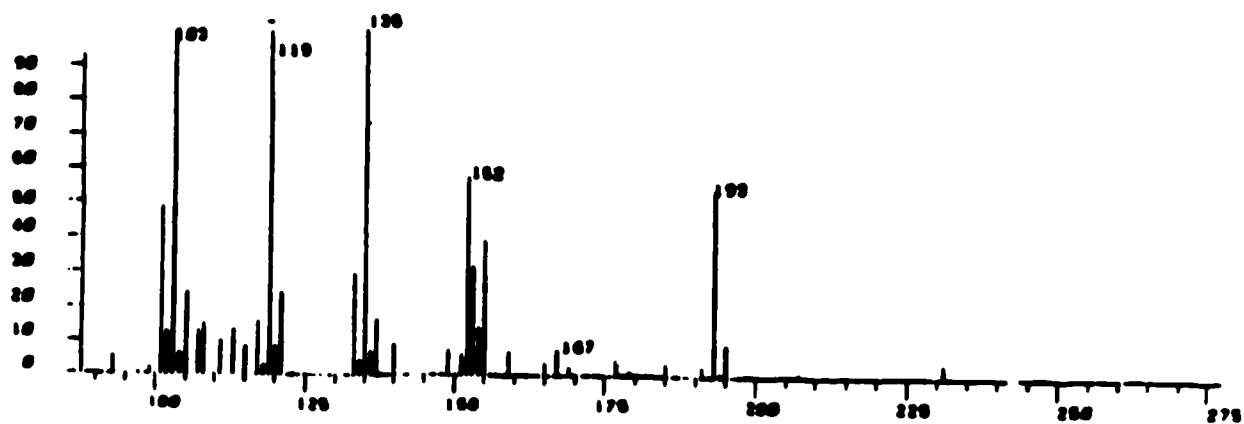
APPENDIX 2

Infrared spectrum of TAHA dissolved in water.



APPENDIX 3

Mass spectra (EI) of TAHA obtained at 180 °C and 240 °C.



APPENDIX 4A

Acid dissociation constants of some common chelates (25 °C,
 $\mu = 0.1 \text{ M KNO}_3$) (reference 30).

Ligand	pK_n
Ethylenediamine N,N,N',N'-tetraacetic acid (EDTA)	$pK_1 = 2.00$ $pK_2 = 2.68$ $pK_3 = 6.16$ $pK_4 = 10.17$
Ethyleneglycol bis-(2-aminoethylether)- N,N,N',N'',N''-pentaacetic acid (EGTA)	$pK_1 = 2.00$ $pK_2 = 2.65$ $pK_3 = 8.85$ $pK_4 = 9.46$
Diethylenetriamine N,N,N',N'',N''- pentaacetic acid (DPTA)	$pK_1 = 1.82$ $pK_2 = 2.65$ $pK_3 = 4.28$ $pK_4 = 8.53$ $pK_5 = 10.45$
Tris (2-aminoethyl) amine (tren)	$pK_1 = 8.41$ $pK_2 = 9.43$ $pK_3 = 8.41$

APPENDIX 4B

Acid dissociation constants of some hexaprotic acids (25 °C, $\mu = 0.1$ M KNO_3) (reference 30).

Ligand	pK_n
Triethylenetetranitrilo-hexaacetic acid (1,4,7,10-tetraazadecane-1,1,4,7,10,10-hexaacetic acid) (TTHA)	$\text{pK}_1 = 2.4 \pm 0.1$ $\text{pK}_2 = 2.7 \pm 0.1$ $\text{pK}_3 = 4.08 \pm 0.2$ $\text{pK}_4 = 6.16 \pm 0.2$ $\text{pK}_5 = 9.44 \pm 0.04$ $\text{pK}_6 = 10.5 \pm 0.4$
1,2,3-Tris[bis(carboxymethyl)amino]propane (1,2,3-triaminopropane-hexaacetic acid) (TAPAA)	$\text{pK}_1 = 2.00$ $\text{pK}_2 = 2.42$ $\text{pK}_3 = 3.54$ $\text{pK}_4 = 4.30$ $\text{pK}_5 = 8.26$ $\text{pK}_6 = 9.88$
Nitrilotris(ethylenenitrilo)hexaacetic acid (triaminotriethylamine-hexaacetic acid)	$\text{pK}_1 = \text{---}$ $\text{pK}_2 = \text{---}$ $\text{pK}_3 = \text{---}$ $\text{pK}_4 = 8.36^1$ $\text{pK}_5 = 8.55^1$ $\text{pK}_6 = 10.65^1$
² Tris(2-aminoethyl)amine-hexaacetic acid (TAHA)	$\text{pK}_1 = 1.82 \pm 0.02$ $\text{pK}_2 = 2.52 \pm 0.01$ $\text{pK}_3 = 2.94 \pm 0.02$ $\text{pK}_4 = 8.12 \pm 0.02$ $\text{pK}_5 = 8.72 \pm 0.03$ $\text{pK}_6 = 10.42 \pm 0.06$

¹ pK_n values measured at 20 °C

² This work

APPENDIX 4C

Acid dissociation constants of ligands (25 °C, μ = 0.1 M KNO₃)
(reference 30).

Ligand	pK _n
N-(2-hydroxyethyl)ethylenedinitrilo-	pK ₁ = 2.6
N,N',N'-triacetic acid	pK ₂ = 5.37
(HEDTA)	pK ₃ = 9.81
1,7-diaza-4-oxaheptane-1,1,7,7-	pK ₁ = ---
tetraacetic acid	pK ₂ = ---
(EEDTA)	pK ₃ = 8.75
	pK ₄ = 9.39